Fatigue Load Monitoring with Standard Wind Turbine Signals

A thesis accepted by the Faculty of Aerospace Engineering and Geodesy of the Universität Stuttgart in partial fulfilment of the requirements for the degree of Doctor of Engineering Sciences (Dr.-Ing.)

by

Nicolai Cosack

born in Celle, Germany

Main referee:	Prof. Dr. Dipl.-Ing. Martin Kühn
Co-referee:	Prof. Dr. rer. nat. Joachim Peinke
Date of defence:	7th of April 2010

Endowed Chair of Wind Energy at the Institute of Aircraft Design
Universität Stuttgart
2010

Acknowledgements

Several people and institutions contributed to the successfull preparation of this thesis and supported this work in many ways. Therefore, I would like to express my gratitude to my supervisor and main referee Prof. Dr. Dipl.-Ing. Martin Kühn, my co-referee Prof. Dr. rer. nat. Joachim Peinke, the staff at the Insitute of Aircraft Design and especially all employees at the Endowed Chair of Wind Energy. I would also like to thank my family and friends for their encouragement throughout the years.

Parts of the work presented in the following have been carried out within the research project ”Verification of Offshore Wind Turbines” (OWEA, FKZ 0327696A) supported by the Federal Ministry for Environment, Nature Conservation and Nuclear Safety (BMU) in the scope of the joint research initiative ”Research at Alpha Ventus” (RAVE). Further I want to acknowledge the cooperation with the Multibrid GmbH and the Energy research Centre of the Netherlands (ECN) which provided me with the possibility to validate the developed approaches on the basis of measured data.

Contents

Nomenclature

If not indicated otherwise, the abbreviations below have been used. Variables which are used only once or in a specific, short paragraph are sometimes explained directly where they appear.

α	momentum parameter in backpropagation training
α_n	bandwidth parameter of order n
Δ_{ji}	change of the weight update between neuron j and i during resilient backpropagation training
γ_3	skewness
γ_4	kurtosis
λ_n	spectral moment of order n and angular frequency ω
μ	learning rate in the backpropagation algorithm
μ_n	central moment of order n
ω	angular frequency
Ω_{gen}	generator rotational speed
$\dot{\Omega}_{gen}$	generator rotational acceleration
ρ	air density
ρ_0	air density at sea level
$\sigma(a_i)$	output of the activation function of neuron i
σ_X	standard deviation of data set X
θ_p	pitch angle
a_i	activation of neuron i
b_i	i-th regression coefficient
E_i	estimation error of data point i
E_{Yaw}	yaw error
f	cyclic frequency
F_r	rotor thrust force
$g(\cdot)$	transfer function from non-Gaussian to Gaussian domain
$G(\cdot)$	transfer function from Gaussian to non-Gaussian domain
h	height above ground
h_r	reference height above ground
$H(x, y)$	joint cumulative distribution function of x and y
I_T	turbulence intensity
$L_{eq,Tref,p}$	equivalent load magnitude with reference time T_{ref} and exponent p
L_u	integral length scale of turbulence
m	exponent for the calculation of equivalent load cycles. $1/m$ corresponds to the slope of the SN-curve when plotted on a double logarithmic scale.
m_n	spectral moment of order n and cyclic frequency f

M_r	rotor torque
M_{ew}	edgewise blade root bending moment
M_{fw}	flapwise blade root bending moment
M_{ip}	in-plane blade root bending moment
M_{op}	out-of-plane blade root bending moment
M_{tb}	longitudinal tower base bending moment
M_{tt}	nodding moment at tower top
N_{ref}	reference number of load cycles for the calculation of equivalent load cycles
$p(\Delta S)$	probability density function of rainflow cycles
$p(L)$	probability density function of load magnitudes
P_{el}	electrical power output
R^2	coefficient of determination
$R_{cor,xx}$	auto-correlation function of variable x
$R_{cor,xy}$	cross-correlation function of variables x and y
$R_{cov,xx}$	auto-covariance function of variable x
ΔS	load range from rainflow counting
$\Delta S_{eq,Nref,m}$	equivalent load range with reference cycle number N_{ref} and exponent m
ΔS_{max}	maximum load range
S_f	power spectral density with cyclic frequency f
S_ω	power spectral density with angular frequency ω
T_{ref}	reference time for the calculation of equivalent load magnitudes
U	wind speed in longitudinal direction
v_0	expected number of up-crossing
v_p	expected numbers of peaks
$Var(X)$	variance of data set X
Δw_{ji}	update of the connection weight between neuron j and i during training
w_{ji}	weight of connection between neuron j and i
w	factor for weighting of equivalent loads
x_p, x_v	peak and valley in the Gaussian domain
$\bar{X}$	mean value of data set X
$\hat{X}_i$	estimated value of data point X_i
X_i	true value of a data point (as opposed to $\hat{X}_i$)
$\ddot{y}_{tt}$	lateral tower top acceleration
$\ddot{z}_{tt}$	longitudinal tower top acceleration
z_0	roughness length
z_p, z_v	peak and valley in the non-Gaussian domain
Z	normalised load range
CDF	cumulative distribution function
MESE	maximum entropy spectral estimate
PDF	probability density function
PSD	power spectral density
TB	method of Tovo-Benasciutti for the calculation of PDFs of rainflow ranges

Executive summary

The loading of wind turbines is in general not monitored and measurements are only performed for the validation of prototypes. A shift towards increased use of load monitoring devices for the forthcoming generation of large multi-megawatt turbines is obvious, as relative costs for measurement devices go down and the benefit from feeding load signals into the turbine control increases. However, it is hard to imagine that this will be the case for turbines with rated power in the range of 1 to 3 MW which are installed in large numbers today.

As a consequence, very little or, in most cases, nothing is known about the load history for more than a few of the many existing turbines. Besides information about energy yield, operating hours and maintenance or repair activities, a turbine's performance and especially its dynamic behaviour is only known from prototype testing. This does not necessarily reflect the real conditions in the series at a particular site properly.

Nevertheless, some standard signals (like rotor speed, electrical power or pitch angle) which are commonly only used for turbine control, are available for these turbines. The objective of this work is to systematically investigate, whether the estimation of wind turbine fatigue loads based on these signals is feasible.

The research comprises the identification of the main drivers for wind turbine fatigue loads and tackles the question, whether these conditions are also reflected in standard wind turbine signals. Furthermore, possible techniques for the set-up of transfer functions to link standard signals and loads are investigated. Because of the many conditions which can potentially influence fatigue loads and the non-linear characteristics of wind turbines, a neural network based approach seems to be the most promising option, at least for loads encountered during normal power production.

Besides discussing the general outline of a load estimation system, different prediction schemes are developed from simulations of a typical 1.5 MW wind turbine. Loads and standard signals are generated using the industrial design tool Flex5. This allows to perform first test of methods for the prediction of equivalent load ranges and equivalent magnitudes from statistical parameters of standard signals. In addition, it is investigated if frequency domain methods can serve as the basis for the estimation of load cycle distributions. Because of the non-linear characteristics of wind turbines

and the non-stationary operational conditions it turns out that these methods can not be applied easily. Therefore, an empirical method which employs fitting of combined probability density distributions to measured loads is developed.

Test and refinement of the methods is performed with measured data. In a first step the developed schemes are validated on the basis of data recorded from measurements at the state-of-the-art 5 MW wind turbine Multibrid M5000. The transferability of the approach to another turbine type and the feasibility to derive accurate predictions from a reduced number of input data is emphasised by additional tests at one 2.5 MW Nordex N80 turbine. First results indicating the applicability of already established transfer functions for load predictions at turbines in a series are derived by utilising measurements from a second N80 turbine. Finally, recommendations for further research activities towards the employment of a load estimation system on an industrial scale are given.

Zusammenfassung

Im Allgemeinen werden die Belastungen, denen eine Windenergieanlage im Laufe ihres Betriebs ausgesetzt ist, nicht aufgezeichnet. Lastmessungen erfolgen häufig lediglich an Prototypenanlagen als Teil der Zertifizierung.

Insbesondere bei den leistungsstarken Anlagen der neuesten Generation ist eine Tendenz zum Einsatz zusätzlicher Hardware zur kontinuierlichen Lastmessung erkennbar. Zum Einen sinken die relativen Kosten für die erforderliche Messtechnik mit dem höheren Anlagenpreis, zum Anderen steigt der sich aus Einbeziehung der Lastinformation in die Anlagenregelung ergebende Nutzen mit der Anlagengröße. Es erscheint allerdings fraglich, ob eine kontinuierliche Lastüberwachung auf Basis konventioneller Messtechnik für die aktuell in großer Zahl installierten Anlagen mit Nennleistungen von 1 bis 3 MW wirtschaftlich sinnvoll ist.

Die Belastungshistorie von Windenergieanlagen ist daher meist unbekannt und oft werden für Serienanlagen routinemäßig nur Basisgrößen wie Ertrag oder Betriebsstunden sowie Informationen zu durchgeführten Wartungs- und Reparaturarbeiten aufgezeichnet. Das grundsätzliche Anlagenverhalten und die Auswirkungen standortabhängiger Umwelteinflüsse sind zwar von Prototypentests bekannt, diese lassen aber natürlich nur in begrenztem Maße Rückschlüsse auf die Belastungen von Serienanlagen an verschiedenen Standorten zu.

Für alle größeren Windenergieanlagen ist jedoch eine Reihe von Signalen verfügbar, die üblicherweise zur Regelung verwendet werden (z. B. Drehzahl, Blattwinkel oder Leistungsabgabe). Eine systematische Untersuchung der Möglichkeiten, diese Signale für eine kontinuierliche Lastüberwachung zu nutzen, ist das Ziel dieser Arbeit.

Dies beinhaltet Untersuchungen zum Einfluss verschiedener Anlagen- und Standorteigenschaften auf Ermüdungslasten aber auch auf die standardmäßig gemessenen Signale. Verschiedene Techniken, um von Standardsignalen auf Lasten zu schließen, werden getestet und bewertet. Wegen der vielen potenziellen Einflussgrößen und des nichtlinearen, betriebszustandsabhängigen Anlagenverhaltens erscheinen insbesondere Transferfunktionen aus neuronalen Netzen vielversprechend, zumindest für Lastprognosen während des normalen Produktionsbetriebs.

Auf Basis dieses Ansatzes wird auch der grundlegende Aufbau eines Systems zur

Lastprognose mittels Standardsignalen erörtert. Konkrete Verfahren zur Schätzung von equivalenten Lasten und von Lastkollektiven werden anhand von Simulationsergebnissen entwickelt. Hierzu werden das in der Industrie häufig eingesetzte Simulationsprogramm Flex5 sowie das Modell einer typischen Windenergieanlage mit einer Nennleistung von 1.5 MW verwendet.

Während die equivalenten Lasten direkt aus statistischen Parametern der Standardsignale geschätzt werden können, ist die Prognose von Lastkollektiven aufwendiger. Obwohl sich Verfahren zur Ermittlung von Lastkollektiven im Frequenzbereich auf den ersten Blick als Grundlage der Prognose anbieten, zeigen nähere Untersuchungen prinzipielle Grenzen für deren Einsatz auf. Daher wurde stattdessen ein Verfahren, basierend auf empirischen, angenäherten Wahrscheinlichkeitsdichteverteilungen, entwickelt.

Weitere Tests der Lastprognoseverfahren erfolgen mit an realen Windenergieanlagen gemessenen Daten. Die grundlegende Praxistauglichkeit wird anhand von Messungen am Prototypen der Multibrid M5000, einer Windenergieanlage mit einer Nennleistung von 5 MW, überprüft. Zusätzliche Schätzungen anhand von Daten der 2.5 MW Anlage Nordex N80 demonstrieren die generelle Eignung des Verfahrens zur Lastüberwachung für drehzahlvariable, pitchgeregelte Anlagentypen. Weiterhin werden erste Ergebnisse von Lastschätzungen für eine zweite N80 Anlage auf Basis der an der ersten Anlage entwickelten Transferfunktionen diskutiert. Die Arbeit schließt mit Empfehlungen zu erforderlichen Folgearbeiten im Bereich der Lastprognose auf Basis von Standardsignalen. Diese sind Voraussetzung für die mögliche Nutzung eines solchen Systems im industriellen Maßstab.

1 Introduction

1.1 Problem and motivation

During the past decades, great efforts have been undertaken to make wind power a viable and competitive source of electricity. This was remarkably successful: At the end of 2008 a capacity of more than 120 GW of wind power was installed worldwide and forecasts predict more than 30 GW of newly installed capacity in 2009. Although the vast majority of turbines is currently installed in Europe, Asia and North America, wind turbines contribute to the power supply of any continent. Even on Antarctica they are employed to provide electrical energy for research stations.

Obviously, today's turbines operate under many different environmental conditions, ranging from extremely cold to very hot climates and from rather flat sites with low turbulence to complex terrain with quite gusty inflow. Unfortunately it is often not known how the individual turbine copes with these conditions and performs at its site. Of course, basic parameters like energy yield, capacity factor and availability are analysed on a regular basis by the operators, but as long as no obvious irregularities are noticed that is often about it. Severe problems and overloads remain hidden until they result in component failures.

Maybe this is a slightly exaggerated image of reality and sometimes the situation is not that bad. Nevertheless, as a matter of fact the loading history of most turbines is unknown. Load measurements are usually only performed for prototype testing and hence very few turbines undergo this procedure. Furthermore, these measurements are carried out for limited periods of time. They are stopped if a sufficient amount of data has been recorded which can frequently be accomplished within half a year. In addition, the chosen test sites often feature benign climatic conditions. Clearly the measured loads and the experienced dynamic behaviour of those prototypes do not necessarily reflect the conditions in the series at a particular site properly.

Other uncertainties are related to the design process of wind turbines. Typically, design loads are derived on the basis of environmental conditions defined in standards. The real site conditions are of course likely to be different. Therefore a site assessment is carried out before a turbine is installed. This approach has lead to the belief that all

turbines are in fact overdesigned, because the assessment ensures that the expected loads at a site are always lower than the design loads. However, there is currently no way to verify this assumption (at reasonable costs). In addition, excessive loads may not only be traced back to wrongly analysed site conditions but also to unforeseen turbine behaviour. A higher number of emergency stops than expected or longer downtimes with engaged mechanical brake are typical examples.

Information on the loading of wind turbines is certainly valuable knowledge and can help to reduce the cost of wind energy. This holds true, no matter whether the monitored loads are below or above those assumed for design. When lower loads are observed, a turbine's operational life could simply be extended beyond the design life. If it seems that the loads are exceeding the design loads, it might be thinkable to adjust the turbine operation to still yield the lowest cost of energy in this particular situation. In any case, the load information will lead to a better understanding of the impact of site and operational conditions on wind turbines. The gained experiences can form the basis for an improved adaptation of turbines to those influences as well as for further optimisations with respect to site selection and wind farm planning.

As stated above, today's turbines in general do not monitor the loading to which they are subjected. The main reasons are the high costs for measurement equipment and the considerable maintenance efforts. In addition, the expected lifetime of a turbine exceeds the lifetime of standard measurement devices (e.g. strain gauges) by far and a replacement would be required occasionally. A shift towards increased use of load measurement devices for the coming generation of multi-megawatt turbines is obvious, as the relative costs for measurement devices (compared to turbine costs) go down and the benefit from feeding load signals into the turbine control increases. However, it is hard to imagine that this will be the case for the turbines which are built in large numbers today.

The majority of today's large turbines feature variable speed and pitch control. For this turbine type, measurement of several signals (denoted as *standard signals* in this work) is required for control purposes. This comprises for example the generator rotational speed, generator rotational acceleration, electrical power output and pitch angle. Similar to loads, standard signals are of course also influenced by changing environmental conditions. To illustrated this, Figure 1.1 displays the rotor thrust and torque along with the generator rotational speed and acceleration. A correlation of distinctive features of these signals with time is clearly visible. From a look at this figure, the idea to also employ standard signals for load estimations suggests itself. The investigation of possible approaches and the general feasibility of this conception for wind turbines

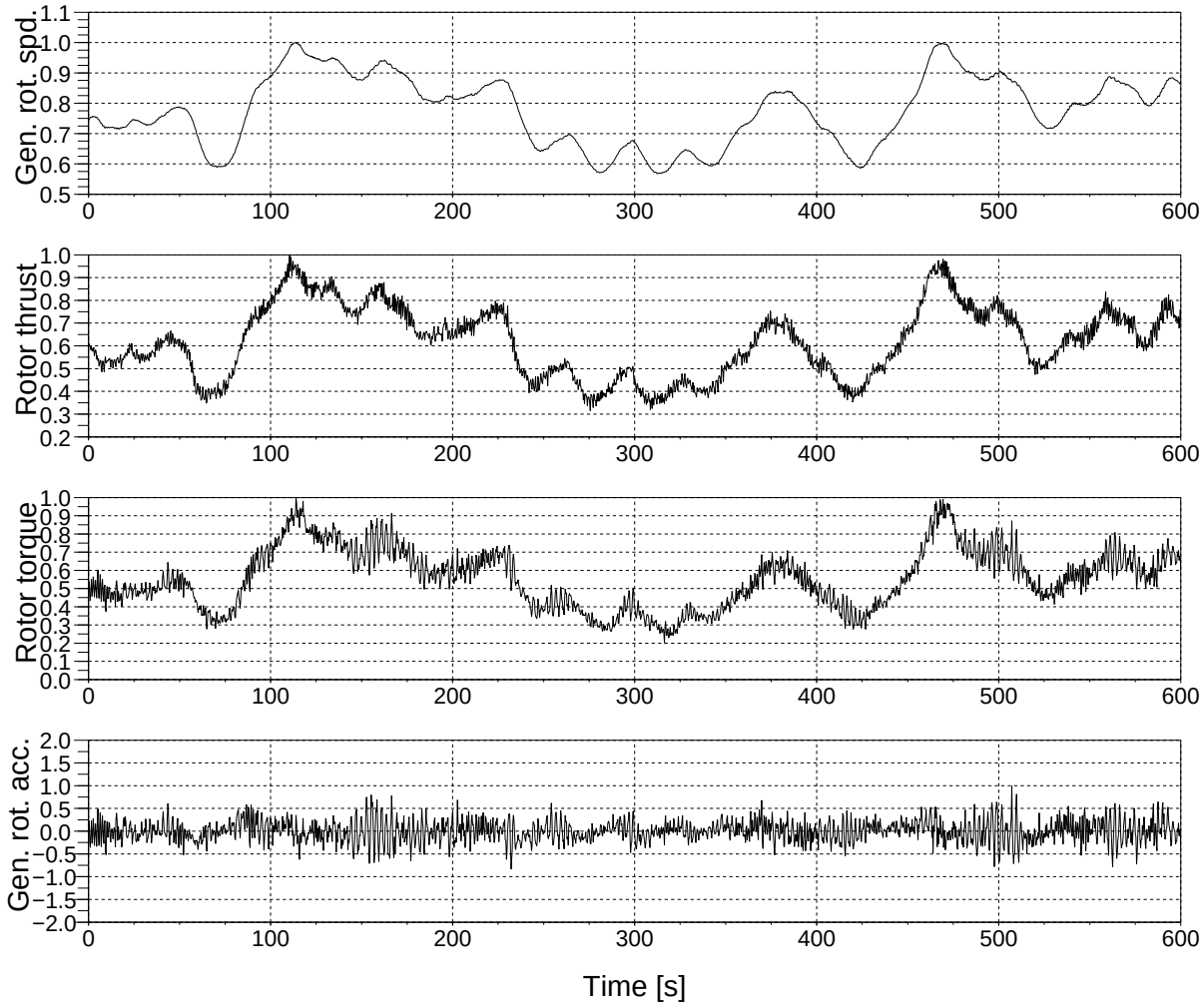

Figure 1.1: Time series of rotor thrust, rotor torque, generator rotational speed and generator rotational acceleration. Often load and standard signals show a correlation of distinctive characteristics.

is the objective of this work.

1.2 Scope and current status

According to the author's best knowledge, fatigue load monitoring with standard signals is currently not performed on an industrial scale in wind energy. However, there are several examples from other industries, where available signals are used to predict the loading of components.

Experience on the prediction of loads from other signals has been gathered especially in aircraft engineering. Several applications can be found in literature mainly in the military sector. Polanco [1] reviews approaches from different authors developed in the 1990's, where flight parameters from helicopters are used to predict component

loads. The cited publications are categorised with respect to the underlying estimation approach such as flight condition recognition, regression models, neural networks and combinations of regression models and neural networks.

In other applications, additional sensors are installed to allow for load predictions. The estimation of the structural loads of an aircraft wing from optical deflection measurements has been investigated by Lizotte and Lokos [2]. Based on laboratory experiments a multiple linear regression model was developed which links deflection and loading. In a test on a real aircraft, accurate estimates of a wing's bending moments were derived.

There are also applications on a larger scale. Azzam et al. [3] describe a fleet and usage management system which has been developed for the UK Ministry of Defence. One part of this system is 'load monitoring and damage detection' and standard flight parameters are employed for this purpose. Similar fleet management techniques are also investigated by the Royal Netherlands Air Force and the National Aerospace Laboratory in the Netherlands [4]. In both cases, prediction results are also used for condition monitoring.

The equivalent to flight parameters of airplanes and helicopters in aircraft engineering are standard signals in wind energy. If the approaches from the aircraft industry are transferable to wind energy, cheap and effective load and condition monitoring can potentially be achieved. In this case the benefits from measuring standard signals which are currently only employed for control purposes are greatly increased, as illustrated in Figure 1.2.

Examples outside the aircraft industry exist as well. A simple one is the estimation of drive torque from motor currents which is frequently done in many applications. In offshore engineering, Lopes [5] proposed to measure jacket displacements. A fatigue damage evaluation was then accomplished on the basis of trained neural networks and allowed monitoring the condition of offshore structures.

It seems that only three investigations related to load estimations from already measured signals have been published in the field of wind energy. Two of them were carried out in parallel to this work: In 2005, Dittmar et al. [6] employed neural networks to predict rainflow cycle distributions of blade root bending moments from rotational speed, electrical power and pitch angle. Their approach, which was tested on simulated and measured data with good success, aimed to directly estimate the numbers of load cycles for fixed ranges. It thereby differs to the method developed in this work, where continuous distributions are employed for this purpose. This reduces the required number of estimations significantly.

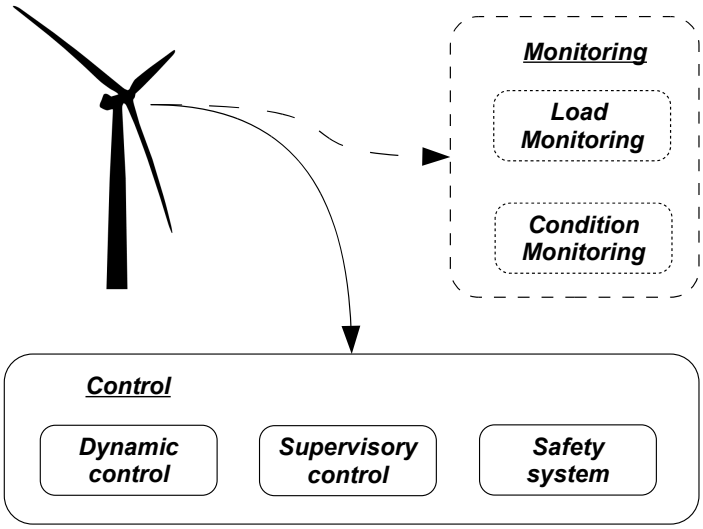

Figure 1.2: Currently standard signals are mainly used for wind turbine control, although they can in general also be employed for monitoring purposes. This research focuses on fatigue load monitoring aspects. However, a condition monitoring is possible as well [9].

In 2009, Obdam et al. [7] described first results derived for their Flight Leader project. This research does not solely rely on standard signals for load predictions. Instead the idea is to also equip one or two turbines in large farms with load measurement devices. The measured loads as well as standard signals are than used to estimate equivalent loads on all remaining turbines.

Hohlen [8] employed a neuro-fuzzy state observer in 2002 to estimate high resolution time series of blade root bending moments from a combination of standard signals, tower bending moments and wind speed data recorded at a separate met mast. One of the main ojectives of the research was to investigate whether the neuro-fuzzy approach can enable a detailed blade load monitoring without the relatively high costs for measurements in a rotating system. Generally, neuro-fuzzy methods offer more insight into an established transfer function compared to pure neural networks, at least if not too many inputs are employed. In his work Hohlen observed a strong deterioration of the transfer function's transparency already if the load estimation required more than four input signals. He also concluded that periodic variations of the blade root bending moments related to the rotation of the rotor can not be estimated well from the available input signals without adding synthetically generated sinusoidal signals.

Even though it is not related to loads, a work by Wiggelinkhuizen et al. [9] should also be mentioned. Besides comparing several common approaches, which require the installation of additional hardware, they also tested the suitability of standard signals derived by SCADA systems for condition monitoring. The results seem to be promising and are an example for the condition monitoring application shown in Figure 1.2.

Although, two publications outside this research already indicate the potential feasibility of fatigue load estimations with standard signals for wind turbines, a systematic investigation is still missing. This work is intended to be a first step to close this gap.

1.3 Methodology and organisation

The work utilises data from wind turbine simulations and measurements. In general, all investigated methods are first tested with simulations and are then validated on the basis of measured data in a preceding step. The industrial design tool Flex5 (Annex A) and the model of a typical 1.5 MW wind turbine (Annex B) are employed for the simulations. Measured data was taken from campaigns carried out at two Nordex N80 turbines and at the prototype of the Multibrid M5000.

Some general concepts on fatigue loads of wind turbines are described in Chapter 2. Based on these considerations, several implications and requirements as well as a number of potential benefits from a load monitoring system are pointed out.

The influence of site and turbine conditions on equivalent loads and statistical parameters of standard signals is investigated in Chapter 3 on the basis of simulations. This includes an evaluation of likely variations of the disturbances. Whenever possible the simulation results are cross-checked with those derived by other authors from a literature review. It is the purpose of this chapter to identify important conditions in terms of fatigue loads and to see if they could potentially be detected from standard signals. At the end, consequences for a load estimation system are summarised.

Chapter 4 evaluates four different methods to relate standard signals and loads, taking the characteristics of wind turbines into account. These are regression techniques, neural networks, physics-based models and state estimation. A complete load estimation system is outlined in Chapter 5, based on neural network transfer functions.

Results from simulations are used in Chapter 6 to establish approaches for the estimation of equivalent loads and fatigue load distributions. In Chapter 7 the developed methods are tested further with measured wind turbine data. The methods are employed first on data from the Multibrid M5000 to evaluate their general suitability while the transferability to other turbines is investigated with data of the Nordex N80 turbines. in a second step. Chapter 8 concludes the work with summary and outlook.

2 Fatigue loads of wind turbines

In this chapter fatigue of wind turbines is discussed purely from a loading perspective. Subjects like stress concentration, crack propagation or fracture mechanics which usually cross one's mind on the word 'fatigue' are not covered[1]. As a consequence, the term 'loading' is also used solely with respect to internal forces and moments acting at certain points of the turbine structure and not for example in the sense of stresses.

It is the overall scope of this chapter to provide a short overview on fatigue loads and how they are currently derived for the design of wind turbines. This offers the opportunity to establish several ideas and definitions which are important basics for the following chapters. Furthermore, a review of the current fatigue load practice allows to draw some conclusions regarding the potential benefits from a load monitoring system and the requirements which such a system has to fulfil.

2.1 Fatigue loads for design

In general, fatigue loads are very important for the design of wind turbines. The dimensioning of practically all major components is at least partially driven by fatigue. Because

- the operational state of a turbine varies constantly due to the ever changing environmental conditions
- turbines usually feature slender structures with low eigenfrequencies which can easily be excited by gusts or even by the operation itself
- they are often designed to endure 20 years of operation or even more, where they produce power for 80 to 90 % of the time

wind turbines have to withstand many load cycles during their design life. Load cycle numbers between 10^8 to 10^9 are frequently the rule rather than the exception.

[1] Compare a report by Sutherland [10] for a comprehensive summary on these subjects with a focus on wind turbines and including some best practice methods.

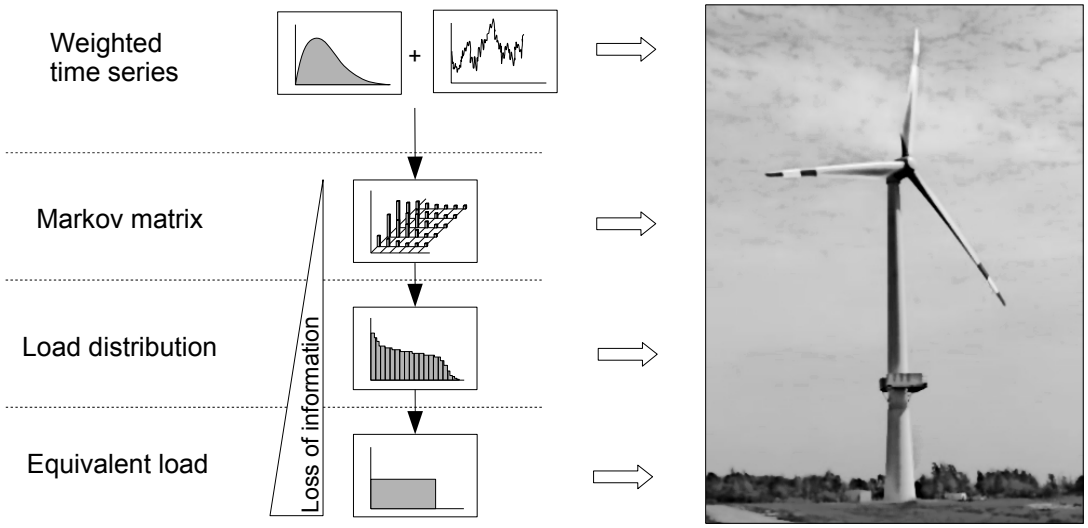

Figure 2.1: Fatigue load formats used for the design of wind turbines

Fatigue loads can be represented in different formats. The most basic one is to describe the variation of a load signal over time as a load time series. Having the time as reference allows to combine the time series of several load components (for example forces and moments). The combined load information can then be used together with a detailed structural model to derive realistic multiaxial stress time series which in turn enables a sophisticated analysis of a structure's fatigue damage.

However, this detailed approach for fatigue analysis of structures is usually quite demanding and time-consuming. Therefore, structural designers sometimes follow simplified methods. These methods do not employ time series, but condensed load formats, some of which are displayed in Figure 2.1. All of them are based on time series, because this format is the only one which contains the complete information on the load history. The time series are processed further and also often weighted to incorporate the occurrence probability of certain turbine states into the condensed formats.

In general, the processed formats suffer from a loss of information which increases with the degree of condensation. Losing load information is of course always undesirable and may potentially lead to faulty designs. It is common practice to counteract those uncertainties by more conservative design strategies. Therefore, the additional costs of overdimensioned structures have to be taken into account when the decision for or against a design approach (and consequently a load format) is made. Considering the constantly high cost pressure on wind turbines in their competition with other sources of electrical energy and also the competition among the various wind turbine manufacturers itself, this is certainly one of the reasons why a trend towards time series based fatigue design (at least for major turbine components) is obvious in recent years.

Because the investigations in the following chapters often refer to load distributions and equivalent loads, some aspects of these formats are discussed below.

Load distributions

Two types of load distributions are mainly used for wind turbine design: rainflow cycle and magnitude distributions. The rainflow cycle distributions (often simply called cycle distributions or rainflow spectra) represent the occurrence probability of load cycles with different ranges. They are usually derived from time series by means of rainflow counting procedures [11]. As an alternative, probability distributions of load cycles can also be calculated in the frequency domain (see Chapter 6). Because of the often non-linear behaviour of wind turbines over their operational range, time domain methods are however much more common than frequency domain approaches.

Knowing the occurrence probabilities of load ranges is a fundamental requirement for fatigue design. Although load cycle distributions are frequently used for their description, these distributions do not contain any information on the mean values around which the load varies. Hence, structural designers have to estimate reasonable means by taking the probability of relevant turbine states into account.

Load magnitude distributions (also denoted as load duration distributions) state how long a certain load level persists. This is an important piece of information especially for gearbox and bearing design [12, 11]. Magnitude distributions do not allow to conclude on the sequence of loads and thus do not indicate the general variation of loads within a given period of time.

As an example, a typical load cycle distribution of the in-plane blade root bending moment and the load magnitude distribution of the rotor torque are shown in Figure 2.2. The distributions have been derived for a 20 year lifetime and only time periods where the turbine is in power production mode have been considered. In both cases, the cumulated distributions are plotted and the abscissa of the cumulated rainflow cycles is given on a logarithmic scale. This is also the most common representation.

These plots can be interpreted and offer the possibility to conclude on some turbine characteristics. The deterministic load cycles due to the static moment of the blade are clearly visible for example. Larger cycles are caused by the influence of aerodynamic forces acting along the blade or by structural dynamics. On average, approximately once per day a load cycle more than two times larger than those caused by the self weight of the blade can be observed.

The cumulated load magnitude distribution of the rotor torque reveals that the turbine operates about 5 years (45000 hours) out of 20 years at rated power. In addition, some

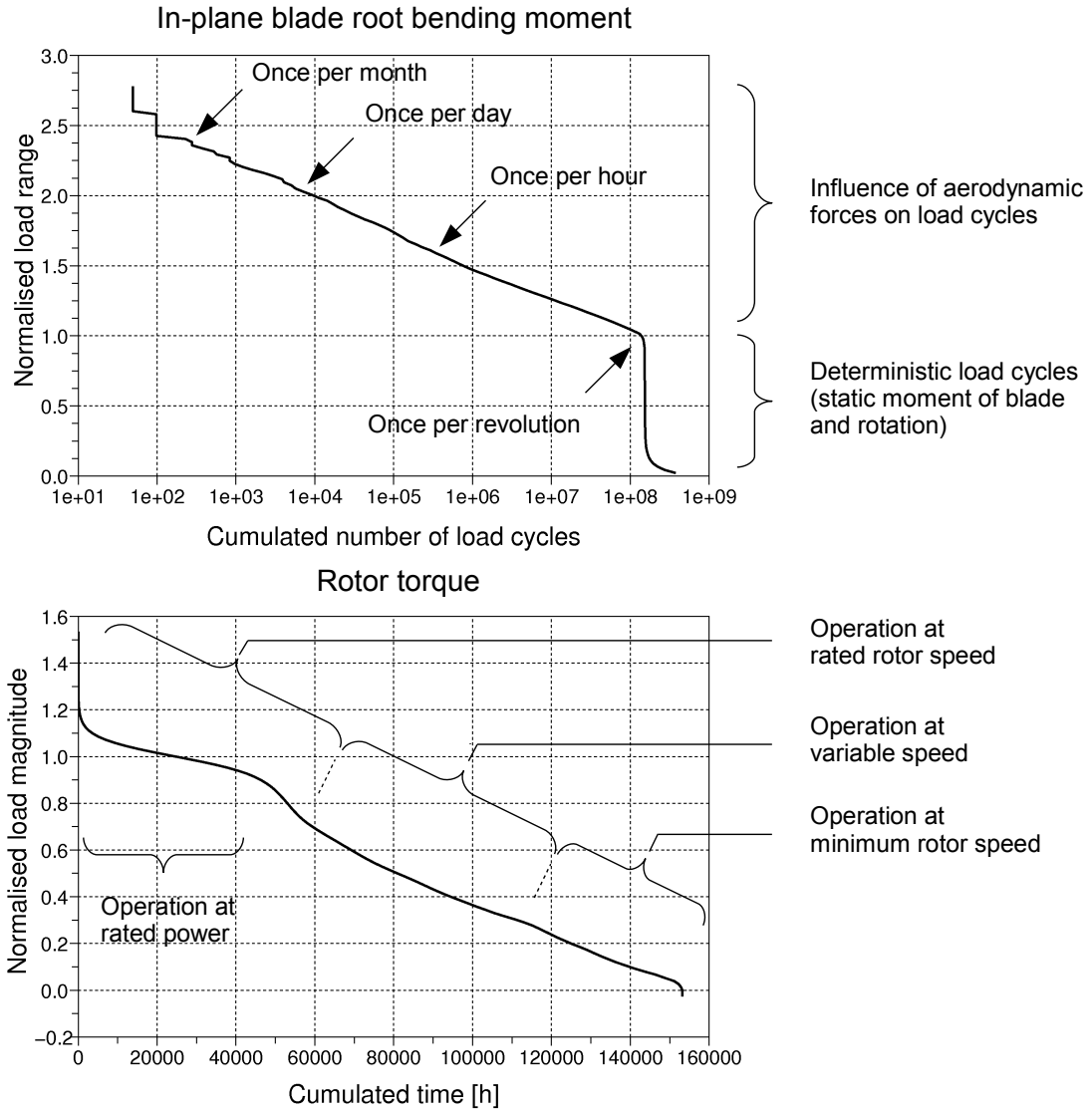

Figure 2.2: Load cycle distribution of the in-plane blade root bending moment (ranges divided by twice the static moment of the blade) and magnitude distribution of the rotor torque (magnitues divided by rated torque). Both distributions also allow to conclude on some turbine characteristics.

kinks in the curve at torque levels below rated torque can also be observed. They allow to conclude on the periods of time where the turbine operates at rated speed, variable speed and minimum speed.

Equivalent loads

Contrary to the multi-stage load distributions discussed above, equivalent loads are condensed further to a single load range (or magnitude). The idea for the reduction of more complicated load distributions to a single value is based on some rather old but fundamental concepts in the field of fatigue [13]. Starting with the first experiments by

Wöhler in the second half of the nineteenth century, it became common to assume an exponential relation between the number of stress cycles with a certain amplitude and the failure of a tested specimen. Furthermore, a linear damage accumulation hypothesis (known as Palmgren-Miner rule) was established in the middle of the last century which allows to calculate a theoretical damage for a specimen under the presence of load cycles with different ranges.

The schematic sketch in Figure 2.3 illustrates the idea of equivalent loads. Because the SN-curve (or Wöhler-curve) is approximately a straight line with the slope $1/m$ when plotted on a double logarithmic scale (with m as a material constant[2]), the damage caused by N load cycles with a range of ΔS will in theory be equal to the damage caused by N_{ref} cycles with a range of

$$\Delta S_{eq,Nref,m} = \sqrt[m]{\frac{\Delta S^m \cdot N}{N_{ref}}} \tag{2.1}$$

If in addition a linear accumulation of damage is assumed, n load ranges with different cycle numbers N_i can be combined to a single equivalent load range which, with the reference cycle number N_{ref}, gives the same damage:

$$\Delta S_{eq,Nref,m} = \sqrt[m]{\frac{\sum_{i=1}^{n} \Delta S_i^m \cdot N_i}{N_{ref}}} \tag{2.2}$$

Once computed, equivalent load ranges can be transferred to other reference cycle numbers with

$$\Delta S_{eq,Nref2,m} = \Delta S_{eq,Nref1,m} \sqrt[m]{\frac{N_{ref1}}{N_{ref2}}} \tag{2.3}$$

Furthermore, k equivalent load ranges can be combined, if derived for the same reference cycle number and exponent:

$$\Delta S_{eq,Nref,m} = \sqrt[m]{\sum_{i=1}^{k} (w_i \cdot \Delta S_{eq,Nref,m,i}^m)} \tag{2.4}$$

where the factor w_i can be used for an individual weighting of the k equivalent loads.

It is obvious, that the above definition of equivalent load ranges is a great simplification of fatigue concepts and that the theoretical damage caused by multi-stage cycle distributions and the corresponding equivalent loads can in fact differ. The main rea-

[2] Typical values for the exponent m range from around 4 for welded steel structures up to 14 for carbon fibre reinforced plastics [12].

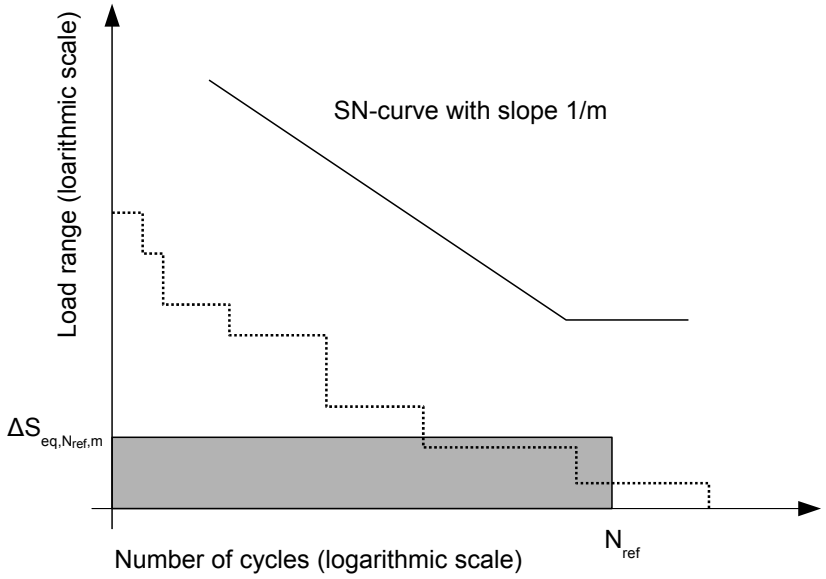

Figure 2.3: Schematic illustration of the idea of equivalent loads: Under certain assumptions, an equivalent load will give the same damage as the corresponding load cycle distribution.

son for deviations is the representation of the SN-curve as a straight line for all cycle numbers. This ignores elastic-plastic deformations for very large load ranges where the linear relationship between range and cycles to failure is not valid. Furthermore, the slope of the SN-curves of certain materials (for example steel) changes significantly when the number of load cycles increases above the so-called endurance limit, something which is also not captured in the above formula.

Equivalent load ranges derived according to Equation 2.2 do not include the influence of a cycle's mean value. At least in some cases the utilisation of equivalent load ranges for fatigue design is therefore debatable. Their usefulness for the comparison of different load cycle distributions is however beyond question - because the ranges are weighted exponentially, different exponents emphasise different regions of the cycle distributions. Equivalent loads which have been derived with large exponents are strongly influenced by the few but very large ranges in a distribution. Contrary to that, equivalent load ranges with small exponents are more sensitive to differences in the small ranges which are commonly present in large numbers. Thus, comparing equivalent loads with different exponents is an easy way to evaluate load distributions.

Similar to the definition of equivalent load ranges, equivalent load magnitudes can be derived from a n-stage magnitude distribution with

$$L_{eq,Tref,p} = \sqrt[p]{\frac{\sum_{i=1}^{n} L_i^p \cdot T_i}{T_{ref}}} \tag{2.5}$$

where T_i is the time share of each load magnitude, T_{ref} is a reference time and p is the exponent for weighting different areas of the distribution. Again, several equivalent magnitudes can be combined to a single value:

$$L_{eq,Tref,p} = \sqrt[p]{\sum_{i=1}^{k}(w_i \cdot L_{eq,Tref,p,i})^p} \tag{2.6}$$

Although in this work the equivalent magnitudes are used simply as load indicators or for comparison of load distributions, they are often also employed for component design. One example is the calculation of equivalent magnitudes for radial and axial loads of bearings inside a gearbox [14].

Influence of occurrence probability on equivalent loads

It is obvious that the occurrence probability of operational states plays an important role in the calculation of fatigue loads. General analysis of its influence on loads is difficult, since it is site dependent of course. Because it has some implications on the functional requirements of a load estimation system, the potential effects are nevertheless discussed briefly in the following in a simple example.

The left hand side of Figure 2.4 shows equivalent load ranges of the out-of-plane blade root bending moment over wind speed. As shown in this example, small equivalent loads can typically be expected at low wind speeds with increasing ranges at higher wind speeds. In the same plot, three possible occurrence probabilities of wind speeds are shown which result in average annual wind speeds of 6, 7 and 8 m/s respectively. Very often Weibull distributions are employed for the approximation of occurrence probability, as in the case here.

On the right hand side, the equivalent loads are weighted according to the time shares calculated from the different Weibull distributions. It is important to note the effect of the exponent m on the weighting: Although they are weighted with large time shares, the equivalent loads at low wind speeds give relatively low equivalent load ranges. Contrary to that, the large equivalent loads at high wind speeds are weighted with almost negligible shares only. Nevertheless, they yield considerable ranges in the right plot. For high wind speeds in particular, rather small variations in time shares can have a substantial impact on fatigue loads.

Significant differences in the weighted overall loads (using Equation 2.4) are computed as well which can mostly be attributed to the different time shares at high wind speeds. The overall equivalent out-of-plane blade root bending moment for an average annual wind speed of 6 m/s is only about 75 % of what is calculated for 8 m/s.

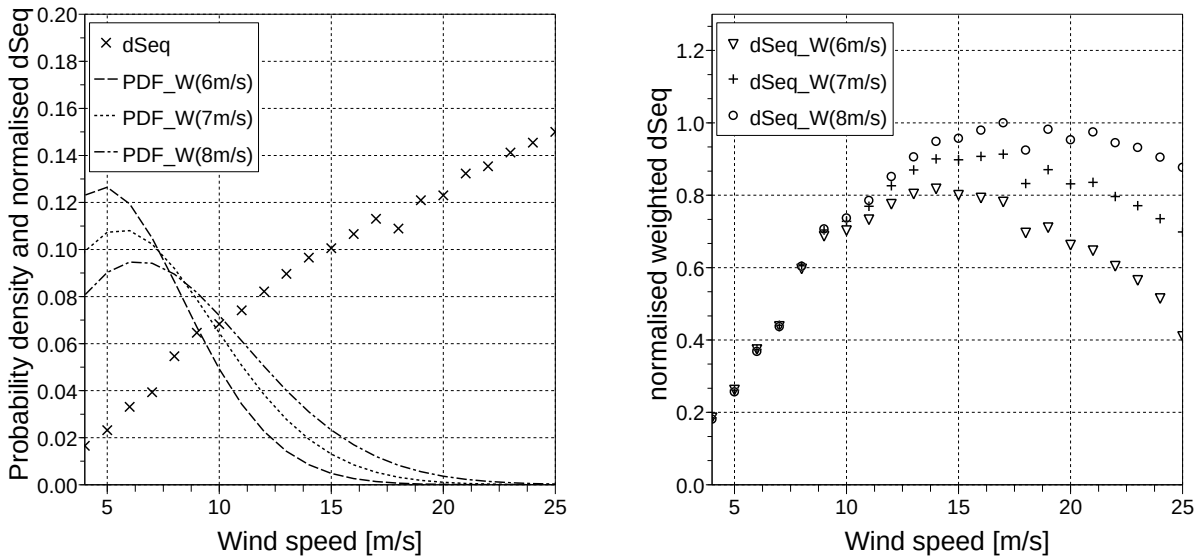

Figure 2.4: Influence of weighting on equivalent loads: Normalised equivalent load ranges of the out-of-plane blade root bending moment (m=9) without weights are shown on the left hand side together with three Weibull probability density functions (average wind speeds of 6, 7 and 8 m/s; shape factor of 2 in all cases). The Weibull weighted equivalent loads are plotted on the right hand side.

Fatigue loads and component damage

At the end of this section, some remarks regarding the relation between fatigue loads and damage are required to put the discussion into a broader context. Because of the assumed exponential relation between load ranges and failure, a small variation in ranges can have a significant influence on fatigue damage. For an exponent of 4 an increase of load ranges by 5 % will for example lead to approximately 20 % higher damage. If an exponent of 10 applies, the increase in damage is much stronger and computes to about 60 %. Thus, in theory fatigue loads have to be calculated with a very high accuracy in order to allow for a reasonable estimation of component damage and lifetime respectively.

But even if the exact fatigue loads would be known, damage and failure can only be assessed in a probabilistic manner. This is because the progress of damage depends not only on the applied load, but also on the component itself. Among the most important influences which can lead to significant variations in fatigue resistance are material quality, tolerances in component geometry as well as surface finish and treatment. In total, these uncertainties lead to a large scatter in the lifetime of specimen which may deviate from the nominal values by factors between 0.3 to 3 [15]. This implies that the lifetime prediction of an individual component on the basis of loads is at least difficult, if not to say impossible. Even if the fatigue loads are exactly known and constant quality and treatment of components is ensured, large prediction errors can still be expected.

These considerations emphasise, that in general a lot of uncertainty is involved in fatigue design. This holds true for both loads and component resistance. As a consequence, quite large safety factors are commonly used in fatigue design. The factors are already partly incorporated into the SN-curves and are partly applied to decrease the characteristic fatigue resistance of a component to a lower design value (usually there are no safety factors on loads). The factors on resistance depend on the material used and also of course on the application, including consequence of failure [16].

2.2 Calculation of fatigue loads

Besides being used for wind turbine design, fatigue loads are also calculated to evaluate the suitability of potential sites for the installation of wind turbines. This shall ensure, that the expected turbine loads for a proposed application are always lower or equal to the design loads. Sometimes this is already obvious from a comparison of environmental conditions at the site of interest to the design conditions and additional calculations can be omitted. But frequently the evaluation requires detailed simulations.

The general steps for the calculation of fatigue loads are displayed in Figure 2.5[3]. If carried out for site evaluations, a reasonable description of the *long-term average site conditions* has to be derived first. This step does not only include the analysis of wind characteristics, but also the assessment of soil and grid conditions for example. Compared to design load calculations, where the site properties are simply taken from standards, the evaluation of real site conditions introduces additional uncertainties into the site specific load assessment.

Of course, the *supervisory control and the safety system* characteristics play an important role as well. These functions determine when and how the turbine changes from one mode of operation to another. To get the complete picture in terms of loads, all relevant states have to be included into the fatigue assessment. In combination with the results from the site analysis, the occurrence probability of those different turbine states can be estimated: At a site which features low wind speeds in general, only very few turbine shut-downs due to high wind speeds and subsequent re-starts will occur, simply because the probability of high wind speeds is low. Similar, in most European countries grid failures are rare events whereas in regions with weak grids the number of stops due to grid problems is usually much higher. Often, experiences with turbines at similar sites can give valuable hints on the occurrence probability of such transients.

[3] Wind turbine loads are commonly derived from time domain simulations. Frequently they show a non-Gaussian, non-stationary behaviour and include deterministic components (compare Figure 6.1). This makes it sometimes difficult to apply frequency domain approaches for their calculation.

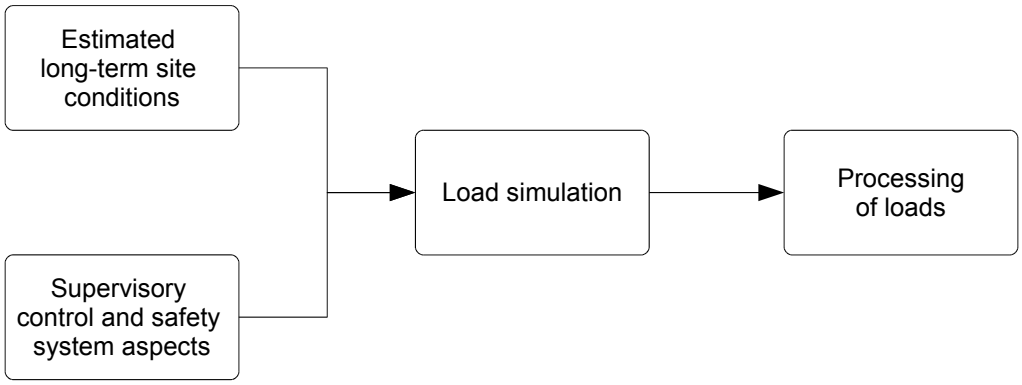

Figure 2.5: Scheme for the calculation of fatigue loads

The *simulation of wind turbines* requires considerable modelling capabilities in different fields. This involves the structural dynamics of the turbine, but also modelling of wind, aerodynamics, turbine control (including actuators) and the mechanical-electrical energy conversion system. Basic modelling strategies can be found in any of the many textbooks on this subject [17, 18, 19, 20]. Commonly only relatively simple modelling approaches are employed in each of the above mentioned areas. Nevertheless, when combined into one model they can make the simulation of wind turbines a complex matter.

Significant efforts are still undertaken to improve the simulation of wind turbines further [21, 22, 23, 24]. However, according to the author's own experiences from research projects related to the structural modelling of wind turbines [25, 26], the designer's enthusiasm for more accurate simulations is sometimes damped by realising the increased computational costs. Design load calculations can easily add up to several thousand single simulations. Because the design of wind turbines is an iterative process, these simulations are usually performed more than once. While transients often take place in less than a minute of real time, power production simulations are usually carried out for 10 minute time periods[4]. In total, the calculation of design loads (at least in the final step of the iteration) easily involves the simulation of about 250 hours of real time or even more. Despite the constantly decreasing costs of computing power, this obviously requires to compromise strongly on the complexity of the applied simulation models in practice.

As a consequence, relatively simple and computational cheap approaches are still

[4] The later is based on the assumption of a gap in the frequency spectrum of wind speed at time periods of around one hour which divides short-term and long-term fluctuations (see for example [27]). This assumption saves the designer from modelling wind speed fluctuations with extremely low frequencies. As a consequence, load cycles originating from such low frequency wind speed variations are commonly neglected which results in non-conservative fatigue loads. Veldkamp [28] found that the increase of equivalent loads due to low cycle fatigue is usually less than 5 %.

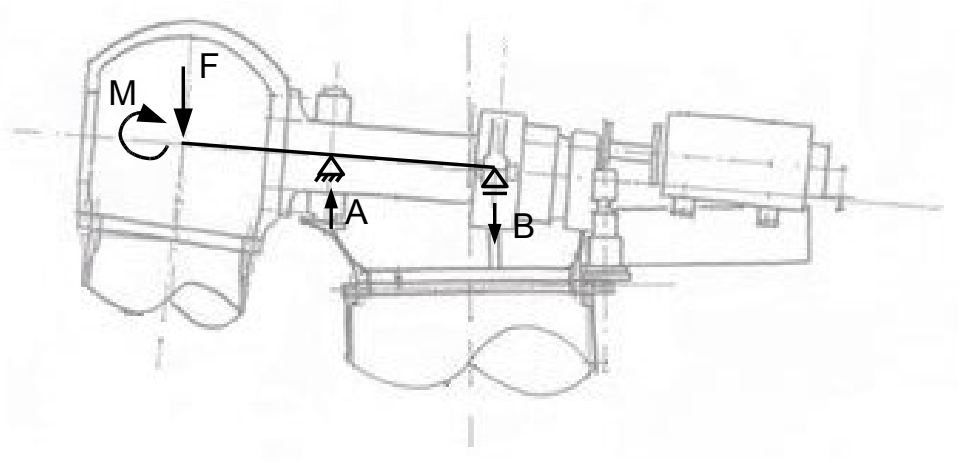

Figure 2.6: Example of a simple static system which can be used to derive bearing loads from forces and moments in the hub centre. Background drawing by Markus Becker (Kenersys GmbH).

very popular today which also includes the representation of the structural dynamics. The employed coarse, primary models are often only capable to compute the internal loads at certain characteristic locations of the structure (for example hub centre or tower base) or at some predefined cross-sections of blades and tower. For detailed fatigue design, further *processing of loads* is required. This step involves utilisation of detailed component models. If these models do not have a direct connection to the primary model, the derived loads have to be transferred first. Simple static models are frequently used for this purpose [11]. One example of a static system which can be employed to transfer loads in the hub centre to the supporting points of the drive train is shown in Figure 2.6. In other cases, the component model may have a direct interface to the primary model already and the calculated loads can be applied directly [29].

A detailed analysis of uncertainties related to simplifications in modelling is beyond the scope of this thesis (Veldkamp [28] analysed some of them in his work on probabilistic fatigue design). Nevertheless, the discussed characteristics of fatigue loads and their calculation suggest some important consequences for a load monitoring system.

2.3 Load monitoring: implications, requirements and benefits

At the end of this chapter, several conclusion regarding the application of load monitoring systems can be drawn. Most of them are independent from the actually applied monitoring method and hold true regardless if load information is derived via estimations or direct measurements. Some *general implications* are that

- a prediction of individual component failure from load data is virtually impossible. There is simply too much scatter in failure statistics, because relatively small variations in material, geometry or loads can have large effects. Hence, load monitoring can not replace condition monitoring systems.
- it is not necessary to base the evaluation of fatigue loads on time series. Instead, condensed load formats, such as load distributions or equivalent loads can be used. For systems which are based on estimated loads, this potentially reduces the required number of predictions considerably.
- if equivalent loads are employed for the monitoring, at least two exponents (a small and a large one) should be used. The rational behind this is the different influence of large and small load ranges on the magnitude of the equivalent loads for different exponents.
- some operational conditions are more important than others. This relates to the encountered loading but also the occurrence probability of these conditions. Because of the logarithmic relation between failure and loading, the important conditions are not always obvious at the first glimpse (see previous discussion on the influence of occurrence probability on equivalent loads).
- load data of power production cases should preferably be collected on a 10 minute basis. This is the standard time period in wind engineering. Because the prediction of component failure is not possible, the potential benefits from a load monitoring system arise from a comparison of a turbine's fatigue load against the design loads or against the loads of another turbine. Capturing low cycle fatigue is not required for this purpose and hence the breakdown of monitored loads into longer time periods is not necessary.

In fact, for the comparison of loads against design loads the application of 10 minute time periods is more of a requirement than just a general implication. Other *requirements* are:

- All relevant site conditions and their impact on turbine loads have to be captured. While this is not at all a point of discussion for directly measured loads, it is probably the biggest challenge for a system which is based on load estimations. This involves the detection of important site conditions as well as to correlate them with the correct loading.
- Transient events like starts or stops have to be included. The turbine behaviour in these states is fundamentally different to the power production mode. In addition, these events usually take place in rather short periods of time. Thus, the

necessity for the adaptation of estimations schemes according to the operational state might arise and the applied estimation approach has to be flexible enough to allow for this.

- Reasonable assumptions regarding the important operational conditions have to be made to set-up a load estimation system. It is a desirable feature that the predictions for the most important operational conditions in terms of fatigue loads are also the ones with the highest accuracy. Unfortunately, the occurrence probability of conditions (which is an important piece of information to determine important conditions) is not known as a priori but differs between sites. Hence, assumptions are required. In the end, it might even prove beneficial to have different estimation systems for the same turbine type, for example one designed for low wind speed sites, another for high turbulent conditions and so forth.

If a load monitoring system meets the requirements above, the derived loads can be used basically in two ways: for the assessment of site specific fatigue loads with respect to the design loads and for the comparison of loads encountered by different turbines.

It is commonly assumed that all wind turbines are overdimensioned for their individual application. This assumption is based on the fact that appropriate site assessments prior to the installation of turbines are carried out. These shall ensure that the turbine loads are below the design loads. Thus a turbine will in theory never be erected at sites which feature more severe conditions than the turbine was intended for. However, a lot of uncertainty is involved in these site assessments. Furthermore, there is usually no way to verify the validity of the assessment especially with respect to site specific loads.

A simple example is the previously discussed occurrence probability of wind speeds at a site. For the vast majority of cases this probability is approximated by a Weibull distribution, but it is often not checked if this is a reasonable assumption (Jaramillo and Borja [30] have evaluated a site where this is certainly not the case). In addition, the method of fitting the distribution can have a significant influence [31]. In practice, these fits aim mainly to yield accurate estimations of the potential energy yield. For this purpose, wind speeds below and around rated are relatively important, but very large wind speeds play a minor role. Clearly this is not the case for loads and hence these fits might not represent the best approximations when it comes to load assessments.

In general, the *comparison of monitored loads against the design loads* allows to

- verify the results from site specific load assessments. Furthermore, the load information can also help to increase the accuracy of future assessments.

- adjust the operational life of a turbine according to the encountered fatigue loads. For example in benign climatic conditions turbines can be operated beyond the design lifetime (for example 20 years)[5].

  Appropriate monitoring strategies would be generally suited to extend the operation of wind turbines beyond the original design lifetime. Similar strategies are applied for conventional power plants. Here, their owners usually aim to operate old plants for as long as possible in order to maximise profits.

- modify the control of a turbine according to the encountered loads. An example is the reduction of power or rotational speed in case of high loading. An individual adjustment of control strategies can also minimise the cost of energy with respect to the site specific conditions. However, one must admit that this is a rather complex task which will require considerably more research efforts.

Usually design loads are only available to the manufacturers of wind turbines, but not for the owners or technical operators. Nevertheless, a comparison of loads encountered by different turbines (of the same type) can still yield valuable information:

- It allows to assess the operation of turbines in a farm according to their fatigue loads. Thereby inspection and maintenance cycles can be optimised. This helps to reduce operational cost and to increase safety at the same time.

- Sites can be compared with respect to energy yield and loads. Hence, favourable (and unfavourable) site characteristics can be identified and future planing of turbine installations can be improved.

- Often the farm layouts are purely driven by considerations regarding energy yield. An evaluation of loads at turbines inside wind farms can lead to enhanced layouts in future.

For sure, the potential benefits from load monitoring systems are promising. This holds true especially if such systems can be based purely on already existing hardware, like sensors and processing units. However, as stated in the requirements above, the greatest challenge for such a system is the detectability of all important disturbances from standard signals. Investigations related to these aspects are therefore carried out in the following chapter.

[5] Authorities usually issue the operational licence for the design lifetime only. For an extension it has to be shown that there is still some margin in fatigue loads left compared to the design loads. This is a hopeless undertaking without a load monitoring system.

3 Influence of disturbances on fatigue loads and standard signals

3.1 Outline of the analysis

Wind turbines operate in permanently changing environmental conditions. In addition, turbines of the same type have similar characteristics, but are not completely identical. Production tolerances, employment of components from different suppliers or site dependent influences give rise to some variation in the overall dynamic response and the loading of apparently identical wind turbines. Several of such aspects, which can in general be considered as *disturbances* to the ideal wind turbine behaviour, are investigated in this chapter more closely.

The purpose of the analysis is to answer the following questions:

1. How do disturbances influence the fatigue loading of wind turbines?
2. Is the presence of a disturbance also reflected in the available standard signals so that its impact on the fatigue loads can be estimated from these signals?
3. What are the subsequent implications for a load monitoring system which has to operate on the basis of standard signals only?

Knowledge of the answers to these questions is crucial to assess the feasibility of a load monitoring system based on standard signals. If a disturbance does not manifest itself in standard signals, its impact on turbine loads can obviously not be detected solely by analysis of these signals. This is not a problem, if the disturbance is of minor importance for the monitored load component, but the accuracy of the monitoring will decrease, if undetectable disturbances have a greater influence on the loading. This holds also true for cases where a disturbance alters a standard signal without changing the loading of the turbine. If the load estimation is based on this signal, a false prediction of fatigue loads will be the consequence.

In the following, the first two questions are discussed directly in the subsections related to the analysed disturbances. For each disturbance, the results are displayed

graphically in two tables using a colour and symbol code explained below. While the first table illustrates the relative impact of the disturbance on the fatigue loads (question 1), the second table shows the detectability of a disturbance from standard signals (question 2). At the end of this chapter the results are summarised at the implications for a load monitoring system are discussed (question 3).

It should be pointed out, that universally valid relations between disturbances, wind turbine loads and standard signals do not exist. Instead, they are of course turbine dependent and are for example likely to differ between turbines with different structural properties or control systems. A standard signal based load monitoring can therefore not be designed without taking the turbine characteristics into account. It is an extremely customised approach and, once designed, fits only to the type of turbine for which it was developed.

Investigated data

The investigations in this chapter are mainly based on wind turbine simulations using the aero-elastic code Flex5 (Annex A) and the NREL 1.5 MW wind turbine model (Annex B). They allow to draw some conclusions on the general feasibility of a standard signal based load monitoring system for turbines with similar properties. Whenever possible, it has also been tried to backup the simulation results by comparisons with findings reported in literature. However, publications on the loading of wind turbines with respect to environmental conditions are rare and those including standard signals even more so.

The operating range of a variable speed pitch-controlled turbine can be roughly classified into two areas, often denoted as ‘below rated’ and ‘above rated’ or ‘partial load’ and ‘full load’ operation. At low to medium wind speeds (partial load) the main objective of the turbine control is to maximise energy output. At high wind speeds (full load), the control tries to maintain rated rotor speed and rated power. Because the behaviour of the turbine is fundamentally different in these operational ranges (see for example the characteristic curves in Annex B), analyses at different wind speeds are required.

For the evaluation of the effect of 10 minute mean wind speed, the wind turbine fatigue loads and standard signals are calculated for all wind speeds within the operational range in steps of 1 m/s. This gives a general impression of their variability and yields baseline values for the subsequent investigations. All other disturbances are investigated at 6, 12 and 18 m/s only which corresponds to partial load operation, the transition region and full load operation.

Whenever turbulent wind fields are used for wind turbine simulations, there is always

Table 3.1: Configuration of baseline simulations

Disturbance	Baseline value
10 minute mean of wind speed	6.0, 12.0 and 18.0 m/s
Longitudinal turbulence intensity	15.0 %
Horizontal turbulence intensity	12 % (0.8 times the longitudinal)
Vertical turbulence intensity	7.5 % (0.5 times the longitudinal)
Integral length scale of turbulence	340 m
Spatial coherence decay factor	12
Roughness length	0.1 m
Vertical inclined flow	0 °
Yaw error (10 minute mean)	0 °
Air density	1.225 kg/m^3
Rotor mass imbalance	none
Rotor aerodynamic imbalance	none
Foundation stiffness	$5{\cdot}10^7$ kNm/rad

some scatter in the results, although the statistical wind field properties of all corresponding simulations are identical. This is due to the stochastic nature of the turbulent wind. In a study presented in [32], variations of the equivalent rotor thrust of about 10 % have been found for different 10 minute stochastic representations of the wind field. To average out such effects, six simulations with different realisations of turbulent wind fields have been performed at all wind speeds.

Obviously, the computed changes of loads and statistical parameters are always relative quantities. Besides the dependence on the variation of the disturbance, they also depend on the background noise. For example, a vertical wind shear might have almost no impact on loads and standard signals at high turbulence conditions. Contrary to that, its relative influence can be greater in more laminar inflow. This effect is also highlighted by Riziotis and Voutsinas [33], where variations in turbulence intensity, yaw error, wind shear and vertical inflow are investigated for flat and complex terrain.

The conditions which are applied in this investigation as a baseline for all following calculations are given in Table 3.1. They have been chosen to reflect typical situations at an onshore site.

Disturbances

Each disturbance is analysed separately and the change in load components and the statistical parameters of standard signals is computed. Typical magnitudes and variations have been chosen for the following disturbances:

Deterministic inflow properties

- Mean wind speed
- Vertical wind shear
- Vertically inclined flow
- Yaw error
- Air density

Stochastic inflow properties

- Overall turbulence intensity
- Horizontal turbulence intensity
- Vertical turbulence intensity
- Integral length scale
- Spatial coherence decay

Turbine properties

- Mass imbalance
- Aerodynamic imbalance
- Soil/Foundation stiffness

Standard signals

It has also been assumed that at least the following standard signals are measured in high resolution (10 Hz and higher) on a state-of-the-art variable-speed pitch-controlled wind turbine:

- generator rotational speed Ω_{gen}
- generator rotational acceleration $\dot{\Omega}_{gen}$ (calculated as derivative of the rotational speed signal)
- electrical power output P_{el}
- pitch angle θ_p
- lateral tower top acceleration $\ddot{y}_{tt}$
- longitudinal tower top acceleration $\ddot{z}_{tt}$

Of course, there are meteorological parameters measured on almost any wind turbine as well, comprising of wind speed and wind direction at least. Nevertheless, meteorological signals are not analysed here. This is because these signals are highly distorted in reality by the influence of the rotor and the nacelle, an effect which is not included in the utilised simulation tool. In addition, the exact value of the wind speed can not be used for accurate load estimations anyway, if the air density is not measured simultaneously (which is often not the case). Therefore, the electrical power, generator speed and pitch angle are frequently more suitable measures and implicitly contain all influences related to the mean wind speed. For a load estimation system running on a real turbine, an averaged wind direction signal can of course be used as an additional indicator of yaw misalignments.

Detectability

In general, a signal can be processed in many different ways to extract the required information. Here, only the mean value ($\bar{X}$), variance ($Var(X)$), skewness (γ_3), kurtosis (γ_4), maximum range (ΔS_{max}) and the first two spectral moments (λ_1 and λ_2) of each signal have been calculated. Frequently, the analysis of those fundamental statistical parameters can already reveal important characteristics. But sometimes information is hidden in noise or superimposed by other more dominant effects. If the influence of a disturbance on a standard signal appears to be weak in this analysis, it might as well be owned to such a situation. In this case, a more elaborate post-processing of signals and the utilisation of additional statistical parameters can help to improve the situation. An example for such an approach is given in Appendix G, where a parameter related to the integral length scale of turbulence is derived.

Of course, the overall variability of a signal's statistical parameters has to be taken into account when the detectability of a disturbance from standard signals is evaluated. Besides a variation of parameters in simulations with identical mean wind speed and turbulence intensity due to the stochastic nature of the wind, another effect can play a role as well: The estimation accuracy of statistical parameters from time series of limited length decreases considerably with increasing order of the parameters. This can cause some additional scatter in the results particularly for higher order statistical parameters.

A condition for detectability is therefore that the variability of at least one statistical parameter of a signal due to the disturbance should be larger than its general scatter. The fulfilment of this condition is tested separately for each investigated operational regions by the following procedure (compare also Figure 3.1):

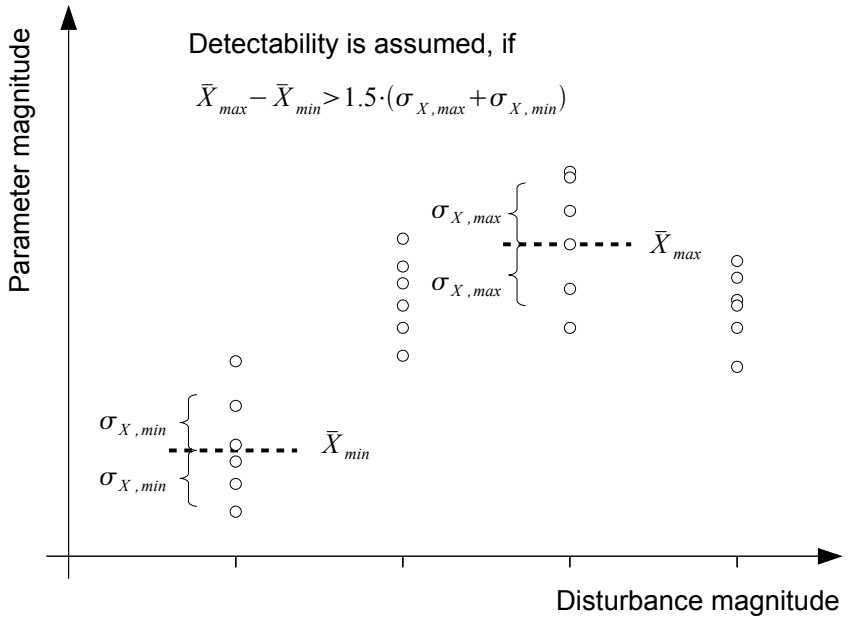

Figure 3.1: Illustration of the applied detectability criteria

1. The overall mean of each statistical parameter is estimated from the six simulations with different turbulent wind fields at the same mean wind speed. This is done for each investigated magnitude of the respective disturbance.

2. The width of the 95 % confidence interval of the overall mean values is calculated for each disturbance magnitude. Normally distributed estimations are assumed and hence the Student's *t* distribution can be employed. Because the overall mean value is always computed from six estimates, the statistical evaluation is based on five degrees of freedom and the confidence interval computes to +/- 1.05 times the standard deviation in each case. In other words, there is a 95 % chance of the true overall mean value not being more than approximately one standard deviation off the estimated value.

3. It is assumed, that the disturbance alters the signal significantly if the difference between the maximum and minimum of the calculated overall mean values is larger than one standard deviation. Taking the 95 % confidence interval into account, this adds up to the sum of 1.5 times the respective standard deviations and yields the expression

$$\bar{X}_{max} - \bar{X}_{min} > 1.5 \cdot (\sigma_{X,max} + \sigma_{X,min}) \tag{3.1}$$

   If condition 3.1 is fulfilled for at least one statistical parameter, the respective standard signal is assumed to be potentially suited for the detection of the disturbance at the investigated wind speed.

Because of the large amount of data from such an analysis, a colour and symbol code (Table 3.2) has been invented to illustrate the results in a comprehensible manner. A table is displayed for each disturbance, where differently shaded cells show fulfilment of Equation 3.1. Shaded summary cells indicate the general potential of the investigated signals and parameters for the detection of disturbances. In addition, each cell contains three symbols, corresponding to the investigated operational states (in the order *below rated*, *rated* and *above rated*). These symbols indicate, if a parameter increases or decreases under the disturbance at a certain operational region.

Analysed fatigue loads

In parallel to the investigation of standard signals, different load components of wind turbines have been compared. They can be classified with respect to their sphere of interference and their relation to standard signals. An overview of the chosen load components and their classification is given in Table 3.3.

All of the analysed standard signals are integral quantities in the nacelle reference system. They include effects which are averaged over the whole rotor plane. In this respect they are similar to loads like the rotor torque or the rotor thrust, but differ to rotating blade loads which are integrated over a single blade only. This can affect the estimations. The rotor torque is directly related to the electrical power and the generator speed for example. Hence, the torque is probably one of the loads which can be predicted with a relatively high accuracy and estimations for other load components might be more challenging.

All equivalent loads are calculated on the basis of an intermediate exponent m or p of 6 and their variability is given in percentage of the baseline loads. An arrow indi-

Table 3.2: Colour and symbol code for the detectability of disturbances from standard signals

Cell	Equation 3.1 not fulfilled for any state
Cell	Fulfilment of Equation 3.1 for at least one operational state
Sum	Signal or parameter potentially less suited
Sum	Signal or parameter potentially suited
Sum	Signal or parameter potentially well suited
$\uparrow$	Maximum parameter value corresponds to larger disturbance value than the minimum parameter value
$\downarrow$	Minimum parameter value corresponds to larger disturbance value than the maximum parameter value
$-$	Equation 3.1 not fulfilled for this state

Table 3.3: Classification of load quantities with respect to their sphere of interference and relation to standard signals

Load quantity	Sphere of interference	Directly related standard signal
Out-of-plane blade root bending moment (M_{op})	Blade	None
In-plane blade root bending moment (M_{ip})	Blade	Generator speed
Nodding moment at tower top (M_{tt})	Rotor	None
Rotor thrust (F_r)	Rotor	Long. tower top acceleration
Long. bending moment at tower base (M_{tb})	Rotor	Long. tower top acceleration
Rotor torque (M_r)	Rotor	Electrical power, generator speed and generator acceleration

Table 3.4: Symbol code for load variations due to disturbances

↑	Equivalent load increases with disturbance
↓	Equivalent load decreases with disturbance

cates whether the load shows a tendency to increases or decreases with an increasing disturbance (Table 3.4).

Additionally, the resulting loads and statistical parameters have also been put into a linear regression. The derived models characterise the influence of each disturbance on fatigue loads and standard signals and allow to predict loads and parameters for other than the simulated magnitudes of disturbances. The regression coefficients are given in Annex E. More details on regression analysis of wind turbine loads are given in Chapter 4.

3.2 Deterministic inflow properties

3.2.1 Wind speed

Modern wind turbines operate typically at wind speeds from approximately 4 to 25 m/s (10 minute mean value). At lower speeds, most turbines are not able to produce enough electricity to cover their own auxiliary power requirements. An upper wind

speed limit for the turbine operation is set, because the turbine loads increase with wind speed. As the occurrence probability of very high wind speeds is usually relatively low, speeds above a certain level contribute only insignificantly to the total energy yield. The limitation of turbine operation to a maximum wind speed is therefore an economical necessity.

Because the objectives of the turbine control in partial load and full load operation are fundamentally different, the loads and standard signals can show significantly different characteristics in these two areas. This is reflected by some of the calculated equivalent loads in Figure 3.2 and 3.3. In these figures, the equivalent loads ΔS_{eq} and L_{eq} are plotted over the typical wind speed range of 4 to 25 m/s for all investigated load components. The transition from partial to full load operation at approximately 12 m/s is clearly visible especially for equivalent magnitudes.

The loads have been derived from the baseline configuration (Table 3.1) and a variation of 10 minute mean wind speeds. Box-whisker-plots are employed to illustrate the results. Here, the centre line corresponds to the median and the borders of the box to the lower and upper quartile of the data. Minima and maxima are marked by the end of the whiskers. In most cases, the boxes seem to be relatively small which means that the equivalent loads from different stochastic realisations of the turbulent wind do not deviate much. Hence, it can be concluded, that average equivalent loads for a given wind speed can be estimated from the six simulated data sets with good accuracy.

In general, the variations in simulated fatigue loads with wind speed are large. This corresponds to commonly known correlations and also becomes obvious from the characteristic curves in Annex B.

The detectability of a change in the mean wind speed has been tested as described before. Results are illustrated graphically in Table 3.5, where a light shaded cell shows the fulfilment of conditions according to Equation 3.1. As the 10 minute mean wind speed itself and no other disturbance at one of the mean wind speeds given in Table 3.1 has been varied, no arrows are shown in Table 3.5.

The shade of the summary cells indicates the general importance of the signal and the statistical parameter respectively. It can be seen, that many statistical parameters are affected from changes in mean wind speed. Therefore, detectability of the 10 minute mean wind speed should be feasible with reasonable accuracy[1].

From the performed analysis it can be concluded, that the 10 minute mean wind

[1] This is also confirmed by a simple test on the basis of neural networks described in Chapter 4. It should however be mentioned that an interaction of several strongly varying disturbances can of course complicate the detectability and give rise to larger estimation errors.

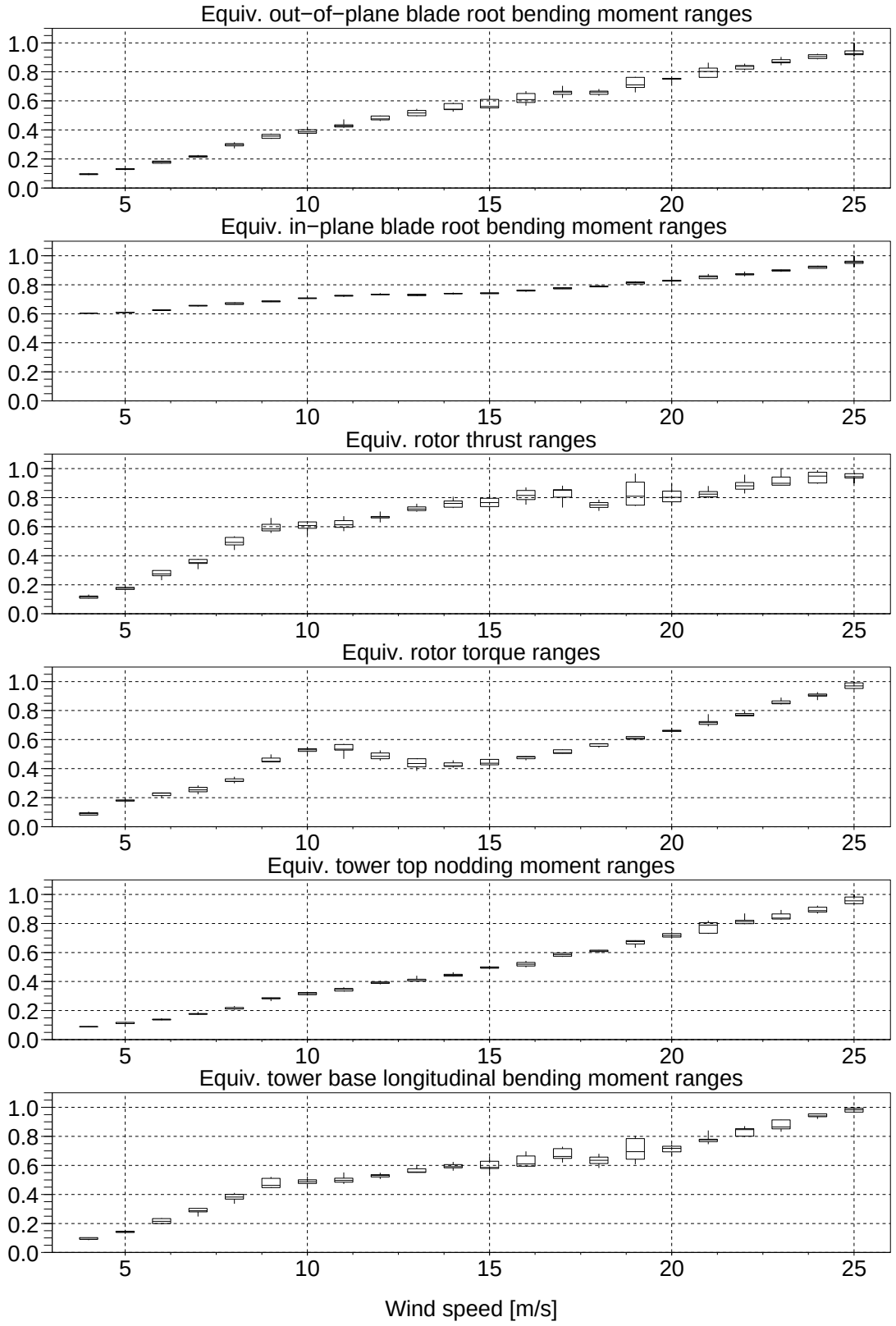

Figure 3.2: Variation of normalised simulated equivalent load ranges ΔS_{eq} from rainflow cycle distributions over wind speed (with exponent m = 6)

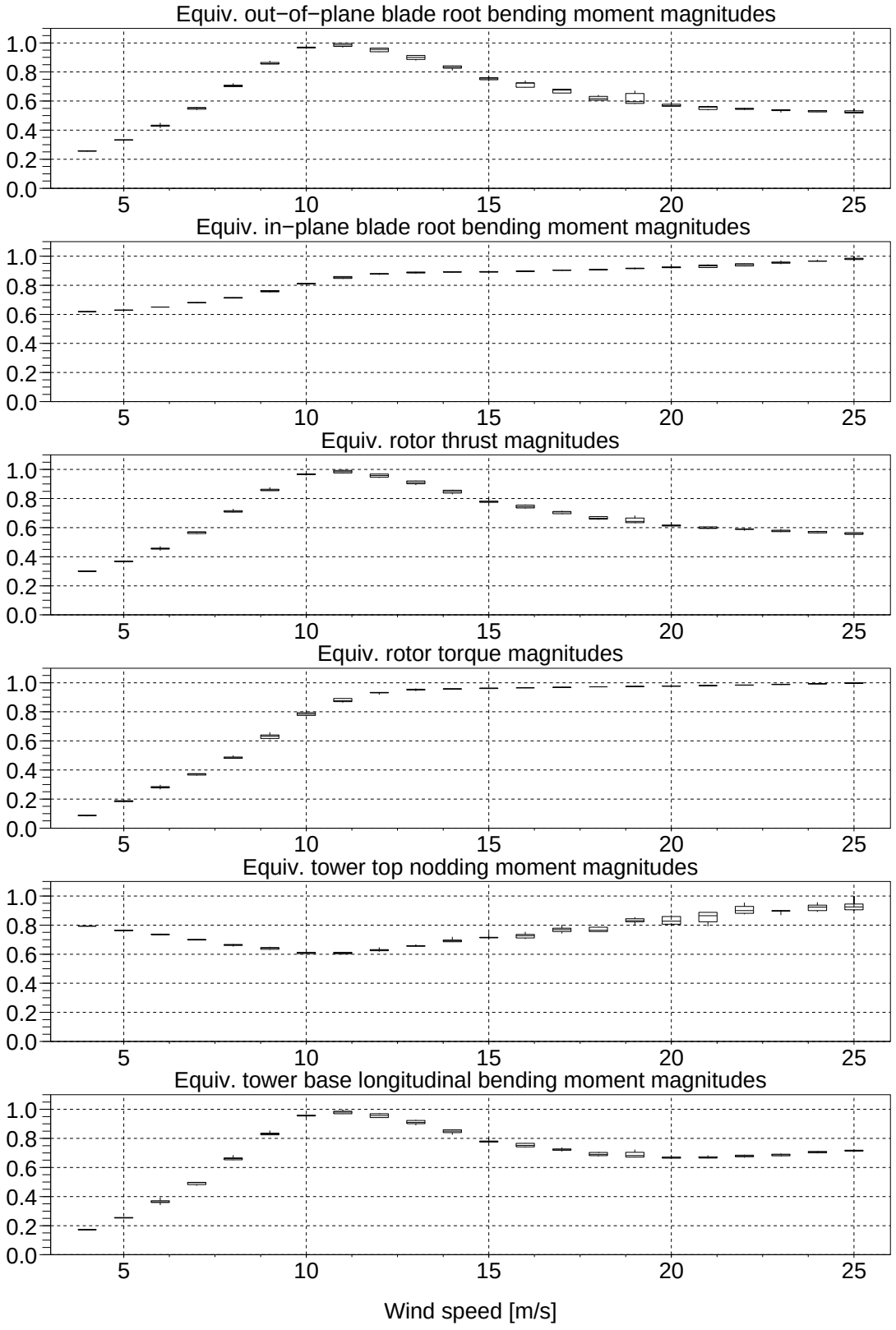

Figure 3.3: Variation of normalised simulated equivalent load magnitudes L_{eq} from magnitude distributions over wind speed (with exponent p = 6)

Table 3.5: Wind speed detectability matrix. Variations from 4 to 25 m/s have been considered

Signal	Statistical parameters							Sum
	$\bar{X}$	$Var(X)$	γ_3	γ_4	λ_1	λ_2	ΔS_{max}	
Ω_{gen}								
$\dot{\Omega}_{gen}$								
P_{el}								
θ_P								
$\ddot{y}_{tt}$								
$\ddot{z}_{tt}$								
Sum								

speed

- has got a very strong influence on all fatigue loads.
- clearly affects most of the analysed statistical parameters of standard signals.

Because loads and statistical parameters vary non-linear with wind speed, the regression analysis in Annex E has not been performed in this case. The linear regression model is not able to reflect the relation of wind speed and loads in an appropriate manner. This is also confirmed by results from Nelson et al. [34], where the coefficients of determination from a linear regression analysis of inflow parameters and loads are found to be relatively small, when calculated for the whole wind speed range.

3.2.2 Vertical wind shear

Usually the average wind speed increases with increasing distance from ground. The two main drivers for this effect, also known as wind shear, are the surface roughness and the conditions in the atmospheric boundary layer. Wind shear is often modelled by the so-called logarithmic law. In neutral stratification, the only inputs to this relation are the roughness length z_0 and a reference wind speed $U(h_r)$ at height h_r, although it can also be extended to incorporate a stability correction based on the Monin-Obuhkov length (not shown here):

$$U(h) = U(h_r) \cdot \frac{ln(h/z_0)}{ln(h_r/z_0)} \tag{3.2}$$

For the design of wind turbines, the potentially high shears in stable atmospheric layering are commonly neglected. This is often justified by arguing, that stable conditions are frequently associated with relatively low wind speeds and turbulence intensities.

They are therefore in general less important for the loading of wind turbines, at least onshore.

Kelley et al. [35] analysed strong nocturnal low level jets in stable stratification at the Great Plains and found shears which differ significantly to what can be modelled with the logarithmic law. They employed these jets for wind turbine simulation and compared the calculated equivalent ranges to those derived for conditions according to IEC 61400-1 type class C. The type class C was chosen, because this type class reflects the very low measured turbulence level at the site best. Some load components increased under the influence of shear, but the difference to loads in type class C was less than 10 % in any case.

To model low level jets measured in Germany, the author extended the simulation software Flex5 with equations given by Emeis [36]. These can be used to efficiently describe an increase of wind speed and a simultaneous wind direction variation with height [37]. Increased equivalent flapwise blade root bending moments in the order of 20 % were calculated, compared to conditions with the same low wind speed and turbulence intensity but without the low level jet. It was also found, that the influence of low level jets increases with hub height and rotor size in the investigated example. However, the measured high shear occured only at low wind speeds and hence the impact on total cumulated fatigue loads will be much smaller when higher wind speeds with usually less stable conditions are included into the comparison.

Sathe and Bierbooms [38] took the distributions of stable, neutral and unstable conditions for two offshore sites and estimated the lifetime fatigue damage from simulations using different wind shear models. Their investigations did not include turbulence and therefore probably strongly overestimate the effect of shear on equivalent loads. Nevertheless, it becomes obvious, that atmospheric stability driven shear will be more important for offshore sites, because offshore, the general level of turbulence intensity is lower and stable conditions occur more frequently than onshore.

In complex terrain, shear can be dominated by local terrain features. For example, Stefanatos et al. [39] reported even negative shears for a complex site in Greece. Depending on the wind direction, Maeda et al. [40] calculated roughness lengths from measured wind profiles ranging from 0 to 1 m for a site characterised as complex near the Japanese coast. Veldkamp [28] recommends to assume no shear at all for complex sites, when no further information is available.

In this investigation, only the influence of the roughness length on shear is considered using Equation 3.2. Lengths from 0.03 m up to 0.3 m are applied. These are

typical values for open farmland to suburbs and wooded countryside [17]. The reference wind speed at hub height $U(h_r)$ is set to 6, 12 or 18 m/s corresponding to the investigated operational region.

As it can be seen from Table 3.6, the influence of the investigated shear due to changes in roughness length on the equivalent ranges is small. The largest deviations of about 4 % occur for the out-of-plane blade root bending moments. For the equivalent magnitudes, the impact on most loads is even smaller. Only in the case of the nodding moment at tower top a noticeable influence is evident. This can be explained by the differences in wind speeds in the upper and lower part of the rotor plane, leading to differences in resulting inflow and angle of attack at the blade sections and hence aerodynamic forces. It should be noted, that the influence of roughness length on the wind speed depends on the height above ground. Therefore, larger effects can be expected for turbines with smaller hub heights or larger rotor diameters.

Riziotis and Voutsinas [33] investigated the influence of a linear shear on equivalent load ranges and found increasing ranges of the flapwise blade root bending moments of approximately 10 to 15 %. Given, that the change in wind shear was about three times the variation which has been applied here, the results are comparable. The small change in other load components is consistent between the two studies as well.

Unfortunately, the detectability matrix is completely blank. The analysed parameters do not seem to be well suited to detect changing wind shears in a load prediction system.

Although dynamic variations in shear are probably difficult to capture, the average shear of a site can still be approximated by using estimates of the roughness length from site properties. This can even be done sector-wise to allow for a more detailed description of the site conditions.

Adaptation of the roughness length to account for seasonal variations is of course possible. Even 24-hour cycles of shear variations could be considered to incorporate diurnal wind shear patters, if this is deemed to be important for the overall load level. Istchenko and Turner [41] investigated such time-of-day corrections for the vertical shear at a site near Calgary and found, that much of the stability related variations are captured by this method. Finally, if significant wind speed variations with height are suspected for a site which can not be approximated by any of the above measures, application of additional signals or a more sophisticated analysis of the available ones can be a solution.

For the analysed conditions it can be concluded, that vertical wind shear

Table 3.6: Variation of equivalent loads in percentage of a baseline case. A change in the roughness length from 0.03 to 0.3 m has been considered, with 0.1 m as baseline.

Load	Equiv. range			Equiv. magnitude		
	6 m/s	12 m/s	18 m/s	6 m/s	12 m/s	18 m/s
M_{op}	2 ↑	2 ↑	4 ↑	0	0	1 ↑
M_{ip}	0	1 ↑	1 ↑	0	0	1 ↑
F_r	0	1 ↑	0	0	0	0
M_r	1 ↑	1 ↑	0	0	0	0
M_{tt}	0	0	1 ↑	2 ↓	5 ↓	7 ↓
M_{tb}	0	1 ↓	0	0	0	0

Table 3.7: Vertical wind shear detectability matrix. A change in the roughness length from 0.03 to 0.3 m has been considered.

Signal	Statistical parameters							Sum
	$\bar{X}$	$Var(X)$	γ_3	γ_4	λ_1	λ_2	ΔS_{max}	
Ω_{gen}								
$\dot{\Omega}_{gen}$								
P_{el}								
θ_P								
$\ddot{y}_{tt}$								
$\ddot{z}_{tt}$								
Sum								

- has got a minor influence on investigated fatigue loads, except for the equivalent magnitudes of the tower top nodding moment.
- can not be detected easily from the analysed parameters of standard signals. The estimation of average site specific roughness lengths, combined with information on seasonal and diurnal variations, might be a cheap workaround.

3.2.3 Vertically inclined flow

Vertically inclined inflow can be considered as a normal operating condition for modern wind turbines. This is due to the fact, that the rotor axis is usually not mounted in a horizontal position, but rotated by a so-called tilt angle. Incorporating such an angle

into the design is an easy way of gaining more tower clearance for the blades and allows to reduce stiffness and mass of the blades. Up to some angle, this economically justifies the resulting loss in power and the increased loading. The power reduction is approximately proportional to the cosine squared of the tilt angle (see Pedersen [42] for example) which means that the loss rapidly increases for larger tilt angles. Studying the product brochures from various turbine manufactures, the tilt angle seems to be around 4 to 5 ° commonly.

When turbines are operating at exposed locations, for example on top of a hill, the inclination of the incoming flow increases. Usually it reduces again with height and even for strongly inclined terrain of 20 to 30 °, an inclined flow of less then 10 ° is likely for common hub heights [28].

For a flat site in Denmark, Dahlberg et al. [43] analysed flow measurements in 30 m height. At relevant wind speeds, the measured inflow angles were in the range of +/- 3 ° only. This variation might be even smaller for larger heights and therefore the main drivers for inclined flow are probably the tilt angle and the inclination of the surrounding terrain.

The IEC 61400-1 standard requires designers to consider an upflow of 8 ° for design load calculations of onshore wind turbines. As guidelines tend to be conservative in their requirements, this indicates that 8 ° can already be considered as a relatively large inclination for most sites. In this investigation, the vertical inflow angle has been varied from +10 (upflow) to -10 ° (downflow). Taking the model's tilt angle of 5 ° into account, this corresponds to a total inclination of +15 to -5 °.

Not surprisingly, the vertical inflow seems to be hard to detect from the chosen statistical parameters. Only the mean value of electrical power and pitch angle are significantly affected. The equivalent loads vary mostly in the range of less than 5 %. An exception is the in-plane blade root bending moment. The inclined flow changes the relative inflow velocity and the angle of attack at the blade sections in the left and right half of the rotor and therefore influences the magnitude of the in-plane load ranges. This holds true especially for larger pitch angles where the lift force has got a larger contribution to the in-plane bending moment. As the load level is weighted exponentially, this effect is also visible in the equivalent magnitudes. At below and around rated, the equivalent magnitude of the nodding moment is also strongly affected.

The relatively small effect on most load components coincides with findings from Riziotis and Voutsinas [33], although only small upflows of about 6 ° were considered. Unfortunately, no information on the in-plane blade root bending moment are given in their report.

Table 3.8: Variation of equivalent loads in percentage of a baseline case. A change in vertically inclined flow from -10 to 10 ° has been considered, with 0 ° as baseline.

Load	Equiv. range			Equiv. magnitude		
	6 m/s	12 m/s	18 m/s	6 m/s	12 m/s	18 m/s
M_{op}	6 ↓	5 ↓	3 ↑	3 ↓	2 ↑	4 ↑
M_{ip}	0	3 ↓	18 ↓	1 ↓	3 ↓	12 ↓
F_r	3 ↓	2 ↓	6 ↑	2 ↓	2 ↑	3 ↑
M_r	2 ↓	5 ↑	0	3 ↓	1 ↓	0
M_{tt}	2 ↓	3 ↓	2 ↓	9 ↑	21 ↑	4 ↓
M_{tb}	4 ↓	1 ↓	1 ↓	4 ↓	1 ↑	3 ↑

Table 3.9: Vertically inclined flow detectability matrix. A change in vertically inclined flow from -10 to 10 ° has been considered.

Signal	Statistical parameters							Sum
	$\bar{X}$	$Var(X)$	γ_3	γ_4	λ_1	λ_2	ΔS_{max}	
Ω_{gen}								
$\dot{\Omega}_{gen}$								
P_{el}	$\uparrow --$							
θ_P	$- \downarrow\downarrow$							
$\ddot{y}_{tt}$								
$\ddot{z}_{tt}$								
Sum								

For the analysed conditions it can be concluded, that a vertically inclined flow

- has got a relatively small influence on the investigated fatigue loads, except for the in-plane blade root bending moment above rated and the nodding moment at tower top below and around rated[2].
- can not be detected easily from the analysed parameters of standard signals. Only the mean of the electrical power and the pitch angle show some significant variation.

[2] It should be mentioned, that varying terrain inclinations can lead to detached flow and the generation of large turbulent eddies, even with reversed flow. This becomes particular relevant for turbines operating for example close to a cliff or behind significant obstacles and the loads arising from such situations are probably much more severe as from simple flow inclinations.

3.2.4 Yaw error

Most wind turbines measure the alignment of the rotor axis with the inflow to actively track the wind direction. Usually at least one wind vane is mounted on top of the nacelle for the purpose of constantly monitoring the yaw misalignment. Because the vane is located behind the rotor and close to the nacelle, the measured local flow conditions are disturbed and differ from the free stream conditions. Commonly this problem is addressed by implementing a transfer function which tempts to correct the measured misalignments with respect to the undisturbed flow. Nevertheless, some uncertainty about the correct alignment of the turbine with the wind direction remains.

Sometimes, additional sources of yaw errors arise from the employed measurement hardware or software. One example is wind direction monitoring with coarse resolution. For instance, frequently found wind vanes with four bit encoding have got a theoretical resolution of only 22.5 °. However, clever positioning of the bit centres and making some additional assumptions allows to derive reasonable estimates of the yaw misalignment which usually deviate less than 5 ° from the real value.

Because the wind direction fluctuates constantly and is not necessarily uniform across the swept rotor area, it is virtually impossible to realise a wind turbine operation without yaw errors. The typical wind direction tracking procedure is therefore, to yaw the turbine only in case that some threshold parameters are exceeded. To adequately cope with slow and fast arising misalignments, several thresholds are often defined. As a simple example the yaw drive could be activated if an error of 5 ° is found to persists for more than 2 minutes, while an error of 20 ° is already tracked after 10 seconds.

For design load calculations, standards require to take yaw misalignments into account. Their magnitude generally depends on the applied control and monitoring system. In the case that no smaller values can be verified, the Germanischer Lloyd recommends to apply misalignments of +/- 8 ° for design calculations [12].

In this evaluation, misalignments of +/- 10 ° have been considered. These values are average errors which persist throughout the whole simulation of 10 minute duration. Because turbulent wind is applied, short term errors are much larger and instantaneous values of around +/- 40 ° have been observed in the simulation.

Although relatively large yaw errors are applied, the deviation of computed equivalent loads is less than 5 % for most load components. The influence of yaw misalignments is strongest for the equivalent ranges of the out-of-plane blade root bending moment and the equivalent magnitudes of the nodding moment at tower top. Both originate

Table 3.10: Variation of equivalent loads in percentage of a baseline case. A change in yaw error from -10 to 10 ° has been considered, with 0 ° as baseline.

Load	Equiv. range			Equiv. magnitude		
	6 m/s	12 m/s	18 m/s	6 m/s	12 m/s	18 m/s
M_{op}	9 ↓	8 ↓	15 ↑	1 ↓	2 ↓	2 ↑
M_{ip}	3 ↓	6 ↓	3 ↑	2 ↓	5 ↓	1 ↑
F_r	2 ↑	2 ↑	4 ↓	1 ↑	1 ↓	2 ↓
M_r	2 ↑	5 ↑	1 ↓	1 ↑	0	0
M_{tt}	1 ↓	2 ↓	4 ↑	7 ↑	11 ↑	27 ↓
M_{tb}	2 ↑	1 ↑	8 ↓	2 ↓	1 ↓	1 ↓

Table 3.11: Yaw error detectability matrix. A change in yaw error from -10 to 10 ° has been considered.

Signal	Statistical parameters							Sum
	$\bar{X}$	$Var(X)$	γ_3	γ_4	λ_1	λ_2	ΔS_{max}	
Ω_{gen}								
$\dot{\Omega}_{gen}$								
P_{el}								
θ_P	$--\uparrow$							
$\ddot{y}_{tt}$								
$\ddot{z}_{tt}$								
Sum								

from the unbalanced inflow to the rotor.

Compared to the vertically inclined inflow, the equivalent in-plane bending moment is much less affected. This is because the additional load oscillations due to yaw errors are not in line with the oscillations due to self weight, but 90 ° phase shifted. The maximum amplitudes therefore remain unchanged and hence the equivalent range is influenced less. The exact opposite happens in case of the out-of-plane moments. Compared to the inclined flow, oscillations due to the yaw error now add up with those from wind shear and tilt angle, yielding much larger increases in the equivalent out-of-plane bending moment.

Riziotis and Voutsinas [33] observed similar changes for the flapwise blade root bending moments. They also confirm the changing sign of the deviations from be-

low rated to above rated operation. However, for above rated operation their computed variations in the tower base bending moments are only around 1 or 2 %.

Yaw errors of the applied magnitude can not be detected probably from standard signals. The mean value and probably also the variance of the wind vane signal would be available as additional signals on real turbines. It is beyond question, that these will certainly help to improve the detectability of such situations.

For the analysed conditions it can be concluded, that moderate yaw errors

- have got a relatively small influence on most investigated fatigue loads, except for the out-of-plane blade root bending moment and the nodding moment at tower top.
- can not be detected easily from the analysed parameters of standard signals. The wind vane signal has not been taken into account in this simulation study and will significantly improve the situation in terms of detectability for real turbines.

3.2.5 Air density

The density of air can be calculated from the air pressure p, temperature T and the gas constant R from

$$\rho = \frac{p}{R \cdot T} \tag{3.3}$$

Typically, the air density is strongly influenced by air pressure and temperature. Because the variation of R is usually of minor importance compared to pressure and temperature, it is often neglected and the value for dry air is used in calculations.

Air pressure strongly depends on altitude[3]. An approximate relation, valid for heights h below 5000 m and international standard atmosphere is given in [19]:

$$p = p_0 - a \cdot h + b \cdot h^2 \tag{3.4}$$

where p_0 is 101.29 kPa, a is 0.011837 kPa/m and b is 4.793·10^{-7} kPa/m^2.

From Equation 3.3 and 3.4 an air density variation of about 11 % is estimated for an elevation change of 1000 m. A variation of air density with similar magnitude can also

[3] In addition to the elevation, the local air pressure is also influenced by large atmospheric systems which result in regions with low or high pressure. Compared to the standard pressure, these systems typically decrease or increase the local pressure by about one or two percent only and hence their impact on air density is commonly small.

Table 3.12: Variation of equivalent loads in percentage of a baseline case. A change in air density from 1.165 to 1.293 kg/m^3 has been considered, with 1.225 kg/m^3 as baseline.

Load	Equiv. range			Equiv. magnitude		
	6 m/s	12 m/s	18 m/s	6 m/s	12 m/s	18 m/s
M_{op}	12 ↑	7 ↑	7 ↑	11 ↑	2 ↑	1 ↓
M_{ip}	1 ↑	1 ↓	2 ↑	1 ↑	1 ↑	1 ↑
F_r	15 ↑	9 ↑	2 ↑	10 ↑	2 ↑	0
M_r	5 ↑	5 ↓	5 ↑	7 ↑	1 ↑	0 ↑
M_{tt}	8 ↑	7 ↑	9 ↑	2 ↓	1 ↑	2 ↑
M_{tb}	16 ↑	9 ↑	3 ↑	14 ↑	2 ↑	2 ↑

Table 3.13: Air density detectability matrix. A change in air density from 1.165 to 1.293 kg/m^3 has been considered.

Signal	Statistical parameters							Sum
	$\bar{X}$	$Var(X)$	γ_3	γ_4	λ_1	λ_2	ΔS_{max}	
Ω_{gen}	$\uparrow --$					$-- \uparrow$		
$\dot{\Omega}_{gen}$					$-- \uparrow$	$-- \uparrow$		
P_{el}	$\uparrow --$							
θ_P	$- \uparrow\uparrow$							
$\ddot{y}_{tt}$			$-- \downarrow$		$-- \uparrow$	$-- \uparrow$		
$\ddot{z}_{tt}$					$\uparrow\uparrow\uparrow$	$\uparrow\uparrow\uparrow$		
Sum								

result from changes in temperature, for example from 273 to 303 K (approx. 0 to 30 °).

Under the assumption of dry air, the density for a site at sea-level is estimated from Equation 3.3 to 1.165 kg/m^3 for 0 °C and 1.293 kg/m^3 for 30 °C. This is also the range of air density variation which has been considered in the performed analysis of loads and standard signals.

The air density has got a significant impact on the operation of wind turbines. This becomes also obvious from the fact that basic momentum theory or kinetic energy relations both depend linearly on mass flow and hence density. Although this linear relation also holds in general for aerodynamic forces and moments, the dynamic turbine control introduces additional effects and the total relation on loads and standard signals

becomes non-linear.

An increase in air density is to some extent comparable to operating the turbine at higher wind speeds. For example, according to fundamental equations, an 11 % increase in density roughly corresponds to an increase of mean wind speed from 6 to 6.3 m/s in terms of loads and 6.2 m/s in terms of energy. These effects are less important for above rated operation, as the turbine simply dumps excessive energy by pitching the blades. But the influence of air density on equivalent loads is significant at below rated operation (compare Table 3.12).

Some standard signals are influenced by the air density variation and the installation of an additional sensor measuring the outdoor temperature (if not already available) can certainly improve the situation further. The estimation of site temperature from meteorological stations in its proximity or simply from weather forecasts could be an alternative.

For the analysed conditions it can be concluded, that air density variations

- have got a noticeable influence on most investigated fatigue loads, especially at below rated operation.
- affect some of the analysed parameters of standard signals. Application of additional temperature sensors or employment of information from weather stations can improve the situation further.

3.3 Stochastic inflow properties

3.3.1 Overall turbulence intensity

The turbulence intensity is an important statistical property of the wind. It is defined as the standard deviation of the wind speed divided by its mean and is a measure of the general magnitude of fluctuations in wind speed.

Turbulence intensity depends on many site and environmental parameters, for example the complexity of the surrounding terrain (mechanically generated turbulence) or the atmospheric stability (thermal turbulence due to convection). In heights of relevance for wind turbines, significant thermal turbulence is usually generated only at low to medium wind speeds, while at higher wind speeds the mechanically generated turbulence dominates.

The range of ambient turbulence intensities at which wind turbines operate is large. Petersen et al. [44] give typical average turbulence intensities in neutral atmospheric conditions for complex terrain ($>$ 20 %), flat open grasland (13 %) and sea (8 %). There are also simple rules of thumb, from which general turbulence levels can be estimated. Equation 3.5 is a popular formular for this purpose and can be found in various text books and standards. Only the roughness length z_0 is required to estimate the average turbulence intensity at height h above ground. An alternative relation (Equation 3.6), based on an additional turbulence profile exponent, has been derived recently by Hansen [45], who validated it against measured wind data from six sites of different complexity.

$$I_T = \frac{1}{ln(h/z_0)} \tag{3.5}$$

$$I_T = 2.4 \cdot \left(\frac{z_0}{h} \cdot e^{0.4}\right)^p \tag{3.6}$$

Plots of measured turbulence intensity over wind speed for about 60 sites, ranging from offshore to mountainous terrains, can be found in [46]. Often, a fairly constant turbulence intensity at medium to high wind speeds can be observed. For low wind speeds the scatter in turbulence intensity increases significantly.

It is commonly known, that the standard deviation of wind speed in the wake of a wind turbine is generally higher than in free stream conditions. In addition, the mean wind speed in the wake is reduced and hence larger wake turbulence intensities are computed. This is of particular importance for turbines operating in wind farms. Frandsen [47] compared average turbulence intensities inside and outside a wind farm and found a wind speed dependent increase in turbulence of up to 40 %.

In [48], single wake measurements in the Vindeby offshore wind farm are reported together with a comparison of wake turbulence predictions from several simulation codes. It is stressed, that the additional wake turbulence decreases with increasing distance from the turbine, but that even at a distance of about 10 rotor diameters from the turbine an increased turbulence level can still be measured. However, the shown measurements have been taken at relatively low ambient turbulence intensities of 6 and 8 %. Therefore, the wake conditions are relatively stable and a stronger diffusion can be expected for higher free stream turbulence.

Seifert and Kröning [49] analysed measurements taken at turbines operating in wake conditions and confirmed a strong increase of turbulence intensity and fatigue loads under full wake conditions. They also observed that turbulence intensity and turbine loads at partial wake operation are even larger than in full wake conditions.

To account for the increased fatigue loading of turbines in wind farms, Frandsen and Thogersen [50] presented a model for the calculation of an effective turbulence intensity, where the turbulence depends mainly on the spacing of turbines, their thrust coefficients and the SN-curve exponent m. This effective turbulence intensity contains all influences of wind farm and wake operation on the fatigue loads of turbines and hence has not a direct physical meaning. It should not be confused with the turbulence intensity measured inside a wind farm.

In the IEC 61400-1 standard [16] the representative turbulence intensity is defined as the average turbulence intensity plus 1.28 times the standard deviation. It is therefore more of a conservative design value than an estimate of a typical average value. Hence, rather large turbulence intensities at low wind speeds are derived and have to be used for the design of wind turbines. At 15 m/s the standard suggests representative turbulence intensities of 13 to 18 %, depending on the chosen turbulence class.

Taking all the above considerations into account, turbulence intensities ranging from 5 to 25 % seem to be common environmental conditions for wind turbine operation. In addition to the longitudinal turbulence intensity, the standard deviation of wind speed in lateral and vertical direction have been modified in this analysis as well. This has been done to maintain the turbulence ratios of 0.8 and 0.5 listed in Table 3.1 and hence the investigated variations correspond to a three-dimensional change in turbulence intensity.

Very large deviations in equivalent ranges for all load components and all operational states have been simulated. The equivalent magnitudes seem to be less sensitive, although the variations are still large. Around rated, some equivalent magnitudes decrease with increasing turbulence. This can be explained by the higher pitching activities of the turbine, leading to more energy being dumped; an effect which is also known from power curve measurements.

Riziotis and Voutsinas [33] computed similar results for a 225 kW pitch controlled turbine. Here, an increase in turbulence intensity from 15 to 25 % at an average wind speed of 18 m/s gave around 50 to 60 % larger equivalent ranges for the flapwise blade root bending moments, the rotor torque and the tower base bending moment. Measurements on a large wind turbine [51, 52] showed 20 % lower equivalent ranges of the flapwise blade root bending moments for a decrease in turbulence intensity from 12 to 6 %. The tower base bending moments went down by as much as 30 %. In both cases, the analysis included a typical distribution of wind speeds at the measurement site. Nelson et al. further also confirm the strong correlation of turbulence intensity and equivalent loads on the basis of regression analysis [34].

Table 3.14: Variation of equivalent loads in percentage of a baseline case. A change in the overall turbulence intensity from 5 to 25 % has been considered, with 15 % as baseline.

Load	Equiv. range			Equiv. magnitude		
	6 m/s	12 m/s	18 m/s	6 m/s	12 m/s	18 m/s
M_{op}	123 ↑	97 ↑	114 ↑	30 ↑	2 ↓	47 ↑
M_{ip}	6 ↑	15 ↑	33 ↑	3 ↑	2 ↑	15 ↑
F_r	143 ↑	93 ↑	136 ↑	22 ↑	8 ↓	19 ↑
M_r	126 ↑	82 ↑	136 ↑	37 ↑	3 ↓	4 ↑
M_{tt}	114 ↑	116 ↑	125 ↑	5 ↑	53 ↑	65 ↑
M_{tb}	148 ↑	97 ↑	146 ↑	41 ↑	7 ↓	25 ↑

Table 3.15: Overall turbulence detectability matrix. A change in the overall turbulence intensity from 5 to 25 % has been considered.

Signal	Statistical parameters							Sum
	$\bar{X}$	$Var(X)$	γ_3	γ_4	λ_1	λ_2	ΔS_{max}	
Ω_{gen}	↑↓ −	↑↑↑			↑↑↑	↑↑↑	↑↑↑	
$\dot{\Omega}_{gen}$		↑↑↑		↑↓ −	↑↑↑	↑↑↑	↑↑↑	
P_{el}	↑↓↓	↑↑ −	− ↓↓	− ↓↑	↑↑↑	− ↑↑	↑↑↑	
θ_P	− ↑↓	− ↑↑			− ↑↑	− ↑↑	− ↑↑	
$\ddot{y}_{tt}$		↑↑↑	↑ − ↑	↑↓ −	↑↑↑	↑↑↑	↑↑↑	
$\ddot{z}_{tt}$		↑↑↑	↓↑↓		↑↑↑	↑↑↑	↑↑↑	
Sum								

If a variation in turbulence intensity has such a huge influence on the general turbine loading, effects on standard signals can be expected. This is confirmed by the detectability matrix (Table 3.15). Most quantities fulfil the criteria of Equation 3.1. Therefore, detection of turbulence intensity variations from standard signals seems to be possible. A simple neural network based detection experiment is described in Chapter 4 and confirms this assumption.

From the above it can be concluded, that the overall turbulence intensity level

- has got a very strong influence on all fatigue loads.
- clearly affects all of the analysed statistical parameters of standard signals.

3.3.2 Lateral and vertical turbulence intensity

In the preceding investigation, longitudinal, lateral and vertical turbulence intensities where changed at the same time to maintain their ratios. Now the lateral and the vertical standard deviations are modified separately, to asses their influence on the equivalent loads and standard signals.

Unfortunately, reports with measured three dimensional turbulence intensities are rare. This makes it difficult to chose appropriate values for this investigation. Nelson et al. [34] published some statistics of the inflow parameters at a wind turbine test site. In average, the lateral and vertical turbulence was found to be 85 % and 54 % of the longitudinal. For a complex terrain site, Mouzakis et al. [53] found average values of 0.82 to 0.98 for the lateral and 0.67 to 0.78 for the vertical ratios. In addition, standard deviations of these ratios from 0.13 to 0.21 and 0.09 to 0.15 were recorded.

The IEC 61400-1 standard [16] requires the minimum lateral and vertical standard deviations to be 70 % and 50 % of the longitudinal one. An informative Annex of [16] recommends to use 80 % and 50 % in conjunction with the Kaimal turbulence model applied here. For sites with complex terrain, equal standard deviations for all directions are suggested.

In this study, variations in the turbulence ratios of 0.6 to 1.0 (lateral) and 0.3 to 0.7 (vertical) have been investigated. Although these variations seem to be large, the influence on the equivalent loads is quite small. This confirms findings by Larsen [54], where similar results from numerical investigation with a validated simulation model of a Vestas V39 turbine [55] were reported.

It also seems, that the ratios of turbulence can not be easily recovered by an analysis of standard signals. However, as the influence on the loading is probably negligible, detectability is not required. From the above it can therefore be concluded, that under the assumed baseline conditions the lateral and vertical wind speed fluctuations

- have got a rather small influence on all fatigue loads.
- can not be easily detected from the analysis of standard signals.

3.3.3 Integral length scale

The integral length scale is related to the average spacial gust length. Measurements show, that it depends at least on the surface roughness and the measurement height above ground (see Counihan [56]). Frandsen et al. [57] also reported a proportionality to wind speed which has been observed at a wind turbine test site in Denmark.

Table 3.16: Variation of equivalent loads in percentage of a baseline case. A change in the lateral turbulence intensity from 9 to 15 % has been considered, with 12 % as baseline.

Load	Equiv. range			Equiv. magnitude		
	6 m/s	12 m/s	18 m/s	6 m/s	12 m/s	18 m/s
M_{op}	1 ↑	2 ↑	2 ↑	1 ↑	0	0
M_{ip}	0	0	0	0	0	0
F_r	1 ↑	2 ↑	1 ↑	0	0	0
M_r	2 ↑	1 ↓	2 ↑	1 ↑	0	0
M_{tt}	1 ↑	1 ↑	3 ↑	0	0	2 ↑
M_{tb}	0 ↑	1 ↑	1 ↑	1 ↑	0	0

Table 3.17: Lateral turbulence detectability matrix. A change in the lateral turbulence intensity from 9 to 15 % has been considered.

Signal	Statistical parameters							Sum
	$\bar{X}$	$Var(X)$	γ_3	γ_4	λ_1	λ_2	ΔS_{max}	
Ω_{gen}								
$\dot{\Omega}_{gen}$								
P_{el}								
θ_P								
$\ddot{y}_{tt}$					$--\uparrow$	$--\uparrow$		
$\ddot{z}_{tt}$								
Sum								

According to Counihan [56], typical average length scales at heights of relevance for modern wind turbines and rural, flat terrain seem to be in the order of 200 m. Frandsen et al. [57] calculated wind speed and height dependent variations from about 150 to 400 m, where the influence of wind speed was much stronger than the one of the measurement height. Wind speeds from 6 to 15 m/s were investigated.

The wind speed dependency is less pronounced for three sites investigated by Veldkamp [28]. Only for the Horns Rev site a significant increase at wind speeds larger than 15 m/s was observed. For most of the other wind speeds and sites, fairly constant values of about 200 m have been calculated.

The general variability in length scale becomes obvious from Petersen et al. [44]. Here, a probability plot of length scales for the Vindeby site shows noticeable occur-

Table 3.18: Variation of equivalent loads in percentage of a baseline case. A change in the vertical turbulence intensity from 4.5 to 10.5 % has been considered, with 7.5 % as baseline.

Load	Equiv. range			Equiv. magnitude		
	6 m/s	12 m/s	18 m/s	6 m/s	12 m/s	18 m/s
M_{op}	1	0	0	0	0	0
M_{ip}	0	0	0	0	0	0
F_r	1 ↑	0	1 ↑	0	0	0
M_r	1 ↑	1 ↓	2 ↑	0	0	0
M_{tt}	1 ↑	1 ↑	1 ↑	0	0	0
M_{tb}	0 ↓	1 ↑	1 ↑	0	0	0

Table 3.19: Vertical turbulence detectability matrix. A change in the vertical turbulence intensity from 4.5 to 10.5 % has been considered.

Signal	Statistical parameters							Sum
	$\bar{X}$	$Var(X)$	γ_3	γ_4	λ_1	λ_2	ΔS_{max}	
Ω_{gen}								
$\dot{\Omega}_{gen}$								
P_{el}								
θ_P								
$\ddot{y}_{tt}$						$--\uparrow$		
$\ddot{z}_{tt}$								
Sum								

rence probabilities of values from below 100 m to more than 2 km. The large variation is confirmed by the author's own investigations for two coastal sites in Germany and the Netherlands, presented in Annex G. Average lengths of about 300 to 350 m have been found, with variations from about 50 to more than 4000 m.

Wake conditions tend to reduce the length scale compared to free stream conditions. Frandsen and Madsen [47] and Vermeer et al. [58] summarise several investigations. In one publication, a reduction to half of the free stream value in a distance of 4 rotor diameters behind the turbine is reported. In the near wake, even larger reductions up to 20 % of the free stream scale seem to be likely.

The integral length scale is also input to many turbulence models, where it is an

Table 3.20: Variation of equivalent loads in percentage of a baseline case. A change in integral length scale from 170 m to 680 m has been considered, with 340 m as baseline.

Load	Equiv. range			Equiv. magnitude		
	6 m/s	12 m/s	18 m/s	6 m/s	12 m/s	18 m/s
M_{op}	3 ↓	12 ↓	11 ↓	2 ↑	2 ↓	0
M_{ip}	1 ↓	3 ↓	4 ↓	0	1 ↓	1 ↓
F_r	3 ↑	15 ↓	17 ↓	2 ↑	1 ↓	0 ↓
M_r	3 ↓	11 ↓	30 ↓	3 ↑	1 ↓	1 ↓
M_{tt}	12 ↓	18 ↓	17 ↓	0 ↓	4 ↓	6 ↓
M_{tb}	1 ↓	19 ↓	29 ↓	4 ↑	2 ↓	2 ↓

Table 3.21: Integral length scale detectability matrix. A change in integral length scale from 170 m to 680 m has been considered.

Signal	Statistical parameters							Sum
	$\bar{X}$	$Var(X)$	γ_3	γ_4	λ_1	λ_2	ΔS_{max}	
Ω_{gen}		$--\downarrow$			$--\downarrow$	$-\downarrow\downarrow$		
$\dot{\Omega}_{gen}$		$\downarrow\downarrow\downarrow$			$\downarrow\downarrow\downarrow$	$\downarrow\downarrow\downarrow$	$--\downarrow$	
P_{el}		$--\downarrow$			$--\downarrow$	$--\downarrow$		
θ_P					$-\downarrow-$			
$\ddot{y}_{tt}$		$\downarrow\downarrow\downarrow$			$\downarrow\downarrow\downarrow$	$\downarrow\downarrow\downarrow$	$-\downarrow\downarrow$	
$\ddot{z}_{tt}$		$\downarrow\downarrow\downarrow$			$\downarrow\downarrow\downarrow$	$\downarrow\downarrow\downarrow$	$\downarrow-\downarrow$	
Sum								

important parameter for the definition of the power spectral density of wind speed. Increasing the length scale shifts energy to lower frequencies and hence increases the probability of low frequency gusts. The IEC 61400-1 standard recommends to apply a constant value of 340 m for the Kaimal turbulence model at all wind speeds.

Table 3.20 summarises the calculated equivalent loads. A change in length scale from 170 to 680 m has been applied which corresponds to halve and to twice the suggested value of 340 m from the standard. All equivalent ranges decrease with increasing length scale. This seems reasonable, as the average gust length is increased and hence the frequency of gust driven load cycles is reduced. The length scale has got a great influence on the equivalent ranges especially for rated and above rated

turbine operation.

Similar results have been derived by Larsen [54] for the blade root bending moments, the rotor torque and the tower base bending moment. This also holds true for the increase of the effects from length scale with increasing wind speed.

At the same time it can be noted, that only acceleration signals are suited for the detection of length scale related disturbances in all operational states. Pitch angle, electrical power and generator speed are most strongly affected in the above rated range.

In general it can be concluded, that under the assumed baseline conditions the integral length scale of turbulence

- has got a noticeable to strong influence on fatigue loads, especially for equivalent ranges at above rated wind turbine operation.
- can potentially be detected from the analysis of standard signals.

Because of the obvious importance of length scale detection for fatigue load estimations, more investigations have been performed and are discussed in Annex G. This includes possibilities for the calculation of length scales from measured data as well as the attempt to define related statistical parameters which can potentially improve the prediction of length scale magnitudes from standard signals.

3.3.4 Spatial coherence decay

Modelling of turbulent wind fields includes the spatial variation of wind speed fluctuations. For this purpose, cross-correlation functions between points in the wind field are required. They account for the fact, that the correlation between wind speeds in two points decreases with increasing distance and with increasing frequency of the wind speed oscillations. To model these effects, so-called coherence functions are defined which are frequently simple exponential functions. As an example, the coherence function recommended by IEC 61400-1 standard for the longitudinal velocity component of the Kaimal turbulence model is defined by

$$Coh(r, f) = exp[-12 \cdot ((f \cdot r/U)^2 + (0.12 \cdot r/L_c)^2)^{0.5}] \tag{3.7}$$

Besides on frequency f and distance r, in this formula the coherence also depends on wind speed U and a coherence length scale parameter L_c. The coherence decay parameter is specified at 12 and the length scale influence factor at 0.12. In a previous version of the standard, the decay parameter was given at 8.8.

If the length scale influence factor is set to zero, the IEC formulation equals the widely used Davenport model. For this model, the decay parameter can be roughly estimated from $a = 12 + 11r/h_{ave}$, where h_{ave} is the averaged height of the two points in space and r their spatial separation.

Saranyasoontorn et al. [59] confirmed the general suitability of the IEC formulation to model the cross-correlation for a test site. Fitting the model to measured data, decay and scale parameter have been found to be 9.7 and 0.13 for lateral separations and 9.7 and 0.06 for vertical separations. They also reported that the decay parameter increases, if large separations are fitted. This means that the coherence at the analysed site in fact decays faster than what the IEC model predicts. The tendency of relatively slow decay of the IEC model compared to measurements is also confirmed from investigations performed by Larsen and Hansen [60].

Besides the IEC coherence model, Saranyasoontorn et al. also fitted the Davenport model to the measured wind data and computed decay parameters in the order of 2 to 2.5 times larger than for the fitted IEC model. Similar to the IEC model, the decay of the Davenport model also underestimates the real decay. When the decay parameters of the Davenport model are calculated from the above formula, the results are by a factor of 1.3 to 1.8 (depending on the separation) lower than what has been fitted by Saranyasoontorn et al..

Hojstrup [61] investigated the coherence in the wake of wind turbines and found, that it is only very little or even not at all affected by wake. Furthermore, the simple Davenport model was able to adequately describe the cross-correlations, except in the near wake.

In general, only very few reports on measured coherences have been found. Because different models are in use, the estimated decay parameters in these reports are difficult to compare. Therefore, in the present sensitivity study the decay parameter of the IEC model has been decreased somewhat arbitrarily from 12 to 8.8 (the value given in the outdated version of the standard) and increased by the same amount to 15.2. This is probably a reasonable assumption for typical variations in coherence decay, although larger variations are presumably possible in complex terrain. The scale parameter has been kept constant.

For these variations, the influence of the spatial coherence decay of turbulence on equivalent loads seems to be less than that of the integral length scale. The largest deviations are visible in the equivalent ranges of the rotor thrust and consequently also

Table 3.22: Variation of equivalent loads in percentage of a baseline case. An increase in the spatial coherence decay parameter from 8.8 to 15.2 has been considered, with 12 as baseline.

Load	Equiv. range			Equiv. magnitude		
	6 m/s	12 m/s	18 m/s	6 m/s	12 m/s	18 m/s
M_{op}	4 ↓	2 ↓	0	2 ↓	0	2 ↓
M_{ip}	0	1 ↑	2 ↑	0	1 ↑	1 ↑
F_r	12 ↓	10 ↓	12 ↓	2 ↓	0	3 ↓
M_r	9 ↓	4 ↓	5 ↑	2 ↓	0	0
M_{tt}	6 ↑	4 ↑	4 ↑	0	3 ↑	3 ↑
M_{tb}	15 ↓	18 ↓	28 ↓	3 ↓	0	6 ↓

Table 3.23: Spatial coherence decay detectability matrix. An increase in the spatial coherence decay parameter from 8.8 to 15.2 has been considered.

Signal	Statistical parameters							Sum
	$\bar{X}$	$Var(X)$	γ_3	γ_4	λ_1	λ_2	ΔS_{max}	
Ω_{gen}		$--\downarrow$			$--\downarrow$	$--\uparrow$		
$\dot{\Omega}_{gen}$		$--\uparrow$			$--\uparrow$	$--\uparrow$		
P_{el}		$--\downarrow$				$--\uparrow$	$--\downarrow$	
θ_P					$-\downarrow\downarrow$			
$\ddot{y}_{tt}$					$\uparrow\uparrow\uparrow$	$\uparrow\uparrow\uparrow$		
$\ddot{z}_{tt}$	$\uparrow --$				$\uparrow\uparrow -$	$\uparrow\uparrow\uparrow$		
Sum								

for the tower base bending moment. These loads decrease with larger decay parameters which can be explained by the smaller lateral and vertical size of the turbulent eddies. When integrating over the whole rotor plane, the flow conditions are more homogeneous and hence the occurrence probability for large load ranges reduces. For simulations of a Vestas V39 turbine [54] it was also found, that the influence of coherence decay variations is strongest for the tower base bending moments. A decrease by almost 10 % for a change in decay parameters from 5 to 7 was calculated.

Each standard signal is affected by the variation in coherence decay. The longitudinal and lateral tower top accelerations are influenced most. Coherence variations manifests themselves in particular in parameters related to the frequency content of a signal, such as the spectral moments.

It can be concluded, that under the assumed conditions the coherence decay

- has got a noticeable influence on fatigue loads, especially for equivalent ranges of the rotor thrust and the tower base bending moment.
- can potentially be detected from the analysis of standard signals.

3.4 Turbine properties

3.4.1 Rotor mass imbalance

It should be clear, that no real wind turbine rotor is exactly balanced. Imbalances result mainly from inevitable production tolerances, where those of the blades have probably got the largest share on the total rotor imbalance. As it is very challenging to push production tolerances below some limits, another approach is often applied: after production, the blades are sorted into different categories, according to their mass and balance point. The rotor of a wind turbine is then assembled only from balanced blades out of the same category. This can obviously reduce the imbalance significantly below what can be expected from the allowed production tolerances.

It is difficult to estimate an order of magnitude for common imbalances, because this data is usually not published. One company which has focused on the removal of rotor imbalances is Deutsche WindGuard Dynamics GmbH. In an article [62] they recommend to take action, if the rotor's centre of gravity is off the rotor axis by more than 0.5 % of the rotor radius. They also state, that significant imbalances on about 20 % of the investigated turbines have been found. Assuming, that these are not all mass imbalances and also, that companies like WindGuard are called mainly if the turbine owner is already suspicious of imbalances, the real number of turbines operating with a severe mass imbalance is probably much lower than 20 %.

Environmental conditions can lead to rotor imbalances as well. Examples are the aggregation of moisture in the blade laminate or icing in cold climate. From the DIBt standard [63], the total ice aggregation on a rotor blade of the simulated 1.5 MW turbine has been estimated to about 6 % of the normal blade mass. Because it has to be assumed, that the ice is distributed unevenly along the blade, the static moment increases by approximately 10 %. In the worst case of having two iced and one clear blade, the total rotor mass eccentricity adds up to about 6 %.

Although icing can have a significant impact on loads and standard signals of wind turbines (see Volund and Antoniou [64] or Frohboese and Anders [65]), such situations are not considered here. Icing is not a major problem for the majority of turbines.

Because of the climatic conditions on most sites, significant icing is relatively unlikely for most of the operational time. Furthermore, manufacturers usually claim to have suitable methods for ice detection and that their turbines will shut down in such cases.

In this investigation, the mass of a single rotor blade was increased to yield a rotor eccentricity of 0.5 %. The additional mass is distributed evenly along the blade and hence the blade mass had to be increased by 1.5 %. It was found, that the investigated equivalent loads are relatively inured to the applied imbalance, except of the equivalent ranges of the longitudinal tower base bending moment around rated.

The imbalance gives mainly additional cyclic loads in lateral direction of course and thus the lateral shear forces at tower top or the lateral tower base bending moment are much more affected than those load components shown in Table 3.24. In this case, an increase in the lateral tower base bending moment (not listed in Table 3.24) of about 20 % in below rated operation and 75 % in above rated operation has been estimated from the performed simulations. In general, the influence of a rotating imbalance on loads also depends on the dynamic properties of the support structure. Here, the frequency of rotation at rated speed is quite close to the first eigenfrequency of the tower which explains the very large effect of the mass imbalance on the lateral tower base bending moment. These loads couple back in the longitudinal direction, partly directly through structural dynamics but also indirectly through the dynamic turbine control.

It is well known, that acceleration measurements can be used to detect imbalances [66]. This is confirmed by the performed analysis of standard signals. However, in the below rated range, the lateral acceleration is classified as less suited. Because of the variable-speed operation, the accelerations from mass imbalance are superimposed by other more dominating effects and an order analysis would be required to detect imbalances in this operational range.

An automated detection of imbalances from installed sensors seems to be feasible and should be performed before the load estimation system is initialised. If imbalances are detected, further investigations with additional sensors are probably required for more exact diagnosis and measures for reduction of the imbalance have to be taken.

For the analysed conditions it can be concluded, that mass imbalances

- are of minor importance for the analysed loads, but significant effects might occur for non investigated load components.
- can be detected from the acceleration signals at tower top, although lateral and longitudinal acceleration measurements probably do not allow for an exact diag-

Table 3.24: Variation of equivalent loads in percentage of a baseline case. A change of mass imbalance on a single blade from 0 to 1.5 % has been considered, with 0 % as baseline.

Load	Equiv. range			Equiv. magnitude		
	6 m/s	12 m/s	18 m/s	6 m/s	12 m/s	18 m/s
M_{op}	0	0	0	0	0	0
M_{ip}	1	2 ↑	2 ↑	1 ↑	1 ↑	1 ↑
F_r	0	1 ↑	1 ↑	0	0	0
M_r	0	1 ↑	0	0	0	0
M_{tt}	0	0	0	0	0	0
M_{tb}	0	10 ↑	3 ↑	0	1 ↑	0

Table 3.25: Mass imbalance detectability matrix. A change of mass imbalance on a single blade from 0 to 1.5 % has been considered.

Signal	Statistical parameters							Sum
	$\bar{X}$	$Var(X)$	γ_3	γ_4	λ_1	λ_2	ΔS_{max}	
Ω_{gen}								
$\dot{\Omega}_{gen}$								
P_{el}								
θ_P								
$\ddot{y}_{tt}$		$-\uparrow\uparrow$			$-\uparrow\uparrow$		$-\uparrow\uparrow$	
$\ddot{z}_{tt}$		$-\uparrow-$			$-\uparrow-$			
Sum								

nosis and classification of the type of imbalance. Detected imbalances should be reduced before the load monitoring begins.

3.4.2 Rotor aerodynamic imbalance

Liersch et al. [67] pointed out, that many rotor imbalances are in fact combinations of aerodynamic and mass imbalances. Besides imperfections on the blade surface, errors in twist or pitch angle are probably the only significant imbalances which can trigger purely aerodynamic imbalances. In practice, the main sources of imbalances are probably pitch angle errors related to improperly positioned blades at the turbine or imprecisely placed reference marks at the blade. Similar to mass imbalances, there

Table 3.26: Variation of equivalent loads in percentage of a baseline case. A change in pitch angle offset on a single blade from 0 to 1 ° has been considered, with 0 ° as baseline.

Load	Equiv. range			Equiv. magnitude		
	6 m/s	12 m/s	18 m/s	6 m/s	12 m/s	18 m/s
M_{op}	3 ↓	1 ↓	3 ↑	8 ↓	7 ↓	8 ↓
M_{ip}	0	1 ↓	0 ↑	1 ↓	3 ↓	5 ↓
F_r	1 ↓	0	3 ↑	2 ↓	1 ↓	0
M_t	2 ↑	2 ↑	1 ↑	0	0	0
M_{tt}	17 ↑	15 ↑	9 ↑	1 ↑	4 ↑	3 ↑
M_{tb}	1 ↑	12 ↑	14 ↑	2 ↓	0	2 ↑

Table 3.27: Aerodynamic imbalance detectability matrix. A change in pitch angle offset on a single blade from 0 to 1 ° has been considered.

Signal	Statistical parameters							Sum
	$\bar{X}$	$Var(X)$	γ_3	γ_4	λ_1	λ_2	ΔS_{max}	
Ω_{gen}								
$\dot{\Omega}_{gen}$								
P_{el}								
θ_P								
$\ddot{y}_{tt}$		$-\uparrow\uparrow$			$--\uparrow$		$-\uparrow\uparrow$	
$\ddot{z}_{tt}$		$-\uparrow\uparrow$			$-\uparrow-$			
Sum								

are also methods for the detection of such offsets available. One often used approach is based on photogrammetry for example, where picture series of all three blades are taken from the ground [62].

The Germanischer Lloyd [12] recommends to assume a total pitch offset of +/- 0.3 ° if no verified tolerances are available. The deviation should be applied at two blades simultaneously, for example by setting blade one to 0 °, blade two to -0.3 ° and blade three to +0.3 °. Hence, a total aerodynamic imbalance of 0.6 ° is present at the rotor. Unfortunately, no information on common pitch imbalances on real wind turbines have been found in literature. It has therefore been decided, to assume slightly larger values than those recommended by the Germanischer Lloyd for this study and offsets of up to 1 ° have been investigated. For simplicity, the whole imbalance was applied to one

blade only.

Contrary to the mass imbalance, the pitch offset also leads to periodic load cycles in the longitudinal direction. This results in an increased equivalent range for the tower top nodding moment. As the rated rotational frequency is quite close to the tower's first eigenfrequency, the effect on the tower base bending moment is also quite large. The impact on the equivalent magnitudes is moderate, with the largest variations occurring for the out-of-plane blade root bending moment of the imbalanced blade itself.

The detectability of aerodynamic imbalances can be rated similar to the ones from mass imbalances. Analysis of longitudinal and lateral accelerations seem to be well suited for this purpose. For the analysed conditions it can be concluded, that significant aerodynamic imbalances

- affect the nodding and blade root equivalent moments especially. Tower base moments are also influenced, depending on the structural dynamic turbine properties.
- can be detected from the acceleration signals at tower top, although lateral and longitudinal acceleration measurements do not probably allow for an exact diagnosis and classification of the type of imbalance. Detected imbalances should be reduced before the load monitoring begins.

3.4.3 Soil and foundation stiffness

For site specific assessments, certification institutions like the Germanischer Lloyd or the Det Norske Veritas require verifications to prove that the actual site conditions are more benign than those assumed for the turbine design (see [12] and [11]). This also involves the soil conditions to ensure compliance with the minimum requirements.

Variations in soil stiffness can influence the dynamic response of the wind turbine. This manifests itself not only in the tower's frequencies of oscillations but also in those of drive train and rotor. Therefore, this investigation can also be regarded as a general sensitivity study related to changes in the structural dynamic properties of the turbine.

Here, the foundation stiffness was increased from $3{\cdot}10^7$ kNm/rad (soft) to $7{\cdot}10^7$ kNm/rad (stiff). This gave the variations in frequencies of oscillation listed in Table 3.30. As expected, the largest deviations of eigenfrequencies were calculated for the first and second tower modes (about 5 to 6 %), but other modes are affected slightly as well.

Reducing the foundation stiffness to the minimum value moves the first tower eigenfrequency quite close to the first rotary excitation frequency of the rotor (the 1P fre-

Table 3.28: Variation of equivalent loads in percentage of a baseline case. A stiffness change from $3{\cdot}10^7$ to $7{\cdot}10^7$ kNm/rad has been considered, with $5{\cdot}10^7$ kNm/rad as baseline.

Load	Equiv. range			Equiv. magnitude		
	6 m/s	12 m/s	18 m/s	6 m/s	12 m/s	18 m/s
M_{op}	0	0	0	0	0	0
M_{ip}	0	0	0	0	0	0
F_r	0	1 $\downarrow$	0	0	0	0
M_r	1 $\downarrow$	2 $\uparrow$	1 $\downarrow$	0	0	0
M_{tt}	0	0	0	0	0	0
M_{tb}	0 $\uparrow$	2 $\uparrow$	1 $\downarrow$	0	0	0

Table 3.29: Soil and foundation stiffness detectability matrix. A stiffness change from $3{\cdot}10^7$ to $7{\cdot}10^7$ kNm/rad has been considered.

Signal	Statistical parameters							Sum
	$\bar{X}$	$Var(X)$	γ_3	γ_4	λ_1	λ_2	ΔS_{max}	
Ω_{gen}								
$\dot{\Omega}_{gen}$								
P_{el}								
θ_P								
$\ddot{y}_{tt}$					$--\uparrow$	$--\uparrow$		
$\ddot{z}_{tt}$								
Sum								

Table 3.30: Variation in coupled eigenfrequencies due to variation of foundation stiffness

Mode description	Frequency [Hz] soft	Frequency [Hz] stiff	Δ [%]
Tower 1st longitudinal	0.35	0.37	5.7
Tower 1st lateral	0.35	0.37	5.7
Shaft torsion, tower 2nd lateral and rotor 1st edgewise (asymmetric)	2.30	2.36	2.6
Tower 2nd longitudinal	2.42	2.53	4.5
Shaft torsion, tower torsion, tower 2nd lateral and rotor 1st edgewise (symmetric)	2.67	2.72	1.9

quency) at rated speed. With 0.35 Hz, it is only about 3 % higher than the 1P. Nevertheless, the effect on equivalent loads is almost not noticeable. This probably results from the fact that the simulated rotor is free of imbalances, something which is a very rare case in reality.

Regarding the loads, the turbine seems to be relatively robust against smaller variations of its dynamic properties. This holds also true for most of the analysed statistical parameters, but unfortunately not for all. The spectral moments of the tower top accelerations show a significant impact. This can potentially be a source for problems. If for example, an important role would be allocated to these parameters within a load monitoring system, frequency variations might become relevant aspects in terms of the accuracy of the monitoring procedure.

For the analysed conditions it can be concluded that significant variations in foundation stiffness, which also induce small changes of the dynamic properties of the wind turbine,

- do not effect the equivalent loads, as long as this does not give rise to resonances.
- are capable of influencing frequency related statistical parameters of standard signals.

3.5 Summary and conclusions for a load estimation system

It is the scope of this chapter to analyse the influence of disturbances on wind turbine fatigue loads. At the same time the potential detectability of the disturbances from standard signals is evaluated. Important findings are summarised below and general conclusions regarding a load estimation system are drawn.

3.5.1 Influence of disturbances on fatigue loads

The investigations in this chapter emphasise, that wind turbines are potentially subjected to many disturbances. Because the nature of disturbances can be fundamentally different, their impact on wind turbine loads is multifaceted. This makes it hard to draw general conclusions in terms of fatigue loads from the above analysis. Nevertheless, in the author's opinion a few statements can be made:

- Typically the variation in 10 minute mean wind speed at sites is large and therefore its impact on fatigue loads is most important.
- The turbulence intensity in longitudinal direction plays an important role as well. Considering typical variations at a site, its effect on fatigue loads is quite pronounced. This makes it the second most influencing variable which has also been confirmed by other authors (see for example [34]).
- Contrary, the lateral and vertical turbulence intensity seem to be the least important inflow parameters for the above analysed load components.

Further evaluation and ranking of disturbances with respect to fatigue loads is difficult. Investigations in this chapter already show that the pure amount of possible disturbances makes the matter quite complex and that many aspects have to be considered. However, a load estimation system has to cope with the same problems exactly which prevent the author from pointing out more general conclusions than the above. Because they have implications of course on a load estimation system, some of the main difficulties are stated below:

- The influence of disturbances depends on the turbine characteristics. For some variations in characteristics, the disturbance-load relations will probably change significantly.
- Ranking disturbances has to also take into account the joint occurrence probability of their magnitude and the operational state of the turbine.
- The impact of a disturbance is always relative and depends on the general conditions: its influence on fatigue loads might be unimportant for very turbulent sites, while it increases significantly in less turbulent conditions.
- Combinations of disturbances, as for example investigated in [33, 37, 52, 38], will also alter their influence on fatigue loads. They might amplify or reduce each others effects.

At the end it should also be pointed out, that the numerical results in this study coincide well with findings from other authors, regardless if these have been derived from simulated or measured data. This indicates, that the simulations are able to capture the effect of disturbances (at least when relative deviations are analysed) and that the applied model reasonably reflects average wind turbine properties.

3.5.2 Detectability of disturbances

From the above analysis it seems, that disturbances with a strong influence on fatigue loads also leave their footprints in wind turbine standard signals. And vice versa, it can be concluded, that unimportant disturbances (in terms of loads) do not affect standard signals significantly in most cases.

However, there can be exceptions to these rules for example as in the case of the out-of-plane blade root bending moment and vertically inclined inflow. Another example are changes of the dynamic properties of the turbine caused by variations in soil and foundation stiffness. Here, the fatigue loads remain essentially unaffected, while statistical parameters vary.

It is obvious, that statistical parameters which are dominated by a certain disturbance and influenced only very little by others can potentially simplify the identification a lot. Unfortunately this is hardly the case. The investigations above emphasise, that disturbances always tend to influence several standard signals and statistical parameters at a time. This poses additional challenges, because the presence and magnitude of a disturbance can not be deduced from a single value in general. Instead, a pattern recognition approach is required which identifies the current environmental conditions from a number of input parameters for example.

When disturbances can not be detected directly, correlations with other better detectable conditions can be exploited (see remarks on atmospherically driven wind shear). If such correlations do not exist, application of further measures, like the estimation of average conditions based on terrain features (for vertically inclined flows), additional campaigns (for the detection and removal of rotor imbalances) or, finally, the installation of additional sensors can be a solution. A rough scheme for the assessment of disturbance detectability which incorporates these considerations is illustrated in Figure 3.4.

3.5.3 Consequences for a load estimation system

For the design of a load estimation system, the influence of disturbances on loads and measured signals has to be analysed first. The reason for this twofold: Most important disturbances in terms of fatigue loads have to be identified and their influence on the standard signals has to be assessed. It is a requirement for a load estimation system, that the disturbances leave a trace in the standard signals. If an important disturbance does not influence any standard signals, its impact on loads can not be incorporated into the estimation and the estimation result is probably subjected to larger errors. This

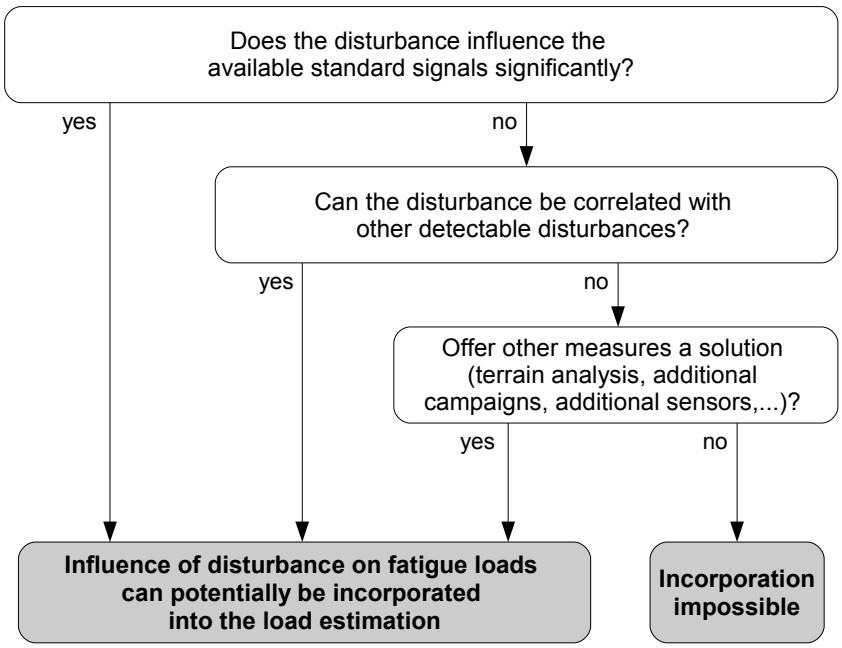

Figure 3.4: Scheme for the assessment of disturbance detectability

analysis has to be carried out for each load component of interest.

Obviously, results from such an investigation are only valid for a specific wind turbine type. Figure 3.5 illustrates that turbine characteristics, likely disturbances and desired estimation targets (the load quantities) are important design drivers for a load estimation system. As a consequence, such a system will be highly customized to specific applications.

Despite the turbine specific design considerations, the exemplary analysis for the fictitious 1.5 MW wind turbine on the basis of simulations revealed several important aspects and potential challenges for a load estimation system:

- It is very likely, that disturbances which have a significant influence on loads also affect standard signals. Hence, there are chances to incorporate corresponding relations into suitable transfer functions. In cases, where statistical parameters of standard signals are not influenced much, workarounds based on terrain analysis or cross-correlations between disturbances are potential solutions.

- Many disturbances are capable of producing significant load variations, but their effect differs with respect to the turbine state (and the operational region). Furthermore, they interfere with each other when several disturbances are present at the same time (a very likely scenario). Thus the required relations between

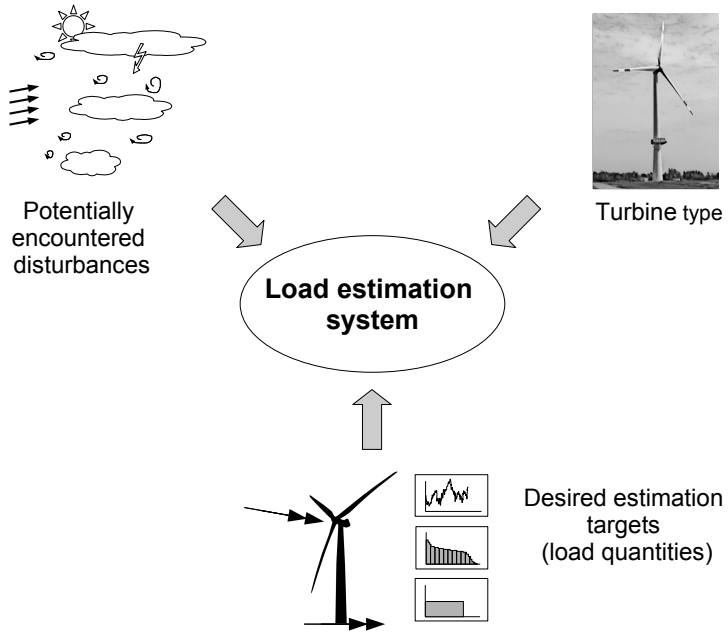

Figure 3.5: Basic design drivers for a load estimation system

fatigue loads and statistical parameters of standard signals are potentially rather complex.

- In theory an endless number of possibilities for combining environmental conditions of different magnitude exist. Even if correlations between them are assumed there are still many cases which have to be investigated. Finding relations between loads and standard signals therefore requires the analysis of large amounts of simulated or measured data.

- It can be expected, that a load estimation system will work better for a single turbine at a flat site than in complex terrains or wind farms. This is because the correlation of disturbances is at least partially removed by the influence of terrain features or surrounding turbines. In addition, in complex terrain the average disturbance magnitudes are much harder to estimate from preceding site analysis. Their larger variability also impose further challenges. Specialised prediction systems which are designed for certain conditions (wake, complex terrain, offshore, etc.) might be required.

4 From standard signals to loads - Evaluation of transfer functions

For the estimation of wind turbine loads, suitable transfer functions have to be available. These functions need to relate information contained in the standard signals to fatigue loads. In this context, the term 'functions' is used in a rather broad sense, including not only traditional mathematical equations, but any method to relate data.

Four different approaches have been analysed and compared to asses their suitability for the prediction of wind turbine loads. These are *classical regression methods*, *neural networks*, *physical model based approaches* and *state estimators*. Because regression models and neural networks seem to be particularly suited for this task, special focus is given to these two methods in the analysis below. While their capabilities are also tested on practical examples, physics-based approaches and state estimators are assessed on the basis of a literature survey and theoretical considerations only.

4.1 Regression techniques

4.1.1 Overview on regression techniques

Regression techniques are widely used in many different fields. They are generally employed to establish relations between data, if the underlying process is unknown or very complicated to describe otherwise. In these cases the most important features of the process are approximated by a statistically valid model which is not based on known mechanical or physical laws [68]. Once such a model has been established it can also be used to predict a response variable from one or more explanatory variables.

In the simplest case the response variable (often also denoted as dependent variable, predictand or target) is estimated from a single explanatory variable (called independent variable, predictor or input) assuming a linear relation:

$$Y = b_0 + b_1 \cdot X \tag{4.1}$$

where Y is the the response, X is the explanatory variable and b_0 and b_1 are the

regression coefficients. Because the regression coefficients are unknown in general, they have to be estimated from a number of n experimental data points using a least squares fitting procedure for example. Thereby the regression coefficients are altered in an iterative manner to yield a global minimum for the sum of the squared estimation errors E_i^2 from the estimations $\hat{Y}_i$

$$\sum_{i=1}^{n} E_i^2 = \sum_{i=1}^{n} (Y_i - \hat{Y}_i)^2 \tag{4.2}$$

The estimated regression coefficients $\hat{b}_0$ and $\hat{b}_1$ can then be used to predict the response values $\hat{Y}_i$ from the explanatory variables X_i:

$$\hat{Y}_i = \hat{b}_0 + \hat{b}_1 \cdot X_i \tag{4.3}$$

Commonly, the remaining errors of the regression are also denoted as residuals. Equation 4.3 is referred to as the regression function and can be interpreted as a transfer function which maps the input to the target values.

For of a load estimation system, a statistical parameter of a standard signal could be a possible input, while an equivalent load might be chosen as target. But very likely, more than just one input variable would be required to yield reasonable prediction results. In such a case, regression models can be extended to include multiple explanatory variables. A multiple regression model using k inputs is defined by

$$\hat{Y}_i = \hat{b}_0 + \hat{b}_1 \cdot X_{i,1} + \hat{b}_2 \cdot X_{i,2} + \hat{b}_3 \cdot X_{i,3} + \ldots + \hat{b}_k \cdot X_{i,k} \tag{4.4}$$

Although almost any non-linear problem can be linearised over a small enough region, sometimes linear relations are not sufficient any more to build a suitable statistical model. This is probably also the case for a wind turbine load estimation application.

For strongly non-linear problems two approaches are usually applied: use of higher order polynomial functions or linearisation by transfer functions. In both cases the regression model still consists of a linear combination of regression coefficients. Despite the fact that the response variable depends in a non-linear way on the explanatory variables, the regression model itself is therefore still considered to be linear.

In the first approach the linear regression function is replaced by a higher order polynomial, whose coefficients are again determined by a least squares fitting procedure. Explanatory variables enter the regression model several times with different regression coefficients and exponents:

$$\hat{Y}_i = \hat{b}_0 + \hat{b}_1 \cdot X_i + \hat{b}_2 \cdot X_i^2 + \hat{b}_3 \cdot X_i^3 + \ldots + \hat{b}_k \cdot X_i^k \tag{4.5}$$

In the second approach, suitable transfer functions are used to linearise the explanatory variables with respect to the response. In doing so, standard regression techniques can still be applied to establish appropriate regression models. As an example, the transformation for power and exponential functions are given below.

Power functions:

$$\hat{Y}_i = \hat{b}_0 \cdot X_i^{\hat{b}_1} \;\rightarrow\; ln(\hat{Y}_i) = ln(\hat{b}_0) + ln(\hat{b}_1) \cdot ln(\hat{X}_i) \tag{4.6}$$

Exponential functions:

$$\hat{Y}_i = \hat{b}_0 \cdot e^{X_i \cdot \hat{b}_1} \;\rightarrow\; ln(\hat{Y}_i) = ln(\hat{b}_0) + ln(\hat{b}_1) \cdot \hat{X}_i \tag{4.7}$$

To evaluate the suitability of a regression model, a coefficient of determination can be computed from the squared error of the single estimations divided by total sum of squares of the responses:

$$R^2 = 1 - \frac{\sum_{i=1}^{n} E_i^2}{\sum_{i=1}^{n} (Y_i - \bar{Y})^2} \tag{4.8}$$

This coefficient indicates how much of the variation of the target value can be explained by the derived regression model and varies between zero (no explanation) and one (full explanation). Typical values from [69] are listed in Table 4.1.

Table 4.1: Assessment of the prediction ability of regression models based on coefficients of determination

$R^2 >$ 0.64	good
0.25 $< R^2 >$ 0.64	average
$R^2 <$ 0.25	poor

It should be noted, that the coefficient of determination can be strongly influenced by sub-samples of data which show significantly different characteristics than the rest of the data. Simple examples are single outliers. Therefore, the coefficient of determination alone is often not sufficient to assess the quality of a statistical model. Instead, it is advisable to analyse other indicators, like for example the mean and standard deviation of residuals, as well.

Regression theory is based on several assumptions, such as linear relationships be-

tween input and target values or uncorrelated, normally distributed estimation errors with an expectation value of zero and constant variance. The validity of these assumptions is often checked visually for example by plotting the estimation errors against explanatory or response variables [70]. If the assumptions are met, some desirable properties of the regression model are that

- the expectation value of the estimations equals the true mean value of the targets (*unbiased model*),
- no other input parameter than the selected will give smaller estimation errors (*efficient model*) and
- the accuracy of the model will improve, if the underlying number of data points is increased. Bias and variance of the estimation error will eventually reduce to zero if the sample size approaches infinity (*consistent model*).

If the relation between input and target values is very non-linear or depends on several input parameters, establishing a regression model gets complicated. Unfortunately, this is the situation for a load estimation system exactly. Here, the choice of appropriate input parameters and transfer functions can be especially challenging. It is likely that many correlations have to be tested and combined to a well working regression model in such a case. The process can be partly automated by means of more elaborate stepwise regression techniques, but still it can not be guaranteed that the found solution performs well.

Establishing regression models for non-linear wind turbine behaviour can potentially be simplified, by dividing the turbine's operational range into several sub-ranges, where approximately linear relations apply. Separate (but simple) regression models can then be derived for each sub-range.

One disadvantage of regression techniques is that they can generally not be used for extrapolation [71]. Although the regression model may provide a good approximation of the real process over the range of samples that have been used for setting up the model, it could be a poor representation outside this region. This means that the developed regression model is only valid, if the explanatory variables are within a defined range.

4.1.2 Estimation of thrust force time series at tower top

To evaluate the suitability of regression techniques for the estimation of wind turbine loads, the method has been tested on a challenging example [32]. Using simulations of the 1.5 MW wind turbine, time series of the thrust force at the tower top and of

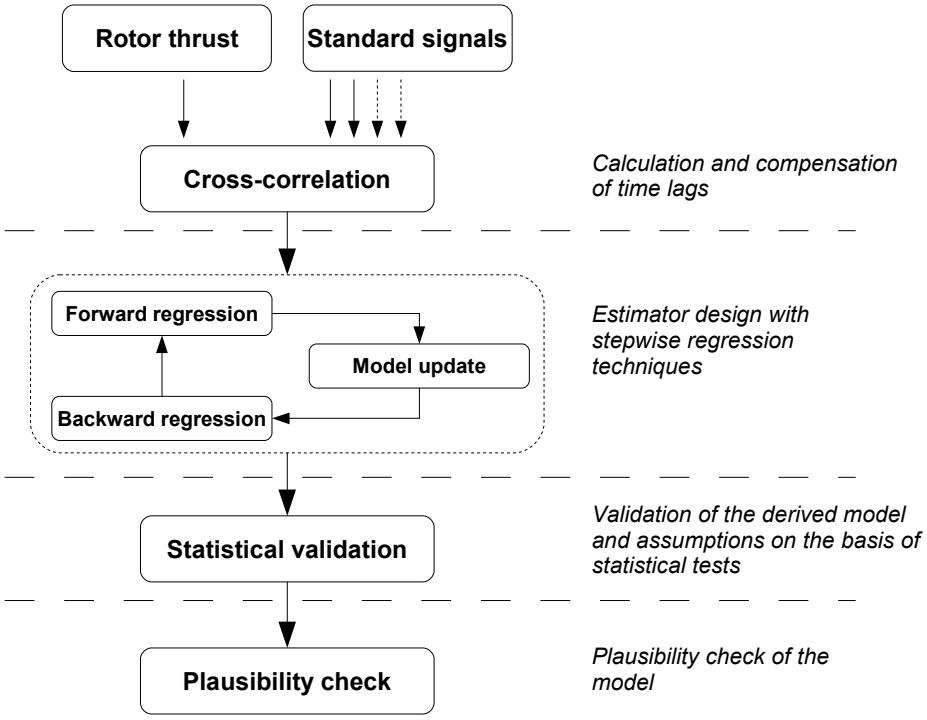

Figure 4.1: Semi-automated set-up of the regression model

relevant standard signals have been generated. Stepwise regression techniques were then applied to establish a suitable estimator for high resolution thrust time series from standard signals.

Setting up a regression model is far from being trivial with many possible input signals and unknown non-linear relationships. To avoid manual testing of different combinations of input signals and transformation functions, the process has been automised and implemented into a script for the numerical computations software *Scilab* [72]. The general approach is illustrated in Figure 4.1.

Because of the mechanical and aerodynamic inertia of a wind turbine it is possible, that the shape of a standard signal time series is very similar to the target signal, but leads (for example pitch angle) or lags (for example generator speed or electrical power) the target signal in time. A compensation of these time shifts improves the quality of the estimations significantly. This has been achieved by computing the time shift between all available input signals and the thrust from the maximum of the cross-correlation:

$$R_{cor,xy}(k) = \frac{1}{n} \cdot \frac{\sum_{i=1}^{n-k}(X_i - \bar{X})(Y_{i+k} - \bar{Y})}{\sqrt{Var(X) \cdot Var(Y)}} \tag{4.9}$$

with $R_{cor,xy}(k)$ as discrete cross-correlation function, n as the number of time steps, k as the sample lags and the variances $Var(X)$ and $Var(Y)$ of time series X and Y.

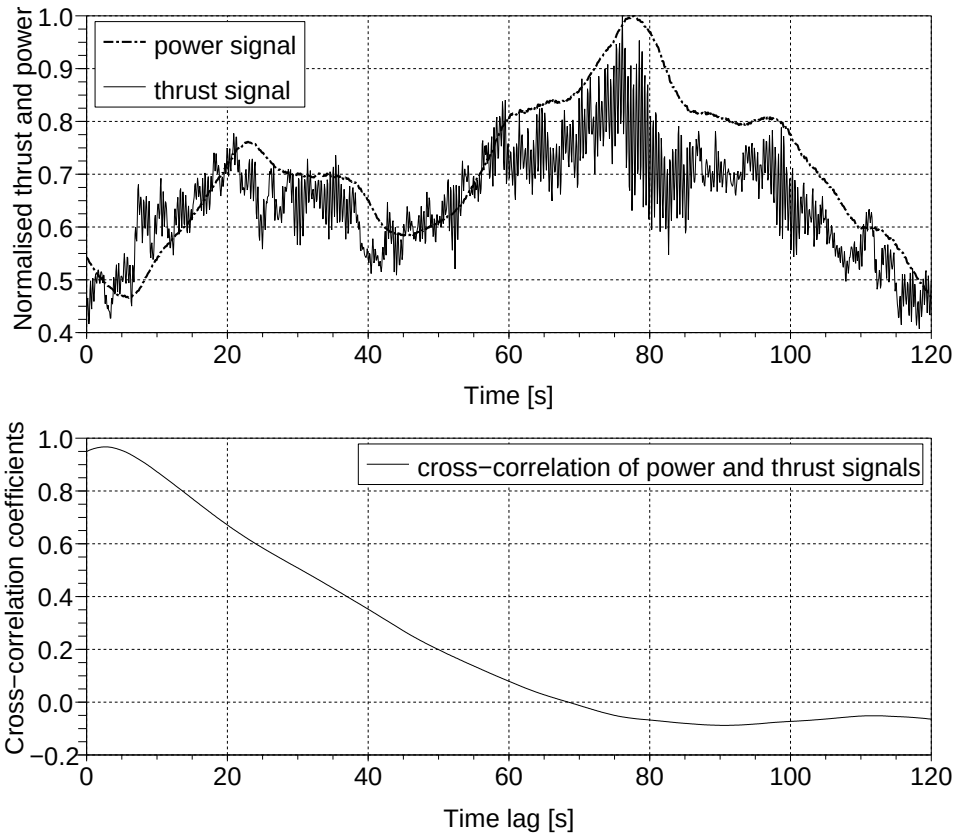

Figure 4.2: Example for cross-correlation of simulated time series of thrust force at tower top and electrical power

As an example, a normalised time series of simulated thrust force at tower top has been plotted in Figure 4.2 together with the normalised electrical power signal and the cross-correlation function of the two signals. The simulation has been carried out with a mean wind speed of 8 m/s and a turbulence intensity of 16 %. Analysis of the cross-correlation revealed that the maximum correlation coefficient can be calculated when the signal of the electrical power is shifted in time by approximately 3 s.

The regression model is assembled in a second step. A stepwise approach (see Figure 4.1) automises the process and aims at the development of the most accurate regression model with the lowest number of input parameters. It is an iterative process based on forward and backward regression.

During forward regression all input parameters are correlated with the target value. Besides linear regression functions, several exponential and power functions as well as a second order polynomial have also been used at each forward regression step. Furthermore, sub-sets of the tower top acceleration signals have been generated by filtering, using band-pass filters with various centre frequencies and bandwidths. All forward regressions are tested for statistical relevance, where the hypothesis of statis-

tical significance is either confirmed or rejected by means of a goodness-of-fit test [69]. At the end of the forward regression, the overall regression function is extended by the statistical significant correlation which gave the highest coefficient of determination in this step.

A goodness-of-fit test is also applied during the backward regression. By doing this it is verified, that all parameters of the overall regression function are still statistically significant and none of them have become redundant because of the model extension in the previous forward regression step. If this is the case, the model remains unchanged and the forward regression is started again. Otherwise, redundant parameters are removed before the next forward regression.

The process is stopped if none of the remaining standard signals can contribute significantly to the explanation of the target signal. Final statistical checks, such as visual inspection of estimation error plots or test of the residuals for normal distribution, are done to confirm the statistical validity of the derived model. Based on some test cases, comparisons of predicted and simulated thrust forces in the time and frequency domain are applied to also verify the physical suitability of the regression function.

Unfortunately, even with this stepwise approach it has not been possible to develop a regression model which is valid over the whole operational range of the simulated wind turbine. Because of the strongly changing thrust characteristics of a pitch controlled turbine around rated wind speed, it became necessary instead to establish separate models for below and above rated operation.

Below rated model (A) for wind speeds of about 5 to 11 m/s:

$$\hat{F}_r(t) = \hat{b}_0 + \hat{b}_1 \cdot P_{el}(t+\delta)^2 + \hat{b}_2 \cdot P_{el}(t+\delta) + \hat{b}_3 \cdot \ddot{z}_{tt,1}(t) + \hat{b}_4 \cdot \ddot{z}_{tt,2}(t)$$

Above rated model (B) for wind speeds of about 12 to 25 m/s:

$$\hat{F}_r(t) = \hat{b}_0 + \hat{b}_1 \cdot \theta_P(t+\delta)^2 + \hat{b}_2 \cdot \theta_P(t+\delta) + \hat{b}_3 \cdot \ddot{z}_{tt,1}(t) + \hat{b}_4 \cdot \ddot{z}_{tt,2}(t)$$

Both models are similar with respect to their general structure and consist of a second order polynomial and two linear terms. Of course, different input signals are required: electrical power P_{el} and band-pass filtered longitudinal tower top accelerations $\ddot{z}_{tt,1}$ and $\ddot{z}_{tt,2}$ for the below rated model and pitch angle θ_P combined with the same acceleration signals in case of the above rated model. For Model A, the coefficients of determination are found to be around 0.95 while they are varying between 0.75 to 0.80 for Model B.

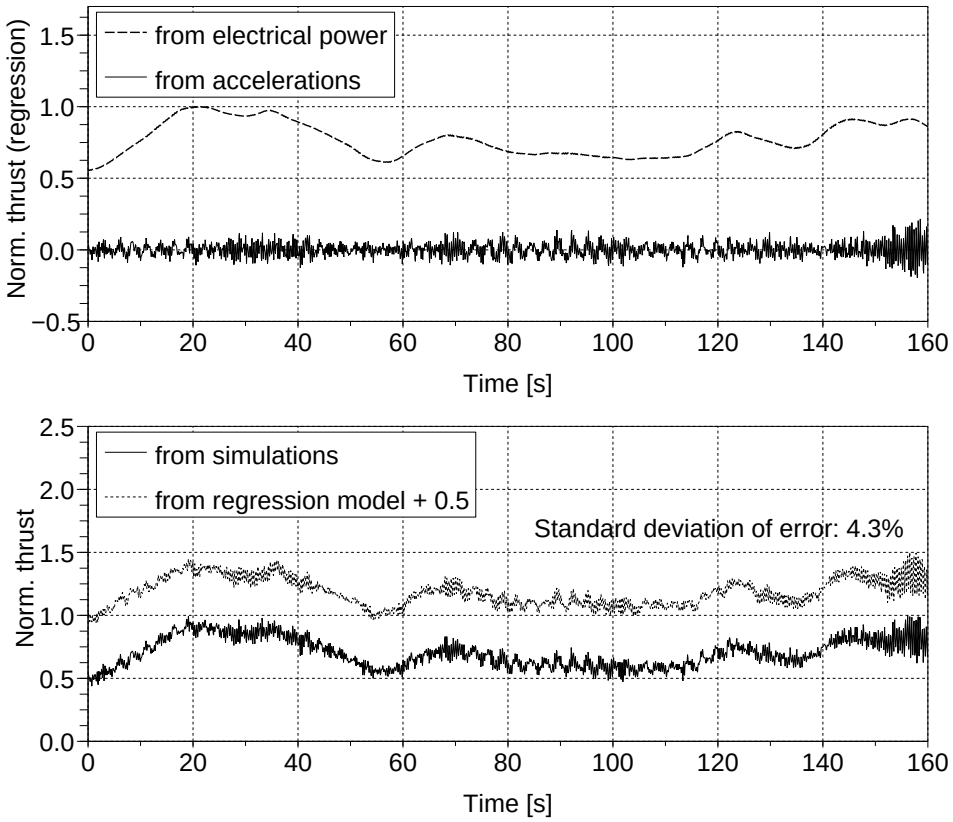

Figure 4.3: Estimation of thrust time series from electrical power and tower top accelerations (Model A)

Table 4.2: Parameters of the developed regression models for the prediction of thrust forces at tower top from standard wind turbine signals

Model	$\hat{b}_0$ [-]	$\hat{b}_1$ [-]	$\hat{b}_2$ [-]	$\hat{b}_3$ [-]	$\hat{b}_4$ [-]	δ [s]
A	21.65	-0.00005	0.2105	82.97	118.36	3.0
B	337.12	0.2044	-15.172	66.36	130.41	-1.0

The regression coefficients as well as the applied time shifts from the cross-correlation analysis δ are given in Table 4.2 for both models. Figure 4.3 shows the results from an estimation of tower top thrust time series from standard signals and Model A. A 10 minute mean wind speed of 8 m/s and a turbulence intensity of 15 % has been used. In the upper plot the results from the explanatory variables, namely electrical power and tower top accelerations, are illustrated separately. It is obvious, that the low frequency change of the mean thrust is captured by the electrical power part of the model, while the high frequency oscillations around this mean are captured on the basis of the accelerations. A comparison of the normalised simulated thrust force and the results from the complete regression model is displayed in the lower plot.

For better visibility the predicted results have been increased by 0.5. The overall shape of the estimated thrust fits the simulation results quite well. The standard deviation of the relative error between the two graphs is relatively small and has been calculated to 4.3 % of the simulated thrust in this example.

More extensive tests have been performed to assess the suitability of regression models for the estimation of wind turbine loads. Based on different stochastic realisations of turbulent wind fields, 40 simulations of ten minutes length each have been carried out, using the model of the 1.5 MW wind turbine. Half of the time series have been simulated with a mean wind speed of 8 m/s to test model A, of which ten were based on a low turbulence intensity of 15 % and ten on a high turbulence intensity of 23.3 %. A mean wind speed of 20 m/s has been used for the other half of the simulations with turbulence intensities of 10 % and 16.5 %, respectively.

Simulation results were used as input to the regression models from which time series of the tower top thrust force were predicted. A rainflow counting procedure was then applied on the predicted time series to compute load cycle distributions which were further simplified to damage equivalent load ranges using exponents of 4 and 10. The relative deviation of equivalent tower top thrust from prediction and simulation is given in Table 4.3, separately for each wind speed and turbulence intensity.

In general, the equivalent loads from predicted thrust time series match the ones from the simulated thrust very well. This holds true in particular for Model B, where the average deviation between damage equivalent loads is around one percent only for both turbulence intensities and exponents.

Model A seems to be well suited in the low turbulence case. However, for higher turbulence intensities the deviation increases to more than 7 percent in average. This can be explained by investigating the probability distributions of wind speeds based on high and low turbulence intensities. Obviously, an increased turbulence leads to a higher occurrence probability of very low and high wind speeds. The probability distribution becomes broader with longer tails and a lower peak. This effect is illustrated in the lower graphs of Figure 4.4. In addition, the steady state thrust curve of the turbine is plotted in the upper part of the figure over wind speed. The rated wind speed has been calculated to about 11.5 m/s and is marked by the dashed line.

As expected, the shape of the thrust curve above and below rated wind speed is completely different which was also the reason why separate regression models had to be derived for the load prediction in each region. Comparing the probability distributions of wind speed, it becomes obvious, that the wind speed can exceed the rated wind speed in case of the high turbulence intensity (hatched area). As Model A is not at

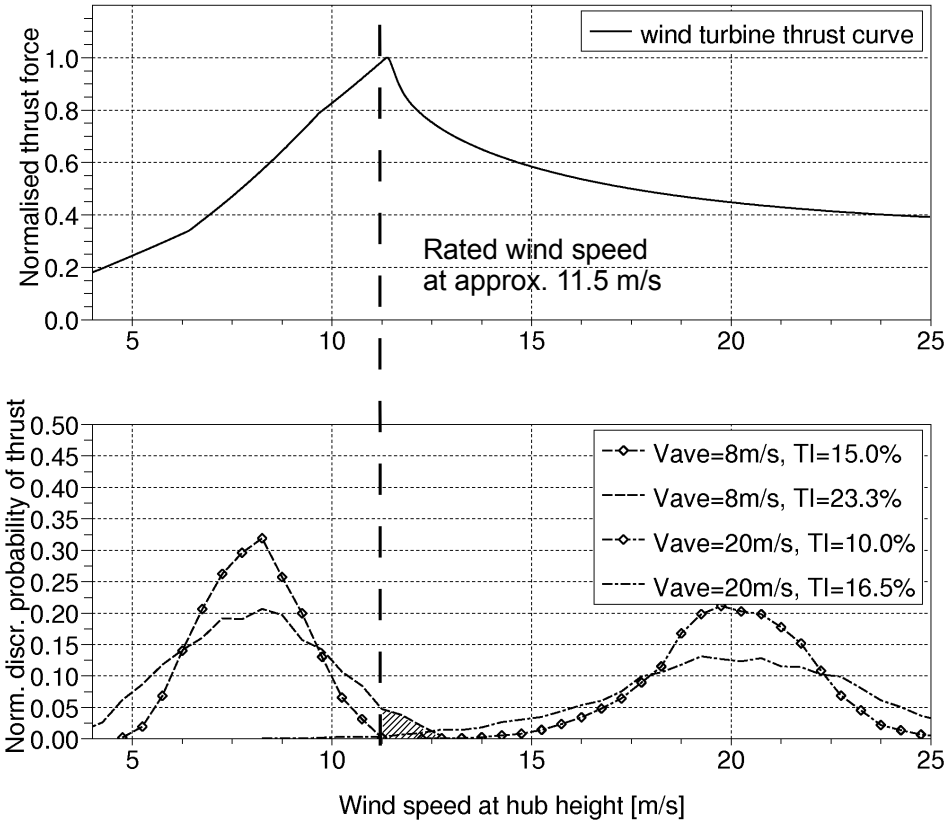

Figure 4.4: Thrust curve and discrete probability density of simulated wind speeds

all suited for predictions above rated wind speed, a false prediction of the corresponding thrust force is the consequence. This effect is then also visible in the calculated damage equivalent loads.

The investigations above demonstrate that regression models might in principal be used for wind turbine load predictions. However, the special challenges of regression analysis for wind turbine applications are also stressed. Setting up a suitable model requires significant efforts. Besides testing all available standard signals for their suitability to serve as explanatory variables, the nature of their relation (for example linear or polynomial) also has to be determined. If the response is highly non-linear, as it has been the case here, probably several models have to be established for different

Table 4.3: Deviation of predicted and simulated equivalent loads

m	$\bar{U}$ = 8 m/s (Model A)		$\bar{U}$ = 20 m/s (Model B)	
	I_T = 15.0 %	I_T = 23.3 %	I_T = 10.0 %	I_T = 16.5 %
4	1.3 %	5.4 %	0.6 %	0.8 %
10	0.1 %	7.3 %	-1.0 %	0.9 %

operational regions. This raises additional difficulties for the design of a load estimation procedure, because suitable switch over procedures between models also have to be defined.

4.2 Neural networks

4.2.1 Overview on neural network techniques

Inspired by research into the processing of information in biological nervous systems, the theory of neural networks has been developed since the fifties. Neural networks have made their way into many engineering applications especially during the past two decades, with ever decreasing costs of computational power. Because networks can be trained to fulfil specific tasks, they are often employed as expert systems for automated decision making, pattern recognition or control. Furthermore, the capability to learn distinctive features of processes allows to apply trained neural networks as black box models in many engineering applications.

One example in wind energy is the forecast of generated wind power. Because of the unsteady nature of the wind, the power generation from wind turbines also fluctuates very much. A wind power forecasting system is therefore required to schedule the reserve power from conventional power plants. In [73], specific neural networks and meteorological parameters from weather forecasts are employed for this purpose and enable a short term wind power prediction of up to 72 hours.

As shown in the left part of Figure 4.5, a neural network consists of several neurons which are linked together with directed connections. The neurons are arranged in multiple layers. Each network at least consists of an input and an output layer, but in almost any application one or more hidden layers of neurons (internal layers) are also present.

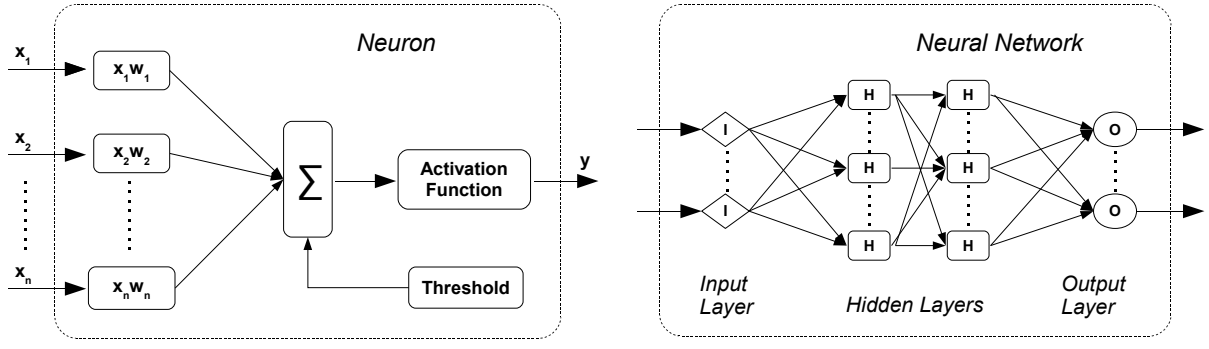

Figure 4.5: Schematic plot of a neuron and a feed-forward neural network

The plotted example is denoted as feed-forward network, because all information is passed through the net in only one direction: from the input layer to the output layer. Many other network types, like recurrent networks with bi-directional connected layers for example exist as well, and the choice of suitable network types in general depends on the application.

Neurons in the input layer are associated with the input data to the network and pass the information on to the neurons in the following layer. All hidden and output neurons receive one or more signals as input. They are weighted and usually simply added together with a threshold value to derive the activation of the neuron. The output is then computed from the activation and the so-called activation function. Common activation functions are the unit step function in case of binary signal processing or differential functions like the sigmoid or the logistic function for non-binary tasks [74]. Hence, a neuron's output can be calculated as:

$$y_i = \sigma(a_i) \tag{4.10}$$

with the activation

$$a_i = \sum_{j=1}^{n}(w_{ji}x_j) - \theta_i \tag{4.11}$$

and i as index of the neuron for which the output is calculated from the activation function $\sigma(w, x, \theta)$, n as the number of incoming connections, w_{ji} as the weight of the connection from neuron j to neuron i, x_j as the output of neuron j and θ_i as threshold of the neuron. In practice, the threshold is often modelled by extending the input and weight vectors of the neuron to $(n+1)$-dimensions with a bias [75], whereby $x_{n+1} = 1$ and $w_{(n+1)i} = -\theta$. In this case, the output of neuron i is therefore

$$y_i = \sigma(\sum_{j=1}^{n+1} w_{ji}x_j) \tag{4.12}$$

Neural networks own much of their popularity to the fact that they are powerful tools for the approximation of arbitrary functions and hence offer the possibility to establish black box models of many processes. Given that a suitable amount of training data is available, training algorithms can be used to teach a network to relate input and output data. If the network is sufficiently large, it is possible to approximate very complex relations in fact by a combination of relatively simple activation functions. Thereby, building and training a neural network is often faster and easier than the set-up of a regression model, especially if complex non-linear relations have to be mapped. This characteristics can be very beneficial for the set-up of a wind turbine load estimation system.

In a neural network, all learned information is contained in the connection weights and the topology. The number of neurons and connections as well as the complexity of the network topology also determine the overall storage capacity of a network. Training of the network is commonly performed by adjusting the connection weights according to some training rules. By changing the weights, the network topology can also be influenced. Setting the weight of a connection to a very low value corresponds to cutting the connection. Similarly, the connection can be reactivated again simply by increasing the low weight.

If input and target values are available from measurements for example, supervised learning is often applied using backpropagation algorithms [76]. Here the input is first propagated forward through the network and a network output is computed. An estimation error is then calculated from the network's output and the real measured target values. The error is propagated back through the network and the connection weights are adjusted accordingly. This procedure is repeated until the error has become sufficiently small or a specified maximum number of training cycles has been reached.

Training of a network can mathematically be interpreted as an attempt in finding the global minimum of the error function. Backpropagation utilises the gradient of the error function to adjust the network weights [75]. As the error is a function of the weights, the gradient of the error in the $(n+1)$-dimensional weight space has to be determined from

$$\nabla E = (\frac{\partial E}{\partial w_{1,1}}, \frac{\partial E}{\partial w_{2,1}}, \cdots, \frac{\partial E}{\partial w_{n+1,k+1}}) \tag{4.13}$$

The individual weights are updated by adding a fraction of the calculated gradient in the respective direction with μ as constant learning rate:

$$\Delta w_{ij} = -\mu \cdot (\frac{\partial E}{\partial w_{ij}}) \tag{4.14}$$

Figure 4.6 illustrates this procedure. Defining the error between the training data t and the network output for the l-th output neuron as

$$E_l = \frac{1}{2} \cdot (t_l - y_l^O)^2 \tag{4.15}$$

the update of the weight Δw_{ml}^O can be derived:

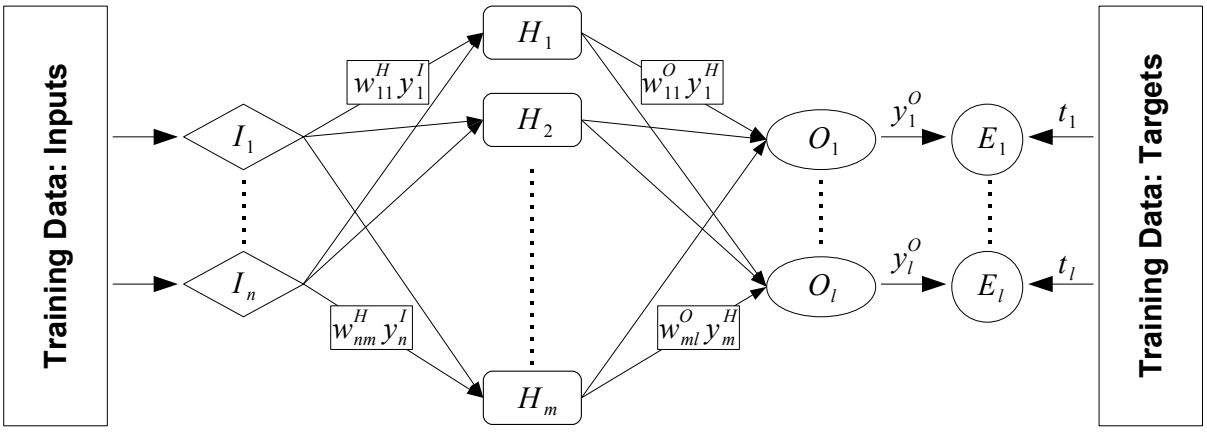

Figure 4.6: Calculation of training error of a network with one input, one hidden and one output layer

$$\begin{aligned}
\Delta w^O_{ml} &= -\mu^O \cdot \frac{\partial E_l}{\partial w^O_{ml}} \\
&= -\mu^O \cdot \frac{\partial E_l}{\partial y^O_l} \cdot \frac{\partial y^O_l}{\partial w_m l^O} \\
&= \mu^O \cdot (t_l - y^O_l) \cdot \frac{\partial y^O_l}{\partial w_m l^O} \\
&= \mu^O \cdot (t_l - y^O_l) \cdot y^H_m \cdot \sigma'(\sum_{i=1}^{m} (w^O_{il} y^H_i) - \theta^O_l) \\
&= \mu^O \cdot (t_l - y^O_l) \cdot y^H_m \cdot \sigma'(a^O_l)
\end{aligned} \tag{4.16}$$

The expression can be arranged more neatly to

$$\Delta w^O_{ml} = \mu^O \cdot \delta_l \cdot y^H_m \tag{4.17}$$

by substituting

$$\delta_l = (t_l - y^O_l) \cdot \sigma'(a^O_l) \tag{4.18}$$

In a similar manner, the change in weight of neurons in the hidden layer is calculated for weight w^H_{nm} as

$$\Delta w^H_{nm} = \mu^H \cdot \delta_m \cdot y^I_n \tag{4.19}$$

using

$$\delta_m = \sum_{k=1}^{l} (w^O_{mk} \delta_k) \cdot \sigma'(a^H_m) \tag{4.20}$$

A closer investigation of the equations 4.17 to 4.20 reveals that the change of weights

Δw_{ji} of neuron i is proportional to

- the learning rate μ. The learning rate is specified at the beginning of a training and is the basic parameter to define the overall rate of weight changes.

- the derivative of the activation function $\sigma'(a_i)$. This implies, that the activation function is differentiable. Remembering that backpropagation is based on the gradient of the error, the requirement is also intuitive. Non-differentiable activation functions would give non-differential error functions, making it impossible to calculate the gradient over the whole weight space.

- the output of predecessor neuron j. An output of neuron j is one of the inputs to neuron i. The weight of this connection is modified to a greater extend, if this value is large. Contrary, the weight is changed only by a small amount, if the value is small and therefore this connection does not contribute much to the output of neuron i (and hence not to the overall error).

- the calculated error E_i (for output neurons) or the weighted sum of changes of all outgoing connections $\sum_{k=1}^{l}(w_{ik}\delta_k)$ (for hidden neurons). Large errors will lead to fast changing weights. This holds true for an output neuron, but also for a neuron with a successor neuron k, where the connection weight w_{ik} has experienced a large change by itself.

Many software tools for the set-up and the training of neural networks exist. Some of them are even available free of charge, like the Java Object Oriented Neural Engine *Joone* [77] or the Java version of the Stuttgart Neural Network Simulator *JavaNNS* [78]. Most of these tools allow the user to define a basic network architecture within minutes and to start the training consecutively with just one mouse click. It is therefore tempting to think that neural networks are easy applicable tools for building black box models of arbitrary processes in an automated manner without any trouble for the user. Because of the following reasons, this is however not the case:

First of all, there are no explicit rules of what a network should look like with respect to a given problem. Analysing and optimising a network is difficult, because so many parameters (for example topology and connection weights) are involved. Since many combinations of parameters may lead to similar output of the network, analysing these parameters individually does not help in understanding the network. With increasing network size, the parameters become virtually uninterpretable very fast and often the network has to be regarded as a self-organised black-box predictor. Therefore, a fair amount of trial and error is required to define a suitable network in most cases.

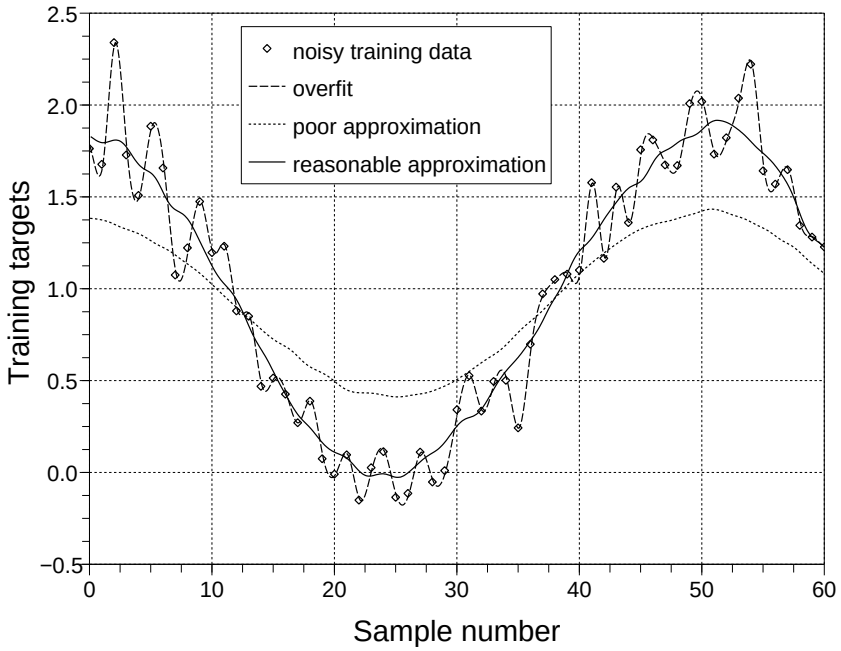

Figure 4.7: Possible predictions from networks with noisy training data

A much followed approach in the search for an appropriate network is to iteratively modify its topology (number of layers, neurons and connections). Here, the investigation of the connection weights can be helpful, as for example low weights might indicate that a connection is in fact superfluous and can be removed [74]. Various pruning algorithms, which have been developed for this task, are available.

Finding a network size close to the optimum is a very important task. If the network is too small, it will not be able to learn the relation between training inputs and targets and give inaccurate prediction results. This is illustrated in Figure 4.7, where the network is obviously unable to map the minimum and maxima correctly. On the other hand, if the network is oversized for the current learning task and has too much storage capacity, overfitting can occur. In this case the network is able to learn a combination of input and target patterns precisely, but has not learned the main features of the process to be modelled. It can therefore not be used for prediction tasks as it has not generalised. In Figure 4.7, possible results of an overtrained network are shown by the dashed line. Clearly, the network has been adapted so much to the training data, that even the scatter and noise of the data is captured well. Such a network will probably give poor results for other than the training data sets.

To avoid overfitting, two data sets are often employed during the training process. One is used for the actual training while the other one serves as a validation set (cross-validation). After each training cycle the validation set is passed through the network and the error is computed. A significantly increasing error of the validation set between

training cycles indicates, that the network has adopted too well to the training data and is therefore overtrained.

Other common issues with neural networks are related to the training algorithms. Again, there is no general rule of which algorithm will yield the best training results for a given approximation problem. Many different training methods are known and more than twenty are implemented into the above mentioned software *JavaNNS* alone [79]. Of course, each method has advantages and disadvantages.

A general training problem is to find the global minimum of the prediction error. As the simple backpropagation algorithm described above relies on the gradient of the error surface only, it is not possible to determine, whether the found minimum is a global or a local one. Furthermore, minima can be jumped over if the backpropagation step is too large. Backpropagation can also get stuck, if an essentially flat area of the error surface has been encountered. In the case where the minimum is very narrow, excessive error oscillations during training are also common problems. Numerous modifications and extensions of the basic method have therefore been developed to enhance the simple backpropagation. Some of them have been tested in this work using *JavaNNS*. Based on these experiences, the following methods seem to be a reasonable compromise with respect to complexity, computational effort and training results for most of the investigated problems and have been used throughout this work:

Backpropagation with momentum

This method includes an additional term into the calculation of the weight changes. The weight is adapted with a weighted average of the current and the previous change of the gradient. In doing so a momentum, often compared to inertia of physical motions, is introduced. This reduces some of the problems with backpropagation and leads to significantly less oscillations in narrow valleys, slower speed up at increasing gradients (can help to not jump over minima) and less deceleration when the gradient reduces (avoids getting stuck at gradients close to zero). The influence of the momentum on weight updates during training is specified by the parameter α:

$$\Delta w_{ij}(t) = -\mu \cdot (\frac{\partial E}{\partial w_{ij}}) + \alpha \Delta w_{ij}(t-1) \tag{4.21}$$

Resilient backpropagation

Most of the above described training problems are related to the proportionality of the weight update to the gradient of the error. Resilient backpropagation tries to get rid of the problems by adjusting the weights only with respect to the sign of the gradient.

Here, the sign of the weight change depends on the sign of the error gradient, whereas the magnitude of the weight change is also modified with respect to the sign of the gradient in the last training cycle. If the gradients of the current and last cycle have the same sign, the sign of the weight stays the same and the magnitude is increased by the constant η. Different signs indicate that a minimum has been missed and therefore the sign of the weight update is changed and its magnitude is decreased. As mathematical expressions:

$$\Delta w_{ij}(t) = -\Delta_{ij}(t) \cdot f(\frac{\partial E(t)}{\partial w_{ij}}) \text{ with } f(x) \begin{cases} 1 & \text{, if } x > 0 \\ 0 & \text{, if } x = 0 \\ -1 & \text{, if } x < 0 \end{cases} \tag{4.22}$$

$$\Delta_{ij}(t) = \begin{cases} \eta^+ \cdot \Delta_{ij}(t-1) & \text{, if } \frac{\partial E(t-1)}{\partial w_{ij}} \cdot \frac{\partial E(t)}{\partial w_{ij}} > 0 \\ \eta^- \cdot \Delta_{ij}(t-1) & \text{, if } \frac{\partial E(t-1)}{\partial w_{ij}} \cdot \frac{\partial E(t)}{\partial w_{ij}} < 0 \\ \Delta_{ij}(t-1) & \text{, otherwise} \end{cases} \tag{4.23}$$

A more detailed explanation of the method, including test results and performance evaluation with respect to other training algorithms can be found in [80].

4.2.2 Estimation of mean and standard deviation of wind speed

For an evaluation of the capabilities of neural networks to serve as load prediction models for wind turbines, a practical example has been carried out [81]. Using a neural network approach, a model for the estimation of mean wind speed and standard deviation from the electrical power and pitch angle signal of the 5 MW wind turbine Multibrid M5000 (see Appendix C) has been developed.

Training and test data were taken from measurements of the Multibrid M5000 prototype at Bremerhaven. The data was recorded from September to December 2005. In total, 250 data sets (each with a length of ten minutes) have been selected, comprising average wind speeds from 4 to 21 m/s and turbulence intensities from 3 to about 25 %. All wind speed measurements were taken from an anemometer on a separate measurement mast. The anemometer was installed at 102 m above ground which corresponds to the hub height of the wind turbine.

Time series of the electrical power and of the pitch angle of the turbine were available as well. As the M5000 is a variable-speed pitch-controlled turbine, the electrical power is almost constant above rated. At below rated operation, the electrical power varies with wind speed. Contrary to that, the pitch angle is constant below rated power and is adjusted at higher wind speeds to maintain the rated rotor speed. Because of this

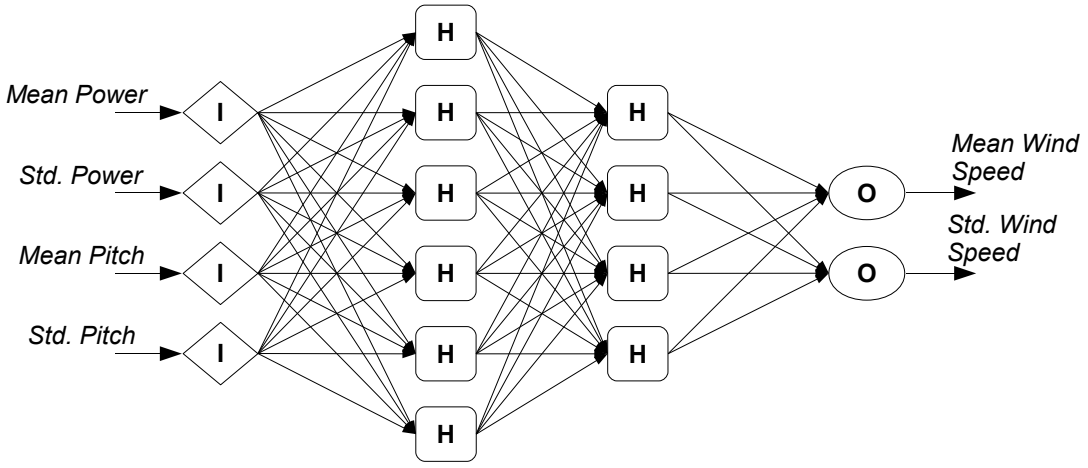

Figure 4.8: Prediction of wind data from power and pitch angle of a wind turbine with a neural network

typical wind turbine characteristics, the pitch angle is not relevant for the prediction if the wind speeds are low to medium. All information is contained in the power signal in this case. At higher wind speeds, the power is futile for this task and the prediction can only be done on the basis of the pitch angle. This is an important feature which the network has to learn. In addition, a relation between wind speed and power as well as between wind speed and pitch angle has to be established of course.

For each data set, the mean value and the standard deviation of wind speed, electrical power and pitch angle have been calculated. 165 sets were used for the training of the network and 85 for testing the network's prediction abilities. After some trials, a network with two hidden layers and a total number of ten hidden neurons had been chosen for this task. *Joone* had been used for the network modelling and a back-propagation with momentum procedure was applied for the training. The subsequent prediction procedure is shown in Figure 4.8.

The prediction results are plotted in Figure 4.9 against the values from the measurements. Obviously the mean wind speed can be estimated from power and pitch angle with reasonable accuracy for all investigated wind speeds. The prediction of the standard deviation of wind speeds is somewhat less accurate.

This is indicated by the higher amount of scatter in the diagram, but can also be seen in Table 4.4 where exact values for the prediction errors are given. The mean of all predictions agrees well with the mean of the measurements for both the mean wind speed and the standard deviation. In addition, the standard deviation of the estimation errors for the mean wind speed is relatively small, so that a prediction error of only about 5 % for a single estimation can be expected. The correspondent standard deviation of wind speed can be predicted with less accuracy and an error of approximately 25 % is likely

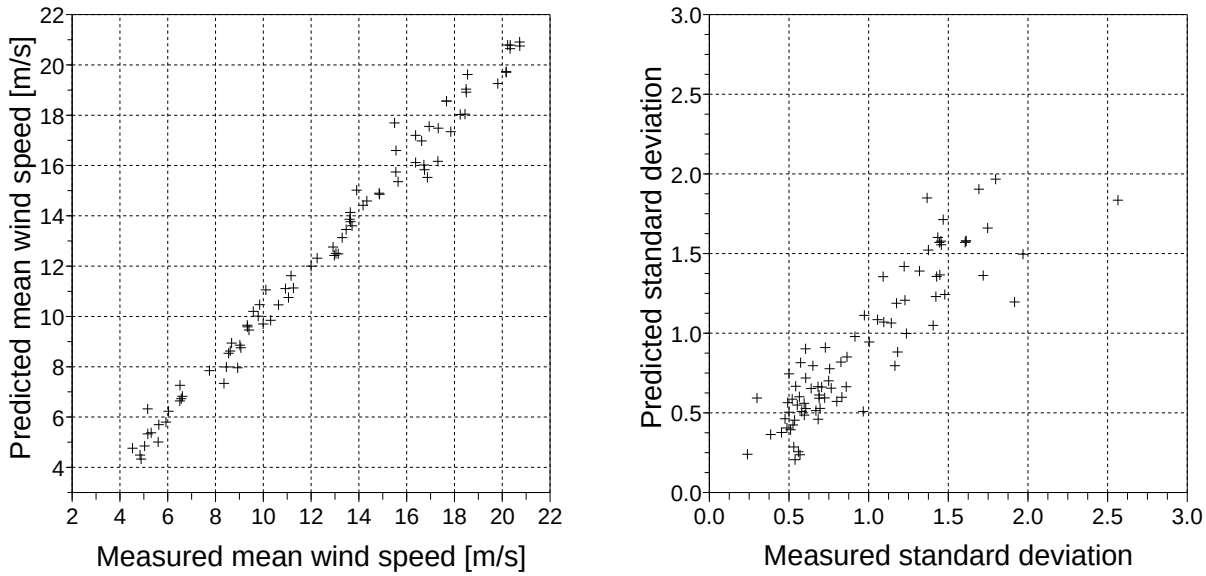

Figure 4.9: Comparison of measured and predicted mean wind speed and standard deviation

Table 4.4: Prediction results of mean wind speed and standard deviation

Prediction targets	Mean error [%]	Std. of error [%]
Mean wind speed	-0.5	5.3
Std. of wind speed	4.5	24.5

to be encountered.

The relatively large standard deviation of errors is not surprising, because only the mean and the standard deviation of the electrical power and the pitch angle have been used for the predictions. If more signals are provided to the network, the results will probably also be more precise. Information on the wind direction and air density could be particularly helpful here. Another explanation for the estimation errors is the fact, that the wind speed is measured in a single point in space only which results in measurement uncertainties because of two aspects. First of all, this point is not exactly located at the wind turbine, but at some distance (about 300 m) away. Secondly, the electrical power and pitch angle are signals which are influenced by the wind speed in the whole rotor plane and not just in a single location [1]. Therefore, the prediction of the standard deviation of wind speeds at the location of the measurement mast from standard wind turbine signals is a relatively demanding task. Taking these considerations into account, the performance of the neural network as a predictor does not seem to be that bad.

Far less manual work was necessary in setting up the network compared to the

[1] Power curve measurements suffer from these two aspects as well and show significant scatter, even if the data is corrected with respect to the impact of varying air density.

classical regression technique. Using a standard training algorithm, it was possible to build a model relatively fast. Although the mapping of complex non-linear relations was required, only a relatively small network was needed. This model was then able to capture the whole range of predictions and the relatively drastic change in the operational behaviour of the wind turbine around rated did not force the development of a second model. Furthermore, assumptions regarding the input-target relations were required only in the respect that the network had to be sufficiently large to be able to approximate the relations with the available number of neurons.

In general, it seems that some of the largest difficulties in the application of regression models for load predictions are far less pronounced when neural networks are employed. However, it should be noted that just as with regression techniques, application of the neural network for predictions is only reliable if the input data are within the range which has been used for the training of the network. An extrapolation is generally not possible.

4.3 Physics-based models

The vast majority of models used in engineering disciplines are based on physical parameters, such as mass or dimension. This is a very intuitive way of modelling for engineers: important mechanical properties of objects are determined and linked with physical laws and theories. Because these models incorporate only known principles and measurable parameters, they are sometimes also called white box models. The response of such a model to some input is deemed to be fully explainable by basic physics. On the contrary, black box models like neural networks for example, only act as transfer functions between input and response. They do not help in answering the question of why an object behaves as it does. Hence, white box models usually offer much more insight into a process.

The behaviour of complex objects as a whole can often not be described by physical laws, because these laws are frequently based on idealisations (a simple example is a body, whose mass is assumed to be concentrated in a single point). Therefore, it is common to model such objects by breaking them down into many small elements, where these idealisations can be applied. The behaviour of the whole object is then calculated as the combined response of the many small elements. If the discretisation of an object is fine enough and appropriate physical laws are applied, the response of the model can match the real response very precisely. Examples, where this approach is applied are finite element models, computational fluid dynamic models or multi body systems.

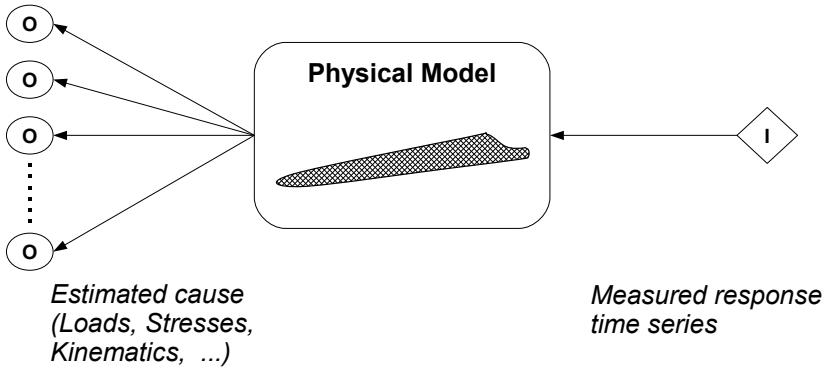

Figure 4.10: Schematics of using a rotor blade model for load monitoring. Loads, stresses or kinematics are estimated at several locations of the model from a measured response.

Physical models typically require the knowledge of many parameters. Sometimes these parameters are hard to determine and have to be estimated. If these estimations do not match the real values, the accuracy of a model of course deteriorates. In fact, the main sources for unsatisfying results from physical models can be related to insufficient discretisation, inapplicability of the chosen physical laws for connecting the discretised elements or wrong estimates of physical properties.

When physical models are applied for load monitoring, high resolutions time series or frequency spectra of deflections, accelerations or strains at one or more locations of the structure are used as input. The loads arising from this input are then calculated from the model. Effectively, this load monitoring approach is an attempt to solve an inverse engineering problem, where the response (measured data) is used to determine its cause (for example the loading) [82]. This is a major difference to common applications of physics-based models.

A physics-based approach allows to propagate responses through the complete model and thereby to derive quantities of interest at many different points simultaneously. This is an advantage compared to regression models or neural networks, where transfer functions between inputs and specific outputs are defined. Figure 4.10 illustrates this feature by showing a model with several estimates from just a single response signal.

However, the figure should not be misunderstood. A single measurement is often not sufficient to allow for an exact estimation of loads in the entire structure. In control theory, this matter is generally addressed as the ‘observability’ of a system. An observable system allows to determine the current status of the system from measured responses precisely. Of course, this is only possible if all independent states of the system are observed. Complex systems commonly feature more than just one independent state

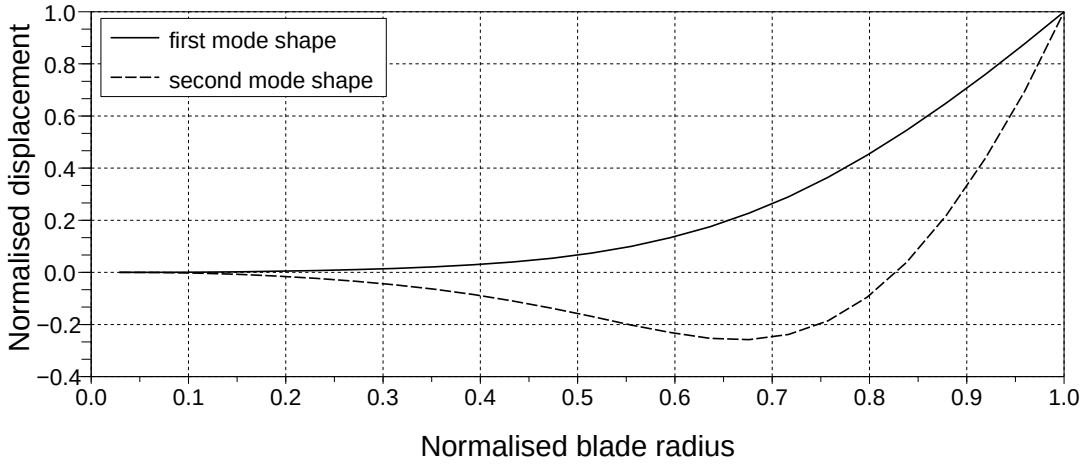

Figure 4.11: First and second flapwise mode shape of a rotor blade model

and hence several response measurements are required.

The importance of the concept of observability becomes evident from a simple example in the field of structural dynamics. Here, slender structures are frequently modelled by means of a mode superposition approach. The individual modes are orthogonal to each other and hence represent independent states of the structure. As a consequence, each mode shape has to be monitored separately to determine the overall status of the system. By way of illustration, Figure 4.11 shows the first two flapwise mode shapes of a rotor blade model. Clearly, a single measured response (for example the vertical displacement at the tip) is not sufficient to distinguish between both modes. At least one additional response measurement is required to observe the two independent states and to monitor the system.

Usually the first few modes of a structure contain most of the system's kinetic or potential energy. If this is the case, only deflections caused by these modes have to be monitored to achieve reasonable load estimation results. In theory, the number of independent measurement signals corresponds to the maximum number of modes which can be captured.

Some applications of physical models for load monitoring are reported in literature, though no example in the field of wind energy has been found. Life cycle management issues for concrete structures are reviewed in [83]. In particular, methods for load monitoring during construction periods are addressed, as these loads can have a significant influence on the long term performance of a building in service. It is shown, how deflections of concrete slabs can be analysed to compute the loading in major load bearing parts of a building. In this example, the slabs in neighbouring floors are connected vertically with shores. Therefore, the displacement of a slab depends not

only on its own loading, but also on the displacement of slabs underneath and above. This knowledge is used to set-up a model of the building (a system of linear equations) from which the shore loads and eventually the loading of each slab is derived. Monitoring the deflection history of slabs therefore allows for an evaluation of the load history of slabs and shores alike.

In other civil engineering applications, fibre optic sensors are used for health monitoring. Several examples, where such sensors are applied successfully to bridges are reported in [84] and [85]. In one application, strains in some locations of a concrete arch were measured. Based on this data and suitable models it was possible to estimate deformations, curvatures in the vertical plane and perpendicular displacements in any location of the whole bridge arch.

It has been pointed out before, that the accuracy of the load estimation will be reduced, if not enough measurements are available. In such cases, the measured response can not be linked with the loading in a unique manner. However, extending the model and introducing additional observers can improve the situation. In [86], the torque exerted from a motor on a work piece had to be monitored to shut the engine down, if the torque exceeded a certain limit. First, a very simple model which involved only a motor torque constant and measurements of the motor currents was used to estimate the motor torque. The estimation accuracy reduced significantly when the motor suddenly accelerated, because the motor required much of the torque for its own acceleration. To solve the problem, the model was extended by a PI-type closed loop observer, where the motor model parameters were estimated from experiments. Taking the motor speed as an additional measurement, the calculated motor torque from the simple model was corrected to give close estimates of the torque on the work piece.

In general it can be concluded, that detailed physical models can be used to relate input data to load quantities. However, these models require very specific input data, like accelerations or deflections at several specific points of the structure. The number of required measurements can be reduced by choosing the response quantities and locations carefully on the basis of theoretical considerations. Still, their number will be large for very complex and dynamic structures. Therefore, the approach is probably well suited for the monitoring of relatively simple objects, but difficult to implement for a whole wind turbine with only a limited number of measurements.

Only high resolution response time series or frequency spectra can serve as input to this method and hence the estimation results will also have a high resolution. This makes the approach expensive in terms of computer power and storage capacities. In

addition, the method has to be coupled with appropriate post processing algorithms to derive more assessable parameters, like for example equivalent loads.

Furthermore, detailed knowledge of structural properties of the physical system that governs the relation has to be available. If the model is not well suited for a prediction and gives unsatisfying results, extending the model on the basis of experiments might be a solution. Often observer based system identification techniques are used for this task.

A major advantage of physical models for load monitoring is related to extrapolation. While this is not possible with regression or neural network techniques, is not an issue with this approach. If the model reflects the real system behaviour correctly, it can be applied at all system states.

4.4 State estimation with database

Very often, the loading of a structure or machinery varies with respect to the environmental and operational conditions. One possibility for establishing a fatigue load monitoring system is therefore, to perform state estimations for the structure in question. In this respect, state estimation is defined simply as classification of the past operational period into pre-defined sub-state categories. For this classification, the most important operational states and conditions in terms of fatigue loads have to be taken into account. Each sub-state is associated with a representative loading. Performing periodic state estimations, for example every ten minutes, allows to derive the load history of the structure or machinery, based on the combination of sets of representative loads.

This approach is also used for the assessment of helicopter operations. The National Aerospace Laboratory in the Netherlands and the Royal Netherlands Air Force have recently developed a fleet life management concept, linking airframe degradation to operational usage. Monitoring of the estimated degradation is then used for the optimisation of maintenance, operational availability and flight safety issues.

The method is based on the recognition of flight regimes and is presented in [4], taking the Chinook helicopter type as an example. Six major flight regimes, such as ‘ascent’, ‘descent’ or ‘hover’, are identified and further refined into a total number of 98 sub-regimes. Test helicopters have been equipped with data-acquisition systems, logging the actual operational data during flights. State identification routines are used to derive basic (short-term) states of the helicopter operation. The overall flight regimes for longer periods of time are then identified from a logical combination of basic state histories.

Each flight regime is associated with a damage index which is considered as a measure for the load transfer through the airframe. In this application, the index serves as the main indicator for the degradation and can be directly linked to maintenance costs and efforts. Combining the damage indices, the past operation of the helicopter can be assessed. In addition, analyses of expected helicopter usage in future can be performed to improve resource and maintenance planning.

More examples for the flight recognition approach in load monitoring systems are given in [1]. Among others, an application for the AH1-W helicopter is described which uses 310 flight regimes in total. Each monitored helicopter signal was binned and a pattern recognition approach was utilised to determine flight conditions from binned signals. Together with information on the sequence and timing of conditions, flight regimes were estimated. The information was processed further and enabled the determination of individual aircraft usage and component fatigue damage from the identified flight condition.

For helicopter monitoring, the loading of a component mostly depends on the flight manoeuvre and on the pilot's technique to perform the manoeuvre. In wind energy, this corresponds roughly to the operational state of the turbine (the manoeuvre) and the contemporaneous environmental conditions (the pilot). An equivalent load monitoring system can therefore look as sketched in Figure 4.12.

First, the overall turbine status has to be determined. This sounds relatively easy, because most turbines log messages which indicate their current status, like for example start, stop, power production and so forth. However, if failure cases have to be classified, the matter gets more challenging according to the author's experience. In such cases, a large number of error messages are often recorded in a relatively short period of time and sometimes the cause-and-effect chain can not be easily determined in an automated manner from the large amount of messages. To make things worse, the sequence in time in which they appear also is not always identical.

As second step, a pattern recognition system is necessary to classify the past period of operation further into sub-states. This requires explicit knowledge of which statistical parameters of the monitored signals are adequate to enter the pattern recognition. Employment of different techniques and parameters can be necessary, depending on the current turbine status. Similar to the examples in [1] and [4], this can also involve the derivation of the statistical parameters of the monitored signals for relatively short time periods and to also take their sequence in time into account.

The pattern recognition identifies the current sub-state of the turbine. This classification determines which entry has to be taken from the database as representative

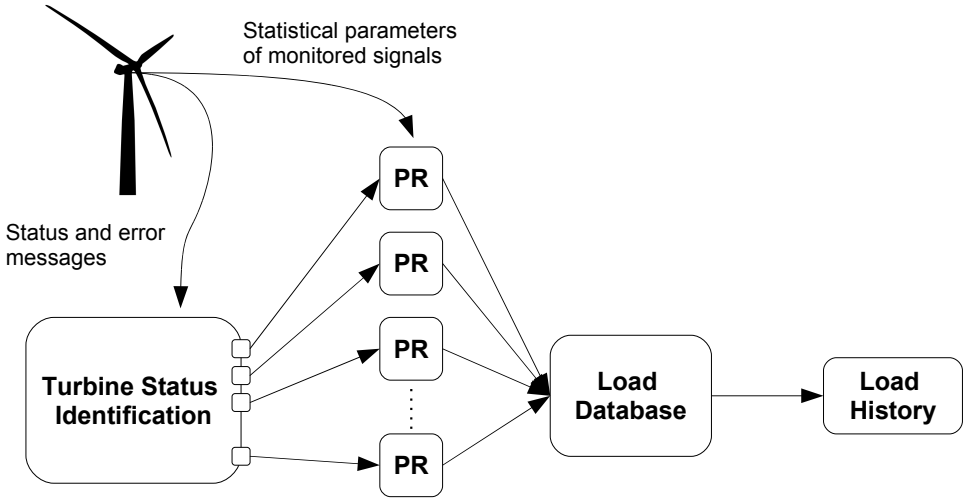

Figure 4.12: Example for the state estimation method for wind turbines

loading for the past period of operation. For each identified state a corresponding load is read from the associated database. Finally the chosen representative loads are combined to an overall fatigue load to derive the load history of the turbine.

The state estimation method is similar to the regression or neural network approach in some way. All methods require a priori knowledge of important parameters, from which the loads are estimated. But while the load information is explicitly given in the database here, it is hidden in the regression function or the connection weights in the other methods.

As it can be seen from all examples, the state recognition approach requires the classification of turbine operation into suitable sub-states and the definition of representative loads for each sub-state. The accuracy of the prediction therefore depends on the accuracy of the pattern recognition, the number and the distribution of sub-states over the operational range, and the validity of the representative loads in the database. Once a sub-state has been identified, data for all load components and in all formats (for example load distributions or equivalent loads) can be extracted from the database.

The set-up of the state estimation approach is simple, as long as the response only depends on one or two statistical parameters of input signals. In addition, the number of required sub states should be small. This implies, that the relation of input parameters and loads should not be too complex.

The method also seems to be particularly suited, if only few measured data sets for establishing a load monitoring system exists. Transients, like starts or stops of the turbine are examples. Using simple indicators for the environmental conditions and the turbine state, for example electrical power and pitch angle at the instance of a grid

failure, these cases can still be classified and at least a rough estimation of the loading can be obtained.

4.5 Comparison and evaluation of methods

A brief comparison of the four methods is given in Table 4.5. It should be noted, that only the most important characteristics, according to the author's view, have been included. Furthermore, the division into advantageous and disadvantageous features is of course subjective. Such a classification depends on the prediction task in question and can change if the scope of the application alters.

From the previous investigations, it seems that physics-based models and regression models are less suited for a load monitoring based on standard signals. Physical models require a lot of information on the structure. In the case of a wind turbine this information is not available, except for the design engineer of the turbine. Furthermore, the utilisation of standard signals only will probably not be sufficient to ensure observability of the most important states of the system. The physical model approach can only be used to predict high resolution time series and a subsequent post-processing is required to derive more comprehensive quantities, for example load distributions or equivalent loads.

Regression models do not require any information on the turbine structure itself. However, the above investigation demonstrates that it can be difficult to define regression models which are capable of reflecting the extremely non-linear turbine characteristics. Setting up such a model is far from easy and requires much manual work. This is an important aspect as separate regression models for each load component and each load format are required.

Neural networks proved to allow for an easier set-up than regression models, especially for non-linear processes and if the prediction target depends on many input variables. Under such conditions, it might even be less laborious than setting up a state estimation approach. The state estimation requires a pattern recognition system, which can even consist of a neural network itself, as well as the identification of necessary sub-states and representative loads. In the neural network approach, these three tasks are already implicitly included in the network, as the network is trained to fulfil all three of them. Although the state estimation allows to associate as much load data as desired to a state (for example data of several load components) and, of course, to extract this information for each identified state in one go, the neural network still seems

to be a more adequate method for load estimations with the turbine in normal power production mode. This holds true at least if not too many different load components have to be predicted with separate networks.

A great advantage of the state estimation is, that it is probably the most suited (and most simple) method for the estimation of loads during transients. Mainly for this reason, a favourable load estimation system consists preferably of a combination of neural networks for the estimation of loads during power production and a state estimation approach for the prediction of loads during transients like manoeuvres of failures.

Table 4.5: Comparison of suitability of estimation methods for load monitoring

	General information	Advantages	Disadvantages
Regression techniques	• Measured input and load data required for set-up • Information stored in regression function	• Regression function offers some insight into input-load relation • Model statistically verified • No detailed information on the wind turbine itself required	• Laborious set-up • Linear(izeable) relation between input and load data necessary • Extrapolation not possible
Neural networks	• Measured input and load data required for set-up • Suitable for all kinds of input-load relations • Information stored in weights and network architecture	• Automated training possible • Semi-automated optimisation of topology possible (with pruning algorithms) • No detailed information on the wind turbine itself required	• Trial and error approach for set-up • Various training issues • Black-box model • Extrapolation not possible
Physics-based models	• Information stored in physical parameters of the model • Very specific input data required for predictions • Based on time domain or linearised frequency domain models	• No measured loads required (although recommended for validation) • Simultaneous load estimates at all locations of the model	• Detailed structural information required • Only for observable systems • Post-processing of time series required
State estimation with database	• Measured input and load data required for set-up • Information stored in database	• Applicable even if only few measurements are available • Suitable for transients	• Sub-states and representative loads required • Pattern recognition needed

5 Synthesis of a load estimation system

5.1 General layout of a load estimation system

A complete fatigue load estimation system does not only consist of an estimation procedure, but also requires a process control and a monitoring scheme. The general layout of such a system is shown in Figure 5.1 and is briefly described in this section.

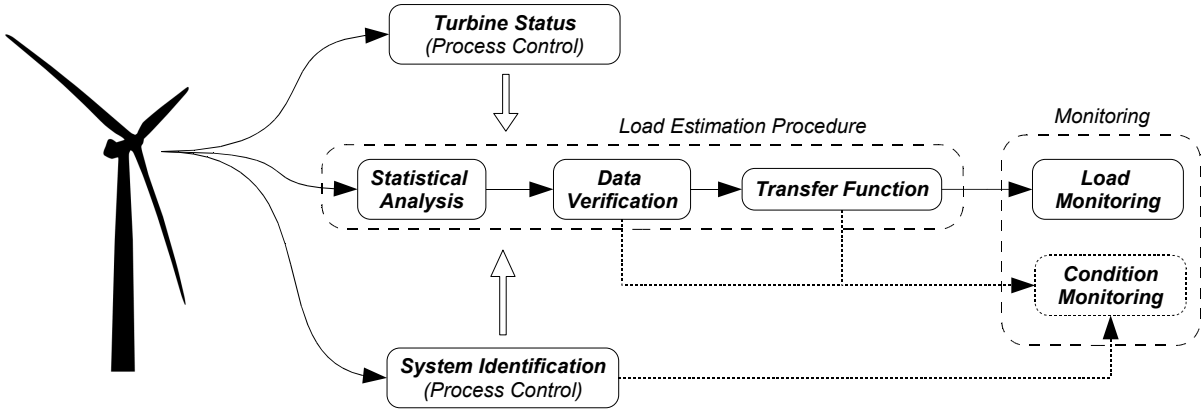

Figure 5.1: Layout of a load estimation system

Process control

System Identification

Accurate estimation results can only be achieved, if the properties of the individual wind turbine are in good agreement with the design assumptions of the estimation system. Due to site specific conditions, for example soil properties, as well as fabrication and assembly tolerances, the system properties of wind turbines in a series can differ to some extend. An exact match of the design assumptions is virtually impossible for this reason. Hence, a system identification step is required to verify that the real turbine properties are not too far off from the design assumptions. The identification should be performed at least once, prior to the initialisation of the estimation system.

Periodical repetitions are required, if significant system degradation over time can be assumed. The detection of immoderate rotor imbalances by system identification and their subsequent removal (see Chapter 3) can serve as a practical example.

The system identification should also comprise an assessment of likely disturbances at the specific site. If the potentially encountered disturbances have not been considered for the design of the load monitoring system, their influence on the estimated loads will not be captured correctly and the prediction error is likely to increase.

Turbine Status

In order to give a complete picture of the situation at a certain site, load predictions have to be performed for all turbine states of relevance for the fatigue loading. The relation between standard signals and loads will certainly be different for the various possible states, such as normal power production, idling, starts and stops. It can therefore be reasonable to adopt the estimation procedure according to the current turbine state. This can be achieved for example by switching between different estimation procedures.

Load estimation procedure

Statistical Analysis

Because all standard signals are also used for the control of wind turbines they are usually measured with high resolution. This continuously monitored high resolution data can either be applied directly for the estimation or divided into sections of equal length, for example 10 minutes, from which suitable statistical parameters can then be derived. The choice of input data format also depends on the desired outcome of the estimation system. If the prediction target is not supposed to be a high resolution time series, statistical parameters are probably sufficient as input in most cases.

Data Verification

This step serves two main purposes. In the first place, the input data has to be checked continuously for plausibility. Single outliers of input parameters as well as sensor malfunctions have to be detected to avoid corruption of the estimation results. Secondly, some estimation procedures can only handle data within a specific range, especially when the estimation is based on empirically derived relations which are not capable of extrapolation of data beyond their calibration range. If incorrect or unusable data has been found, a suitable method of correction and handling of these data has to be defined to make sure that no periods of time are neglected for the fatigue load estimation.

Transfer Function
The transfer function is the key part of the estimation. Some possible methods like neural networks and state estimation with database have been described and compared in Chapter 4. As stated there, a neural network approach seems to be the most promising option for power production cases. Consequently, this approach is utilised and tested on simulated and measured wind turbine data in the following chapters. For transients, a state estimation with an associated data base is an alternative. Because the measured turbine data does not include transients, detailed investigations of this method are not carried out.

Monitoring

Load Monitoring
The individual short-term fatigue load estimations would usually be cumulated to give the overall long-term fatigue load. Cumulated loads are then compared against the design loads or to loads derived for other turbines and allow for an assessment of the past operation. When making some additional assumptions regarding the long-term environmental conditions at a site, it is also possible to extrapolate the fatigue loads to the design life of the wind turbine. However, this method requires choosing representative loads as a basis for the extrapolation and is therefore more complicated than the simple load accumulation. If done correctly, the lifetime extrapolation allows for a better assessment of the turbine operation compared to the load accumulation, especially at the beginning of the monitoring period.

Condition Monitoring
Without much additional effort the above load estimation system can be extended to incorporate a basic monitoring that aims for the prediction of the overall turbine condition. The information from a periodically performed system identification and the result of the data verification can both be analysed to safeguard the compliance of the wind turbine with specifications and design assumptions. Furthermore, the predicted loads can be analysed with respect to trends to detect wear and tear of the turbine as well as long-term degradation.

Examples for the application of standard wind turbine signals for condition monitoring purposes are given by Wiggelinkhuizen et al. [9]. In their research they analysed high resolution time series as well as statistical parameters of 10 minute data sets derived via SCADA systems with promising results.

5.2 Set-up of a load estimation procedure

The estimation procedure is the core part of the load estimation system. Therefore, some aspects of this procedure are outlined here in more detail. These are the choice of estimation targets and input data as well as some considerations regarding the development of neural network based transfer functions.

5.2.1 Estimation targets

In general, fatigue loads are described in various formats which can all serve as targets for an estimation procedure (compare also Chapter 2). Among these formats are:

- time series
- multi stage distributions, for example load cycle or magnitude distributions
- single stage distributions, such as equivalent load ranges or equivalent load magnitudes

Time series are the most complex format and are not easily assessable. They have to be processed further into distributions or equivalent loads for an evaluation. Instead of time series, these post-processed load formats can be chosen as estimation targets. In doing so, the load monitoring system simplifies, because the common post-processing of time series can be omitted.

Multi stage load distributions are usually determined from time series by appropriate counting procedures. An example is the so-called rainflow counting which is used to derive load cycle distributions from time series. Besides the rainflow cycle distribution, multi stage load magnitude distributions are often used to characterise the loading of a wind turbine. The magnitude distributions are a measure of how long certain load levels are present.

Both types of distributions can be simplified further to equivalent loads which, under certain assumptions, will give the same fatigue damage as the multi stage distributions. Because their computation involves exponential weighting, the resulting equivalent load depends non-linearly on the choice of the exponent m and p, respectively. If it is calculated with a large exponent, large load ranges will have a relatively large impact on the result compared to calculations with small exponents for example. A comparison of equivalent loads from different exponents reveals additional information, as it indicates the ratio of large to small load ranges in the underlying process.

Of all possible estimation targets, equivalent loads are probably the most favourable. They allow to characterise the fatigue load with just a single or very few values. Therefore, they offer a good compromise regarding the estimation costs and benefits. Of course, estimations from several periods can again be combined to an overall equivalent load, if the underlying reference numbers and exponents are identical.

The estimation of load distributions is more elaborate. One method, which is based on predefined ranges, has been proposed by Dittmar et al. [6]. Other methods are investigated in Chapter 6.

5.2.2 Input data

For practical reasons, equivalent loads or multi stage load distributions will be the preferred targets for a load monitoring procedure in most cases. These load formats are calculated from time series of some length and hence characterise the loading for that period of time. Therefore, statistical parameters of standard signals, derived for the same time periods as the loads, are sufficient as input to a load estimation procedure.

Variable-speed pitch-controlled wind turbines monitor several signals related to the overall turbine status, such as electrical power output, generator rotational speed, pitch angles and tower top accelerations. Furthermore, wind direction deviations and yaw activities are recorded. Secondary signals like rotational accelerations or pitch rates can be derived from these primary data if necessary.

In a pre-processing step, adequate statistical parameters which reflect the turbine activities during the past time period have to be calculated. If the chosen parameters do not describe the turbine behaviour well or if relevant information has been omitted, the accuracy of the estimation result is likely to be decreased.

Some understanding of the relations between disturbances, loads and standard signals is crucial for the design of an estimation procedure and, in the author's opinion, a well functioning system can not be designed without it. This requires a detailed investigation of possible disturbances and their likely influence on loads and standard signals. The choice of relevant input parameters and suited sets of training data should be based on results from this analysis. In addition, such a study allows to draw first conclusions regarding the possible accuracy of the load estimation procedure. The investigations described in Chapter 3 can serve as an example.

A meaningful characterisation of a time series always comprises more than just one statistical parameter. Preferably, the selected parameters should be related to important signal properties, such as its distribution, variability and frequency content. A classification of possible parameters is shown in Figure 5.2. These are also the statistical

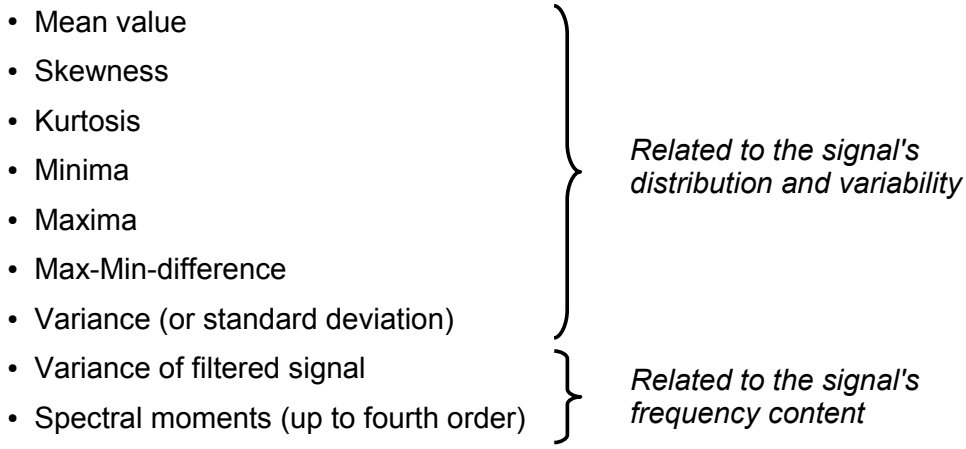

Figure 5.2: Selection and classification of utilised statistical parameters

parameters which have been used within this work.

Parameters related to distribution and variability

The mean values of standard signals indicate the average operation point of a turbine while standard deviations or variances are basic measures of the variability of the operation around this point. A more detailed description of the operation is possible if higher order statistical parameters like skewness γ_3 and kurtosis γ_4 are taken into account. These parameters are calculated from the third and fourth central moments of a signal (μ_3 and μ_4), normalised by the standard deviation σ. They can be used to describe basic deviations of the signal distribution from the normal distribution (where the skewness equals zero and the kurtosis equals three):

$$\gamma_3 = \frac{\sum_{i=1}^{n}(X_i - \bar{X})^3}{\sigma^3} = \frac{\mu_3}{\sigma^3} \tag{5.1}$$

$$\gamma_4 = \frac{\sum_{i=1}^{n}(X_i - \bar{X})^4}{\sigma^4} = \frac{\mu_4}{\sigma^4} \tag{5.2}$$

As illustrated in Figure 5.3, the skewness indicates the deviation of the distribution peak from the mean of the distribution, while the kurtosis is related to the relative flatness of the distribution.

Frequency domain related parameters

Besides knowing the variability of a signal, the frequency content of the oscillations is also an important information. Similar to the central moments in the time domain, the spectral moments are basic parameters to characterise the distribution of the signal's oscillations in the frequency domain.

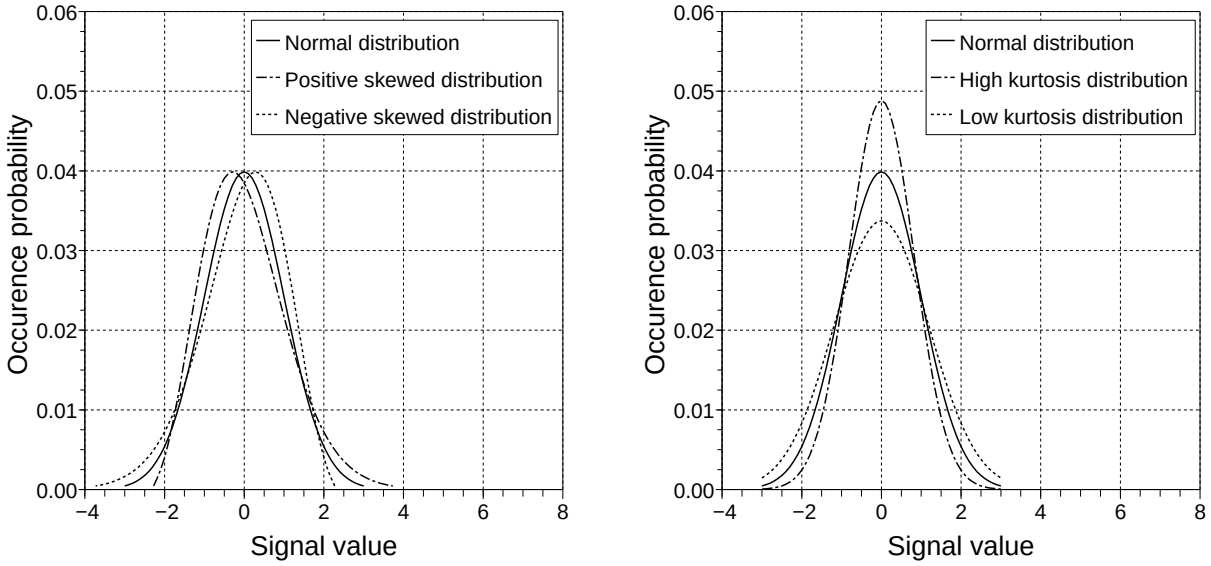

Figure 5.3: Variation of skewness and kurtosis

To derive the spectral moments, time series are usually transferred into the frequency domain to yield the power spectral density (PSD) of a signal as shown in Figure 5.4. Often traditional Fast Fourier Transform based spectral estimation methods, for example the periodogram or the correlation method, are applied for this task. Other approaches utilise autoregression models, where the autoregression coefficients are derived from the autocorrelation function of a signal. The coefficients can then be related to the power spectral density. These models are computationally more expensive but can give better results than the traditional approaches, especially if relatively short sequences of a signal are analysed. Furthermore, they do not rely on the assumption, that the signal is composed of harmonically related sinusoids [87]. It should be mentioned that there are also methods to derive spectral moments directly from time domain representations of a process. Several approaches for the calculation of spectral moments have been tested during this work and are summarised in Annex F.

If the PSD has been derived, the calculation of the spectral moments of different orders n can be performed. Both the utilisation of the cyclic frequency f and the angular frequency ω can be found in literature:

$$m_n = \int_0^\infty f^n \cdot S(f) df \tag{5.3}$$

$$\lambda_n = \int_0^\infty \omega^n \cdot S(\omega) d\omega \tag{5.4}$$

Whatever definition is applied, it is obvious, that the contribution of high frequencies

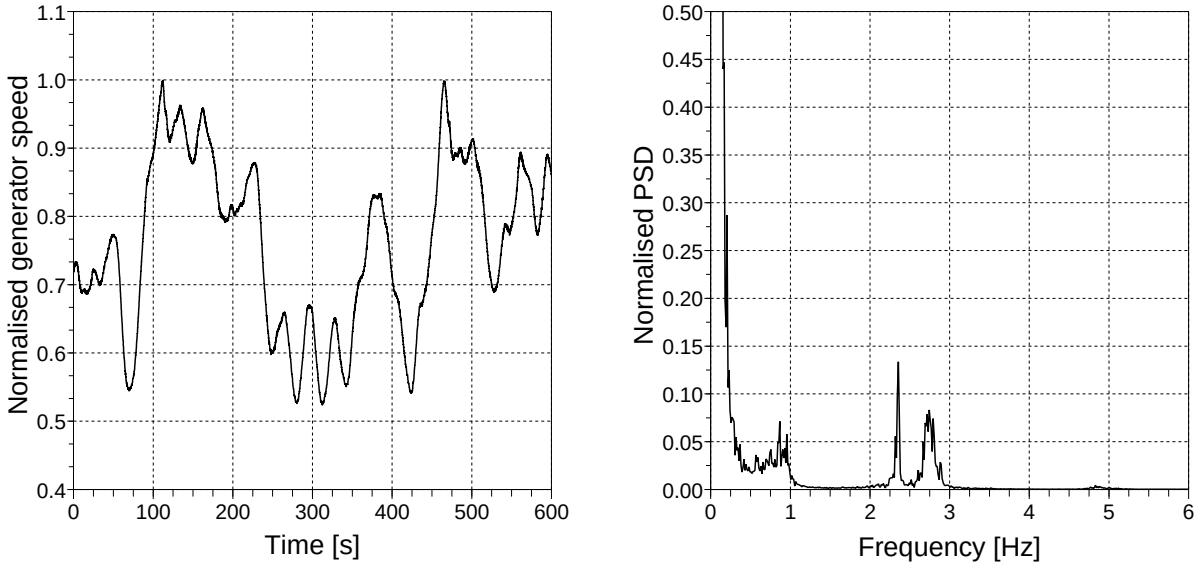

Figure 5.4: Normalised generator rotational speed signal as time series and power spectral density

to the spectral moment increases with increasing order of the moment[1]. A comparison of moments of different order can therefore be used to conclude on the characteristics of the PSD and hence on the distribution of energy of the process.

Time series which feature significant oscillations with periods that are relatively large compared to the length of the time series are often denoted as being trended. Trends in wind speeds make the comparison of measured wind turbine data more complicated, because they tend to distort some signals and their statistical parameters more than others. Therefore, trended data sets are often excluded when measured data is analysed.

In case of a load estimation system, excluding data sets is not an option, because all time periods have to be captured. Instead, the introduction of trend related parameters into the estimation process is preferred. Besides utilising spectral moments of different orders, it is also possible to compare the total variance of the signal to the variance of the same but low-pass or high-pass filtered signal for example (see also Annex G).

[1] Particular care should be given to the selection of a suitable cut-off frequency when Equation 5.3 or 5.4 is implemented numerically, since this can have a significant influence on the computed value of higher order moments.

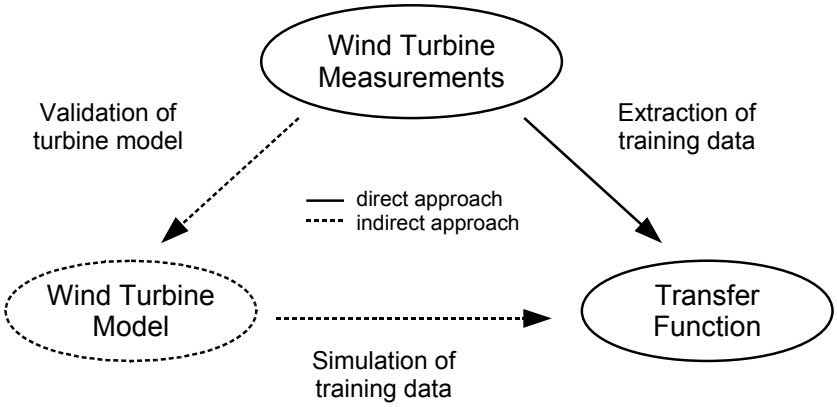

Figure 5.5: Measured data forms the basis for the transfer function set-up. The training itself can then be performed with measured and simulated data.

5.2.3 Development of a neural network based transfer function (training aspects)

The investigations in Chapter 4 indicate that neural networks are particular suited to serve as transfer functions in a load estimation procedure. This holds true at least when the turbine is in normal power production state. Prior to the estimation, the network has to be trained to map the relations between the input data and target values. Suitable training data has to be available for this purpose.

Load measurements are a fundamental requirement to obtain training data, although the training itself can also be performed with simulated data. This is illustrated in Figure 5.5. Two general approaches can be distinguished: In the direct approach, specific training data is extracted from measured data and utilised for establishing a neural network based transfer function. The indirect approach uses measured data for the set-up and validation of a wind turbine model. Based on this model, suitable training data is simulated and employed for the training. Although not shown, hybrid approaches which are made up from a combination of measured and simulated data are also imaginable.

Both approaches have their benefits and drawbacks. Ideally, the training should include all conditions which a turbine can potentially encounter. This is particularly difficult, when only measured data is employed. Because it is very likely that not all situations can be measured at one turbine, data from several measurement campaigns at various locations will be required to assemble a complete set of training data.

This is not the case, when a validated simulation model is available, because all relevant conditions can be included in the simulations. However, setting up a simulation model requires detailed knowledge of the wind turbine which in most cases is available only to the turbine designer. Furthermore, the validation of a simulation model requires great efforts and is not an easy task, according to the author's experience.

In any case, the accuracy of the estimation will depend to a large extent on the quality of the training data. Inaccuracies in measurements and simulations will directly be passed on to the transfer function via the training and lead to a decreased prediction accuracy. Examples are calibration errors of measuring sensors or simulation tools with insufficient capabilities to reproduce the real turbine loads and standard signals. Finding appropriate training data can be considered as one of the fundamentals for establishing an appropriate load estimation procedure.

Within this work only the direct approach has been employed for setting up the transfer functions. Measured data from two different wind turbine types have been available for this task. The indirect method via the validation of a simulation model could not be tested [2]. Unfortunately, simulation models for the two turbines where not accessible.

In general, it is advisable to keep the employed neural networks as simple as possible. In the author's view, application of simple transfer functions is a fundamental requirement to assure the practical applicability of the load estimation approach, because an increased complexity is often accompanied by a higher susceptibility. Therefore, common feed-forward networks with only one hidden layer have been used in this work. Training of the network was performed on the basis of standard algorithms such as backpropagation with moment term or resilient backpropagation (see Chapter 4).

The utilisation of separate data sets for training and test of the training success, often denoted as cross-validation, is a standard technique for neural networks. A reasonable evaluation of the trained network with this technique requires similar properties and feature distribution of the training and test data sets. If this can not be guaranteed, other methods such as k-fold cross validation or bootstrap methods [75] provide the possibility to analyse the network quality. However, within this work similar training and test data sets have been used and hence the cross-validation approach has always been applied. Of course, the training data has to also resemble reality which is an implicit supposition throughout this work.

Examples for the applied networks can be found in the following two chapters. Here, the general suitability of the neural network approach for the load estimation is tested and refined with simulated and measured data. Methods for the prediction of equivalent loads and load distributions are developed.

[2] Simulated turbine data is used in Chapter 6. Because the applied model is a generic turbine model (see Annex B), it can not be assigned to any real turbine and be used for testing of the indirect approach.

6 Test and refinement with simulated data

6.1 Training and test data

In this chapter, the general feasibility of a load estimation procedure with neural networks is investigated. For this purpose, neural network based transfer functions have to be established. These functions relate statistical parameters of standard signals to the desired target values.

Of course, the networks have to be trained accordingly which requires a sufficiently large number of representative data sets. In this case, the data sets have been derived by means of simulations. A total number of 660 simulations have been carried out using Flex5 (Annex A) and the model of a variable-speed pitch-controlled wind turbine with a rated power output of 1.5 MW (Annex B).

The mean wind speeds of the simulations have been varied from 4 to 25 m/s and thereby cover the typical operational range for this type of wind turbine. Turbulent wind fields were calculated according to the standard IEC 61400-1 [16]. Adjusting the parameter I_{ref} resulted in turbulence intensities of 14, 16, 18, 20 and 22 % at an average wind speed of 15 m/s, while the characteristic shape of the IEC turbulence distribution over wind speed was maintained. The shaded area in Figure 6.1 indicates the combinations of average wind speeds and turbulence intensities in the training data.

For performance evaluation of the designed estimation procedures on the basis of cross-validation, 132 additional simulations were carried out. This time, wind speeds and turbulence intensities were chosen randomly. As a constraint, their combination had to be inside the shaded area of Figure 6.1.

Methods for the estimation of equivalent load ranges and magnitudes as well as rainflow range and load magnitude distributions are developed in the following sections. Estimated and simulated loads are compared and the accuracy of the load predictions

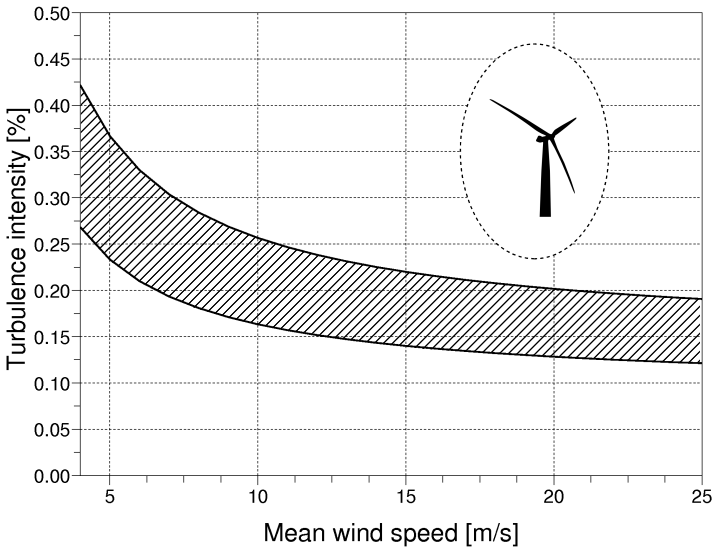

Figure 6.1: Average wind speeds and turbulence intensities of simulated training data

is assessed on the basis of the test data sets.

The feasibility studies within this chapter are performed taking the rotor torque as an example. This is an important quantity which characterises the loading of the drive train and hence of several major turbine components. Furthermore, two directly related standard signals are usually measured: the electrical power and the rotational speed of the generator (see Table 3.3). It can therefore be assumed, that the rotor torque is among those load components which can be predicted most successfully. This makes it particularly suited for the feasibility investigations. Other load components are investigated on the basis of measured data in Chapter 7.

The rotor torque is also an interesting and challenging test case, because it contains many characteristics which are typical for load components of wind turbines. At partial load operation, the torque varies with wind speed and is non-stationary. In addition, its probability distribution deviates significantly from the Gaussian distribution, mainly because the torque varies non-linear with wind speed (see also Figure B.1). At full load operation, the properties are fundamentally different and the rotor torque is almost stationary with a probability distribution quite close to Gaussian.

Figure 6.2 illustrates this behaviour. Here, data derived from three simulations at different mean wind speed and turbulence intensity are displayed. All plots on the left side show the behaviour of the rotor torque at partial load operation, while those on the right are derived from operation at full load. The transition is illustrated by the graphs in the middle.

Plots of example time series (a) and of the variance derived from moving sections

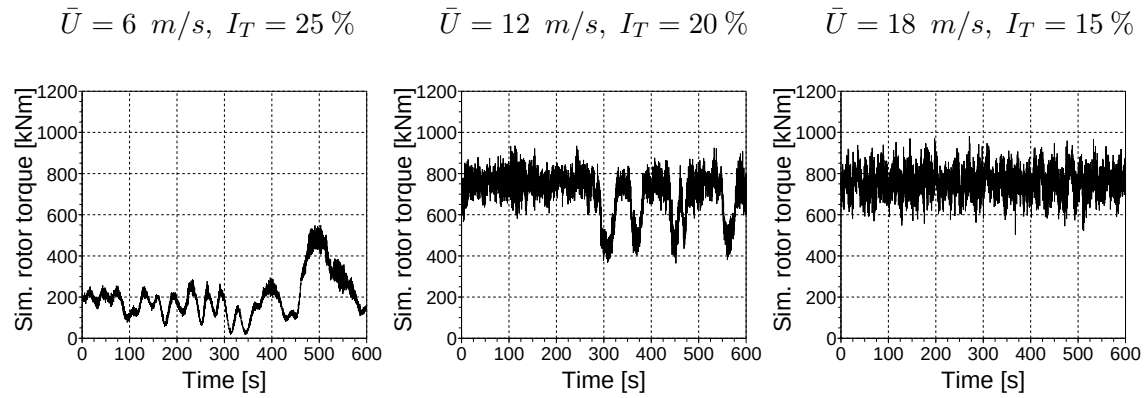

(a) Simulated time series of rotor torque

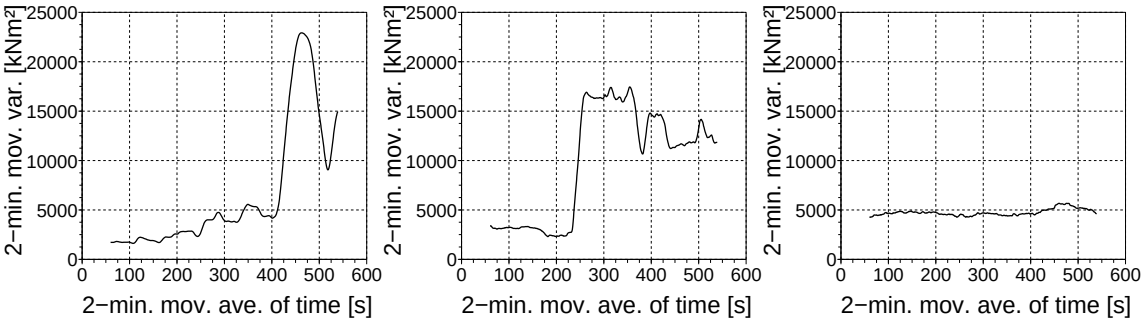

(b) Variance of moving sections of 2-min. length

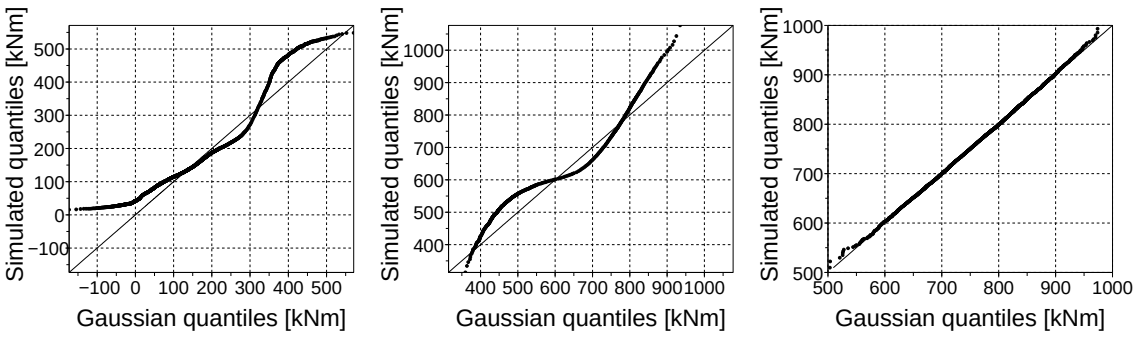

(c) Quantiles of simulated torque against quantiles of Gaussian distribution

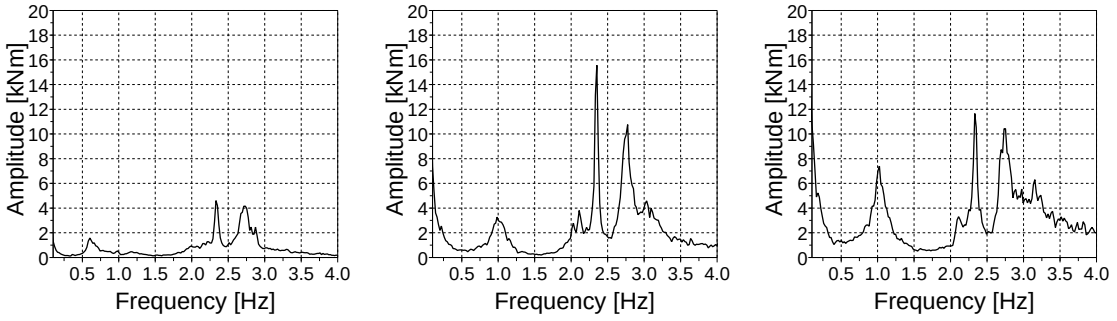

(d) Amplitude spectra

Figure 6.2: Illustration of rotor torque characteristics with respect to stationarity and Gaussianity for different operational conditions. Figures on the left: 6 m/s and 25 %, figures in the middle: 12 m/s and 20 %, figures on the right: 18 m/s and 15 %.

Table 6.1: Skewness and kurtosis of the example time series displayed in Figure 6.2 (a). For Gaussian distributions the skewness equals zero and the kurtosis equals three.

	Partial load $\bar{U} = 6\ m/s,\ I_T = 25\%$	Transition $\bar{U} = 12\ m/s,\ I_T = 20\%$	Full load $\bar{U} = 18\ m/s,\ I_T = 15\%$
Skewness	1.19	-1.09	-0.05
Kurtosis	4.46	3.56	2.96

of 2-min. length (b) demonstrate the non-stationary behaviour of the mean and the variance of the torque at partial load and at the transition region. At full load operation, the torque appears to be much more stationary.

Quantile plots (c) illustrate that the probability distribution of the torque almost matches the Gaussian distribution at full load. This is also confirmed by the skewness and the kurtosis derived from the example time series (compare Table 6.1). In contrast, the probability distributions at below rated and at the transition region substantially deviate from Gaussian.

The amplitude spectra in Figure 6.2 (d) show that the rotor torque features a wide band of frequencies. Some distinctive peaks are visible which reflect properties of the turbine model related to structural dynamics (compare eigenfrequencies given in Annex B) and cyclic excitations for example with 3P frequency.

6.2 Equivalent load ranges and load magnitudes

In its most basic form, a load estimation procedure aims for the prediction of simple parameters which are related to the current load level. Although in general, statistical load parameters such as mean values and standard deviations of loads are also possible estimation targets, the prediction of equivalent loads is preferred. Equivalent loads are directly related to fatigue damage and allow for a meaningful evaluation of the past operation.

In the following investigations on the rotor torque, equivalent load ranges and load magnitudes are estimated for different exponents. These values were derived with standard counting procedures for each training and test data set. In addition, statistical parameters of the standard signals were calculated. They served as input to the neural network during training and also for the prediction.

In a first step, neural networks were trained to transfer the input parameters into equivalent loads. Separate networks were set-up for each target value. Several network architectures and combinations of input parameters were examined and tested

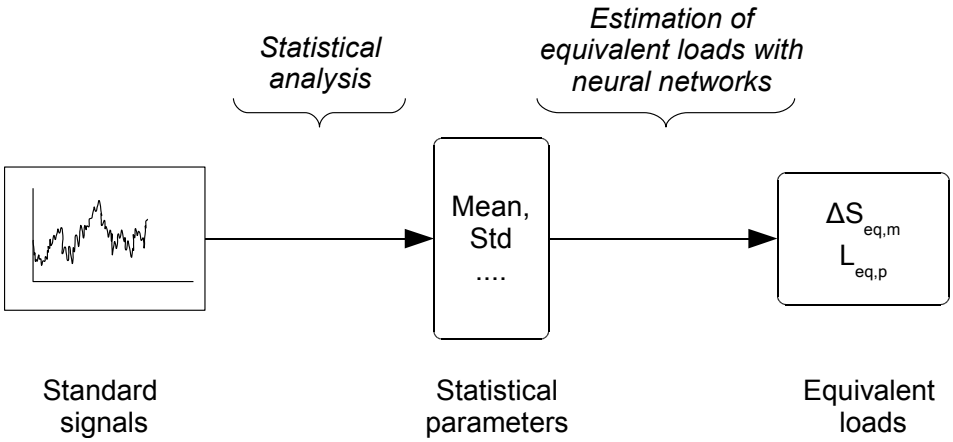

Figure 6.3: Scheme for the estimation of equivalent loads from statistical parameters of standard signals

manually with a trial-and-error method[1]. In all cases, relatively small networks proved to be sufficient. Only one hidden layer with a maximum of six neurons was required to already achieve very accurate estimation results. In addition, only very few input parameters were necessary. The prediction of equivalent load magnitudes was performed on the basis of the mean value and the standard deviation of the rotational speed and the power signal. For the equivalent load ranges, the rotational acceleration of the generator was included as an additional signal and the kurtosis as an additional statistical parameter. The general estimation scheme is illustrated in Figure 6.3.

After training was completed, the statistical parameters of the 132 test data sets were fed successively into the networks and equivalent loads were estimated for each data set. Figure 6.4 shows a comparison of estimated and directly calculated equivalent loads for the exponents of 4 and 10. For an exact match between these two, all dots would be located on an imaginary diagonal line. Obviously, this is not the case. Nevertheless, the estimation seems to be quite accurate and only a small scatter is visible. This is confirmed from the results of a linear regression analysis. Calculation of the coefficients of determination for the residuals (compare Chapter 4) yields values larger than 0.96 in any case. This means that more than 96 % of the variation in equivalent loads can be reproduced by the neural network based transfer function. The largest scatter occurs for the equivalent load ranges and an exponent of 10, while estimations of the equivalent load magnitudes matched the directly calculated values almost perfectly.

Numerical values of the estimation errors E are given in Table 6.2. The results

[1] A more systematic optimisation using network pruning has been employed during the analysis of data from a real wind turbine in Chapter 7.

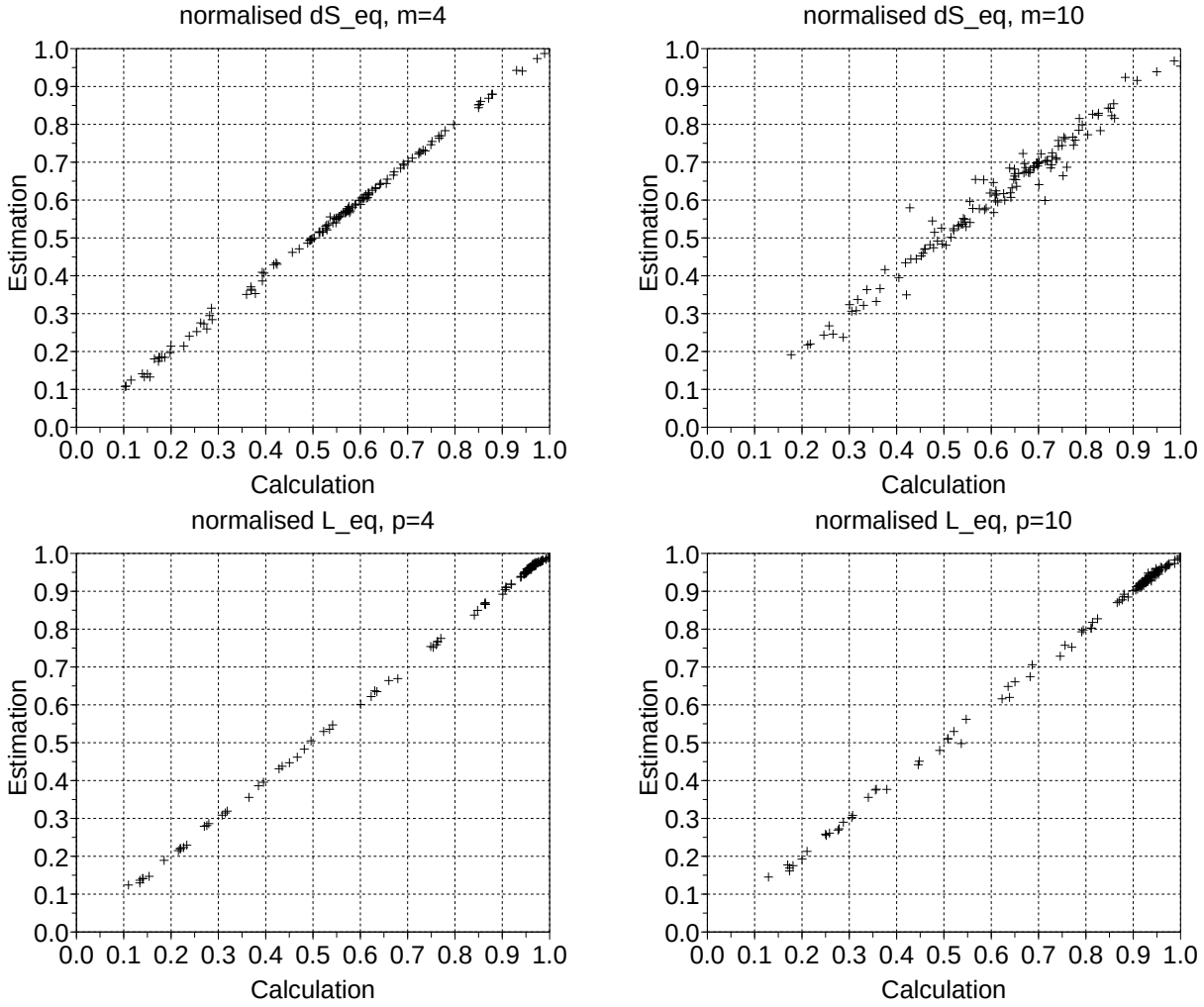

Figure 6.4: Estimated versus calculated equivalent loads from simulations (normalised values)

have been classified and grouped with respect to the average wind speed during the simulation. This classification also corresponds to the operational states of the turbine: below rated from 4 to 8 m/s, around rated from 9 to 16 m/s and above rated from 17 to 25 m/s. Out of the 132 analysed time series, 30 were categorized as below rated, 48 as rated and 54 as above rated. The averaged errors for the exponents 4 and 10 are given, where a positive value indicates an overestimation of the equivalent load. In addition, the standard deviations of errors σ_E are listed. They are measures of the error which can be expected for a single estimation.

In general, the estimated loads coincide very well with the directly calculated values. This holds true for all operational states. The standard deviation of errors is largest for low wind speeds, probably due to the potentially large variation in equivalent loads in the below rated operational states (compare also Figures 3.2 and 3.3). An error of about 10 % can be expected for a single estimation of the equivalent load ranges, but

Table 6.2: Estimation errors E and standard deviations of errors σ_E of the equivalent rotor torque ranges ΔS_{eq} magnitudes L_{eq} from simulations

	Equivalent load ranges ΔS_{eq}			
	m = 4		m = 10	
Average wind speed m/s	E %	σ_E %	E %	σ_E %
4.0 - 8.0	0.2	5.5	-0.5	10.1
9.0 - 16.0	0.0	1.4	0.1	5.0
17.0 - 25.0	0.0	0.4	-0.4	2.2
Accumulated	0.0	2.8	-0.3	5.8
Extrapolated (IEC TC II)	-0.2	-	-1.2	-
	Equivalent load magnitudes L_{eq}			
	p = 4		p = 10	
Average wind speed m/s	E %	σ_E %	E %	σ_E %
4.0 - 8.0	0.4	2.9	0.1	3.9
9.0 - 16.0	0.2	0.5	0.1	0.9
17.0 - 25.0	0.1	0.3	-0.1	0.5
Accumulated	0.1	1.4	0.0	2.0
Extrapolated (IEC TC II)	0.2	-	0.2	-

it reduces for higher wind speeds.

The averaged errors for the different operational states as well as the error of the accumulated loads are quite small. This indicates an unbiased estimation where the single estimation errors eventually average out. Based on the wind speed distribution according to type class II of the IEC standard [16], the estimated and calculated loads have also been extrapolated to 20 years lifetime. Calculation of the prediction error shows almost an exact match for equivalent ranges and equivalent magnitudes.

It should be emphasised, that these results are based on simulations which feature well defined ‘laboratory’ conditions. Therefore, they are probably close to the possible maximum regarding their accuracy and load predictions with measured data will be more challenging. However, the efforts to achieve these results were also kept within reasonable limits, so that there is certainly room for improvements as well. Among these are the application of more sophisticated training algorithms, optimisation of network topology or the combination of networks to ensembles for an improved generalisation [88]. Examples for a systematic optimisation of network topology and input data selection with network pruning are given in Chapter 7 on the basis of measured data.

6.3 Load cycle distributions

6.3.1 Frequency domain methods for the calculation of load cycle distributions

Typically, load cycle distributions are derived from measured or simulated time series by means of appropriate counting algorithms. Besides this direct time series counting, there are several analytical or semi-empirical approaches for the calculation of load cycle distributions from statistical parameters. These approaches are usually based on the frequency domain representation of a signal. From this representation the spectral moments of the signal can be calculated first and then the distribution of rainflow cycles can be derived. Application of such methods as the basis for load predictions seems to be very attractive, as only a few parameters have to be estimated to enable the computation of the whole load cycle distribution.

Usually, these analytical or semi-empirical approaches relate statistical parameters of the time and frequency domain to the probability density distribution (PDF) of load cycles. A varying number of parameters is included depending on the method. It is not yet fully understood as to which parameters are theoretically required to give accurate results and hence have to be included. However, in 1990, Bishop and Sherratt demonstrated, that an exact theoretical relation between the PSD and the PDF of load cycles exists [89, 90], at least for Gaussian processes. Given that the PSD does not contain any phase information this can not be taken as self-evident. Nevertheless, up to now a universally valid relation has not been found and the determination of dependencies between the distribution of fatigue cycles and statistical parameters is still a research objective [91, 92].

Parameters which characterise random loadings in the frequency domain are often calculated from the spectral moments λ_n. These moments indicate the distribution of a signal's energy with respect to its frequency content. Therefore, they are often utilised to characterise the bandwidth of a process. Among others, an important family of spectral moment based bandwidth parameters is defined as:

$$\alpha_n = \frac{\lambda_n}{\sqrt{\lambda_0 \lambda_{2n}}} \tag{6.1}$$

where often only the first one or two parameters are used:

$$\alpha_1 = \frac{\lambda_1}{\sqrt{\lambda_0 \lambda_2}}, \quad \alpha_2 = \frac{\lambda_2}{\sqrt{\lambda_0 \lambda_4}} \tag{6.2}$$

In narrow-band processes α_n approaches zero, while advancing one for broad-band processes.

Based on results from Rice [93], the spectral moments can also be related to the expected number of up-crossings υ_0 per unit time for stationary Gaussian processes:

$$\upsilon_0 = \frac{1}{2\pi}\sqrt{\frac{\lambda_2}{\lambda_0}} \tag{6.3}$$

The term $\sqrt{\lambda_2/\lambda_0}$ equals the radius of gyration of the PSD about the origin and can hence be interpreted as a mean equivalent frequency of the random process [94]. Dividing by 2π (because λ_n is based on the angular frequency) yields the rate of occurrences of up-crossings per unit time.

Similarly, the expected number of peaks per unit time which also corresponds to the number of expected load cycles can be calculated from:

$$\upsilon_p = \frac{1}{2\pi}\sqrt{\frac{\lambda_4}{\lambda_2}} \tag{6.4}$$

where $\sqrt{\lambda_4/\lambda_2}$ is the radius of gyration of the PSD about the origin of the derivative of the process. Often, an irregularity factor of a process is calculated from the number of up-crossings and peaks as υ_0/υ_p. In case of stationary Gaussian processes this yields the expression for α_2 exactly.

As stated before, a method which is able to relate these frequency domain parameters to load cycle distributions for general processes is not available yet. Analytically derived solutions or approximations only exist for some special cases, for example harmonic or stationary narrow-banded processes.

One of the most popular approaches, the one from Dirlik [95], has been derived empirically by fitting PDFs of load cycles to simulated data. Application of the method is restricted to stationary Gaussian signals, although relatively accurate results are reported even for cases where the requirement of Gaussianity is not met [90]. Another approach has recently been developed by Tovo and Benasciutti [96]. Their method can handle non-Gaussian data, but still maintains the requirement of stationarity.

Stationary is a general requirement for all available PSD methods and dealing with non-stationary data is not straightforward. However, most wind turbine load signals do not fulfil this requirement. Varying wind conditions and the different characteristic frequencies of the wind turbine are reflected in the load signals and therefore they often feature a non-stationary behaviour with a wide band of frequencies (compare

Figure 6.2). The performance of the Dirlik and the TB method under such conditions is evaluated in the following. The results are compared to rainflow cycle distributions derived from time domain counting.

Dirlik's expression for stationary Gaussian processes

Dirlik [95] approximated the amplitude probability distribution of stationary Gaussian processes by a combination of an exponential and two Rayleigh distributions. The parameters of these distributions can be calculated from four spectral moments only. To derive analytical relations between spectral moments and the parameters of the three distributions, Dirlik analysed several simulated stationary Gaussian processes. Fitting procedures were then applied to approximate the resulting amplitude densities from time domain counting by the selected distributions.

Due to its simplicity, the Dirlik approach is probably the most widely used frequency domain method for the calculation of rainflow cycle distributions. Although in general it is limited to stationary Gaussian processes, it often gives reasonable results even if these requirements are not fully met.

The overall PDF of rainflow ranges $p(\Delta S)$ can be computed from a weighted linear combination of the three single distributions as:

$$p(\Delta S) = D_1 \cdot p^{exp}(\Delta S) + D_2 \cdot p^{vR}(\Delta S) + D_3 \cdot p^{sR}(\Delta S) \tag{6.5}$$

with

- the exponential distribution

$$p^{exp}(\Delta S) = \frac{1}{2\sqrt{\lambda_0}} \cdot \frac{1}{Q} e^{-\frac{Z}{Q}} \tag{6.6}$$

- the variable Rayleigh distribution

$$p^{vR}(\Delta S) = \frac{1}{2\sqrt{\lambda_0}} \cdot \frac{Z}{Var^{vR}(Z)} e^{-\frac{Z^2}{2Var^{vR}(Z)}} \tag{6.7}$$

- and the standard Rayleigh distribution

$$p^{sR}(\Delta S) = \frac{1}{2\sqrt{\lambda_0}} \cdot Z e^{-\frac{Z^2}{2}} \tag{6.8}$$

and

$$Z = \frac{\Delta S}{2\sqrt{\lambda_0}}$$

All weighting factors and remaining parameters are calculated from the spectral moments of the PSD and the above given bandwidth parameters respectively. Dirlik derived the following expressions by fitting $p(\Delta S)$ to the shape of empirically derived rainflow range distributions:

$$D_1 = \frac{2(x_m - \alpha_2^2)}{1 + \alpha_2^2} \quad , \quad D_2 = \frac{1 - \alpha_2 - D_1 + D_1^2}{1 - \sqrt{Var^{vR}(Z)}}$$

$$D_3 = 1 - D_1 - D_2 \quad , \quad Q = \frac{1.25(\alpha_2 - D_3 - \sqrt{Var^{vR}(Z)}D_2)}{D_1}$$

$$\sqrt{Var^{vR}(Z)} = \frac{\alpha_2 - x_m - D_1^2}{1 - \alpha_2 - D_1 + D_1^2} \quad , \quad x_m = \alpha_1 \cdot \alpha_2$$

The method of Tovo-Benasciutti for stationary processes

In 2005, Tovo and Benasciutti (TB) published an approach for the calculation of the PDF of load ranges from PSD data which also is applicable to non-Gaussian processes [96, 97]. This method is more complex than Dirlik's approach and only a brief overview can be given here.

The basic idea is that, for Gaussian processes, the expected damage given by the results from the rainflow counting method $E(D_{RF})$ is bound by the expected damage from two other cycle counting procedures: the one from level crossing $E(D_{LC})$ and range-mean counting $E(D_{RM})$. In addition it can be shown, that the damage from level crossing equals the damage from a so-called narrow-band approximation $E(D_{NB})$ and therefore:

$$E(D_{RM}) \leq E(D_{RF}) \leq E(D_{NB}) \tag{6.9}$$

This relation can now be exploited to give an estimate of the expected rainflow damage from a linear combination of the damages from the narrow-band approximation and the range-mean method:

$$E(D_{RF}) = bE(D_{NB}) + (1 - b)E(D_{RM}) \tag{6.10}$$

In [96] Tovo and Benasciutti suggested an approximation for b which was calibrated on simulation results from Gaussian random processes with different spectral densities and bandwidth parameters:

$$b \cong \frac{(\alpha_1 - \alpha_2)[1.112(1 + \alpha_1\alpha_2 - (\alpha_1 + \alpha_2))e^{2.11\alpha_2} + (\alpha_1 - \alpha_2)]}{(\alpha_2 - 1)^2} \tag{6.11}$$

However, Karlsson [98] argues that b can be outside the interval [0,1] and hence

suggest to use $\tilde{b}$ instead of b where

$$\tilde{b} = \begin{cases} 0 & \text{, if } b \leq 0 \\ b & \text{, if } 0 \leq b \geq 1 \\ 1 & \text{, if } b \geq 1 \end{cases} \tag{6.12}$$

The application of the TB method for non-Gaussian processes is feasible, because it is not based on probability density functions of load cycles. Instead, it utilises joint probability distributions for combinations of peaks x_p and valleys x_v to characterise load cycle occurrence probabilities. This has got the advantage, that load cycles can be resized by adjusting peaks and valleys in case of non-Gaussian processes. Similar to equation 6.10, the joint cumulative distribution function (CDF) can be approximated by:

$$H_{RF}(x_p, x_v) = bH_{NB}(x_p, x_v) + (1-b)H_{RM}(x_p, x_v) \tag{6.13}$$

where $H_{NB}(x_p, x_v)$ and $H_{RM}(x_p, x_v)$ turn out to be:

$$\begin{aligned} H_{NB}(x_p, x_v) = &\left[P_p(x_v) + \alpha_2(e^{-\frac{x_v^2}{2\lambda_0}} - e^{-\frac{x_p^2}{2\lambda_0}})I(x_p + x_v)\right] I(-x_v) \\ &+ \left[P_v(x_v) - \alpha_2 e^{\frac{x_p^2}{2\lambda_0}}\right] I(x_v) \end{aligned} \tag{6.14}$$

$$\begin{aligned} H_{RM}(x_p, x_v) = &\Phi\left(\frac{x_v}{\sqrt{\lambda_0(1-\alpha_2^2)}}\right) - \alpha_2 e^{-\frac{x_p^2}{2\lambda_0}} \Phi\left(\frac{x_v - x_p(1-2\alpha_2^2)}{2\alpha_2\sqrt{\lambda_0(1-\alpha_2^2)}}\right) \\ &+ \alpha_2 e^{-\frac{x_v^2}{2\lambda_0}} \left[\Phi\left(\frac{x_p - x_v(1-2\alpha_2^2)}{2\alpha_2\sqrt{\lambda_0(1-\alpha_2^2)}}\right) - \Phi\left(\frac{\alpha_2 x_v}{\sqrt{\lambda_0(1-\alpha_2^2)}}\right)\right] \end{aligned} \tag{6.15}$$

with the cumulated distribution of peaks $P_p(x_p)$ and valleys $P_v(x_v)$, the standard normal distribution $\Phi(\cdot)$ and an indicator function $I(\cdot)$ which equals zero for negative values and otherwise equals one.

Non-Gaussian processes can be treated with this approach, if suitable transfer functions for peaks and valleys are available. In this case, the function $G(\cdot)$ transforms data from the Gaussian into the non-Gaussian domain, while $g(\cdot)$ does the inverse:

$$(z_p, z_v) = (G(x_p), G(x_v)) \tag{6.16}$$

$$(x_p, x_v) = (g(z_p), g(z_v)) \tag{6.17}$$

Hence, the joint CDF can be transferred from one domain to the other simply by trans-

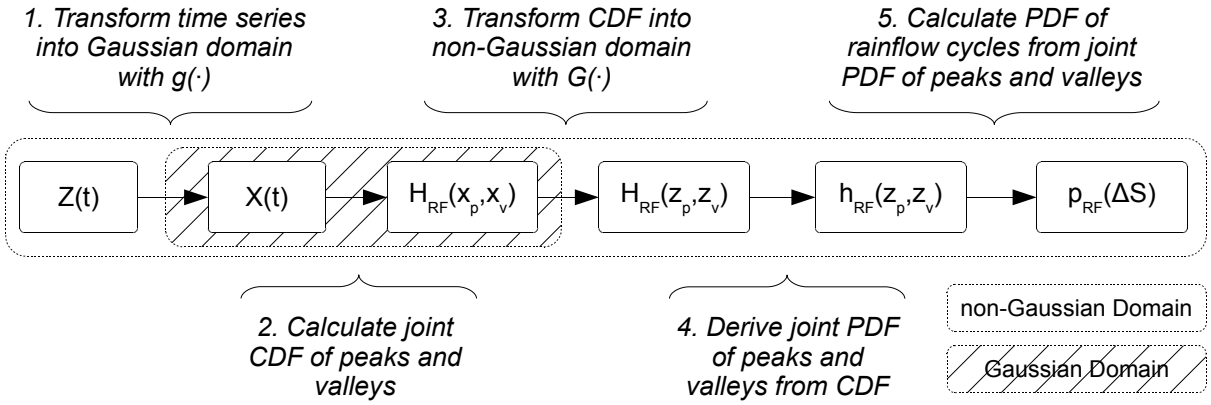

Figure 6.5: Steps of the Tovo-Benasciutti approach for the calculation of the probability density function of rainflow cycles for stationary non-Gaussian processes

forming the peaks and valleys:

$$H_{RF}(z_p, z_v) \Longrightarrow H_{RF}(g(z_p), g(z_v)) = H_{RF}(x_p, x_v) \tag{6.18}$$

The general treatment of non-Gaussian load time series with the TB method is illustrated in Figure 6.5. In a first step, a suitable transfer function is established which corrects the time series for non-Gaussianity. In the Gaussian domain, the spectral moments are computed from which the joint CDF of peaks and valleys $H_{RF}(x_p, x_v)$ is calculated using Equation 6.11 to 6.15. The cumulative distribution is transferred back into the non-Gaussian domain, where the joint PDF of peaks and valleys and finally the PDF of load cycles are derived.

Figure 6.5 displays the process as proposed by Tovo and Benasciutti. However, in practice it turns out to be more efficient to define the discrete peaks and valleys directly in the non-Gaussian domain and to calculate $H_{RF}(g(z_p), g(z_v))$ in the Gaussian domain. In doing so, the inverse transfer function $G(\cdot)$ is not required and step 3 can be omitted.

The degree of non-Gaussianity of a process is often measured by its skewness and kurtosis (see Equations 5.1 and 5.2). These two parameters indicate, how close the third and fourth moment of a signal match the theoretical values of a Gaussian process. Therefore, one or both parameters also frequently serve as parameters of Gaussian transfer functions. Several methods for the transformation of time series from the Gaussian into the non-Gaussian domain and vice versa exist. Some of them have been summarised by Benasciutti in [97].

Because Winterstein's Hermite moment models [99] correct both the skewness and the kurtosis of a process, they have been applied here in conjunction with the TB method. The method employs Hermite polynomials to resemble the transfer functions in both directions. Winterstein related the coefficients of the polynomials to the skew-

ness and the kurtosis and thereby established second order Hermite models. Different models are required for so-called softening ($\gamma_4 > 3$) and hardening ($\gamma_4 < 3$) processes and hence four transfer functions are required in total. Further details are given in Annex H.

Unfortunately, the transformation functions are not monotonic for all combinations of skewness and kurtosis. Therefore, not all processes can be treated with the Winterstein transformation and the method works only if the deviation from Gaussian is sufficiently small. To improve the modelling and simulation of non-Gaussian processes, Gurley [100, 101] proposed a modification to the Hermite transformation. He extended the Winterstein models with an optimisation procedure. This procedure is designed to minimise the error between the target skewness and kurtosis and the skewness and kurtosis measured after the transformation. Minimising the error provides the values of $\tilde{\gamma_3}$ and $\tilde{\gamma_4}$ which are the optimal coefficients of the Hermite model for the desired transformation. These values do not correspond to the measured skewness and kurtosis of the process anymore and hence do not have a direct physical meaning. Nevertheless, the modified transformation is supposed to give more accurate results than the pure Winterstein transformation. Both approaches have been applied in conjunction with the TB method and the results are discussed in the next section.

6.3.2 Evaluation of the methods in case of non-Gaussian and non-stationary processes

For test purposes, the 660 time series of the rotor torque, which were initially generated for network training purposes, have been analysed with the approaches discussed above. The resulting load cycle distributions, extrapolated to 20 year lifetime according to the IEC standard, are displayed in Figure 6.6. It can be seen that the method of Dirlik and the TB approach yield quite similar results, if the Gaussian transformation is omitted. However, both seem to overestimate the true load cycle distribution from rainflow counting in the time domain. This holds true especially for large and medium size ranges.

The situation for large ranges can be improved by including the Gaussian transformation on the basis of Winterstein's Hermite moment models. At the same time, the difference to the rainflow counting results for medium ranges increases. Further improvements for the large load ranges can be achieved with the modified Winterstein transformation proposed by Gurley. Nevertheless, the difference to the rainflow counting results is still significant.

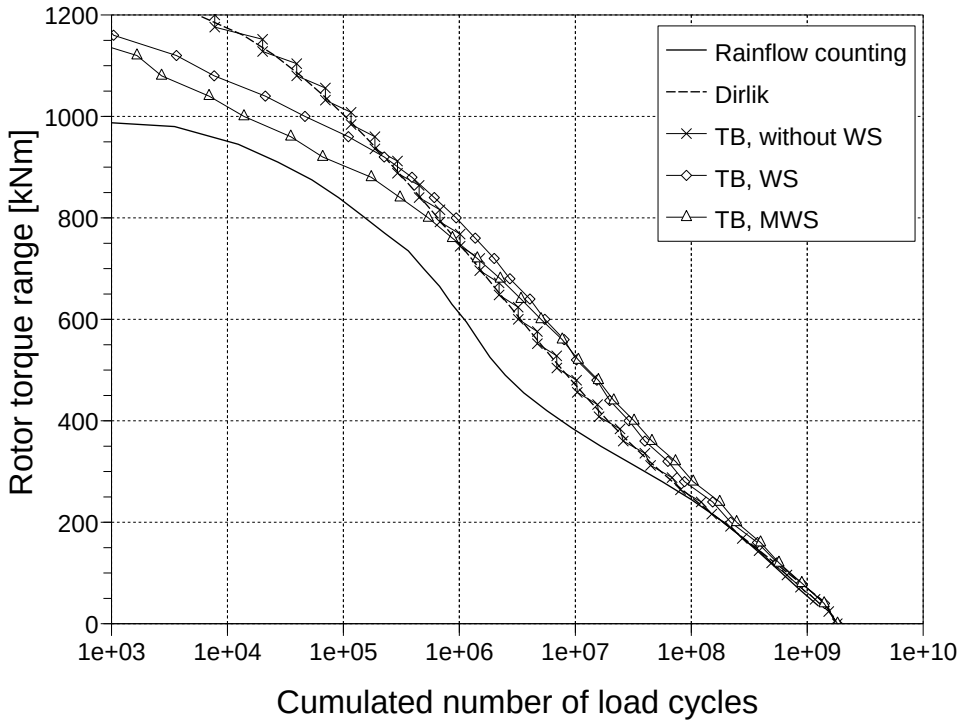

Figure 6.6: Load cycle distributions of the simulated rotor torque from rainflow counting, Dirlik's method, TB method without any correction for non-Gaussianity, TB method with Winterstein transformation and TB method with modified Winterstein transformation

The performance of the Dirlik approach for wind turbine loads has been investigated by other authors in the past. Ragan and Manuel [102] analysed field data from a 1.5 MW wind turbine and compared the results with those from rainflow counting. They found that the accuracy of Dirlik's method differs significantly depending on the investigated load component. Relatively good agreement was observed for tower base bending moments which also corresponds to results derived for offshore wind turbines by van der Tempel [103]. For the investigated blade loads, Ragan and Manuel got much higher fatigue loads from Dirlik's approach compared to the rainflow counting procedure. They argued, that blade loads contain considerable periodic components and do not fulfil the requirements of Gaussianity and stationarity.

This argument certainly applies in the presented investigation of the rotor torque as well. However, in the case of the TB approach the non-Gaussianity has been taken into account. To exclude all possibility of doubt regarding the Gaussian transformations, additional investigations have been carried out: Empirical transfer functions were developed for each time series so that their CDF after the transformation exactly matches the CDF of a Gaussian signal. These transfer functions which yield ideal Gaussian signals were than applied in conjunction with the TB method. It was found that the results are quite comparable to the ones from the modified Winterstein transformation.

This confirmed the good transformation capabilities of the modified Hermite moment models.

If the Gaussian transformation works with satisfying accuracy, the non-stationarity of the signals is left as the reason for the poor prediction. This hypothesis is substantiated by the fact, that the deviations between rainflow counting and TB method turned out to be much larger for operation below and around rated (also confirmed by Ragan and Manuel [102]). In these operational states a slowly varying wind speed generates large low-frequency load cycles. Given the limited length of simulated time series of 10 minutes, such load cycles can appear as non-stationarity (compare Figure 6.2). On the contrary, the results at above rated operation, where such large low-frequency load cycles are not present in the rotor torque, agree much better with the ones from rainflow counting.

It should be mentioned, that the extrapolation of a limited number of time domain simulations probably does not contain the largest load cycles occurring within 20 years and that the rainflow counting tends to give non conservative results. Albeit this is certainly true, it seems to be more likely that most of the mismatch is due to the non-stationary time series caused by the non-linear wind turbine characteristics.

Stationarity is a condition which has to be met in all cases where PSD data is applied for load cycle calculations. Sherratt et al. [91] recommend to ensure stationarity by analysing only sufficiently small time periods. Another workaround is to split the signal into a low and high frequency part and to analyse each part separately. Similar approaches are known for example from the analysis of bi-modal processes. In general, the combined PDF of two independent variables can be derived as the convolution of their independent density functions. The assumption of independence might be justified here, if one argues that the low frequency oscillations are caused by the varying wind conditions, while the high frequencies are mainly due to the dynamics of the structure. In this case the convolution yields

$$\begin{aligned} p(\Delta S) &= p_{LF}(\Delta S) \ * \ p_{HF}(\Delta S) \\ &= \int_{-\infty}^{+\infty} p_{LF}(\Delta S - \varsigma) p_{HF}(\varsigma) d\varsigma = \int_{-\infty}^{+\infty} p_{HF}(\Delta S - \varsigma) p_{LF}(\varsigma) d\varsigma \end{aligned} \tag{6.19}$$

where $p_{LF}(\Delta S_s)$ and $p_{HF}(\Delta S_s)$ are the PSDs of the low and high frequency parts with ς as the shift between the distributions.

Figure 6.7 shows the results of such an analysis. The simulated time series have been filtered and thereby split into two series: one containing the low frequency and

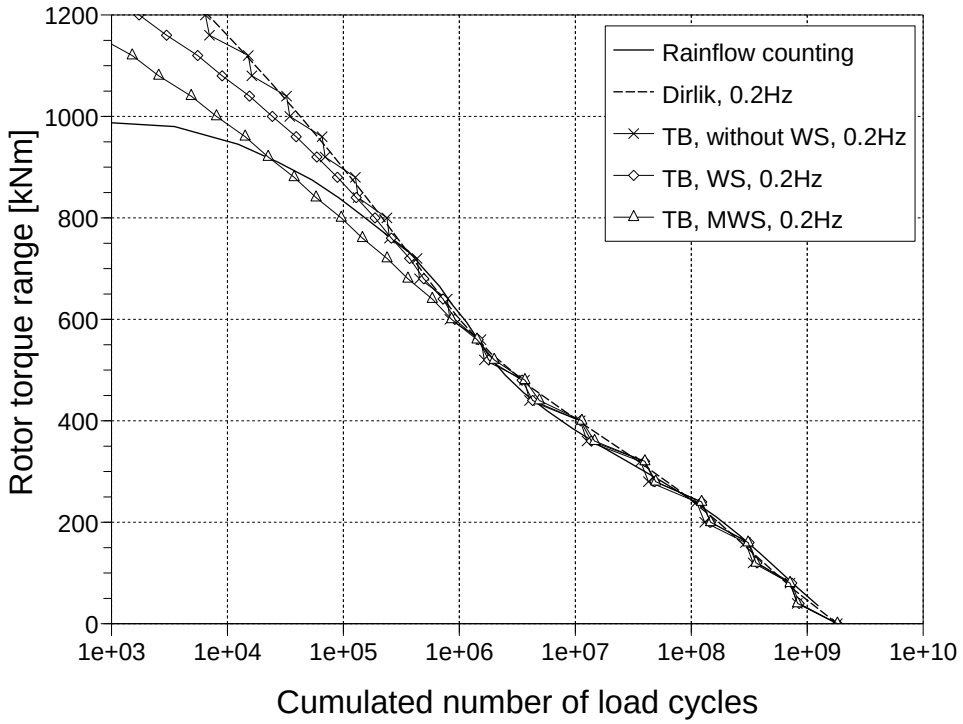

Figure 6.7: Load cycle distributions of the simulated rotor torque from rainflow counting, Dirlik's method, TB method without any correction for non-Gaussianity, TB method with Winterstein transformation and TB method with modified Winterstein transformation. The low and high frequency parts have been analysed separately with a cut-off frequency of 0.2 Hz

the other the high frequency oscillations. A frequency of 0.2 Hz has been chosen as the cut-off frequency, because a spectral gap was visible around this frequency, particularly for the time series below and around rated (compare Figure 6.2).

The agreement of all methods for medium load ranges with the rainflow counting results is much better now compared to Figure 6.6. Still, very large load ranges are not approximated well. Even if the analysis is done with the modified Winterstein transformation, the ranges only agree in an average sense. Unfortunately, the large ranges are frequently the most important ones regarding the fatigue life and therefore a good prediction accuracy for these ranges is compulsory in practice.

In the author's opinion, the investigations indicate, that the existing frequency domain techniques for predicting fatigue loads can not be easily applied for all wind turbine load signals. This is somewhat disappointing, because the general idea behind this techniques, namely the computation of complete fatigue load distributions from only a few parameters, suits the needs of a load estimation system perfectly.

More efforts towards the handling of non-stationarity might lead to a better match with rainflow counting results. However, this does not necessarily improve the situation

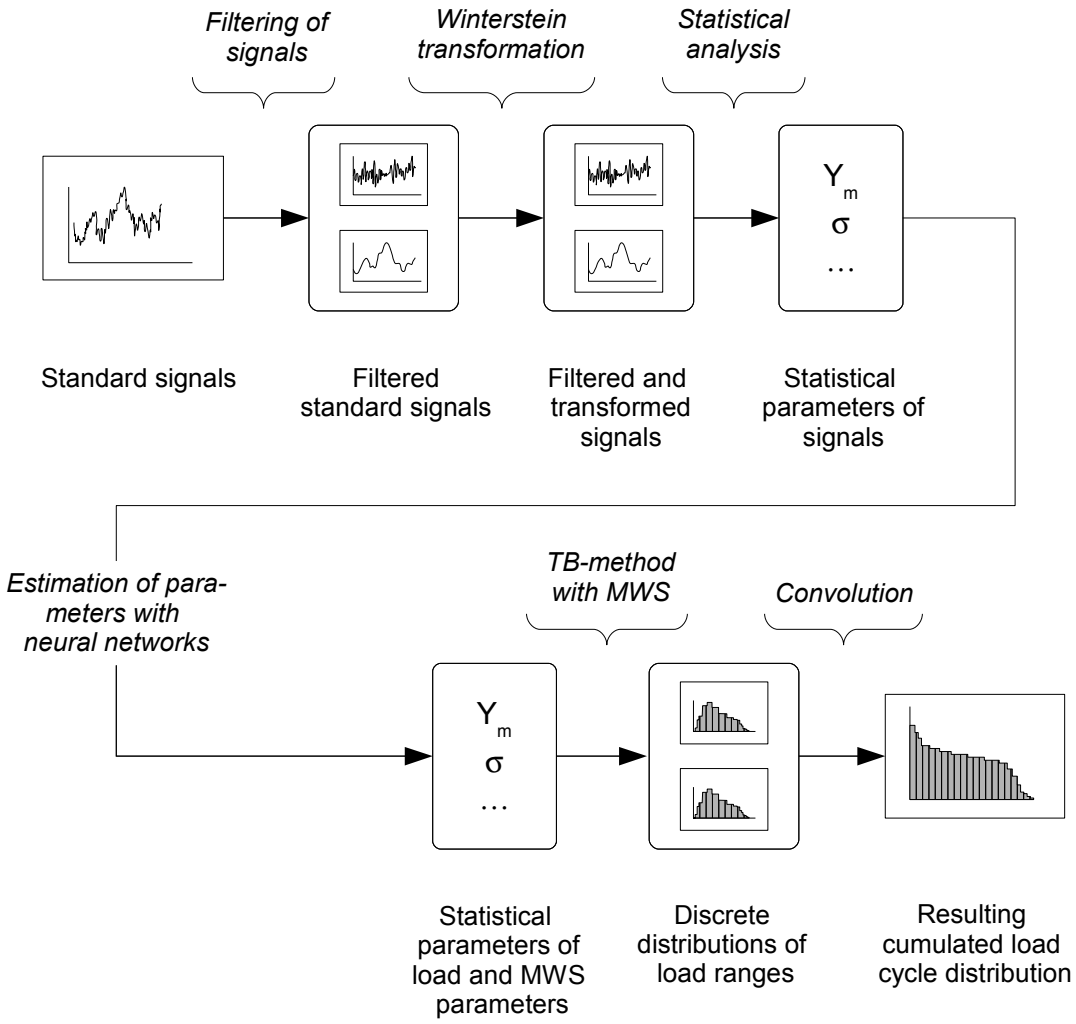

Figure 6.8: Complex load estimation procedure based on the TB method and Gurley's modified Winterstein transformation. The signal is split up into a low and high frequency part to improve performance for non-stationary signals.

for a load estimation system, because the approach will almost certainly become more complex. The performed splitting of time series into a high and low frequency part already doubles the number of parameters which have to be estimated from standard signals. A total number of 16 parameters is required for each load estimation in this approach, eight for each frequency part: mean value, variance, skewness and kurtosis in the non-Gaussian domain as well as four spectral moments of the signals in the Gaussian domain.

The corresponding neural network based estimation scheme on the basis of the TB method and the modified Winterstein transformation is shown in Figure 6.8. Application of this procedure for the estimation of simulated rotor torque ranges has been presented in [104]. The accuracy of the results was comparable to those of the directly calculated ones shown in Figure 6.7, with a good agreement of small and medium sized

ranges and an average matching of the large ranges. In this example, the standard signals have also been filtered prior to the calculation of statistical parameters. This was done because the neural networks ability to estimate the statistical parameters of the low and high frequency load signals improved, when statistical data of filtered standard signals were available as input.

Nevertheless, the displayed estimation procedure (Figure 6.8) is probably already too complex for practical application in a load estimation system. It can therefore be concluded, that the analytical methods currently available to derive load range distributions from statistical parameters are not suited to serve as the core of a robust load estimation system for wind turbines. Instead, an alternative approach on the basis of empirically derived probability density functions of load ranges is developed in the following.

6.3.3 Development and test of an empirical approach for load cycle estimations

The development of an approach for the estimation of load ranges with empirically derived probability density distributions is inspired by work from Wang and Sun [105, 94] and Bishop [106]. These authors adopted and modified Dirlik's empirical approach according to their needs.

Wang's extension to Dirlik's formula

Similar to Tovo and Benasciutti, Wang investigated methods for the calculation of PDFs of load ranges for non-Gaussian processes from frequency domain data. However, he stayed much closer to Dirlik's idea of fitting appropriate distributions. Wang replaced Dirlik's standard Rayleigh distribution by a lognormal distribution. The rational behind this step is the desire for a more accurate approximation of the tail distributions. Hence, the density distribution of load ranges is given by

$$p(\Delta S) = W_1 \cdot p^{exp}(\Delta S) + W_2 \cdot p^{vR}(\Delta S) + W_3 \cdot p^{ln}(\Delta S) \tag{6.20}$$

with

$$p^{ln}(\Delta S) = \frac{1}{\sigma_Z^{ln}\sqrt{2\pi}Z} e^{-\frac{1}{2}\left(\frac{lnZ-\bar{Z}^{ln}}{\sigma_Z^{ln}}\right)^2} \tag{6.21}$$

and $p^{exp}(\Delta S)$ and $p^{vR}(\Delta S)$ similar to Equations 6.6 and 6.7 respectively.

The distributions are defined by 6 parameters in total of which only 5 are independent

(because $W_1 + W_2 + W_3 = 1$). Wang proposed to derive the 5 distribution parameters from fitting procedures and gave recommendations for suitable methods. In addition, he developed expressions for these parameters himself which depended on the kurtosis γ_4, the bandwidth parameter α_2 and x_m (see Dirlik's formula) as independent process variables.

Bishop's calculations including deterministic components

Bishop [106] and Bishop et al. [90] applied Dirlik's approach for the calculation of wind turbine blade fatigue loads. These loads include significant deterministic components and therefore in fact fall outside the limits of applicability of this method (compare Figure 2.2). As a consequence, in particular the edgewise load cycle distributions derived from frequency domain parameters showed large deviations from the rainflow counting results. Bishop concluded, that one reason for this is the non-stationarity of the load signals. However, he considered the significant deterministic load component due to the gravity of the blade as far more important for the mismatch.

To improve the capability of Dirlik's PDF to capture deterministic load components, Bishop replaced the standard Rayleigh distribution by a Gaussian distribution:

$$p(\Delta S) = B_1 \cdot p^{exp}(\Delta S) + B_2 \cdot p^{vR}(\Delta S) + B_3 \cdot p^{G}(\Delta S) \tag{6.22}$$

with

$$p^{G}(\Delta S) = \frac{1}{\sigma_Z^G \sqrt{2\pi}} e^{-\frac{(Z-\bar{Z}^G)^2}{2\ \sigma_Z^G}} \tag{6.23}$$

and again $p^{exp}(\Delta S)$ and $p^{vR}(\Delta S)$ similar to Equations 6.6 and 6.7.

Bishop generated a large number of test cases, consisting of combinations of different PSDs and deterministic components and fitted $p(\Delta S)$ to approximate the combined load range distributions. Unlike Dirlik and Wang, no analytical equations were derived to relate the parameters of the fitted PDF to independent process variables, such as the spectral moments or bandwidth parameters. Instead he employed neural networks to establish a relationship between the test PSDs and the PDF parameters from the fitting procedure.

Both of the above examples demonstrate, that Dirlik's approach can be modified to yield more accurate results, for example in the case of non-Gaussian processes (Wang) or for data with significant deterministic components (Bishop). In addition, Bishop demonstrated that a sophisticated transfer function, which links PSD data and

PDF parameters, is suited to reduce inherent limitations of frequency domain methods.

A similar approach can be applied for a load estimation system as well. In a first step, density distributions have to be defined which are able to approximate the rainflow counting results. Secondly, a transfer function has to be derived. Here, neural networks are used for this task. They map statistical parameters of the standard signals to the parameters of the chosen PDF types.

Such an empirical approach can also be used to deal with two common problems related to the calculation of load cycle distributions with frequency domain methods:

- Expected total number of load cycles
  Equation 6.4 has been derived for stationary Gaussian processes only. Nevertheless, it is also applied to calculate the expected number of load cycles in the TB method. Benasciutti argues that transformation of a broad-band non-Gaussian process into the Gaussian domain influences the magnitudes of peaks and valleys, but not the total number of load cycles [97].

  For non-stationary processes or if relevant deterministic components are present, the real number of load cycles can be significantly different to those given by Equation 6.4. This effect is reported by Bishop from his investigations on deterministic components [106] and also appeared in the investigations above. Although it is hard to spot due to the logarithmic scale in Figures 6.6 and 6.7, the total number of load cycles from rainflow counting is about 25 % lower than from frequency domain methods. This deviation can probably be reduced, if the expected number of load cycles are directly estimated by means of trained neural networks from statistical parameters of standard signals.

- Expected maximum load ranges
  Wind turbines are non-linear systems and the behaviour of the turbine adapts to external conditions (for example via a control system). One key purpose of this adaptation is the limitation of maximum and minimum loads. Therefore, the possible extreme load ranges during normal operation are limited in practice as well. However, frequency domain methods are commonly derived on the basis of linear processes. For such processes, the extreme load ranges are not bound by any physical limitations, although the occurrence probability decreases for increasing load ranges. As a consequence, some theoretical probability remains even for extremely large load cycles which do not occur in practice because of the non-linear behaviour of real systems.

  The possible overestimation of large load cycles remains for any approach which utilises continuous distributions for the approximation of the PDF of load cycles.

A solution to this problem is the estimation of the largest expected load cycle from standard signals. Knowledge of the largest expectable range can then be used to limit the estimated PDF of load ranges accordingly.

It should be noted, that estimation of maximum load ranges will not give the theoretically likely maximum load ranges of a process. The reason for this is, that the estimation procedure is developed on the basis of time series of finite length. Hence, only the maximum value for the given period of time can be predicted. Because the estimated loads will usually be compared with other data of limited length, for example to results from load measurements or simulations, this is rather a desirable feature than a disadvantage.

An empirical approach for the estimation of PDF or CDF of load cycles requires three major steps (compare Figure 6.9). Two of them are part of the pre-processing and are performed only during the set-up of the load estimation procedure.

First, the parameters of empirically fitted distributions have to be derived. This also includes the identification of suitable but simple distributions which can be fitted to the amplitude probability density distributions of the analysed time series. The calculated parameters, including the maximum ranges and the total number of load cycles, have to be recorded so that they can be used as target values for the estimation.

In a second step the neural network has to be trained to predict the target values from statistical parameters of standard signals. The quality of the result will be influenced by several decisions regarding the selection of adequate statistical parameters, the network architecture, the applied training algorithms and the choice of appropriate training data sets.

Once these steps have been accomplished the actual estimation procedure can be performed. It consists of the following tasks:

1. Analysis of the measured standard signals to derive the required statistical parameters

2. Application of the trained neural network for prediction of the target values on basis of the previously derived input parameters

3. Calculation of the empirical probability density distribution of amplitudes and further processing of the PDF into a CDF of load cycles

Similar to the investigations in Section 6.2, the feasibility of this approach has been tested on simulated data of the rotor torque. First, several single distributions as well as combinations of distributions have been evaluated regarding their suitability to approximate the PDFs derived from simulations. Only the simulated training data was

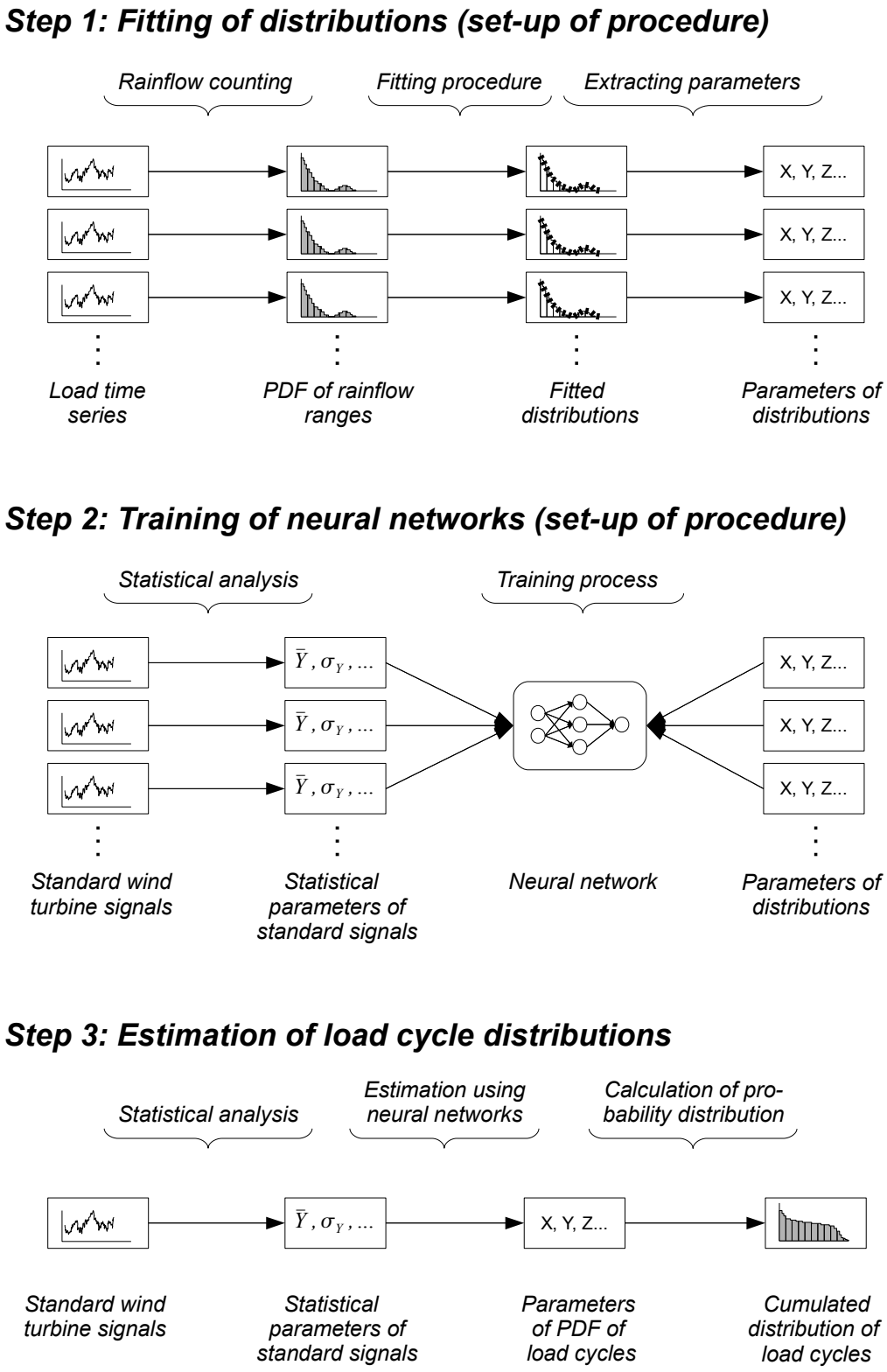

Figure 6.9: Set-up and application scheme of an empirical approach for the estimation of load cycles from standard wind turbine signals.

employed for this investigation. It turned out, that utilisation of one or two distributions for the fit is already sufficient to give relatively accurate results.

In Figure 6.10, the results from a fitted lognormal distribution $p^{ln}(\Delta S)$ as well as those from a combination of a variable Rayleigh and a lognormal distribution $p^{lnR}(\Delta S)$ are compared to load cycles of the rotor torque from rainflow counting. These distributions are defined as:

$$p^{ln}(\Delta S) = \frac{1}{2\sqrt{\lambda_0}} \left(\frac{1}{\sigma_Z^{ln}\sqrt{2\pi}Z} e^{-\frac{1}{2}\left(\frac{lnZ-\bar{Z}^{ln}}{\sigma_Z^{ln}}\right)^2} \right) \tag{6.24}$$

$$p^{lnvR}(\Delta S) = \frac{1}{2\sqrt{\lambda_0}} \left(\frac{C_1}{\sigma_Z^{ln}\sqrt{2\pi}Z} e^{-\frac{1}{2}\left(\frac{lnZ-\bar{Z}^{ln}}{\sigma_Z^{ln}}\right)^2} + \frac{C_2 Z}{Var^{vR}(Z)} e^{-\frac{Z^2}{2Var^{vR}(Z)}} \right) \tag{6.25}$$

with Z as defined by Dirlik and $C_1 + C_2 = 1$.

Both distributions approximate the ranges from rainflow counting quite well, although the combined distributions seem to give a slightly better match. However, two additional parameters, $Var(Z)^{vR}$ and either C_1 or C_2, would enter the fitting, the training and the estimation. The additional costs are probably not justified by the relatively small improvements which can be expected from the better approximation of rainflow ranges.

The results of the performed estimations on the basis of the lognormal distributions are also illustrated in Figure 6.10. Only five variables had to be predicted for each of the 132 data sets by previously trained neural networks: the distribution parameters σ_Z^{ln} and $\bar{Z}^{ln}$, the spectral moment λ_0 (equal to the variance of the time series), the expected number of cycles and the maximum load range. Relatively simple networks with only one hidden layer, consisting of six to ten neurons were used. In most cases, mean value and variance of the electrical power, the generator speed and the rotational acceleration proved to be sufficient as input to the networks.

Table 6.3 gives the error of the equivalent loads with respect to the rainflow counting results for the exponents 4 and 10 (extrapolated to 20 years lifetime according to the IEC standard). The deviation is only a few percent in any case. This not only emphasises the good approximations of the rainflow counts by the fitted distributions for the training data, but also the accurate results of the estimation procedure with the test data.

The above investigations demonstrate the general feasibility of the presented empirical approach for the estimation of load cycle distributions. Chances are, that less parameters are involved into the process than for any analytical frequency domain technique and hence less estimations are required. In addition, better approximation

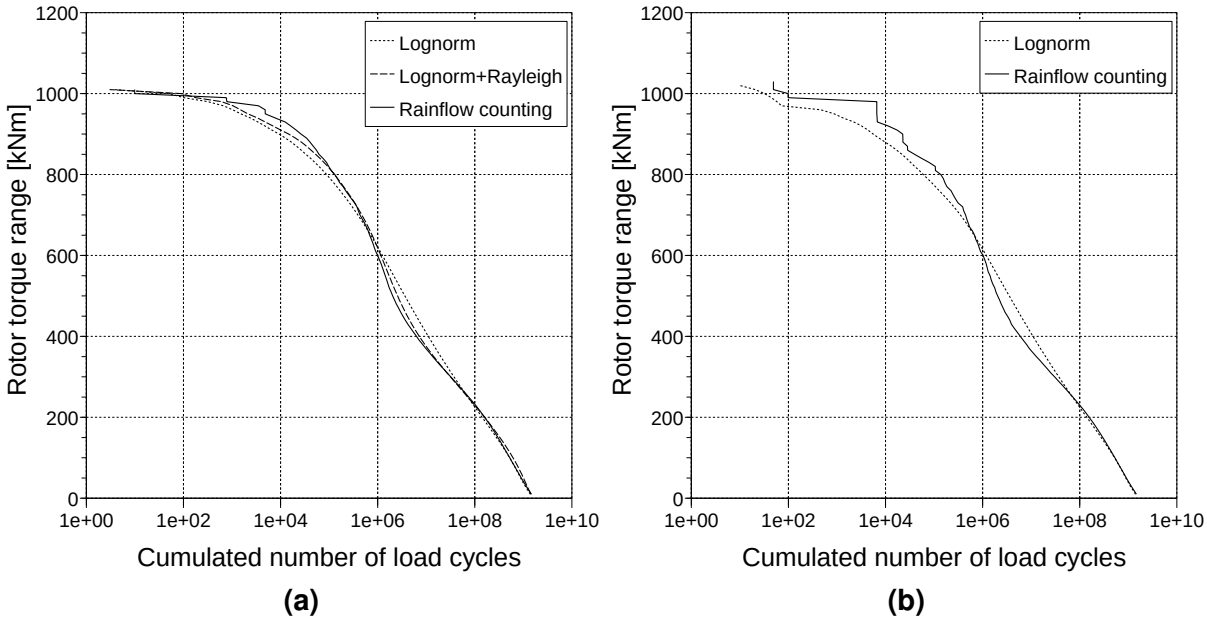

Figure 6.10: (a) Approximation of the rainflow counted load cycle distribution of the rotor torque by fitting a lognormal distribution as well as a combination of a variable Rayleigh and a lognormal distribution (training data only) (b) Results of the complete estimation procedure on the basis of the lognormal distributions and 132 test data sets

of results from rainflow counting can be expected, at least for non-stationary processes. Further validation of the method is performed in Chapter 7 with measured data.

6.4 Load magnitude distributions

The previously developed approach for load cycle distributions can easily be adapted to magnitudes distributions. At the same time, this is also a very intuitive method for load magnitudes, because the employed empirical distributions are frequently used to describe time domain representations of signals in a statistical manner. The resulting cumulated load magnitudes are derived from superposition and accumulation of many

Table 6.3: Deviations of extrapolated equivalent load ranges from rainflow counting and empirical distributions.

	Fitting rainflow cycle distributions by empirical PDFs		Using fitted PDF for prediction
	Lognormal E in %	Lognormal+Rayleigh E in %	Lognormal E in %
m = 4	3.5	3.3	3.5
m = 10	0.0	-1.4	-2.3

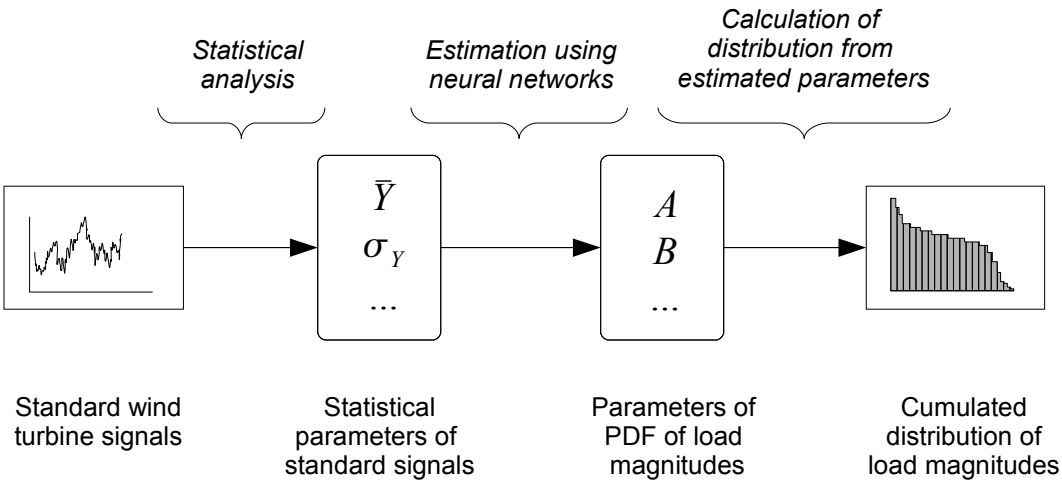

Figure 6.11: Estimation scheme for load magnitude distributions

individual probability distributions.

Similar to the scheme shown in Figure 6.9, two pre-processing steps for setting up the method are required. In a first step, either a single distribution or combinations of distributions are fitted to approximate the statistical representation of the load signal. Neural networks are then trained to transfer statistical parameters of standard signals into the coefficients of fitted distributions. Once the training is completed, the neural networks can be employed in a procedure for the estimation of load magnitude distributions (Figure 6.11).

In this example, the probability distribution of the rotor torque has been approximated by a Gaussian distribution:

$$p^G(L) = \frac{1}{\sigma_L\sqrt{2\pi}} e^{-\frac{1}{2}\left(\frac{L-\bar{L}}{\sigma_L}\right)^2} \tag{6.26}$$

The Gaussian distribution is defined by a mean value $\bar{L}$ and the standard deviation σ_L only. These parameters can be calculated directly from the load time series. The first set-up step can therefore be omitted, as fitting is not required. For the same reasons as in the case of the maximum load ranges, the estimations also involve the expected minima and maxima.

The approximation of the PDF of load magnitudes by a Gaussian distribution can be improved, if the skewness and the kurtosis are considered as well. This requires computation of γ_3 and γ_4 from the load time series and inclusion into the training of neural networks. In the load estimation step, these parameters also have to be predicted from standard signals. Finally, the estimated Gaussian distribution of the rotor torque has to be transferred into the non-Gaussian domain.

Figure 6.12 shows three cumulated distributions of load magnitudes, derived for the

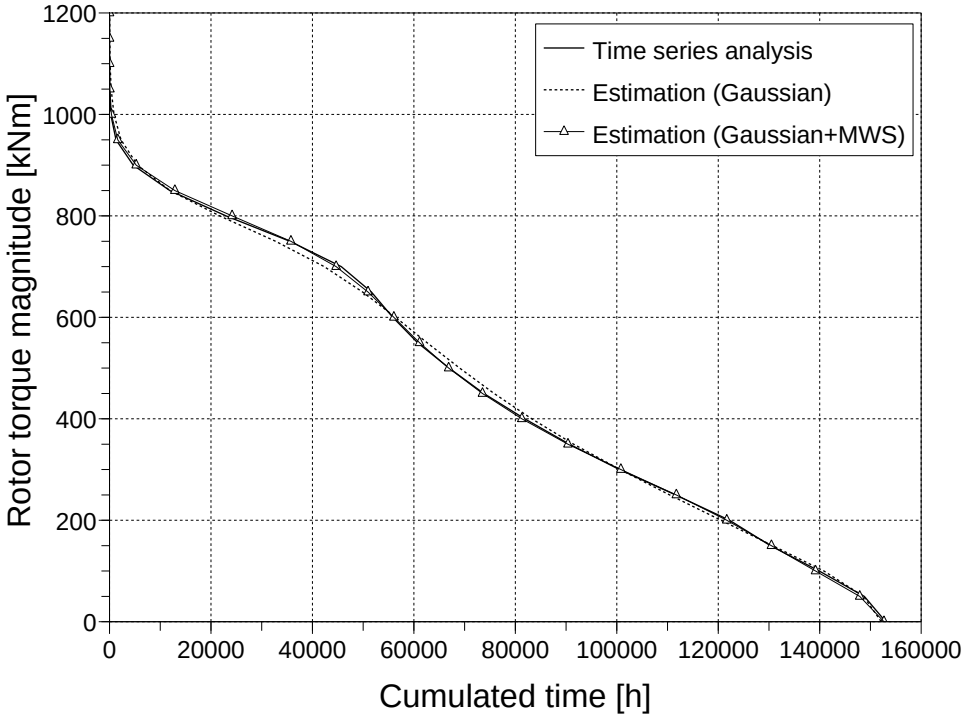

Figure 6.12: Estimated load magnitude distributions from simulated data of the rotor torque. Results from direct analysis of load time series, estimations using a Gaussian distribution and estimations using a Gaussian distribution and the modified Winterstein transformation for non-Gaussian corrections are shown.

132 test data sets and extrapolated to 20 years lifetime according to the IEC standard. Two of them are based on estimated distributions (using the procedure in Figure 6.11), while one has been computed directly from the load time series for comparison. The required neural networks were trained with data calculated from the 660 training sets.

For one of the graphs, a simple Gaussian distribution has been employed and only the mean and the standard deviation of load time series as well as the expected minima and maxima had to be estimated. For the other, the skewness and kurtosis of the modified Winterstein transformation were also predicted and the Gaussian PDFs were transformed accordingly. Hence, six variables were involved in total.

It can be seen, that a correction of the Gaussian distribution with skewness and kurtosis gives the closest approximation of the directly calculated distribution, with almost an exact match. However, the difference between the results (with and without the correction) is quite small. In practice, this might justify to omit the non-Gaussian transformation and to get away with four estimations per data set instead of six. The relatively good accuracy of the estimations is also documented by the deviations of equivalent load magnitudes which have been derived from the two graphs (see Table 6.4).

In the author's view, the above results indicate that the estimation of load magnitude distributions can be performed by predicting parameters of fitted distributions. The method is very similar to the proposed estimation of load cycle distributions. A simple Gaussian distribution already seems to be sufficient as a basis for the prediction of the cumulated distribution of the rotor torque from simulations with high accuracy.

Table 6.4: Deviations between equivalent load magnitudes from load time series analysis and estimated distributions. The distributions have been extrapolated to 20 years lifetime prior to the calculation of equivalent load magnitudes.

	Gaussian E in %	Gaussian+MWS E in %
p = 4	0.0	0.4
p = 10	1.4	0.9

7 Validation on the basis of measured data

Within this chapter, the previously derived methods for the estimation of loads from standard signals are validated on the basis of measured wind turbine data. For this purpose, recorded time series from measurement campaigns at the Multibrid M5000 prototype turbine at Bremerhaven (Annex C) and two Nordex N80 turbines at Wieringermeer (Annex D) have been used. While the Endowed Chair of Wind Energy at the Universität Stuttgart (SWE) was directly involved in the measurements at the M5000, the N80 data was made available for this work by the Energy research Centre of the Netherlands (ECN).

First, the methods for the estimation of equivalent loads as well as load distributions are evaluated with data from the M5000. A systematic approach for the set-up of neural networks is discussed followed by an analysis of inputs and targets of the estimation procedure. In a second step, the general transferability of methods to another turbine type, the N80, is tested. Because ECN records data at two turbines, transfer functions which are first derived at one of the N80 turbines are also used for load estimations at the other one. This allows to draw first conclusions on the practical suitability of the monitoring approach for its intended industrial usage: to perform load estimations for a series of wind turbines of the same type.

7.1 Validation with data from the Multibrid M5000 turbine

The data which is used in this section has been recorded during a load measurement campaign in winter 2005/2006 for certification purposes. About 150 hours have been extracted from all measured data sets (divided into data sets of 10 minutes each), reflecting typical site conditions with wind speeds between 4 and 22 m/s and turbulence intensities ranging from 3 to 17 %. Only measured time series, where the turbine was in normal power production mode have been considered.

For each of the available standard signals

- generator rotational speed
- generator rotational acceleration (calculated as derivative of the rotational speed signal)
- electrical power
- pitch angle
- lateral tower top acceleration
- longitudinal tower top acceleration
- nacelle wind vane signal (yaw error)

the following statistical parameters have been derived

- mean value
- total variance and ratio of variances (compare Annex G)
- normalised third and fourth central moments (skewness and kurtosis)
- maxima, minima, maximum range
- first to fourth spectral moments

In total, this yields 84 potential input values to the estimation procedure. About 120 hours of data have been used to train neural networks which have then been employed to predict fatigue loads on the basis of the derived statistical parameters. This was performed for the remaining 30 hours of data which were not part of the training process.

Both equivalent loads and load distributions have been estimated. The following evaluation also includes an investigation of the utilised input signals and parameters as well as an analysis of the estimated target values. In the case of the load distributions, the necessity for the adaptation of the method according to the estimation targets is demonstrated.

7.1.1 Equivalent loads

In general, networks with reasonable approximation capabilities can often be designed on the basis of theoretical considerations and best guesses. This approach has been used in Chapter 6, and also for load estimations at the M5000 presented previously in [107]. However, sometimes a systematic approach for the set-up of networks is

required. Network pruning is an example for such a method. It can be used to derive network configurations which are optimised in terms of computational costs and accuracy.

Estimations with pruned networks

Pruning is an iterative process and starts from a baseline network configuration. After each training, one connection within the network is removed according to some criteria. Training is repeated and connections are deleted until the training error exceeds a specified limit. In the following examples, pruning was carried out simply on a magnitude basis, where always the connection with the smallest weight is removed. Input and hidden neurons without any remaining connection are deleted after each training as well. With this approach, not only the connection weights but also the network architecture becomes variable and each iteration step leads to lower estimation costs. This obviously not only holds true for the network processing itself (which in the investigated examples has only low computational costs) but also holds true for all pre-processing steps within the load estimation procedure (for example the computation of statistical data). Of course, deleting too many neurons and connections will tend to deteriorate the networks capabilities to adapt to training data and consequently this results in larger estimation errors. Hence, pruning designed networks always reflect a compromise with respect to cost and accuracy, relative to the chosen baseline network configuration.

In this application, two sets of neural networks were established with different optimisation intentions. The procedure is illustrated in Figure 7.1. For the first sets of networks, pruning was stopped after the sum of squared training errors[1] increased by 5 % compared to the baseline network. In a second step, the networks were pruned further until removing the connection with the smallest weight alone increased the sum of squared training errors by 5 %. While the first networks focus on estimation accuracy and only the least important connections are removed, the second set allows larger estimation errors for the benefit of reduced computational costs.

Equivalent loads of the blade root bending moments, rotor torque, rotor thrust and longitudinal tower base bending moment[2] have been predicted using two exponents (4 and 10) for each load quantity. The blade root bending moments are estimated as in-plane and out-of-plane moments in a fixed coordinate system as well as edge- and flapwise moments in a pitching coordinate system. For each load quantity and each

[1] The training error is defined as the difference of target value and network output in this context.

[2] For this turbine, a container platform 29 m above ground is denoted as ‘tower base’. The concrete sections below the platform are considered as part of the foundation.

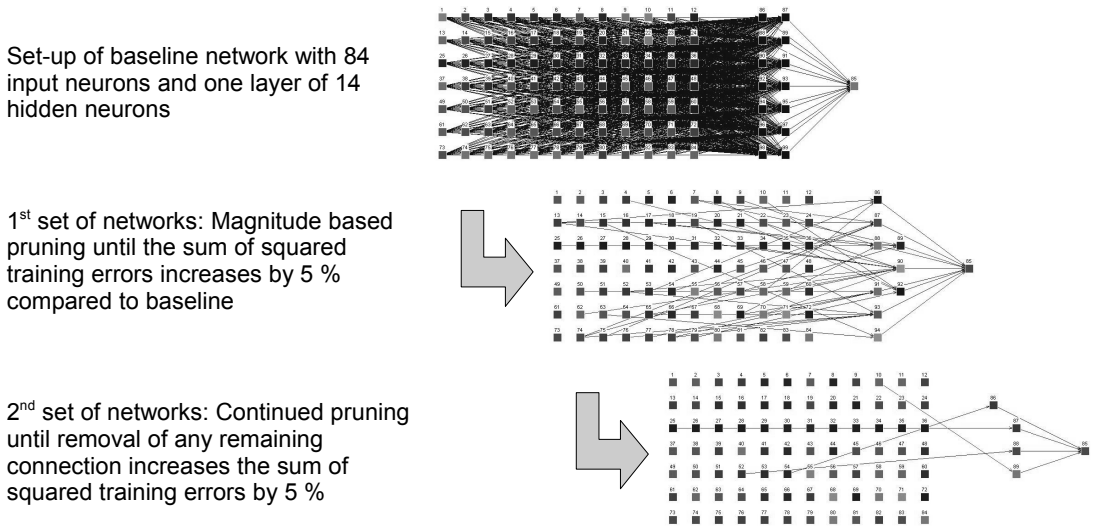

Figure 7.1: Procedure for establishing two sets of networks by magnitude based pruning.

exponent an individual neural network has been trained.

All results have been compared with equivalent loads from standard time series counting procedures and the deviations have been computed to assess the accuracy of the estimations. The estimation errors of equivalent load ranges $\Delta S_{eq,N_{ref},m}$ and magnitudes $L_{eq,T_{ref},p}$ are displayed in Figure 7.2. Only errors derived with the first set of networks are shown, where

- E are the errors of the cumulated equivalent loads and thus are a measure for the overall prediction error.
- σ_E are the standard deviations of errors calculated from all single test data estimations. Hence, they indicate the error which can be expected for the estimated load of a single 10 minute data set.

For all load components the cumulated error is relatively small. In most cases, it is below 2.5 %, except for the longitudinal tower base bending moment, where a prediction error of about -5 % has been computed. Further investigations revealed that most of this error results from the false prediction of a single data set (see 'Output analysis' below).

There is no significant difference in terms of accuracy between the estimated blade loads and those of integral quantities of the rotor, for example the torque. This applies even for the out-of-plane blade root bending moment which is not directly related to any of the available standard signals (compare Table 3.3). In fact, the most accurate predictions have been derived for the in-plane and edgewise blade root bending moments respectively. These quantities are dominated by deterministic oscillations originating from the self weight of the blade and the rotation of the rotor. As the weight is constant

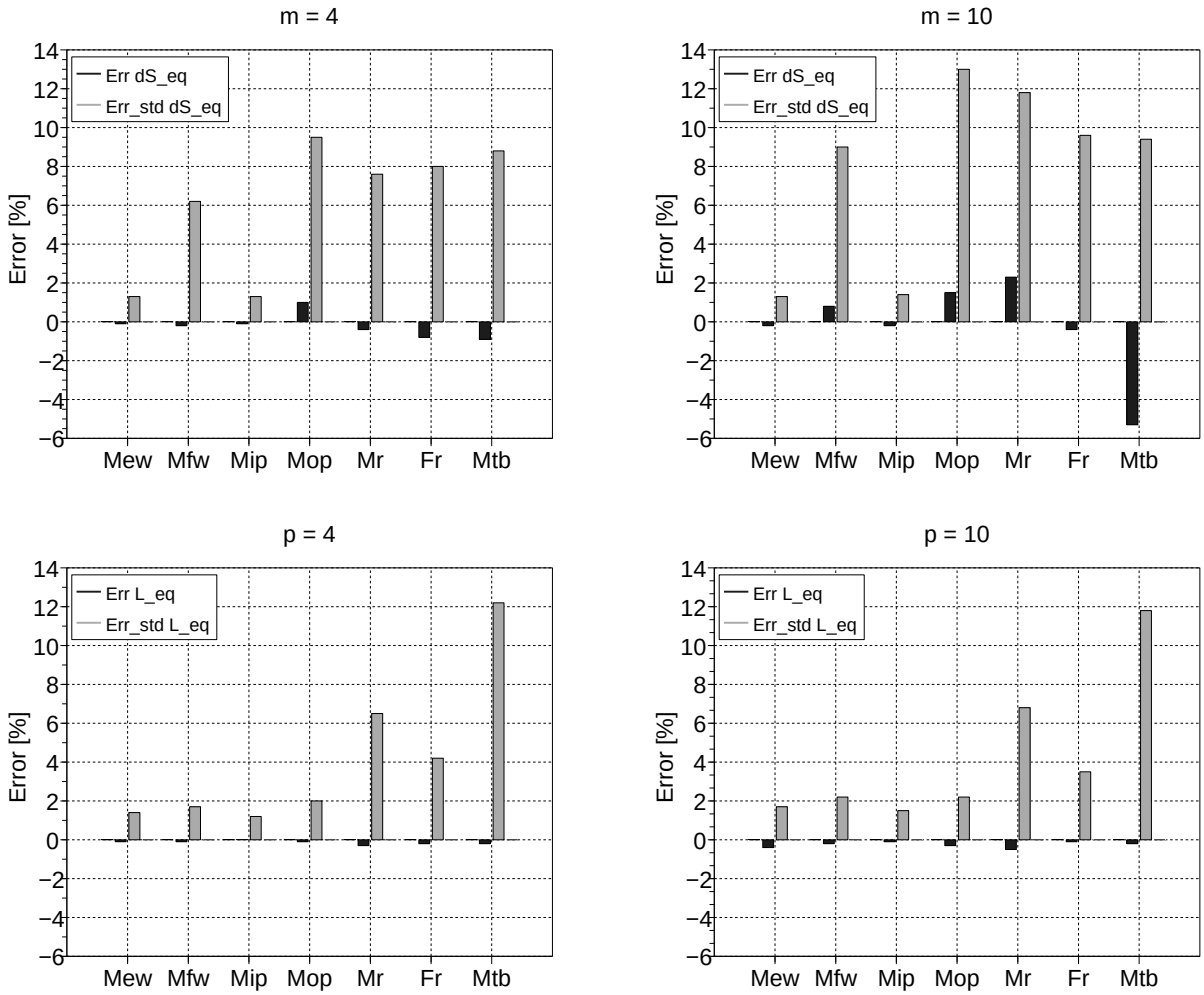

Figure 7.2: Error of cumulated equivalent loads and standard deviation of errors for estimations with the first set of networks for edgewise (M_{ew}), flapwise (M_{fw}), in-plane (M_{ip}), out-of-plane (M_{op}) blade root bending moments and longitudinal tower base (M_{tb}) bending moment as well as rotor torque (M_r) and rotor thrust (F_r).

and the rotational speed is a direct input to the neural networks, a good estimation result can be expected.

The maximum standard deviation of errors is about 13 % for the equivalent ranges of the out-of-plane blade root bending moment and an exponent of 10. On average, an error of only 6 to 12 % can be expected for a single estimation of most load components. When results from several estimations are cumulated, this error eventually averages out quite well and in most cases no significant bias remains.

Because their standard deviations of errors are somewhat lower, it seems that in general equivalent load magnitudes can be predicted with a higher accuracy than equivalent ranges. This is probably due to the fact, that magnitudes are driven mostly by the mean values of time series which are obviously easier to predict than load ranges.

At least for the load ranges, the standard deviations for an exponent of 4 appear to be

Table 7.1: Estimation errors E of cumulated loads and standard deviations of errors σ_E from pruned networks. The numbers are averages of absolute values over all load components.

		E (abs) in %		σ_E in %	
		exp = 4	exp = 10	exp = 4	exp = 10
1st set	ΔS_{eq}	0.5	1.5	6.1	7.9
	L_{eq}	0.1	0.3	4.2	4.2
2nd set	ΔS_{eq}	0.8	2.3	10.7	11.0
	L_{eq}	0.2	0.6	9.0[3]	5.3

slightly lower than those for an exponent of 10. For large exponents, few large ranges can have a significant influence on the equivalent load ranges. Therefore, equivalent loads with large exponents are often subjected to higher scatter which is in turn reflected in the prediction errors.

Table 7.1 lists the prediction errors of cumulated loads and the standard deviations of errors, averaged over all load components. Indeed there seems to be a tendency, that magnitudes can be predicted better than ranges and equivalent loads with small exponents better than those with large exponents. In addition, Table 7.1 also gives averaged results of the estimations with the second set of networks. Regarding the cumulated loads, the prediction accuracy deteriorated slightly. Furthermore, a higher standard deviation of errors compared to the first set of networks can be observed particularly for the equivalent load ranges. This seems to be reasonable, because during set-up of these networks with the pruning approach, larger errors were allowed. Nevertheless, the second set of networks still gives quite accurate results, at least on an average basis.

Output analysis

One important reason for the small errors of the cumulated equivalent loads are effects due to averaging. In most cases, the prediction error is already reduced significantly, if the sum of relatively few estimates is considered. This holds true even for the second set of networks which, in general, feature a larger standard deviation of errors.

It seems, that for the majority of predicted load components eventually none or only a small bias remains. An example of a noticeable deviation of equivalent loads from estimations and measurements is the longitudinal tower base bending moment. As

[3] This value is dominated by a few false predictions of the longitudinal tower base bending moment which in turn cause a quite large standard deviation. Without this load component, the average standard deviation of errors yields 3.5 %.

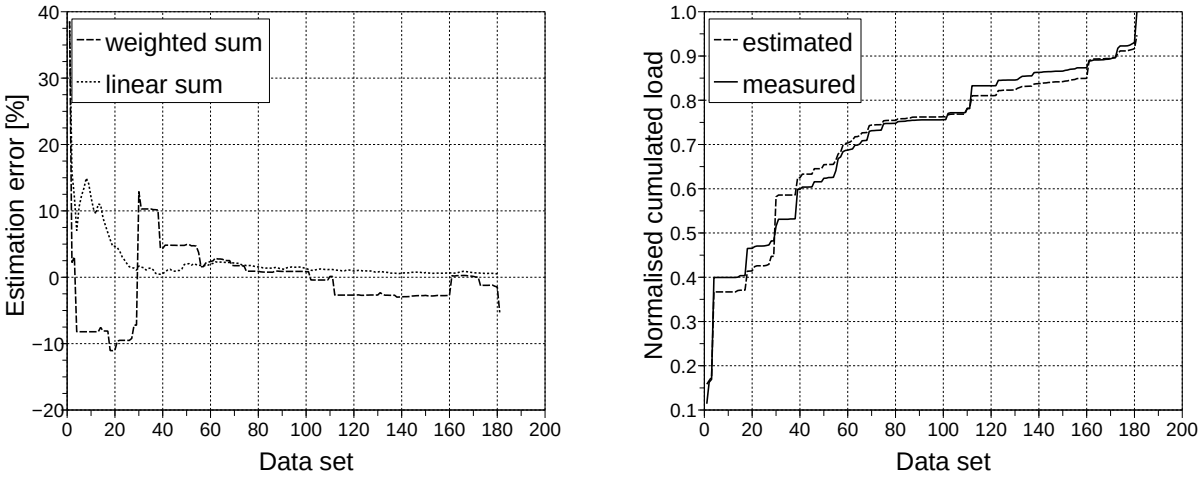

Figure 7.3: Estimation errors as linear and exponentially weighted running sums (left) and normalised cumulated sums (right) of the longitudinal tower base bending moment from estimations and measurements.

shown in Figure 7.2, an error of approximately -5 % remains for the equivalent ranges with an exponent of 10. However, closer investigations reveal, that the error is not caused by a biased estimation, but more by the exponential weighting of the equivalent loads during cumulation.

This is illustrated in Figure 7.3, where two running averages of errors are displayed: a linear sum of errors and the error of cumulated loads (which according to Equation 2.4 corresponds to an exponentially weighted sum). While the linear sum of errors approaches zero in a more or less consistent manner, the errors of the weighted sum show a different behaviour: In the weighted sum, data sets with large equivalent loads have a much greater influence during cumulation compared to those with small equivalent loads.

In Figure 7.3 this becomes obvious by the steps in the weighted sum. For the corresponding data sets, the estimation errors are not exceptionally large and consequently they do not have a significant influence on the linear sum. But the equivalent loads of these data sets themselves are quite large and hence a prediction error of a common size has an exceptional impact on the weighted sum. Thus, much of the remaining prediction error results from only a few estimations. In this particular case, the equivalent load ranges of the longitudinal tower base bending moment of the very last data set was underestimated by about 11 %. Unfortunately, this data set contained by far the largest equivalent ranges and hence its influence (and the one of the corresponding prediction error) on the cumulated load is large.

As a general rule, this characteristic of the load cumulation should already be accounted for during training of the network. The leading thought is, to teach the network

that an accurate prediction is more important for large equivalent loads than for small ones. There are at least two possibilities to achieve this: data selection and weighting of errors. Both are commonly applied methods which are frequently used when analytical models are fitted to measured data as for example in the field of regression techniques.

In the present case of neural networks, the first approach can be implemented by selecting the distribution of training data according to the relative importance of equivalent loads. Hence, the training data would consist of a relatively large proportion of data with large equivalent loads. This approach requires to establish separate sets of training data for different load components and exponents and also involves taking into account the expected occurrence probability of relevant conditions at average sites.

For the second possibility, the equivalent loads can be weighted in principle prior to the training, for example according to the employed exponent and an assumed probability of occurrence. Thus, large equivalent loads contribute to the network training according to their true importance for the cumulated equivalent load. Propagating the computed training error back through the network will yield correspondingly conditioned networks.

Unfortunately, it was not possible to follow any of these methods in this example. Selecting the training data according to the relative importance of the equivalent loads failed simply because not enough data with large equivalent loads was available. The application of weighted targets turned out to be not practical in this case as well. Because of the required exponential weighting, the general range of target values became much broader (with several orders of magnitude) which in turn complicated the learning and deteriorated prediction abilities of the employed networks.

The suitability of networks for load predictions can also be assessed in a statistical sense by means of a coefficient of determination (see Equation 4.8 and Table 4.8). This number indicates, how much of the target data's variance can be explained by the established model. The coefficient is estimated directly from the residuals and is not subjected to effects related to exponential weighting. Therefore, the coefficients of determination have been calculated for each equivalent load in addition to the estimation errors. Average coefficients as well as the minimum and maximum encountered values are given in Table 7.2.

On average, the neural networks are able to correctly reflect at least 91 % of the variation on equivalent loads. The analysis also confirms the previously derived results, even if the differences are almost neglegible: loads with a small exponent can be predicted slightly better than those with large exponents and the estimated magnitudes

are more accurate than the ranges.

Table 7.2: Coefficients of determination from estimation results with two sets of networks. Average coefficients over all load components are given, together with the corresponding minimum and maximum values for individual load components.

		Coefficients of determination average (minimum, maximum) exp = 4	exp = 10
1st set	ΔS_{eq}	0.97 (0.96, 0.98)	0.95 (0.90, 0.97)
	L_{eq}	0.99 (0.98, 1.0)	0.99 (0.97, 1.0)
2nd set	ΔS_{eq}	0.94 (0.87, 0.97)	0.91 (0.86, 0.94)
	L_{eq}	0.98 (0.96, 1.0)	0.98 (0.95, 0.99)

Network analysis

In statistics, the evaluation of prediction errors, the so-called residuals, plays an important role for the assessment of a model's quality. Because the application of common statistical methods usually requires that the residuals feature certain properties, they are analysed routinely. As an example, a Gaussian distribution of errors is a requirement for the calculation of confidence intervals or statistical hypothesis testing. Furthermore, scatter plots of the residuals allow to investigate, how well a model has been adapted to measured data. The rational behind this is, that in efficient models, the estimation errors are distributed randomly and hence follow a Gaussian distribution. When a model has not captured all the important features of the data, this can not be assumed. A distribution of residuals which significantly differs from the normal distribution indicates, that the predictions suffer from a systematic error, at least for some parts of the models's intended area of validity. In these cases, either relevant effects are not reflected in the input data or the model does not process the information correctly.

These kind of investigations have been carried out for all derived estimation results. In general it has been found, that the scatter plots of residuals from all networks of the first set and for most of the second set do not feature distinctive shapes and the errors seem to be distributed randomly. However, for a few plots this was not the case. Figure 7.4 shows such an example. Here, estimation errors of the equivalent tower base bending moment magnitudes with an exponent of 4 are displayed. While the residuals from estimations with the first set of networks look like random scatter, a pattern is visible for errors from the second set of networks.

Although the residuals are still quite small (the coefficient of determination is 0.99 in both cases), the pruning obviously had some influence on the distribution of errors.

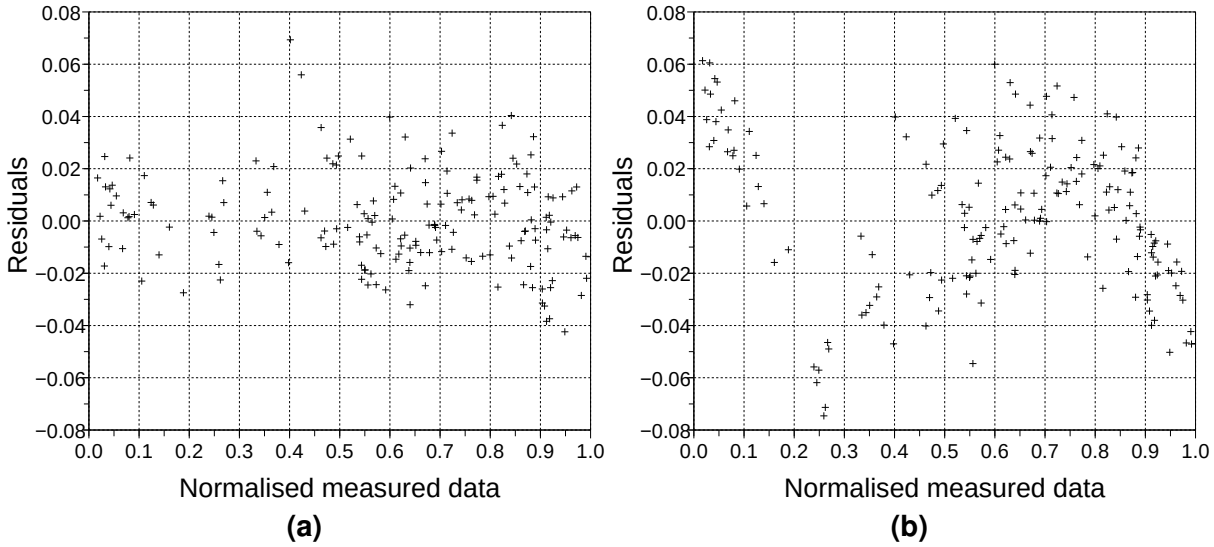

Figure 7.4: Residuals from equivalent magnitude estimations of the longitudinal tower base bending moment with an exponent of 4. Prediction errors for the first (a) and second (b) set of networks are displayed.

Either this pattern appeared because of the removed inputs or the reduced network size. Small networks are sometimes not flexible enough to adapt to all characteristics of the training data. Nevertheless, in practice the reduced computational costs for data processing can sometimes justify the deterioration of model capabilities.

The advantage in size of the second set of networks becomes obvious from Table 7.3. On average, the networks of the first set consist of 18 input, 7 hidden and 1 output neuron. These are linked together with 33 connections. A typical network of the second set is much smaller: only 3 input, 2 hidden and 1 output neuron with a total number of 6 connections are required. Table 7.3 also states the average size of networks where the target values have the property in the first column in common (for example an exponent of 4) . At least for the first set of networks this analysis reveals, that the largest models are required for the estimation of equivalent load ranges with an exponent of 10. Contrary, prediction of equivalent magnitudes and exponents of 4 can be performed with significantly smaller networks.

Pruning of networks is not exclusively applied for their optimisation with respect to prediction accuracy and costs, but also to analyse the utilisation of input data by the network. If the pruning is performed until the training error increases by a relatively small amount, as it is the case for the first set of networks, only unimportant input neurons are removed. Continuing the process up to significantly larger errors (the second set of networks) only leaves the most efficient inputs.

Table 7.3: Average number of input neurons, hidden neurons and connections of the established neural networks.

	1st set of networks			2nd set of networks		
	Input neurons	Hidden neurons	Connections	Input neurons	Hidden neurons	Connections
exp = 4	17	7	31	3	2	5
exp = 10	20	7	35	4	3	6
ΔS_{eq}	22	8	40	4	3	6
L_{eq}	14	6	26	3	2	5
All networks	18	7	33	3	2	6

In Figure 7.5 the remaining number of inputs for the first and second set of networks are displayed. While the plots in the upper row result from summing all inputs involved in the estimation of equivalent ranges, the required inputs for the estimation of equivalent magnitudes are given in the lower row. The statistical parameters are plotted on the abscissae and the standard signals on the ordinate.

As expected, parameters related to oscillations (for example the variance) and to the frequency of oscillation (for example the spectral moments) are relevant inputs to the prediction of equivalent load ranges. The networks retrieve this information preferably from the lateral and longitudinal tower top acceleration as well as from the rotational acceleration of the generator.

The mean value of the electrical power is not used in any of the second set of networks for equivalent load range prediction. This is surprising, because one would assume, that the average operational state below rated can be estimated quite well from the electrical power signal. Probably such information is derived from the mean values of the generator speed and pitch angle, since these parameters are often employed

Equivalent load magnitudes are closely related to mean values of load signals and obviously the mean values of generator speed, electrical power and pitch angle are by far the most important inputs to their estimation. The tower top accelerations, which were often applied for the prediction of equivalent ranges, are not used at all in the second set of networks for the estimation of equivalent magnitudes.

In general, the yaw error signal from the nacelle wind vane seems to be relatively unimportant. One reason for this is that the turbine generally manages to keep yaw errors low and hence no operation with large misalignments is present in the training data. Furthermore, as investigated in Chapter 3 with simulations of a 1.5 MW turbine, small yaw errors only have a relatively small impact on most of the load components,

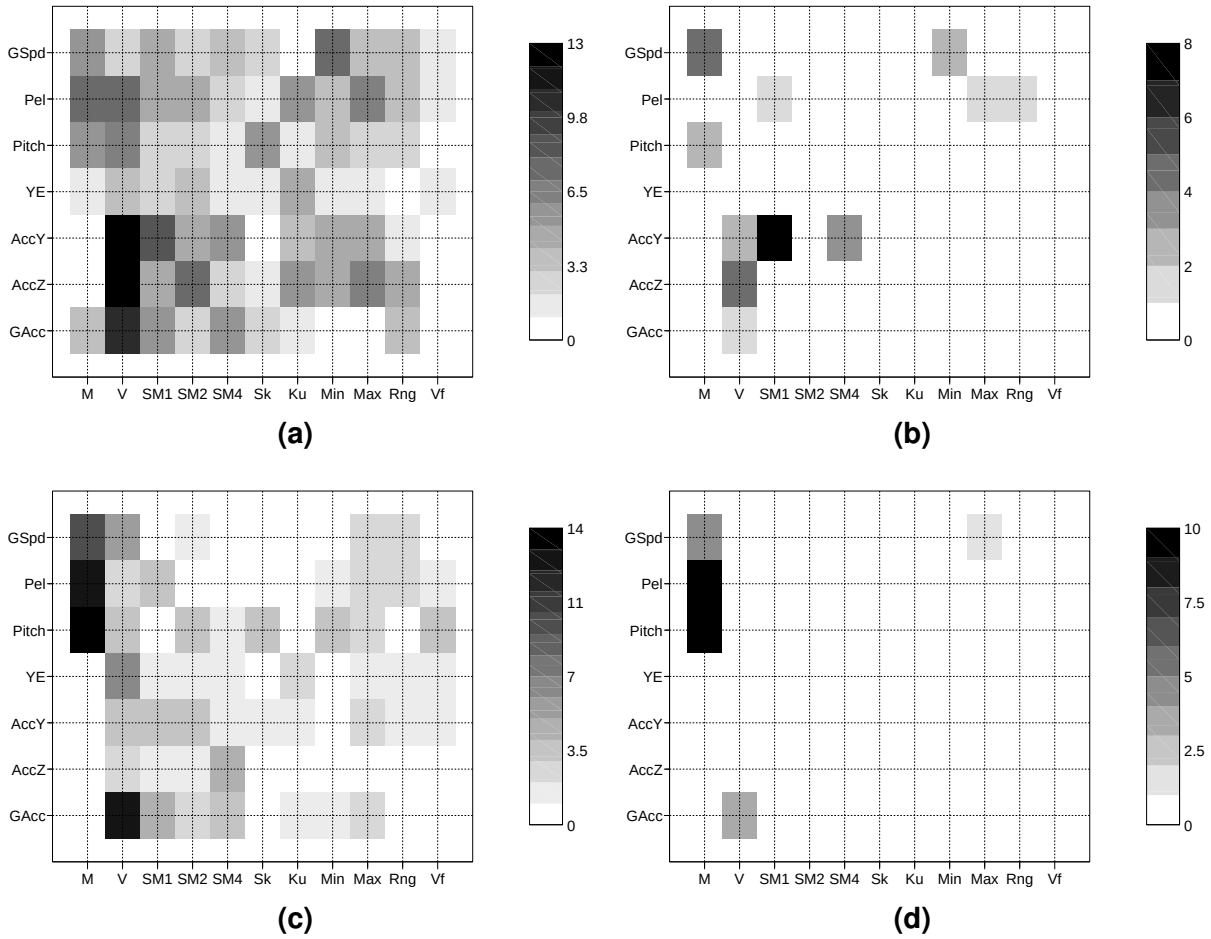

Figure 7.5: Remaining number of network inputs after pruning, subdivided into statistical parameters (abscissae) and standard signals (ordinate). Inputs are given as sum over all load components for equivalent ranges (1st set (a) and 2nd set (b)) as well as for equivalent magnitudes (1st set (c) and 2nd set (d))

except for the out-of-plane (and flapwise) blade root bending moment.

Skewness and kurtosis are not applied in any of the second set of networks. These two parameters describe the deviation of a load signal's distribution from Gaussian, an important characteristic which significantly affects fatigue loads (see for example an investigation on the effect of skewness by Wang [108]). Both parameters also play an important role for the calculation of rainflow ranges from statistical parameters (compare Chapter 6). Nevertheless, the networks obviously do not require skewness and kurtosis from standard signals to capture their effect on equivalent loads.

The inputs to the networks have also been analysed in detail. It has been found, that often physical relations are reflected by the chosen inputs. For example, all predictions of the equivalent ranges of in-plane blade root bending moments include the mean rotational speed. This makes sense from an analytical point of view, because self

weight and rotational speed are by far the main drivers for the in-plane load ranges. Similar, the prediction of the rotor torque incorporates electrical power and generator speed.

The utilisation of physically meaningful relations in neural networks can not be taken for granted. During training, the network is free to employ any correlation between input and target data that it can find. As a consequence, the risk that spurious correlations are applied for predictions is always existent and the designed networks should be evaluated carefully. However, this is not an easy task in particular with large networks.

As a final remark it should be emphasised, that results from the analysis of estimation inputs via pruning have to be interpreted with caution. Such an analysis allows to find inputs which can be omitted without affecting the estimation accuracy by more than a predefined limit. The reverse conclusion, namely that the application of the remaining signals and parameters is compulsory to get reasonable results, is not valid for the following reasons:

First, information might be available redundantly in the input data. During pruning, the network keeps those inputs which it can utilise most efficiently. Nevertheless, this does not mean, that the network is not able to employ other inputs to retrieve the same information, in case these efficient inputs are not available.

Second, pruning aims to keep the variation of errors from single estimations below a limiting value. However, for a fatigue load estimation system, the accuracy of a single prediction is not the determining criteria. Instead, the cumulated load from many estimations is much more important. As long as the removal of an input only yields larger standard deviations of prediction errors and not a systematic prediction bias, the designed load estimation system can still give accurate cumulated results.

7.1.2 Load distributions

In Chapter 6, an empirical approach for the estimation of load distributions has been developed. This approach is further tested and validated in the following with data measured at the M5000 turbine. For each of the investigated load components, the set-up according to Figure 6.9 has been followed.

In a first try, the distribution of load cycles of the rotor torque and the rotor thrust have been estimated. It was expected that these quantities are among those loads where the most accurate results can be derived, because closely related standard signals, such as generator speed, power output, pitch angle and tower top accelerations are available as input signals for the estimation (compare Table 3.3).

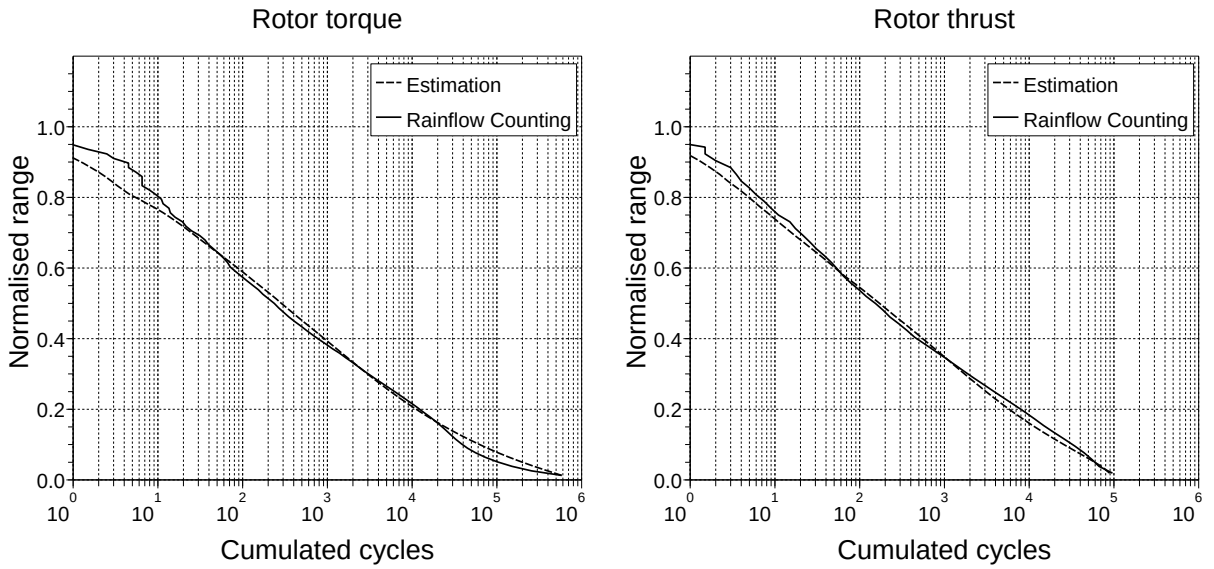

Figure 7.6: Comparison of estimated load cycle distributions of rotor torque and thrust with rainflow counting results from measured data.

During set-up, several distributions have been evaluated with respect to their suitability for capturing the important characteristics of the measured probability densities. Eventually, the simple lognormal distribution from Equation 6.24, which had already been applied successfully for the estimation of simulated rotor torque cycles, proved to be sufficient. As a consequence, a total number of only five variables had to be estimated for each test data set.

The networks were designed on the basis of theoretical considerations and a number of experiments. For the rotor torque, electrical power, generator rotational speed, generator rotational acceleration and lateral tower top accelerations were chosen as input signals. The estimation of rotor thrust utilised electrical power, generator rotational speed, pitch angle and longitudinal tower top accelerations. In both cases, mean value, variance, skewness, kurtosis, maximum ranges and a variance ratio were available as statistical parameters for all signals. Networks with just one hidden layer containing a maximum of eight neurons were employed for the predictions.

From the five estimated distribution variables, density distributions for each 10 minute set of test data were established. Based on the predicted number of cycles, discrete probabilities were then derived and processed further to cumulated distributions of load cycles. Figure 7.6 illustrates the results. Also plotted are the load cycle distributions which have been calculated directly from time series analysis of measured data.

In general, the estimated distributions are reasonable approximations of the measured ones. However, the very large load ranges are slightly underestimated particu-

Table 7.4: Errors of equivalent loads calculated from estimated cycle distributions of the rotor torque and thrust with respect to results from measured data.

	Rotor torque E in %	Rotor thrust E in %
m = 4	1.5	-2.6
m = 10	-3.2	-2.7

larly for the rotor torque.

To assess the estimations in a quantitative manner the distributions have been reduced to equivalent load ranges. The deviations between equivalent loads derived from estimations and measurements are listed in Table 7.4 for two exponents. While the equivalent ranges with small exponents are mainly driven by the frequently occurring oscillations with small amplitudes, those with large exponents are significantly influenced by the few large ranges. The results given in Table 7.4 confirm the overestimation of small ranges and the underestimation of large ranges in case of the rotor torque. For the thrust, a slight underestimation for both exponents has been computed. Nevertheless, the deviations are small which supports the good visual agreement in Figure 7.6.

As stated above, in the example of rotor torque and thrust a simple lognormal distribution has been applied to fit measured probability density distributions. This turned out to be quite convenient as it is made up from only very few variables. However, such simple distributions do not yield accurate approximations in all cases, especially under the presence of deterministic influences. For some load components, combining two or more distributions can give greatly improved results which might be well worth the costs of additional variables. The in-plane blade root bending moment can serve as an example in the following.

From the 30 hours of measured test data, probability densities have been derived by rainflow counting. The resulting distribution is shown in Figure 7.7. Besides a relatively large probability for the occurrence of small load ranges, there is also a significant probability for rainflow ranges with a normalised amplitude of 0.6 to 0.8. This peak in the distribution corresponds to the load ranges caused by self weight and rotation of the blade. Clearly, such a shape can not be approximated well by one simple distribution. A plot of estimated probability densities based on the lognormal distribution in the same figure confirms this. Although the fit looks poor, for a lognormal distribution this is probably close to the best achievable result.

Nevertheless, the accuracy of the predicted densities is unsatisfying. For a better

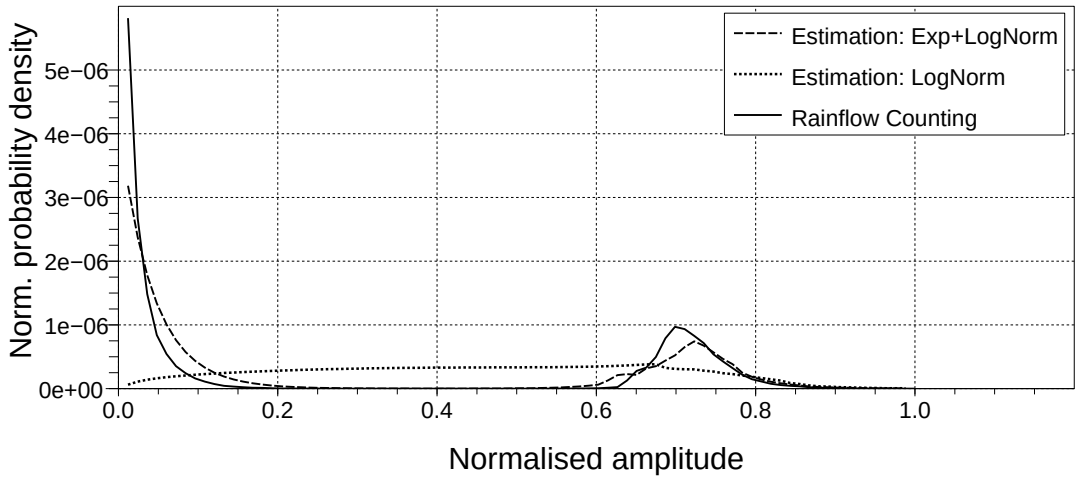

Figure 7.7: Probability densities of the in-plane blade root bending moment from rainflow counting of measured test data and predictions based on a lognormal and a combination of an exponential and a lognormal distribution.

approximation more complex distributions are required. As a demonstration, a combination of an exponential and a lognormal distribution is employed in the following. The combined distribution $p^{eln}(\Delta S)$ is defined by

$$p^{eln}(\Delta S) = \frac{1}{2\sqrt{\lambda_0}} \left(\frac{C_1}{J} e^{-\frac{Z}{L}} + \frac{C_2}{\sigma^{ln}_{\Delta S}\sqrt{2\pi} Z} e^{-\frac{1}{2}\left(\frac{lnZ - \bar{Z}^{ln}}{\sigma^{ln}_{\Delta S}}\right)^2} \right) \tag{7.1}$$

with Z as defined by Dirlik (see Chapter 6) and $C_1 + C_2 = 1$.

As additional variables, one of the weighting coefficients C_1 or C_2 and the scale parameter J have to be predicted. The increased prediction efforts are however justified by a much better approximation of measured densities. Results from predictions with the combined distribution are also shown in Figure 7.7. Obviously, the estimated occurrence probabilities of the small and large ranges are much closer to the measured distributions now.

The importance of the applied density distribution is emphasised by a comparison of measured and predicted cumulated rainflow ranges displayed in Figure 7.8. The step in range of the in-plane moment is due to self-weight and rotation and corresponds to the peak in the previously discussed density plot. While the prediction based on the combined exponential and lognormal distribution is able to match even this sharp step, the results from the simple lognormal distribution approximate the measured data only on an average basis.

For the out-of-plane blade root bending moment the difference is less pronounced. Nevertheless, the combined distribution is more accurate here as well, especially for the prediction of small ranges. The error in equivalent loads, derived from the estimated

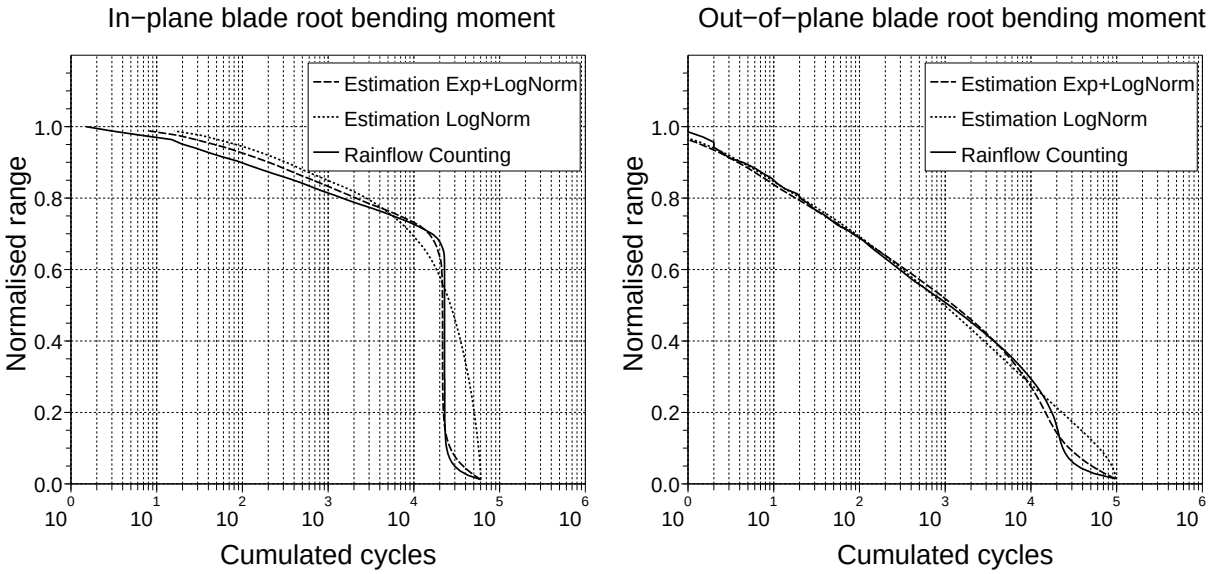

Figure 7.8: Comparison of estimated cycle distributions of in-plane and out-of-plane blade root bending moment with measured data. Estimations have been carried out with a simple lognormal and a combination of an exponential and a lognormal distribution.

Table 7.5: Errors of equivalent loads from estimated cycle distributions of in-plane and out-of-plane blade root bending moments with respect to results from measured data.

		In-plane E in %	Out-of-plane E in %
Lognormal	m = 4	-0.3	-0.9
	m = 10	-0.1	-0.1
Exp + Lognormal	m = 4	-0.9	-0.5
	m = 10	0.7	0.0

load ranges given in Table 7.5, does not reflect this. Here, the calculated deviations are rather small for both approaches, confirming the average match of predictions with the lognormal distribution.

7.1.3 Conclusions

In the present investigations, neural networks have been successfully applied for the prediction of fatigue loads at the Multibrid M5000, a state-of-the-art 5 MW wind turbine. This indicates the potential of the approach for fatigue load monitoring. Quite accurate results were derived for the 30 hours of test data for equivalent loads as well as load cycle distributions, although it should be stressed, that the data had been recorded at a relatively flat site excluding wake operation.

Furthermore, the processing of measured data emphasised the following:

- Relatively small networks with only a few inputs are sufficient to derive accurate estimations
- The prediction of equivalent ranges tend to be less accurate than those for the equivalent magnitudes.
- Because of larger scatter, the estimation of equivalent loads with large exponents seems to be more difficult than estimations for small exponents.
- The exponential weighting during the calculation of cumulated loads increases the impact of individual data sets with large equivalent loads. Individual estimation errors can therefore have a significant effect. This can be accounted for by an appropriate choice of training data sets.
- The previously developed approach for the estimation of load distributions has been successfully applied. A relatively simple distribution proved to be sufficient as the basis for the empirical approach.
- Deterministic load variations can significantly influence the probability densities of load ranges. As a consequence, predictions have to be carried out using a combination of distributions which can capture all relevant features of a process.

7.2 Transferability of methods - Tests at Nordex N80 turbines

In 2002, ECN installed five Nordex N80 wind turbines at their wind turbine test location at Wieringermeer (see Annex D). Initially one turbine (T6) and later a second (T8) were equipped with measurement devices. The measured loads and standard signals from the two measurement turbines as well as SCADA data from all five turbines are used to support ECN's research activities.

Some of the data was made available by ECN for the further validation of the methods developed within this work. It is employed in the following for investigations regarding the transferability of the approach to other turbines. First transferability to another turbine type, the N80, is tested. Second, networks trained with data from one N80 turbine are used to predict loads for the other one.

About 145 hours of high resolution time series of loads and standard signals from turbine T8 and 22 hours of T6 are employed for this purpose. The data was chosen

to reflect typical conditions of the site. Time series for turbine T8 were selected from data recorded from May to December 2008 while those of turbine T6 were measured in May and June of the same year. The data sets of T8 yield an average wind speed of 8.3 m/s with an average turbulence intensity of 9.5 %. For the sets of T6 an average wind speed of 7.4 m/s and an average turbulence intensity of 8.2 % was computed. As for the previous investigations on the Multibrid M5000, only operation at normal power production is considered. Furthermore, the data only contained undisturbed inflow conditions and hence situations where for example one turbine operated in the wake of the other are not investigated.

In total, 30 potential inputs to the neural networks were calculated. This, in comparison to the M5000, rigorous reduction of inputs was driven by considerations regarding the robustness of the approach. Because statistical parameters of higher order tend to be sensitive against small signal variations, only parameters of second order and below were applied.

Regarding the available standard signals, it is the author's experience, that tower top accelerations are often recorded as root-mean-square-values and are additionally averaged over short time periods. Obviously, the informative value of such a signal for the purpose of load monitoring is rather limited. Therefore, the renouncement of tower top accelerations in the present investigation can give hints regarding the applicability of estimation procedures for those kind of turbines.

Based on these considerations, the estimation procedure is carried out with the following signals

- generator rotational speed
- generator rotational acceleration (calculated as derivative of the rotational speed signal)
- electrical power output
- pitch angle
- nacelle wind vane signal (yaw error)

and statistical parameters

- mean value
- total variance and ratio of variances
- maximum range
- first and second spectral moment

As before for the M5000, equivalent load ranges and magnitudes are estimated and compared to values derived from direct analysis of the measured data. This is done for the in-plane and out-of–plane blade root bending moments, the rotor torque and thrust as well as for the longitudinal tower base bending moment.

7.2.1 Estimations for another turbine type

In a first step, networks were trained with about 80 % of the available data from turbine T8 which corresponds to approximately 115 hours. The established networks were similar to those developed for the M5000 regarding topology and size. With the trained networks predictions of equivalent loads have been carried out for the remaining 30 hours of data.

The results are listed in Table 7.6. Estimation errors of cumulated equivalent loads as well as standard deviations of errors for exponents of 4 and 10 are given. In general, the errors of cumulated loads are quite small for all load components. The largest error occurred for the equivalent ranges of the longitudinal tower base bending moment with an exponent of 10. A detailed analysis showed that most of this error is caused by the false prediction of a single value. Similar to the M5000, quite a large equivalent load of one data set was underestimated by about 10 %. Because of the exponential weighting, this had a significant impact on the cumulated load cycles (compare Figure 7.3).

The standard deviation of the estimation errors are comparable to those encountered for the load predictions at the M5000 (Figure 7.2 and Table 7.1). Again the scatter of residuals is significantly lower for the equivalent magnitudes than for the cycles. The tendency to get better predictions for small exponents than for large ones can also be observed, even though it is not very pronounced.

As stated earlier, only the most robust signals and parameters were used for these predictions. This included the renouncement of the tower top accelerations in particular. In the previous analysis on the M5000 the variance and the first spectral moment of the tower top accelerations were often employed for the estimation of equivalent ranges. The fact, that predictions with comparable accuracy are achieved in this case without tower acceleration signals, indicates that the networks were able to retrieve about the same knowledge from other parameters. Thus, this information seems the be contained redundantly in the input data.

Table 7.6: Averages estimation errors and standard deviations of equivalent load ranges and magnitudes for the N80 turbine T8.

	Equivalent load ranges ΔS_{eq}			
	E in %		σ_E in %	
	m = 4	m = 10	m = 4	m = 10
M_{ip}	0.0	-0.1	1.3	1.7
M_{op}	-0.6	0.9	15.2	16.0
M_r	-1.8	-2.2	4.7	5.7
F_r	0.9	-3.4	10.9	11.9
M_{tb}	-0.1	-4.1	11.0	10.8
Average (abs)	0.7	2.1	8.6	9.2
	Equivalent load magnitudes L_{eq}			
	E in %		σ_E in %	
	p = 4	p = 10	p = 4	p = 10
M_{ip}	0.0	-0.1	1.6	2.2
M_{op}	0.1	-0.2	4.1	3.6
M_r	-0.1	-0.1	8.4	7.1
F_r	-0.1	0.0	2.9	3.7
M_{tb}	0.0	-0.3	3.5	4.0
Average (abs)	0.1	0.1	3.9	4.1

7.2.2 Application of established procedures for another turbine of the same type

The networks which have been trained with data from turbine T8 were applied for the prediction of loads at the turbine T6 for the available 22 hours of test data. Details of the estimation results are given in Table 7.7.

The results are similar to those derived for the turbine T8 for some load components. This holds true for example in case of the rotor thrust and the longitudinal tower base bending moment. The equivalent magnitudes of the rotor torque also feature the same level of accuracy. Surprisingly, some of the prediction errors are much larger than the errors observed for estimations at turbine T8. Because the turbine types are identical, the turbine locations are only about 600 m away from each other and the wind conditions in the two data sets are comparable, such huge false predictions have not been expected.

The following differences to the previously derived results at the turbine T8 are particularly eye-catching:

1. The error of the cumulated equivalent ranges of the in-plane blade root bending moment is much larger.

Table 7.7: Average estimation errors and standard deviations of equivalent load ranges and magnitudes for turbine T6. Networks for the prediction of equivalent loads have been trained with measured data from turbine T8.

	Equivalent load ranges ΔS_{eq}			
	E in %		σ_E in %	
	m = 4	m = 10	m = 4	m = 10
M_{ip}	7.3	7.8	2.2	2.5
M_{op}	4.6	-3.1	30.0	31.0
M_r	1.6	-1.2	38.1	32.3
F_r	-0.5	2.8	16.6	19.2
M_{tb}	0.5	-5.7	18.1	14.8
Average (abs)	2.9	4.1	21.0	20.0
	Equivalent load magnitudes L_{eq}			
	E in %		σ_E in %	
	p = 4	p = 10	p = 4	p = 10
M_{ip}	-1.7	-6.9	3.9	4.1
M_{op}	7.6	6.4	6.4	7.0
M_r	-5.0	-0.2	7.2	9.2
F_r	-3.3	-2.3	5.7	6.1
M_{tb}	-2.9	-2.3	5.4	6.8
Average (abs)	4.1	3.8	5.7	6.6

2. Standard deviations of errors for the equivalent ranges of the out-of-plane blade root bending moment and the rotor torque increased significantly.

3. Standard deviations of errors for the equivalent ranges of the rotor torque increased significantly.

4. Equivalent load magnitudes of the out-of-plane blade root bending moment are strongly overestimated.

To investigate the reasons for this surprising results, the measured loads have been analysed for both turbines. In fact, it turned out that most deviations can be justified by a comparison of measured data. Some of the data has been plotted in Figure 7.9 to support the following explanatory statements:

1. Both the mean value and the standard deviation of the measured in-plane blade root bending moment differ significantly between turbine T6 and T8 (Figure 7.9 (a) and (b)). The standard deviation, which is related to the load cycles, is significantly larger for T8. If the network is trained with data from T8, it will tend to overestimate the equivalent load ranges at T6.

In theory, the difference in standard deviation could be due to different static moments of the blades. However, the quantitative difference corresponds approximately to a 6 to 10 % larger mass of the blade at T8 which seems to be an unrealistic large deviation. Instead, an issue with the measurement calibrations is a more likely explanation. This guess is also supported by the large deviations of the measured mean values which can not be explained otherwise.

2. The standard deviations of the out-of-plane blade root bending moments (Figure 7.9 (d)) are comparable at both turbines and hence can not be the reason for the large increase in the standard deviation of prediction errors. Further investigations revealed that some of the small equivalent ranges are overestimated to more than twice the measured values. This influences the standard deviation of errors significantly without affecting the error of cumulated load ranges much.

3. On the contrary, the increased standard deviation of the torque can again be related to measured data. Figure 7.9 (e) illustrates that the small equivalent ranges are systematically overestimated. This can be traced back to a significant deterministic oscillation of the measured torque at turbine T8. Because of this oscillation, relatively large standard deviations of the torque are derived, even for the lowest power levels. While the standard deviations of torque at T6 get close to zero for low power output, this is not the case for T8. The relative influence of the deterministic oscillation reduces with increasing power, because other effects dominate. This is also reflected by the estimation results which get more and more accurate for large equivalent torque ranges.

   The exact reason for the deterministic oscillation is unknown. It's frequency matches the 1P frequency of the rotor and hence one might assume a rotor imbalance as a simple explanation. If this assumption applies, deterministic oscillations should be visible in other signals, for example the rotational acceleration of the generator, as well. However, this is not the case. Instead, the influence of main shaft bending which couples back into the torque measurements might be an explanation.

4. Similar to the deviations of mean values in the in-plane blade root bending moments, those of the out-of-plane moments also differ between turbine T6 and T8 when plotted over power output (Figure 7.9 (c)). Clearly, this explains why the neural network overestimated the equivalent magnitudes of this load component.

A detailed discussion on whether the deviations in measured loads between the two turbines are real or because of measurement errors (or a mixture of both) is beyond the

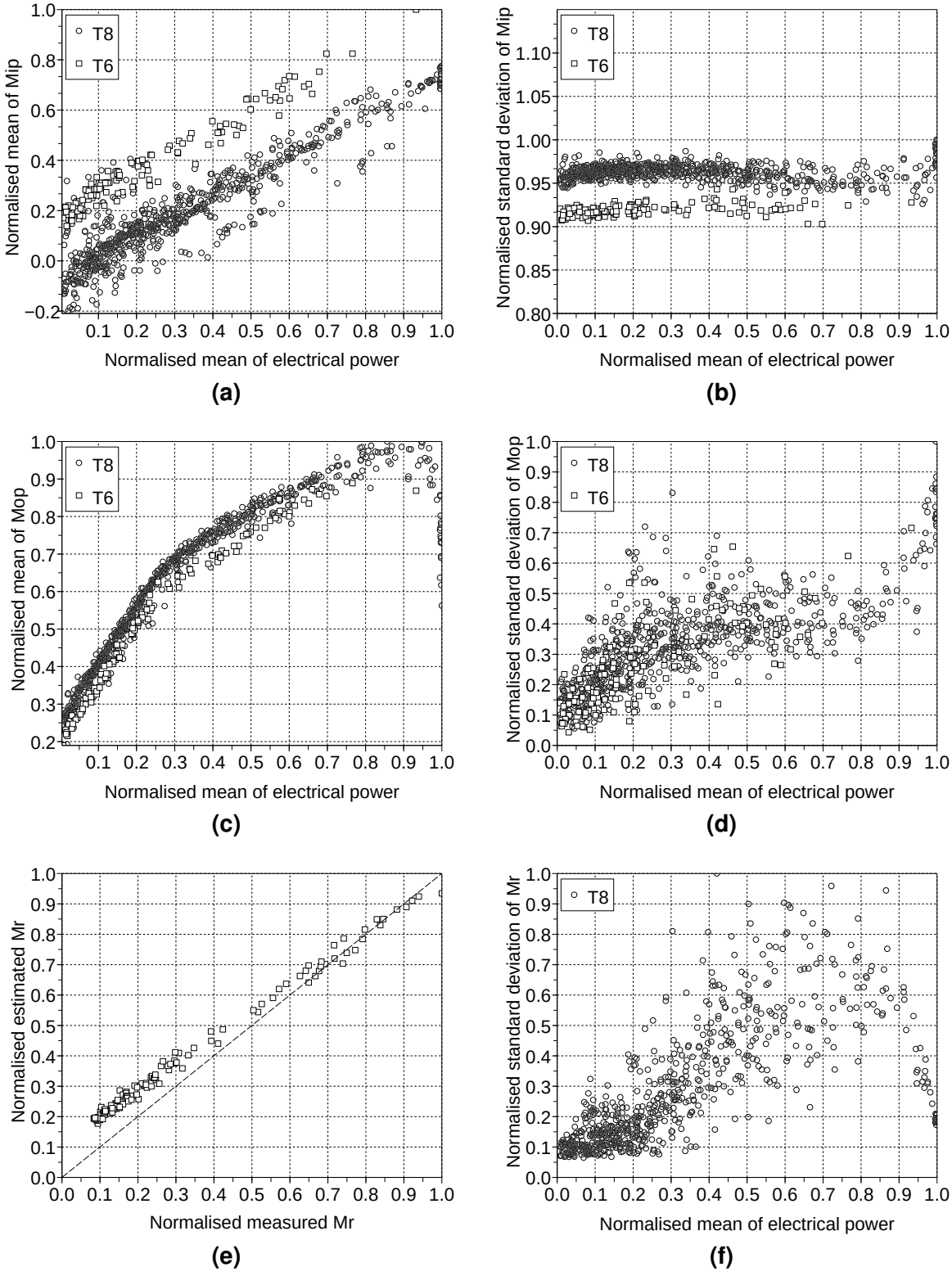

Figure 7.9: Comparison of measured mean values and standard deviations of in-plane ((a) and (b)) and out-of-plane ((c) and (d)) blade root bending moments over power. For the rotor torque, estimation results (e) and measured standard deviations (f) are shown.

scope of this work. Nevertheless, it can be concluded, that the deteriorated prediction results can be clearly related to these deviations in most cases. In other words, the neural networks correctly transfer the input data to equivalent loads according to the relations learned at turbine T8, but for some reasons these relations do not fully apply at turbine T6.

This also emphasises, that predicted loads have to be interpreted with care. Properties of turbines which significantly deviate from those encountered at turbines used to derive the data for establishing the transfer functions can influence the estimation accuracy. In case that load characteristics deviate, as it happened in the analysis above, the result is obvious: These deviations will simply not be captured and predicted loads will correspond to those included in the training data. If, however, the characteristics of input signals change, the situation is different. This data is passed through the network and thereby affect the predictions in one way or another. The potential impact on estimation results can be hard to assess, because the way the network processes the input data is difficult to analyse.

In any case, these considerations emphasise the importance of the system identification step during initialisation of a load estimation system and also of the continuous data verification outlined in Chapter 5. An additional example for the continuous verification requirement has been encountered during analysis of the power signal of turbine T6:

Towards the end of June 2008, the characteristics of the second spectral moment suddenly changed (compare Figure 7.10), yielding much larger values than before. Furthermore, this change was not observed in any other of the derived statistical parameters. The reason turned out to be an oscillation in the power signal with a frequency $>$ 5 Hz which was not present in data recorded before. Occurrence of the oscillation coincided in time with a derating of the turbine from 2.5 to 2 MW. Whether derating of the turbine caused the change in the second spectral moment, or this change reflects some kind of turbine failure which in turn was the reason for the derating, is not known. If the later applies, this example could even be quoted with respect to condition monitoring capabilities of a load estimation system.

7.2.3 Conclusions

An estimation of equivalent loads with neural networks has been carried out for two Nordex N80 turbines. Again the data was measured at an essentially flat site and wake operation was not included.

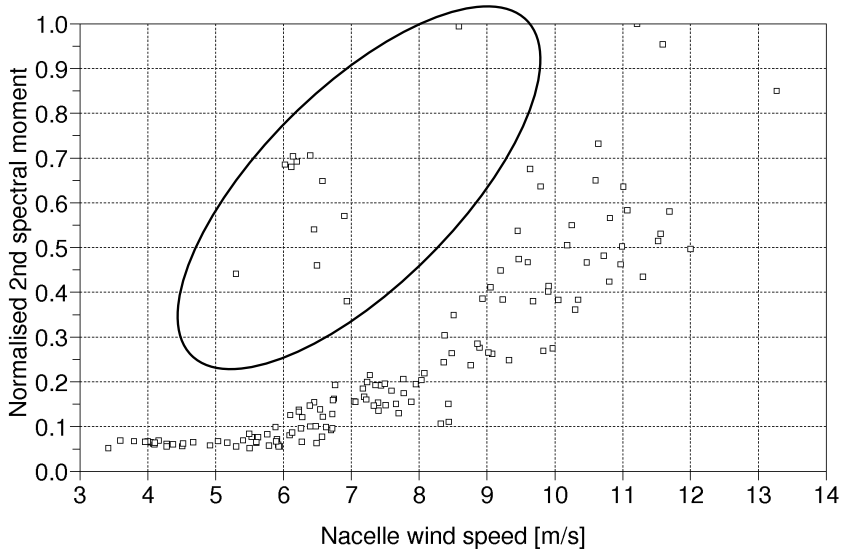

Figure 7.10: Second spectral moment before and after derating of turbine T6 plotted over mean wind speeds measured by the nacelle anemometer. The data recorded after derating have been encircled.

In terms of accuracy, the results are comparable to those derived previously for the Multibrid M5000 turbine. Although no tower top accelerations were available as input and only the most robust statistical parameters were used, the estimations errors did not deteriorate significantly. This also indicates, that the neural network based approach is generally suited to predict fatigue loads of variable speed pitch-controlled turbines. Because this type of turbine is currently the most often installed one and will probably dominate wind energy conversion within the foreseeable future, this is an important result.

In general, accurate results have also been derived, when networks which had been trained with data from turbine T8 were used to predict loads for turbine T6. For some load components large estimation errors were observed however. Obviously, the deviations were caused by differences in the loads measured at the two turbines under comparable external conditions (indicated by identical power output). Whether these differences are real or due to measurement errors could not be clarified.

For sure, a final assessment of transferability requires more investigations and experiments with additional turbines. Nevertheless, there seems to be a realistic chance of success to establish load estimation systems which can be applied for load predictions in a turbine series.

8 Summary and outlook

The investigations on fatigue load monitoring with standard wind turbine signals emphasise several aspects which have to be considered for the design of a load estimation system. The most important ones are summarised below. Based on the results of this study, recommendations for further areas of research are given.

Main findings

Because the load estimation system relies on an analysis of standard signals, it is a fundamental requirement that variations in fatigue load level manifest themselves also in standard signals. This is apparently the case for large load variations in the investigated examples. However, the influence of some environmental conditions on loads seems to be hard to detect from standard signals. Such situations occur, if averaging over the whole rotor plane reduces the impact of the disturbance significantly and, at the same time, only rotor averaged standard signals are employed for the monitoring. In these cases, a more sophisticated analysis of standard signals or the utilisation of information from a site analysis can improve prediction results.

A wind turbine is constantly subjected to many disturbances which all act differently on loads and standard signals. Furthermore, superposition can potentially alter their effects. For the design of an estimation system these influences have to be known and hence a large amount of representative measured or simulated data is required. Obtaining all necessary information is for sure one of the key aspects to establish a well working system.

Analysis of the data with conventional statistical methods like regression techniques is quite challenging. On the one hand because of the large number of influencing variables, on the other hand because of the non-linear wind turbine characteristic. Similar, the application of physical models for load estimations seem to be difficult. A lot of information on the turbine is required which often might not be available. In addition, wind turbines are already relatively complex systems and hence the measured standard signals are probably not sufficient to conclude on observability. Thus, at least for power production states, application of neural networks seems to be a suitable method to relate standard signals and fatigue loads. State estimation with database can be an

alternative, especially for transients.

Although utilisation of neural networks is probably the most convenient of the investigated methods to transfer standard signals into loads, the approach has some drawbacks. Usually networks have to be considered as black boxes. The analysis of networks is challenging and the potentially gained knowledge limited, because many different networks may give comparable results. Hence, such an analysis will not lead to a better understanding of the underlying processes.

The difficulties in the analysis of neural network based transfer functions in addition to the fact that each turbine type might react differently to disturbances, complicates the transfer of experiences gained at one load estimation system to another. As a consequence, the general feasibility of performing load predictions has to be assessed for each turbine type individually by taking the likely to encounter operational conditions into account.

Equivalent loads are particularly well suited estimation targets. They are closely related to fatigue damage and summarise a period of operation in just a single number. Therefore, the evaluation of an operational period in terms of fatigue loads can be performed on relatively few estimates.

For a more detailed analysis of fatigue loads, a procedure for the prognosis of load distributions has been developed. Because this method relies on probability density distributions, only a small number of estimates is usually required for each time period. To include effects of the non-linear and non-stationary wind turbine behaviour on the distributions, quantities like the expected total number of load cycles, maximum ranges and the maximum and minimum load levels have to be estimated as well.

These typical wind turbine characteristics are also the reason, why common frequency domain techniques for the calculation of load cycle distributions could not be applied. Because of some inherent limitation of these methods related to processes which are non-Gaussian, non-stationary or include significant deterministic components, their utilisation for wind turbines is not straightforward.

All developed prediction methods have been tested on the basis of measured wind turbine data with good success. In general, relatively accurate results are achieved for the estimation of equivalent loads and also for load distributions. Even when predictions are performed for another turbine of the same type, the accuracy of the results does not deteriorate much. In those cases where larger errors between predictions and measurements appeared, these could be related to deviations in the measured loads on both turbines. Whether the differences in measured loads are real or due to the measurements themselves could not be investigated in depth.

A final assessment of load estimation based on standard wind turbines from this work is difficult. The extensive analysis above revealed at least no insurmountable obstacles. It is therefore not unrealistic to assume, that such a system could work in practice and would enable wind turbine operators to benefit from the potentially large advantages of load monitoring (compare Chapter 2). Nevertheless, it should be stressed that more investigations are necessary to gain a better understanding of possibilities and requirements of a load estimation system. Some of these aspects are outlined below.

Recommendations for future work

- Most wind turbines are not installed as single turbines but in clusters. It is well known that turbines in a wind farm influence each other and that their behaviour and loading in wake differs from free stream operation. The impact of wake has not been investigated in this thesis, although the accuracy of load estimations in wake operation is certainly an important aspect for the general applicability of a load monitoring based on standard signals. First investigations by Obdam et al. [7] indicate that wake conditions have to be included into the training data of neural networks. Otherwise the estimations might underrate the real fatigue load level.

- For similar reasons, more investigations with measured data from real turbines at exposed and complex locations should be performed. For such sites, relations derived from flat terrain might not be fully valid anymore.

- Information from a site analysis or from correlating certain environmental conditions can potentially improve load predictions, especially for conditions which are hard to detect only from an analysis of standard signals. In addition, the design and the utilisation of statistical parameters of standard signals which can be linked to certain disturbances in a unique manner can simplify the load estimation (see Annex G for an example). Benefits and limitations of such approaches should be explored.

- For a working load estimation system, not only the influence of a single disturbance, but also those from combinations of disturbances have to be known. Thus, a large amount of data has to be collected to establish such a system. The process simplifies of course, if simulated data can be employed. Investigations towards hybrid estimation systems which are partly established with measured and partly with simulated data should therefore be carried out.

- Further optimisation of the load estimation procedure should be performed. This involves testing of other methods for establishing transfer functions than those investigated in this work. It will also be beneficial to include the uncertainty of the prediction into the monitoring. This can for example be achieved by using different transfer functions in parallel and to derive the uncertainty on the basis of the individual predictions. Another possibility is the prediction of probability density distributions from mixture density networks ([109]).

- Cost efficient load measurements using simple data loggers can simplify the collection of load and standard signal data, especially as detailed information on the wind conditions from separate measurements is not required. A feasibility study and practical tests could demonstrate this and further promote the application of load estimations.

- Transients have not been investigated in this work at all. However, depending on the number of occurrence and the reaction of the turbine to such situations, they can significantly influence fatigue loads. It has been concluded here, that state estimation with database is a suitable method to incorporate the effect of transients into the load estimation system. Because no measured transients were available, a practical evaluation of this assumption could not be carried out.

- The extrapolation of monitored loads and a comparison of results against the design load is an attractive option for making use of the potential benefits from an estimation system. However, this includes the automated selection of data sets which are representative of the past and the future operation and knowledge of the typical site conditions. This is not an easy task, but it allows to asses the fatigue loads of turbines already after relatively short monitoring periods.

- Furthermore, it is possible to predict a site dependent lifetime, defined as the moment in time where the real fatigue loads will equal the design loads. Based on these predictions authorities might agree to extend the service life of a turbine beyond the design life. This is probably one of the main reasons to employ load estimations in practice, because it offers the potentially largest benefit for a wind turbine operator.

In general, the above emphasises that there is still much research left to be done. Several issues have to be investigated further and solved in order to establish load estimation systems for wind turbines. Nevertheless, the assumption that such a system could be designed and applied on an industrial scale within the next years does not seem to be completely out of touch with reality.

Bibliography

[1] F.G. Polanco. Estimation of structural component loads in helicopters : a review of current methodologies. Technical Report DSTO-TN-0239, Aeronautical and Maritime Research Laboratory, Melburne, Australia, 1999.

[2] A.M. Lizotte and W.A. Lokos. Deflection-based structural loads estimation from the active aeroelastic wing F/A-18 aircraft. Technical Report NASA/TM-2005-212871, NASA Dryden Flight Research Center, Edwards, USA, 2005.

[3] H. Azzam, J. Cook, M. Wallace, A. Smith, P. Foote, and J. McFeat. The loads and damage detection techniques of a fleet and usage management system. In *9th Joint FAA/DoD/NASA Conference on Aging Aircraft*, Atlanta, USA, March 2006.

[4] A.A. ten Have and P.J.H.H. de Witte. Delivering fleet life management to the operator. Technical Report NLR-TP-2007-574, National Aerospace Laboratory NLR, April 2008.

[5] T.A.P. Lopes. Neural networks on fatigue damage prediction. In *International Conference on Neural Networks*, Houston, USA, June 1997.

[6] R. Dittmar, S. Müller, and S. Schwartz. Restlebensdauer von Windenergieanlagen bestimmen. *Erneuerbare Energien*, 3:20–22, March 2005.

[7] T. Obdam, L.W.M.M. Rademakers, and H. Braam. Flight leader concept for wind farm load counting and performance assessment. In *European Wind Energy Conference*, Marseille, France, March 2009.

[8] H. Hohlen. *Ein Neuro-Fuzzy-Zustandsbeobachter zur Bestimmung der Blattwurzelbelastungen von Windenergieanlagen*. PhD thesis, Technische Universität Berlin, 2002.

[9] E.J. Wiggelinkhuizen, T.W. Verbruggen, H. Braam, L.W.M.M. Rademakers, J. Xiang, S. Watson, G. Giebel, E. Norton, M.C. Tipluica, A. Maclean, A.J. Christensen, E. Becker, and D. Scheffler. CONMOW: Condition monitoring for offshore wind farms. In *European Wind Energy Conference*, Milan, Italy, May 2007.

[10] H.J. Sutherland. On the fatigue analysis of wind turbines. Technical Report SAND99-0089, Sandia National Laboratories, Albuquerque, USA, June 1999.

[11] Det Norske Veritas and Wind Energy Department of Risø National Laboratory. Guidelines for Design of Wind Turbines, 2002. 2nd edition.

[12] Gemanischer Lloyd Wind Energy GmbH. Rules and Guidelines - IV - Industrial Services, Guideline for the Certification of Wind Turbines, November 2003.

[13] W. Schutz. A history of fatigue. *Engineering Fracture Mechanics*, 54(2):263–300, 1996.

[14] P. Dahlhoff, A. Dombrowski, R. Grzybowski, F. Pollicino, B. Niederstucke, S. Subramanian, M. Wöbbeking, L. Krutschinna, and H. Idelberger. Forschungsvorhaben ELA - Erweiterte Lebensdaueranalyse für Windenergieanlagen. Technical Report 71048, Germanischer Lloyd Wind Energie GmbH, Hamburg, Germany, August 2003.

[15] D.E. Newland. *Introduction to random vibration, spectral and wavelet analysis*. Dover Publications, New York, USA, 3rd edition, 2005.

[16] International Electrotechnical Commission. International Standard IEC 61400-1 Ed.3, Wind Turbines - Part 1: Design Requirements, 2005.

[17] T. Burton, D. Sharpe, N. Jenkins, and E. Bossanyi. *Wind Energy Handbook*. John Wiley & Sons, Chichester, UK, 2001.

[18] R. Gasch and J. Twele, editors. *Wind Power Plants*. James & James, London, UK, 2002.

[19] J. F. Manwell, J. G. McGowan, and A. L. Rogers. *Wind Energy Explained - Theory, Design and Application*. John Wiley & Sons Ltd., Chichester, UK, 2003.

[20] M.O.L. Hansen. *Aerodynamics of wind turbines*. Earthscan, London, UK, 2nd edition, 2008.

[21] T. Sant. *Improving BEM-based Aerodynamic Models in Wind Turbine Design Codes*. PhD thesis, Delft University of Technology, 2007.

[22] J. Peeters. *Simulation of Dynamic Drive Train Loads in a Wind Turbine*. PhD thesis, University of Leuven, 2006.

[23] D.-P. Molenaar. *Cost-effective design and operation of variable speed wind turbines*. PhD thesis, Delft University of Technology, 2003.

[24] R. Mikkelsen. *Actuator Disc Methods Applied to Wind Turbines*. PhD thesis, Technical University of Denmark, 2003.

[25] S. Hauptmann, S. Mulski, N. Cosack, M. Kühn, and L. Mauer. Aero-elastic simulation of a wind turbine and drive train resonance analysis using the multi-body simulation code SIMPACK. In *German Wind Energy Conference (DEWEK)*, Bremen, Germany, November 2006.

[26] D. Kaufer, N. Cosack, C. Böker, M. Seidel, and M. Kühn. Integrated analysis of the dynamics of offshore wind turbines with arbitrary support structures. In *European Wind Energy Conference*, Marseille, France, March 2009.

[27] E. D. Eggleston and R.N. Clark. Cut-in note 1: Wind speed power spectrum analysis for Bushland, Texas, USA. *Wind Engineering*, 24(1):49–52, 2000.

[28] D. Veldkamp. *Chances in Wind Energy - A Probabilistic Approach to Wind Turbine Fatigue Design*. PhD thesis, Delft University of Technology, 2006.

[29] T.J. Knill. The application of aeroelastic analysis output load distributions to finite element models of wind. *Wind Engineering*, 29(2):153–168, 2005.

[30] O.A. Jaramillo and M.A. Borja. Bimodal versus weibull wind speed distributions: an analysis of wind energy potential in La Venta, Mexico. *Wind Engineering*, 28 (2):225–234, 2004.

[31] H. Basumatary, E. Sreevalsan, and K.K. Sasi. Weibull parameter estimation - a comparison of different methods. *Wind Engineering*, 29(3):309–316, 2005.

[32] N. Cosack and M. Kühn. Überwachung von Belastungen an Windenergieanlagen durch Analyse von Standardsignalen. In *7. Aachener Kolloquium für Diagnose, Instandhaltung und Anlagenüberwachung*, Aachen, Germany, November 2006.

[33] V.A. Riziotis and S.G. Voutsinas. Fatigue loads on wind turbines of different control strategies operating in complex terrain. *Journal of Wind Engineering and Industrial Aerodynamics*, 85(3):211–240, 2000.

[34] L.D. Nelson, L. Manuel, H.J. Sutherland, and P.S. Veers. Statistical analysis of wind turbine inflow and structural response data from the LIST program. *Journal of Solar Energy Engineering*, 125:541 – 550, 2003.

[35] N.D. Kelley, B.J. Jonkman, and G.N. Scott. The great plains turbulence environment: Its origins, impact and simulation. In *AWEA WindPower Conference*, Pittsburgh, USA, June 2006.

[36] S. Emeis. Vertical wind profiles over an urban area. *Meteorologische Zeitschrift*, 13(5):353–259, 2004.

[37] N. Cosack, S. Emeis, and M. Kühn. On the influence of low-level jets on energy production and loading of wind turbines. In *Euromech Kolloquium 464b on Wind Energy*, Oldenburg, Germany, October 2005.

[38] A. Sathe and W. Bierbooms. Influence of different wind profiles due to varying atmospheric stability on the fatigue life of wind turbines. *Journal of Physics: Conference Series*, 75, 2007.

[39] N. Stefanatos, F. Mouzakis, B. Binopoulos, F. Kokkalidis, and Papadopoulos P. Verification of power performance of active power control wind turbines in complex terrain. In *European Wind Energy Conference*, Athens, Greece, March 2006.

[40] T. Maeda, S. Homma, and Y. Ito. Effect of complex terrain on vertical wind profile measured by SODAR technique. *Wind Engineering*, 28(6):667–678, 2004.

[41] R. Istchenko and B. Turner. Extrapolation of wind profiles using indirect measures of stability. *Wind Engineering*, 32:433–438, 2008.

[42] T. F. Pedersen. On wind turbine power performance measurements at inclined airflow. *Wind Energy*, 7(3):163–176, 2004.

[43] J.-A. Dahlberg, T. F. Pedersen, and P. Busche. ACCUWIND - methods for classification of cup anemometers. Technical Report R-1555 (EN), Risø, Roskilde, Denmark, May 2006.

[44] E.L. Petersen, N.G. Mortensen, L. Landberg, J. Hojstrup, and H.P. Frank. Wind power meteorology. Part I: climate and turbulence. *Wind Energy*, 1(1):2–22, 1998.

[45] K.S. Hansen and C.G. Larsen. Characterising turbulence intensity for fatigue load analysis of wind turbines. *Wind Engineering*, 29(4):319–329, 2005.

[46] G.C. Larsen and K.S. Hansen. Database on wind characteristics - contents of database bank. Technical Report Risø-R-1472(EN), Risø National Laboratory, Roskilde, Denmark, 2004.

[47] S. Frandsen. Spatially average of turbulence intensity inside large wind turbine arrays. In *European Seminar on Offshore Wind and other Marine Renewable Energies in Mediterranean and European Seas*, Naples, Italy, April 2003.

[48] K. Rados, G. Larsen, R. Barthelmie, W. Schlez, B. Lange, G. Schepers, T. Hegberg, and M. Magnisson. Comparison of wake models with data for offshore windfarms. *Wind Engineering*, 25(5):271–280, 2001.

[49] H. Seifert and J. Kröning. Recommendations for spacing in wind farms. In *European Wind Energy Conference*, Madrid, Spain, June 2003.

[50] M. L. Frandsen, S.; Thogersen. Integrated fatigue loading for wind turbines in wind farms by combining ambient turbulence and wakes. Technical report, Risø National Laboratory, 1999.

[51] K. Bleibler. Untersuchung der meteorologischen Einflüsse auf das Leistungs- und Lastverhalten des Prototypen der Multibrid M5000 Windenergieanlage. Master's thesis, Universität Stuttgart, Endowed Chair of Wind Energy at the Institute of Aircraft Design, 2006.

[52] K. Bleibler, T. Kramkowski, N. Cosack, and K. Braun. The influence of meteorological parameters on the operational behavior of multi-megawatt WEC. In *German Wind Energy Conference (DEWEK)*, Bremen, Germany, November 2006.

[53] F. Mouzakis, E. Morfiadakis, and P. Dellaportas. Fatigue loading parameter identification of a wind turbine operating in complex terrain. *Journal of Wind Engineering and Industrial Aerodynamics*, 82(1):69–88, 1999.

[54] G.C. Larsen. Consequences of variations in spatial turbulence characteristics for fatigue life time of wind turbines. Technical Report Risø-R-1052(EN), Risø National Laboratory, Roskilde, Denmark, April 1998.

[55] G.C. Larsen and P. Volund. Validation of an aeroelastic model of Vestas V39. Technical Report Risø-R-1051(EN), Risø National Laboratory, Roskilde, Denmark, April 1998.

[56] J. Counihan. Adiabiatic atmospheric boundary layers: A review and analysis of data from the period 1880-1972. *Atmospheric Environment*, 9:870–905, 1975.

[57] S. Frandsen, H.E. Jorgensen, and J.D. Sorensen. Relevant criteria for testing the quality of turbulence models. In *European Wind Energy Conference*, Milan, Italy, May 2007.

[58] L. J. Vermeer, J. N. Sorensen, and A. Crespo. Wind turbine wake aerodynamics. *Progress in Aerospace Sciences*, 39:467–510, 2003.

[59] K. Saranyasoontorn, L. Manuel, and P.S. Veers. A comparison of standard coherence models for inflow turbulence with estimates from field measurements. *Journal of Solar Energy Engineering*, 126(4):1069–1082, 2004.

[60] G.C. Larsen and K.S. Hansen. Database on wind characteristics - analyses of wind turbine design loads. Technical Report Risø-R-1473(EN), Risø National Laboratory, Roskilde, Denmark, June 2004.

[61] J. Hojstrup. Spectral coherence in wind turbine wakes. *Journal of Wind Engineering and Industrial Aerodynamics*, 80:137–146, 1999.

[62] A. Grunwald, M. Melsheimer, C. Heilmann, and J. Liersch. Unwuchtbestimmung mit Ampelfunktion. *Erneuerbare Energien*, pages 28–31, August 2007.

[63] Deutsches Institut für Bautechnik. Richtlinie für Windenergieanlagen, 2003.

[64] P. Volund and I. Antoniou. Measured ice loads on Avedoere 1 MW test turbine. Technical Report Risø-R-1026(EN), Risø National Laboratory, Roskilde, Denmark, December 1997.

[65] P. Frohboese and A. Anders. Effects of icing on wind turbine fatigue loads. *Journal of Physics: Conference Series*, 75:012061 (13pp), 2007.

[66] P. Caselitz and J. Giebhardt. Rotor condition monitoring for improved operational safety of offshore wind energy converters. *Journal of Solar Energy Engineering*, 127(2):253–261, 2005.

[67] J. Liersch, M. Melsheimer, and K. Ohde. Schwingungsberuhigung von Windenergieanlagen - Unterscheidung von aerodynamischer und massenbedingter Unwucht. In *German Wind Energy Conference (DEWEK)*, Wilhelmshaven, Germany, October 2004.

[68] R.V Hogg and J. Ledolter. *Engineering Statistics*. Macmillan Publishing Company, New York, 1987.

[69] L. Fahrmeir, R. Künstler, I. Pigeot, and G. Tutz. *Statistik*. Springer, Berlin, 5th edition, 2004.

[70] R.A. Johnson and D.W. Wichern. *Applied Multivariate Statistical Analysis*. Prentice Hall, New Jersey, 3rd edition, 1992.

[71] W. Mendenhall and T. Sinich. *Statistics for Engineering and the Science*. Prentice Hall, New Jersey, 4th edition, 1995.

[72] S. L. Campbell, J.-P. Chancelier, and R. Nikoukhah. *Modelling and Simulation in Scilab/Scicos*. Springer, Berlin, 2006.

[73] K. Rohrig and B. Lange. Application of wind power prediction tools for power system operations. In *IEEE Power Engineering Society General Meeting 2006*, Montreal, Canada, June 2006.

[74] B. Müller and J. Reinhard. *Neural Networks - An introduction*. Physics of Neural Networks. Springer, Berlin, 1991.

[75] R. Rojas. *Neural Networks - A Systematic Introduction*. Springer, Berlin, Germany, 1996.

[76] K. Gurney. *An introduction to neural networks*. UCL Press, London, 1997.

[77] P. Marrone. *Joone - Java Object Oriented Neural Engin: The complete guide*. January 2007, available from www.sourceforge.net/projects/joone/.

[78] I. Fischer, F. Hennecke, C. Bannes, and A. Zell. *JavaNNS - Java Neural Network Simulator*. University of Tübingen. User Manual, Version 1.1, available from www.ra.cs.uni-tuebingen.de/software/JavaNNS/.

[79] A. Zell et al. *SNNS - Stuttgart Neural Network Simulater*. University of Stuttgart and University of Tübingen. User Manual, Version 4.2, available from www.ra.cs.uni-tuebingen.de/SNNS/.

[80] H. Braun. *Neuronale Netze - Optimierung durch Lernen und Evolution*. Springer, Berlin, 1997.

[81] L. Dong. Internship report. Technical report, Universität Stuttgart, Endowed Chair of Wind Energy at the Institute of Aircraft Design, 2007.

[82] J. Holnicki-Szulc, editor. *Smart Technologies for Safety Engineering*. John Wiley & Sons, Chichester, England, 2008.

[83] A.M. El-Shahhat and W.F. Chen. Toward a life cycle analysis of concrete structures. Technical Report CE-STR-94-13, Purdue University, 1994.

[84] H.-N. Li, D.-S. Lia, and G.B. Song. Recent applications of fiber optic sensors to health monitoring in civil engineering. *Engineering Structures*, 26(11):1647–1657, 2004.

[85] J.R. Casas and P.J.S. Cruz. Fiber optic sensors for bridge monitoring. *Journal of Bridge Engineering*, 8(6):362–373, 2003.

[86] M. C. Tsai, E. C. Tseng, and M. Y. Cheng. Design of a torque observer for detecting abnormal load. *Control Engineering Practice*, 8(3):259–269, March 2000.

[87] S.M. Kay and S.L. Marple. Spectrum analysis - a modern perspective. In *Proceedings of the IEEE*, volume 69, pages 1380–1419, November 1981.

[88] M.P. Perrone and L.N. Cooper. *When networks disagree: Ensemble methods for hybrid neural networks*. Artificial Neural Networks for Speech and Vision. Chapman and Hall, London, 1993.

[89] N.W.M. Bishop and F. Sherratt. A theoretical solution for the estimation of rainflow ranges from power spectral density data. *Fatigue and Fracture of Engineering Materials and Structures*, 13(4):311–326, 1990.

[90] N.W.M. Bishop, H. Zhihua, and F. Sherratt. The analysis of non-Gaussian loadings from wind turbine blades using frequency domain techniques. In *Proceedings of the13th BWEA conference*, pages 317–323, Swansea, UK, April 1991.

[91] F. Sherratt, N.W.M. Bishop, and T. Dirlik. Predicting fatigue life from frequency domain data: Current methods. Technical report, 2005. Expanded version of an article in the September 2005 issue of the Engineering Integrity Society from www.e-i-s.org.uk/.

[92] G. Petrucci and B. Zuccarello. On the estimation of the fatigue cycle distribution from spectral density data. *Journal of Mechanical Engineering Science*, 213(8): 819–831, April 1999.

[93] S.O. Rice. *Mathematical analysis of random noise*. Selected Papers on Noise and Stochastic Processes. Dover Publications, New York, USA, 1954.

[94] J.-Q. Sun. *Stochastic Dynamics and Control*. Elsevier, Amsterdam, The Netherlands, 2006.

[95] T. Dirlik. *Applications of Computers in Fatigue Analysis*. PhD thesis, University of Warwick, England, 1985.

[96] D. Benasciutti and B. Tovo. Fatigue life assessment in non-Gaussian random loadings. *International Journal of Fatigue*, 28:733–746, 2005.

[97] D. Benasciutti. *Fatigue Analysis of Random Loadings*. PhD thesis, University of Ferrara, 2005.

[98] M. Karlsson. Evaluation of approximate methods for rainflow damage of broad-banded non-Gaussian random loads. In *International Mechanical Engineering Congress and Exhibition*, Orlando, USA, November 2005.

[99] S.R. Winterstein. Nonlinear vibration models for extremes and fatigue. *Journal of Engineering Mechanics*, 114(10), Oktober 1988.

[100] K.R. Gurley. *Modelling and Simulation of Non-Gaussian Processes*. PhD thesis, University of Notre Dame, 1997.

[101] K. Gurley and A. Kareem. Simulation of correlated non-Gaussian pressure fields. *Meccanica*, 33:309–317, 1998.

[102] P. Ragan and L. Manuel. Comparing estimates of wind turbine fatigue loads using time-domain and spectral methods. *Wind Engineering*, 31:83–99, 2007.

[103] J. van der Tempel. *Design of Support Structures for Offshore Wind Turbines*. PhD thesis, Delft University of Technology, 2006.

[104] N. Cosack and M. Kühn. Prognose von Ermüdungslasten an Windenergieanlagen mittels Standardsignalen und neuronaler Netze. In *Tagungsband des Dresdner Maschinenelemente Kolloquiums*, Dresden, Germany, Dezember 2007.

[105] X. Wang and J.Q. Sun. Multi-stage regression fatigue analysis of non-Gaussian stress processes. *Journal of Sound and Vibration*, 280(1-2):455 – 465, 2005. ISSN 0022-460X.

[106] N.W.M. Bishop, R. Wang, and L. Lack. A frequency domain fatigue predictor for wind turbine blades including deterministic components. In *Proceedings of the17th BWEA conference*, pages 53–58, Warwick, UK, October 1995. BWEA.

[107] N. Cosack and M. Kühn. An approach for fatigue load monitoring without load measurement devices. In *European Wind Energy Conference*, Marseille, France, March 2009.

[108] X. Wang and J.Q. Sun. Effect of skewness on fatigue life with mean stress correction. *Journal of Sound and Vibration*, 282:1231 – 1237, 2005.

[109] Christopher M. Bishop. Mixture density networks. Technical Report NCRG/94/001, Aston University, Dep. of Computer Science and Applied Mathematics, Birmingham, UK, February 1994.

[110] S. Øye. Simulation of loads on a wind turbine including turbulence. In *Proceedings of IEA-Meeting on Wind Characteristics of Relevance for Wind Turbine Design*, Stockholm, Sweden, 1991.

[111] R.W. Clough and J.R. Penzien. *Dynamics of Structures*. McGraw-Hill, Singapore, second edition, 1993.

[112] P.S. Veers. Three-dimesional wind simulation. Technical Report SAND88-0152, Sandia National Laboratories, Albuquerque, USA, March 1988.

[113] D.J. Malcolm and A.C. Hansen. WindPACT turbine rotor design study. Technical Report NREL/SR-500-32495, National Renewable Energy Laboratory, Golden, USA, August 2002.

[114] J.T. Petersen, H.A. Madsen, A. Björck, P. Enevoldsen, S. Øye, H. Ganander, and D. Winkelaar. Prediction of dynamic loads and induced vibrations in stall. Technical Report Risø-R-1045(EN), Risø National Laboratory, Roskilde, Denmark, May 1998.

[115] Multibrid GmbH. M5000 - technical data. Bremerhaven, Germany, June 2008. Booklet available at www.multibrid.com.

[116] Erneuerbare Energien. Wind turbine market 2007. Magazine, SunMedia publishing, Hannover, Germany, 2007.

[117] Nordex AG. N80/2500 and N90/2300. Norderstedt, Germany, January 2009. Booklet available at www.nordex-online.com.

[118] N.D.P. Barltrop and A.J. Adams. *Dynamics of fixed marine structures*. Butterworth-Heinemann Ltd, Oxford, UK, 3rd edition, 1991.

[119] M. Kühn. *Dynamics and Design Optimisation of Offshore Wind Energy Conversion Systems*. PhD thesis, Delft University of Technology, 2001.

[120] S. Holm. Spectral moment matching in the maximum entropy spectral analysis method. *IEEE Transactions on Information Theory*, IT-29(2):311–313, March 1983.

[121] S. Holm and J.M. Hovem. Estimation of scalar ocean wave spectra by the maximum entropy method. *IEEE - Journal on Oceanic Engineering*, OE - 4(3):76 – 83, July 1979.

[122] E.L. Petersen, N.G. Mortensen, L. Landberg, J. Hojstrup, and H.P. Frank. Wind power meteorology. Technical Report Risø-I-1206(EN), Risø National Laboratory, Roskilde, Denmark, December 1997.

[123] S. Frandsen. Turbulence and turbulence generated structural loading in wind turbine clusters. Technical Report Risø-R-1188(EN), Risø National Laboratory, Roskilde, Denmark, January 2007.

[124] P.L. O'Neill, D. Nicolaides, D. Honnery, and J. Soria. Autocorrelation functions and the determination of integral length with reference to experimental and numerical data. In *Proceedings of the Fifteenth Australasian Fluid Mechanics Conference*. University of Sydney, December 2004.

[125] G.J. Van Fossen and C.Y. Ching. Measurements of the influence of integral length scale on stagnation heat transfer. In *Fifth Symposium on Transport Phenomena and Dynamics of Rotating Machinery*, 1994.

[126] G.I. Taylor. The spectrum of turbulence. *Proceedings of the Royal Society of London. Series A, Mathematical and Physical Sciences*, 164(919):476–490, 1938. ISSN 00804630.

[127] S. de Waele, A. van Diek, P. Broersen, and P. Duynkerke. Estimation of the integral time scale with time series models. In *15th Conference on Boundary Layer and Turbulence*, 2002.

A Flex5

The computer program FLEX5 has been developed at the Department of Fluid Mechanics at the Technical University of Denmark [110]. It has been specially designed to model the behaviour of horizontal axis wind turbines operating in various wind conditions including simulated turbulent wind. The turbine model has got only relatively few but important degrees of freedom, combined with a fully non-linear calculation of loads and response.

Structural dynamics of the turbine are modelled using modal shape functions for the deflections of the tower and the blades and stiff bodies connected by flexible hinges to model the nacelle, rotor shaft and hub. Generalised global mass and stiffness matrices are then assembled from the generalised masses and stiffnesses of these sub systems. Setting up the stiffness matrix is straightforward, because no coupling in terms of stiffness is assumed and hence the stiffness matrix is diagonal. Coupling of the sub systems is achieved only via the off diagonal elements of the mass matrix. With all degrees of freedom activated, the maximum matrix size is 28 x 28.

The response of the structure to external forces is calculated in the time domain with a numerical approximation step-by-step approach. An explicit Runge-Kutta method of second order, based on numerical integration and the assumption of constant acceleration in between the steps, is applied for this purpose (see for example Clough and Penzien [111] for details on this step-by-step approach and the set-up of generalised mass and stiffness matrices).

The aerodynamic loads are calculated by the Blade-Element-Momentum (BEM) method. Also several additional models are applied to account for effects that are not captured by the BEM approach, such as dynamic wake, tip losses and dynamic inflow. Their implementation mostly agrees with descriptions given by Hansen in [20]. No iterations, for example for the computation of induction factors, are performed. Instead it is assumed, that the time steps required for the structural response calculation are sufficiently small, so that the variations in aerodynamics from one step to another are small as well and hence no additional iteration at the single time steps is necessary.

Flex5 licences include the delivery of the source code which then has to be maintained by the licence holder. As each owner probably modifies the code, many derivatives exists today. Some features of the basic version are listed below.

Wind and aerodynamic modelling

- Superposition of deterministic and stochastic wind
- Deterministic: mean wind speed and direction, wind shear, tower shadow
- Stochastic: three-dimensional turbulence using the Veers method [112]
- Aerodynamic loads calculated according to the unsteady BEM Theory
- Inlcudes tip loss correction (Glauert/Prandl), turbulent wake state correction (Glauert), dynamic inflow model (Øye), yawed flow model (Glauert/Øye) and dynamic stall simulation (Øye)
- Drag loads on hub, nacelle and tower are included

Structural modelling

- 28 degrees of degrees of freedom in total
- Viscous damping for all degrees of freedom
- Blades: beam model with distributed mass and stiffness; coupled edge and flapwise modes; pre-curved initial shape possible.
- Hub: stiff body with mass and mass moments of inertia
- Shaft: spring with two bending and one torsional degree of freedom; gearbox transmission ratio; mass moment of inertia on high speed side
- Nacelle: stiff body with mass and mass moments of inertia
- Tower: beam model with distributed mass and stiffness
- Foundation: stiff body with mass and mass moments of inertia
- First order models for generator, brake and yaw system
- Second order model for pitch system

Table A.1: Possible degrees of freedom in FLEX5

Blades	Nacelle	Tower	Foundation
1st flapwise	1st shaft bending[1]	1st longitudinal	1st translational[2]
2nd flapwise	1st torsional	2nd longitudinal	1st rotational[2]
1st edgewise	rotational	1st lateral	
2nd edgewise		2nd lateral	

[1] in two perpendicular directions
[2] in three perpendicular directions

B NREL 1.5 MW WindPACT turbine

The National Renewable Energy Laboratory NREL (Colorado, USA) has developed a simulation model of a generic wind turbine. Although the model has originally been intended for the WindPACT (Wind Partnership for Advanced Component Technologies) research project [113] it has been used as a baseline for other research activities at NREL during the past years as well. The model is also included in the wind turbine simulation package FAST which can be obtained from the NREL homepage.

Flex5 and FAST are quite similar in their general methods of how a wind turbine is modelled. Nevertheless, some small adjustments of the model have been necessary in order to implement it into Flex5. According to the author's experience, the overall characteristics of the model are consistent with those of real, commercial wind turbines. The main properties are listed below to give an overview of the wind turbine model used.

Turbine data

- variable-speed, pitch-controlled, 3-bladed wind turbine
- 1.5 MW rated power
- rotor speed range from 12.0 to 22.5 rpm with rated speed at 20.5 rpm
- gearbox transmission of 87.965
- overall efficiency at rated power 92.5 %

Geometrical data

- 70 m rotor diameter
- 84 m hub height
- tilt angle of 5 $^{\circ}$
- maximum blade chord length of 2.74 m
- hub overhang of 3.30 m (from tower axis)

Structural data

- blade mass: 4440 kg

- hub mass: 15500 kg
- nacelle mass: 52000 kg
- blade eigenfrequencies flapwise: 1.12/3.40 Hz ($1^{st}/2^{nd}$)
- blade eigenfrequencies edgewise: 1.77/6.05 Hz ($1^{st}/2^{nd}$)
- shaft torsional eigenfrequency: 3.55 Hz
- tower bending eigenfrequencies: 0.39/2.52 Hz ($1^{st}/2^{nd}$)
- tower torsional eigenfrequency: 2.14 Hz

Eigenfrequencies of the turbine model

The frequencies of the lowest coupled modes are given in Table B.1. They are derived from the non-rotating, stationary model and hence exclude centrifugal and gyroscopic forces. For a complete analysis of stability or possible resonances, those forces have to be included of course as their effect on frequencies and modes can be significant (see for example Petersen et al. [114]).

Table B.1: Coupled eigenfrequencies of the NREL 1.5 MW model from FLEX5 simulations (neglecting effects from rotation and damping)

Mode description	Frequency in Hz
Mainly 1^{st} longitudinal tower mode	0.37
Mainly 1^{st} lateral tower mode	0.37
Combined nacelle yaw and 1^{st} flapwise blade modes	1.04
Combined nacelle tilt and 1^{st} flapwise blade modes	1.12
Mainly 1^{st} flapwise blade modes	1.15
Mainly 1^{st} edgewise blade modes	1.76
Mainly 1^{st} edgewise blade modes	1.78
Combined shaft, 2^{nd} lateral tower and 1^{st} edgewise blade modes	2.34
Mainly 2^{nd} longitudinal tower mode	2.50
Combined shaft, tower torsion, 2^{nd} lateral tower and 1^{st} edgewise blade modes	2.70
Combined nacelle yaw and 2^{nd} flapwise blade modes	2.95
Mainly 2^{nd} flapwise blade modes	3.42
Mainly 2^{nd} flapwise blade modes	3.48
Combined shaft and 2^{nd} edgewise blade modes	4.80

Description of the control strategy

The model is operated as a variable-speed pitch-controlled turbine. The main control variables are generator speed, power output and pitch angle. The actuating variables are pitch angle and generator torque. Two separate loops (for torque and pitch) are

used to control these variables.

Torque control loop:

- The demanded generator torque is determined from PI-control, using generator speed as input.
- Below rated speed the torque control is used to maintain the optimum tip speed ratio (variable speed control).
- At rated speed, the torque control is used to maintain rated speed until the torque reaches an upper limit (rated power output, start of pitch control).
- At full load operation the torque is adjusted to yield rated power.
- The torque set points are band-stop filtered to remove unwanted frequencies.

Pitch control loop:

- The demanded pitch angle is determined via PI-control, using generator speed as input.
- At partial load operation the pitch angle is kept constant.
- At full load operation the pitch angle is used to maintain rated generator speed.
- A secondary pitch control loop monitors power output and thereby ensures decoupling of pitch and torque control.

If the torque control is set to maintain rated power at full load operation, the damping of the drive train becomes negative (an increase in generator speed will result in a reduction of generator torque). To avoid excessive oscillations of the drive train, an active damping mechanism is commonly implemented at real turbines. Typically, the shaft oscillations with the frequencies of interest are monitored and the generator torque is adjusted to damp the oscillations actively [17].

To keep the control algorithm of the simulated turbine simple, the problem is handled differently here. Instead of implementing a damper, only a band stop filter for the torque set points is applied. This avoids additional excitation of the torsional shaft modes by the generator, but does not include an active reduction of resonances. As a consequence, the general level of vibration within the drive train might be slightly higher, than what can be expected for a commercial turbine with a proper damping algorithm.

Characteristic curves

Figure B.1 shows some important operational and load signals. The data has been derived by slowly increasing the wind speed from 3 to 25 m/s. Only deterministic wind

without turbulence has been used. Most degrees of freedom have been deactivated in this simulation. A straight line with negative inclination has been added to the upper branch of the torque-speed curve to illustrate that the torque is adjusted to maintain rated power at full load operation.

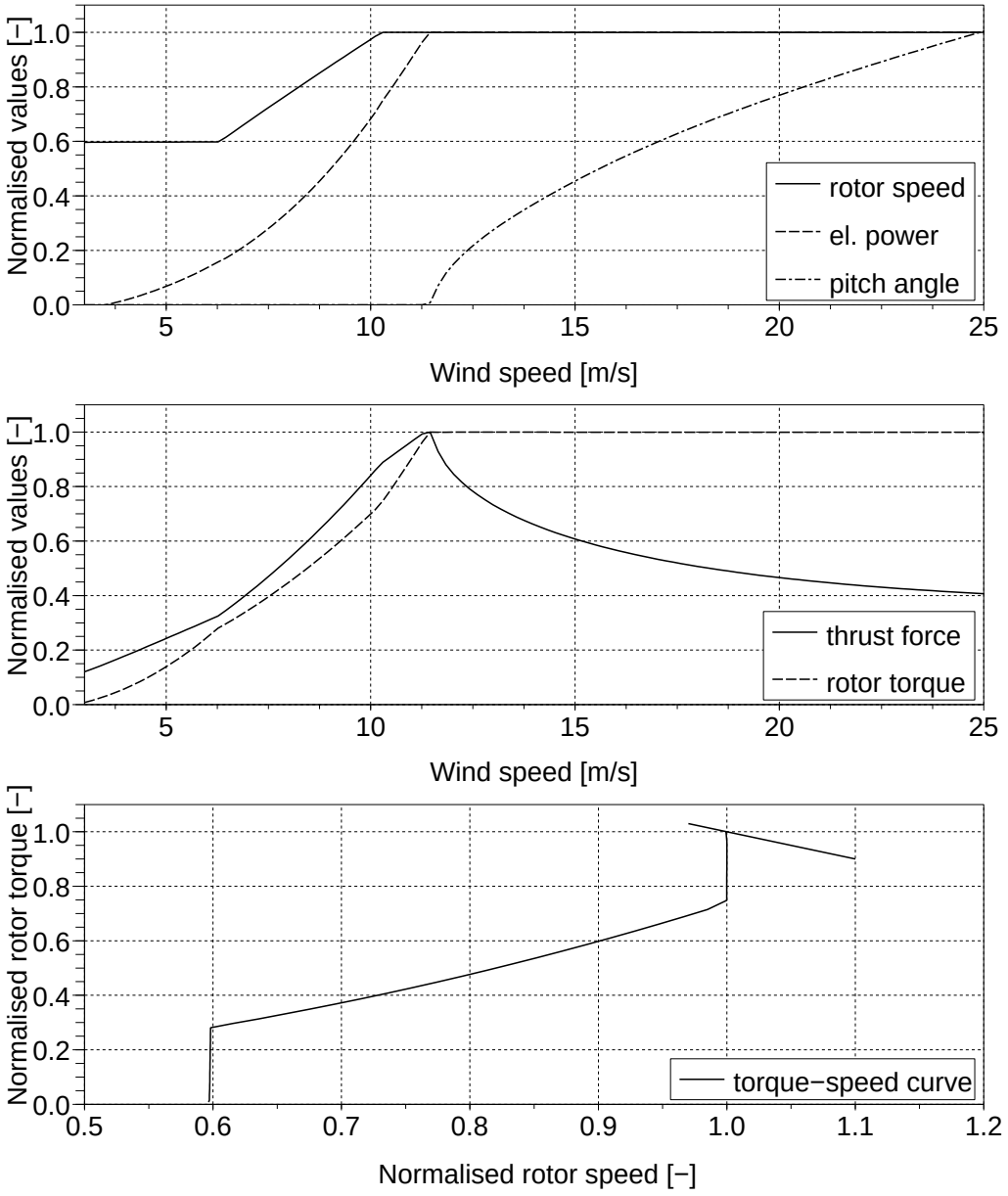

Figure B.1: Characteristic curves of the NREL 1.5 MW model: rotor speed, power, pitch angle, thrust and torque over wind speed and the torque-speed curve

C Multibrid M5000 prototype turbine

C.1 Turbine description

The Multibrid M5000 turbine is a state of the art multi-megawatt wind turbine with a rotor diameter of 116 m and a rated power of 5 MW. A special feature of this turbine is its concept for the mechanical-electrical energy conversion. Here, a gearbox consisting only of one planetary stage is used for the torque-speed transmission. An electrically excited synchronous generator, rotating at a medium pace, transfers the mechanical energy finally to electrical energy. This concept can be considered as a hybrid between the directly driven and the conventional gearbox drive trains.

Because main bearing, gearbox and generator are highly integrated (into each other and the machine housing), the turbine is relatively lightweight. It has been designed with a strong focus on offshore applications which is typical for a turbine of this size. Some public available information from [115] has been summarized below.

Turbine data

- variable-speed pitch-controlled 3-bladed wind turbine
- 5 MW rated power
- rotor speed range from 5.9 to 16.3 rpm with rated speed at 14.8 rpm
- gearbox transmission of 9.92
- overall efficiency at rated power 90.2

Geometrical data

- 116 m rotor diameter
- 102 m hub height
- tilt angle of 5 $^\circ$
- hub cone angle of 2 $^\circ$

Structural data

- blade mass: 16500 kg
- hub mass: 60100 kg
- nacelle mass: 200000 kg

C.2 Description of site and measurements

The prototype of the Multibrid M5000 wind turbine had been erected close to the town of Bremerhaven, Germany in December 2004. Since 2005 load and power measurements have been performed in several campaigns. Besides fulfilling certification requirements, the data is also used at the Endowed Chair of Wind Energy at the Universität Stuttgart for research purposes. Only a rough overview on the taken measurements is given here.

As it can be seen from Figure C.2, the prototype site is relatively flat. This is also reflected in the turbulence intensities of the measured data which are mostly in the region of 8 to 12 %. The annual average wind speed of the site is approximately 8 m/s with south-south-west as the main wind direction. Overall, the site characteristics seem to be typicall for a location in Germany close to the North Sea.

The meteorological conditions are measured with sensors installed on a separate met mast. It is located approximately 2.5 rotor diameters (about 290 m) south-west to the turbine (see Figure C.1). There are several anemometers and wind vanes installed at heights of 44m, 74m, and 102m above ground. A Thies 1st anemometer is used as a reference anemometer at hub height. Besides wind speed and direction, the atmospheric pressure, temperature and moisture are recorded as well.

Load data is measured with conventional strain gauges which have been installed at the turbine. From the monitored strains, the loads at several locations are derived. Among others these involve the

- blade bending moments in two directions at three blade sections, including the blade root
- tower top bending moments in two directions
- tower section bending moments at 29 m height above ground in two directions
- tower top torsional moments

Other load quantities, for example the thrust forces and the rotor torque, are calculated from these primary signals. In addition to the loads, the corresponding standard

signals of the wind turbine are also logged. Within this work, the tower top acceleration in lateral and longitudinal direction, generator speed, electrical power, pitch angle, wind direction and wind speed are mainly used. Loads and standard signals are recorded with a frequency of 50 Hz.

All measurements are classified with respect to the wind direction during the recording of the data. There are three categories:

- NOP1: Relatively undisturbed inflow to the turbine, with wind directions from 196° to 306°. Most of the measurements fall into this category, as this also corresponds to the main wind direction.
- NOP2: Wind directions from 10° to 55°. The met mast is in the wake of the turbine. Hence, the measured wind conditions are disturbed.
- NOP3: The prototype operates in the wake of other turbines (Vestas V39 and V44 turbines several hundred meters away) and some larger buildings.

Obviously, data from the first category is preferably used in general, because the inflow to the turbine is relatively well known from the meteorological met mast data and not disturbed by other turbines or buildings. Therefore, only this data is employed for load and performance validations (and consequently also within this work). In 2008, some other turbines (Repower 5M and Enercon E82) were erected close by, so that the size of sector NOP1 has been somewhat reduced.

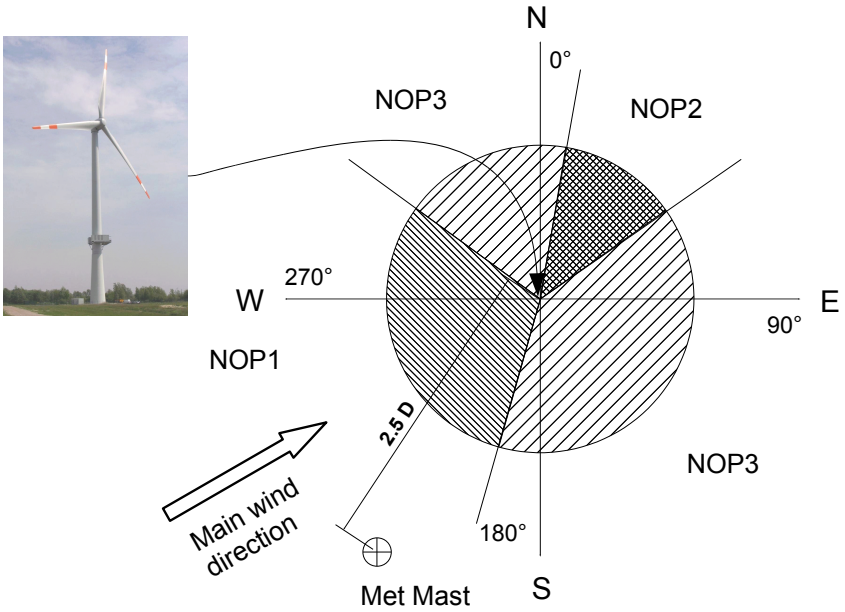

Figure C.1: Measurement categories and main wind direction

315° 0° 45°

45° 90° 135°

135° 180° 225°

225° 270° 315°

Figure C.2: View to the North, East, South and West from the top of the Multibrid M5000 prototype. Pictures taken by Andreas Rettenmeier (SWE).

D Nordex N80 turbines at EWTW

D.1 Turbine description

Nordex's N80 turbine is a typical example of a modern wind turbine. It features a classical distributed drive train with one main bearing, a gearbox and a double-fed asynchronous generator. Compared to its rotor radius the rated power of this turbine is relatively high and hence gives also a relatively large rating. This indicates its intended use for sites with high wind speeds.

Contrary to the Multibrid M5000, the turbine has already been built in large numbers during the past years. In autumn 2008, Nordex celebrated the production of the 1000th unit[1]. Some key figures of the turbine are summarised below [116, 117].

Turbine data

- variable-speed pitch-controlled 3-bladed wind turbine
- 2.5 MW rated power
- rotor speed range from 10.8 to 18.9 rpm
- gearbox transmission of 68.7
- double-fed asynchronous generator

Geometrical data

- 80 m rotor diameter
- 80 m hub height (of turbines at EWTW)

Structural data

- blade mass: 9000 kg
- hub mass: 25000 kg
- nacelle mass: 91000 kg

[1] This number also includes the N90 turbine type which is the 'low wind speed version' of the N80.

D.2 Description of EWTW and measurements

The ECN Wind turbine Test location at Wieringermeer (EWTW) is located in a flat, rural area in the north of the Netherlands, only a few hundred meters to the west of the IJsselmeer. It consists of nine wind turbines in total which are arranged in two rows with a distance of approximately 1.5 kilometres in between. The five Nordex N80 turbines form the northern row of the test site (see Figure D.1).

For the investigations within this work, only free stream conditions are considered. Therefore, only such data sets were employed where the mean wind direction was between 120 ° and 250 ° (from south-east to south-west). There are almost no obstacles in this directions except one smaller turbine approximately 11 D from the Nordex turbines as well as several farm houses and a couple of trees in about the same distance.

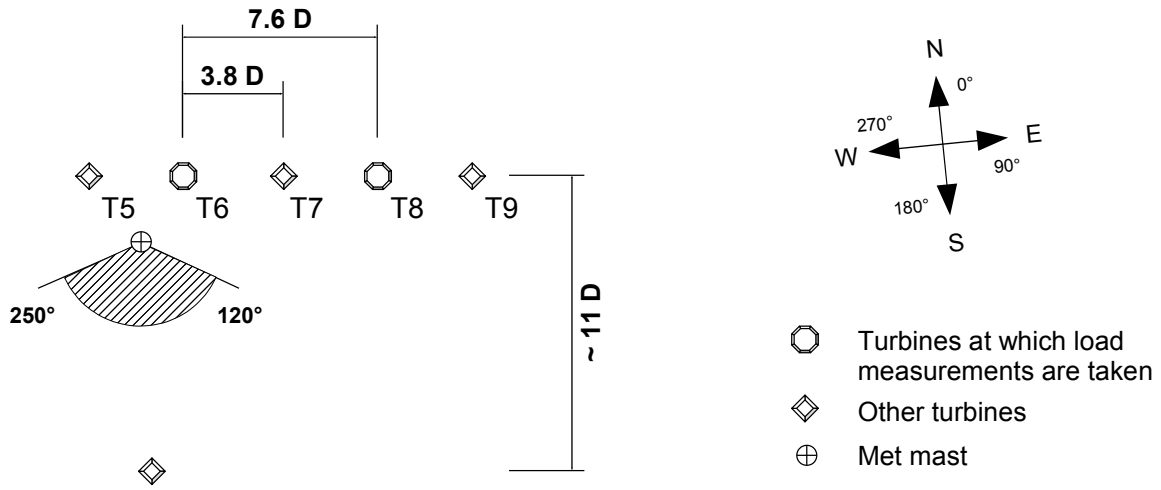

Figure D.1: Layout of the northern turbine row with Nordex N80 turbines at the EWTW

Wind measurements are taken at a met mast close to turbine T6. They consist of typical quantities like wind speeds and wind directions, recorded at two different heights above ground (52 m and 80 m). Loads are measured in high resolution at the turbines T6 and T8 from which the following quantities are used in this work:

- in-plane and out-of-plane blade root bending moments
- rotor thrust
- main shaft torque
- longitudinal tower base bending moment (fore-aft)

Of these signals, only the main shaft torque is measured directly. All other channels are computed by ECN using additional measured signals. The in-plane and out-of-plane blade root bending moments are based on two orthogonal measured bending

moments in the blade and the current pitch angle. These quantities and the rotor azimuth position are also used to calculate the rotor thrust force. Tower base bending moments are derived from orthogonal measurements at the tower base and the nacelle position.

Furthermore, several standard signals are recorded. Within this work, the following data is employed:

- generator rotational speed
- electrical power output
- pitch angle
- nacelle wind vane signal (yaw error)

In addition, the rotational acceleration of the generator, calculated as the derivative of the rotational speed signal, is also applied.

E Regression models for the NREL 1.5 MW WindPACT turbine

Based on the simulation results of the NREL 1.5MW wind turbine from Chapter 3, simple linear regression models have been derived. These are suited to describe the influence of a disturbance on equivalent loads and statistical parameters of standard signals. For each operational state (below rated, rated and above rated), separate regression models have been established which corresponds to fitting a straight line through the simulation results. The inclination of this line is given as a result and indicates, how much a load or a statistical parameter changes with respect to variations of the disturbance (see Figure E.1).

Table E.1 and E.2 list loads and parameters of standard signals derived from simulations of the baseline cases (compare Sections 3.1 and 3.2.1). These are averaged values from six simulations of 10 minute length with different stochastic wind fields. All equivalent loads are given for exponents of 6 and per unit hour of operation. A reference cycle number of 10^8 load cycles and a reference time of 175000 h has been used.

The inclinations of the regression lines are given in the tables following the baseline data. They indicate the change of the baseline values in percent with respect to a disturbance. Each disturbance has been added separately to the baseline configuration in the simulations. Hence, the given regression models can not be used to estimate combined effects from superimposed disturbances.

It should be noted, that in general loads and statistical parameters do not depend linearly on a disturbance. Nevertheless, if the variation of the disturbance is not too large, a linear approximation is acceptable in most cases. Because of the linearisation, results from the regression models may differ from those given in Chapter 3. The magnitude of the difference can serve as a measure for the adequacy of the linear approximation.

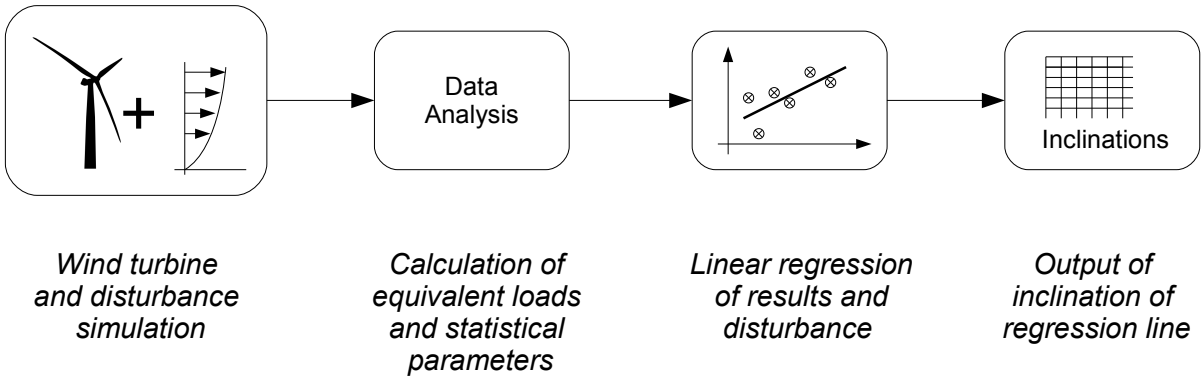

Figure E.1: Scheme for the analysis of loads and statistical parameters with respect to disturbances

Examples:

Reducing the baseline turbulence intensity by 5 % to 10 % lowers the mean value of the generated power at 6 m/s from 216 kW by -5 · 0.9 = -4.5 % to 206 kW, while at 12 m/s the power increases by -5 · -0.6 = 3.0 % to 1449 kW (compare Table E.2 and E.16).

In a similar manner, the tables in this annex can be used to estimate variations of equivalent loads due to changes in the environmental conditions. If the operation of a turbine within 20 years is thought to be concentrated at the operational states 6, 12 and 18 m/s with time shares of 85000, 55000 and 15000 hours, the equivalent load ranges of the rotor thrust are calculated from an inner product of vectors as:

$$\Delta S_{eq,Thrust,N_{ref},m} = (\vec{t} \cdot \vec{A})^{1/6} \quad \text{, with} \quad \vec{t} = \begin{bmatrix} 85000 \\ 55000 \\ 15000 \end{bmatrix} \qquad \vec{A} = \left(\begin{bmatrix} P_6 \\ P_{12} \\ P_{18} \end{bmatrix} \begin{bmatrix} 4.5 \\ 11 \\ 12 \end{bmatrix} \right)^6$$

For the baseline configuration the percental differences P_6, P_{12} and P_{18} are all 1 and the equivalent load ranges of the thrust compute to 72.3 kN. If the overall turbulence intensity at 6 m/s is increased by 5 % to 20 % and at 18 m/s decreased by -5 % to 10 %, the percental differences (see Table E.15) are P_6 = 1 - 5 % · 0.071, P_{12} = 1 and P_{18} = 1 + 5 % · 0.068. In this case the equivalent rotor thrust ranges yield 68.3 kN. Hence, the equivalent load ranges will be reduced by approximately -6 % in 20 years, if the turbulence intensity changes as assumed above.

Table E.1: Equivalent loads of the **baseline configuration** per unit hour of operation (N_{ref} = 10^8 and T_{ref}=175000 h). Values are given in units of kN and kNm.

Load	Equiv. range, m=6			Equiv. magnitude, p=6		
	6 m/s	12 m/s	18 m/s	6 m/s	12 m/s	18 m/s
M_{op}	44	118	162	76	169	110
M_{ip}	133	156	168	54	72	75
F_r	4.5	11	12	13	28	19
M_r	18	39	45	30	99	103
M_{tt}	39	111	172	95	82	100
M_{tb}	404	991	1075	806	2110	1520

Table E.2: Parameters of standard signals of the **baseline configuration**. Applied basic units are rpm, rpm/s, kW, ° and m/s

Signal	Below rated operation - 6 m/s						
	$\bar{X}$	$Var(X)$	γ_3	γ_4	λ_1	λ_2	ΔS_{max}
Ω_{gen}	1110	5210	1.4	5.1	330	260	360
$\dot{\Omega}_{gen}$	0.0	170	-0.1	3.8	1960	$3.3{\cdot}10^4$	120
P_{el}	216	7920	0.6	3.5	460	330	435
θ_P	0.0	0.0	0.0	0.0	0.0	0.0	0.0
$\ddot{y}_{tt}$	0.0	0.001	0.01	3.3	0.02	0.3	0.3
$\ddot{z}_{tt}$	0.0	0.003	0.02	3.1	0.02	0.3	0.3
Signal	Rated operation - 12 m/s						
Ω_{gen}	1780	3375	-1.3	5.9	685	2720	345
$\dot{\Omega}_{gen}$	0.0	2530	0.0	3.2	$4.2{\cdot}10^4$	$8.2{\cdot}10^5$	405
P_{el}	1407	$3.8{\cdot}10^4$	-2.1	6.2	3580	2935	790
θ_P	4.0	11.5	0.4	2.1	1.1	0.9	12.3
$\ddot{y}_{tt}$	0.0	0.02	0.001	3.0	0.3	7.9	1.0
$\ddot{z}_{tt}$	0.0	0.02	-0.004	3.2	0.2	2.8	1.2
Signal	Above rated operation - 18 m/s						
Ω_{gen}	1800	4380	-0.1	2.8	1660	6030	375
$\dot{\Omega}_{gen}$	0.0	5810	0.0	3.0	$9.7{\cdot}10^4$	$2.1{\cdot}10^6$	585
P_{el}	1500	173	0.1	3.1	375	4075	97
θ_P	16.3	10.9	-0.6	3.8	1.1	0.7	19
$\ddot{y}_{tt}$	0.0	0.04	-0.01	3.0	0.7	16.5	1.6
$\ddot{z}_{tt}$	0.0	0.06	0.001	3.0	0.5	7.9	1.7

Table E.3: Regression analysis: Variation of equivalent loads in percent per increase in the logarithmic of the **roughness length** of 1. Roughness length of 0.03, 0.07, 0.1, 0.2 and 0.3 m have been considered, with 0.1 m as baseline.

Load	Equiv. range, m=6			Equiv. magnitude, p=6		
	6 m/s	12 m/s	18 m/s	6 m/s	12 m/s	18 m/s
M_{op}	0.7	1.0	1.6	0.0	0.1	0.4
M_{ip}	0.0	0.2	0.5	0.0	0.1	0.3
F_r	0.1	0.1	0.1	-0.1	0.0	0.0
M_r	0.1	0.2	0.0	-0.1	0.0	0.0
M_{tt}	0.1	-0.1	0.2	-0.8	-2.3	-2.8
M_{tb}	0.1	-0.1	0.0	0.0	0.1	0.2

Table E.4: Regression analysis: Variation of statistical parameters of standard signals in percent per increase in the logarithmic of the **roughness length** of 1. Roughness length of 0.03, 0.07, 0.1, 0.2 and 0.3 m have been considered, with 0.1 m as baseline.

Signal	Below rated operation - 6 m/s						
	$\bar{X}$	$Var(X)$	γ_3	γ_4	λ_1	λ_2	ΔS_{max}
Ω_{gen}	0.0	-0.4	-0.3	-0.1	0.0	-0.3	-0.1
$\dot{\Omega}_{gen}$	0.0	-0.3	1.7	-0.9	-0.6	-0.6	-0.2
P_{el}	-0.1	-0.1	-0.4	-0.2	0.2	0.0	-0.1
θ_P	0.0	0.0	0.0	0.0	0.0	0.0	0.0
$\ddot{y}_{tt}$	0.0	0.9	57.0	-0.9	0.0	-0.2	1.0
$\ddot{z}_{tt}$	0.0	-0.2	11.0	-0.1	0.2	0.3	0.9
Signal	Rated operation - 12 m/s						
Ω_{gen}	0.0	0.6	-0.6	-0.6	0.2	0.2	-0.2
$\dot{\Omega}_{gen}$	0.0	0.3	7.7	-0.1	0.2	0.0	-0.7
P_{el}	0.0	0.5	-0.4	-0.7	0.2	-0.2	0.1
θ_P	-0.2	-0.1	1.3	0.2	0.0	0.6	0.0
$\ddot{y}_{tt}$	0.0	-0.1	-13.5	0.0	-0.4	-0.6	-2.2
$\ddot{z}_{tt}$	0.0	-0.1	-45.0	0.1	-0.1	0.0	0.3
Signal	Above rated operation - 18 m/s						
Ω_{gen}	0.0	-0.1	-0.1	0.0	-0.1	-0.1	0.0
$\dot{\Omega}_{gen}$	0.0	-0.1	0.5	0.0	-0.1	-0.1	0.4
P_{el}	0.0	-0.1	-0.6	0.0	-0.1	-0.1	-0.2
θ_P	0.0	0.1	0.2	0.2	0.1	0.1	0.2
$\ddot{y}_{tt}$	0.0	0.1	-15.4	0.0	0.1	0.0	0.6
$\ddot{z}_{tt}$	0.0	-0.1	15.3	0.0	-0.2	-0.2	0.2

Table E.5: Regression analysis: Variation of equivalent loads in percent per increase in the **vertical flow angle** of 1 degree. Flow angles of -10, -5 and 0 degrees have been considered, with 0 degree as baseline.

Load	Equiv. range, m=6			Equiv. magnitude, p=6		
	6 m/s	12 m/s	18 m/s	6 m/s	12 m/s	18 m/s
M_{op}	-0.5	-0.5	-0.1	-0.3	0.1	0.2
M_{ip}	0.0	-0.2	-1.0	0.0	-0.1	-0.7
F_r	-0.1	0.0	0.3	-0.2	0.1	0.2
M_r	0.0	0.4	0.0	-0.3	-0.1	0.0
M_{tt}	-0.1	-0.2	-0.1	0.5	1.0	-0.3
M_{tb}	-0.3	-0.1	-0.1	-0.3	0.1	0.2

Table E.6: Regression analysis: Variation of statistical parameters of standard signals in percent per increase in the **vertical flow angle** of 1 degree. Flow angles of -10, -5 and 0 degrees have been considered, with 0 degree as baseline.

Signal	Below rated operation - 6 m/s						
	$\bar{X}$	$Var(X)$	γ_3	γ_4	λ_1	λ_2	ΔS_{max}
Ω_{gen}	-0.1	-1.3	-0.1	0.3	-0.2	-0.1	-0.4
$\dot{\Omega}_{gen}$	0.0	-0.1	3.9	0.5	-0.4	-0.5	0.2
P_{el}	-0.6	-0.2	-0.5	-0.4	0.3	0.3	-0.2
θ_P	0.0	0.0	0.0	0.0	0.0	0.0	0.0
$\ddot{y}_{tt}$	0.0	0.8	7.4	0.0	-0.1	-0.3	0.3
$\ddot{z}_{tt}$	0.0	-0.2	4.6	-0.1	-0.3	-0.3	-0.6
Signal	Rated operation - 12 m/s						
Ω_{gen}	0.0	1.9	1.5	0.8	0.9	0.9	1.0
$\dot{\Omega}_{gen}$	0.0	0.7	2.8	0.0	0.6	0.4	0.4
P_{el}	-0.1	2.1	-1.5	-2.4	1.4	1.3	0.6
θ_P	-0.8	-0.5	5.0	0.3	-0.2	0.1	-0.3
$\ddot{y}_{tt}$	0.0	0.4	-4.6	0.0	0.3	0.2	-0.2
$\ddot{z}_{tt}$	0.0	0.0	-59.7	-0.1	-0.1	-0.2	-0.7
Signal	Above rated operation - 18 m/s						
Ω_{gen}	0.0	0.2	-0.4	0.0	0.1	0.1	0.1
$\dot{\Omega}_{gen}$	0.0	0.1	-1.1	-0.1	0.1	0.0	-0.4
P_{el}	0.0	0.0	-0.1	0.0	0.0	0.1	0.0
θ_P	-0.2	0.6	0.5	0.1	0.7	0.6	0.3
$\ddot{y}_{tt}$	0.0	-0.2	19.0	0.1	0.0	0.0	-0.1
$\ddot{z}_{tt}$	0.0	-0.3	-61.1	0.0	-0.3	-0.4	-0.2

Table E.7: Regression analysis: Variation of equivalent loads in percent per increase in the **vertical flow angle** of 1 degree. Flow angles of 0, 5 and 10 degrees have been considered, with 0 degree as baseline.

Load	Equiv. range, m=6			Equiv. magnitude, p=6		
	6 m/s	12 m/s	18 m/s	6 m/s	12 m/s	18 m/s
M_{op}	0.0	0.0	0.3	0.0	0.1	0.2
M_{ip}	0.0	-0.2	-0.8	0.0	-0.1	-0.6
F_r	-0.1	-0.1	0.3	0.0	0.1	0.1
M_r	0.0	0.2	0.0	0.0	0.0	0.0
M_{tt}	0.0	-0.1	0.0	0.4	1.1	-0.1
M_{tb}	-0.1	-0.1	-0.1	0.0	0.0	0.1

Table E.8: Regression analysis: Variation of statistical parameters of standard signals in percent per increase in the **vertical flow angle** of 1 degree. Flow angles of 0, 5 and 10 degrees have been considered, with 0 degree as baseline.

Signal	Below rated operation - 6 m/s						
	$\bar{X}$	$Var(X)$	γ_3	γ_4	λ_1	λ_2	ΔS_{max}
Ω_{gen}	0.0	-0.1	0.1	0.0	-0.3	0.3	-0.1
$\dot{\Omega}_{gen}$	0.0	0.2	-3.1	0.4	0.5	0.5	0.2
P_{el}	0.1	-0.3	0.2	0.0	-0.4	-0.6	-0.2
θ_P	0.0	0.0	0.0	0.0	0.0	0.0	0.0
$\ddot{y}_{tt}$	0.0	-0.1	-8.2	0.2	0.1	0.1	0.2
$\ddot{z}_{tt}$	0.0	0.0	-4.0	0.1	0.0	0.0	0.2
Signal	Rated operation - 12 m/s						
Ω_{gen}	0.0	-0.6	-0.4	-0.4	-0.2	0.3	-0.5
$\dot{\Omega}_{gen}$	0.0	0.4	-6.7	0.1	0.4	0.3	0.5
P_{el}	0.0	-0.2	-0.2	-0.3	0.0	0.4	-0.1
θ_P	-0.4	-0.7	2.2	0.4	-0.3	0.0	-0.3
$\ddot{y}_{tt}$	0.0	0.0	32.6	0.1	-0.1	-0.2	0.6
$\ddot{z}_{tt}$	0.0	0.0	-7.8	0.0	-0.1	-0.2	0.0
Signal	Above rated operation - 18 m/s						
Ω_{gen}	0.0	0.0	-0.2	0.0	0.0	0.1	0.0
$\dot{\Omega}_{gen}$	0.0	0.1	-5.1	0.0	0.1	0.0	0.0
P_{el}	0.0	0.0	-0.9	-0.1	0.0	0.1	0.0
θ_P	-0.2	0.3	0.1	0.0	0.5	0.4	0.2
$\ddot{y}_{tt}$	0.0	0.1	-2.7	0.0	0.2	0.2	-0.3
$\ddot{z}_{tt}$	0.0	-0.2	-51.2	0.1	-0.3	-0.3	0.2

Table E.9: Regression analysis: Variation of equivalent loads in percent per an increase in **yaw misalignment** of 1 degree. Misalignments of -10, -5 and 0 degree have been considered, with 0 degree as baseline.

Load	Equiv. range, m=6			Equiv. magnitude, p=6		
	6 m/s	12 m/s	18 m/s	6 m/s	12 m/s	18 m/s
M_{op}	-0.7	-0.7	0.4	0.0	-0.2	-0.2
M_{ip}	-0.1	-0.3	0.1	-0.1	0.2	0.0
F_r	0.2	0.2	-0.4	0.1	-0.1	-0.2
M_r	-0.1	-0.4	0.0	0.1	0.0	0.0
M_{tt}	0.0	-0.2	0.2	0.3	0.5	-1.6
M_{tb}	0.1	0.1	-0.7	0.1	-0.1	-0.1

Table E.10: Regression analysis: Variation of statistical parameters of standard signals in percent per an increase in **yaw misalignment** of 1 degree. Misalignments of -10, -5 and 0 degree have been considered, with 0 degree as baseline.

Signal	Below rated operation - 6 m/s						
	$\bar{X}$	$Var(X)$	γ_3	γ_4	λ_1	λ_2	ΔS_{max}
Ω_{gen}	0.0	0.6	0.3	0.2	0.1	-0.2	0.3
$\dot{\Omega}_{gen}$	0.0	-0.4	1.5	-0.7	-0.5	-0.4	-0.6
P_{el}	0.2	0.3	0.3	0.1	0.0	0.2	0.2
θ_P	0.0	0.0	0.0	0.0	0.0	0.0	0.0
$\ddot{y}_{tt}$	0.0	-0.2	-12.9	-0.1	-0.2	-0.2	0.1
$\ddot{z}_{tt}$	0.0	-0.2	7.6	0.0	-0.2	-0.1	-0.2
Signal	Rated operation (12 m/s)						
Ω_{gen}	0.0	-0.3	-0.3	0.0	-0.1	-0.5	-0.2
$\dot{\Omega}_{gen}$	0.0	-0.8	2.5	-0.4	-0.7	-0.6	-0.4
P_{el}	0.1	-0.6	0.5	0.7	-0.5	-1.1	-0.2
θ_P	0.5	0.8	-2.7	-0.3	0.4	-0.5	0.4
$\ddot{y}_{tt}$	0.0	0.2	-3.7	-0.2	0.0	0.0	-0.4
$\ddot{z}_{tt}$	0.0	-0.3	-39.4	0.0	-0.1	-0.1	0.3
Signal	Above rated operation - 18 m/s						
Ω_{gen}	0.0	0.1	-0.7	-0.1	0.0	0.1	-0.1
$\dot{\Omega}_{gen}$	0.0	0.1	8.6	0.0	0.0	0.0	-0.2
P_{el}	0.0	0.0	2.3	-0.1	0.1	0.1	-0.2
θ_P	0.2	-0.3	-0.6	-0.3	-0.5	-0.3	-0.2
$\ddot{y}_{tt}$	0.0	0.1	8.7	0.1	0.1	0.1	0.4
$\ddot{z}_{tt}$	0.0	-0.2	50.6	-0.1	-0.2	-0.3	-0.2

Table E.11: Regression analysis: Variation of equivalent loads in percent per an increase in **yaw misalignment** of 1 degree. Misalignments of 0, 5 and 10 degree have been considered, with 0 degree as baseline.

Load	Equiv. range, m=6			Equiv. magnitude, p=6		
	6 m/s	12 m/s	18 m/s	6 m/s	12 m/s	18 m/s
M_{op}	-0.2	-0.2	1.1	-0.1	0.0	0.2
M_{ip}	-0.1	-0.3	0.2	-0.1	-0.3	0.1
F_r	-0.1	0.0	0.3	0.1	0.0	0.0
M_r	0.1	0.5	-0.1	-0.1	0.0	0.0
M_{tt}	0.0	0.0	0.3	0.4	0.5	-1.2
M_{tb}	-0.2	0.0	0.0	-0.2	0.0	0.1

Table E.12: Regression analysis: Variation of statistical parameters of standard signals in percent per an increase in **yaw misalignment** of 1 degree. Misalignments of 0, 5 and 10 degree have been considered, with 0 degree as baseline.

Signal	Below rated operation - 6 m/s						
	$\bar{X}$	$Var(X)$	γ_3	γ_4	λ_1	λ_2	ΔS_{max}
Ω_{gen}	0.0	-0.6	0.1	0.2	-0.3	-0.3	-0.2
$\dot{\Omega}_{gen}$	0.0	-0.1	-5.4	0.2	-0.2	-0.2	0.2
P_{el}	-0.2	-0.3	-0.1	-0.2	-0.2	-0.2	-0.2
θ_P	0.0	0.0	0.0	0.0	0.0	0.0	0.0
$\ddot{y}_{tt}$	0.0	-0.6	-0.8	-0.2	-0.2	-0.1	-0.5
$\ddot{z}_{tt}$	0.0	-0.2	-2.7	0.0	-0.2	-0.3	0.1
Signal	Rated operation (12 m/s)						
Ω_{gen}	0.0	0.5	-0.1	0.1	0.5	1.0	0.1
$\dot{\Omega}_{gen}$	0.0	1.2	-1.1	0.8	1.1	0.8	1.3
P_{el}	-0.1	0.7	-0.6	-0.8	0.8	1.6	0.1
θ_P	-0.5	-0.6	3.4	0.7	-0.4	0.0	-0.2
$\ddot{y}_{tt}$	0.0	0.8	-2.6	0.1	0.3	0.1	0.7
$\ddot{z}_{tt}$	0.0	0.3	61.6	0.4	0.0	-0.1	1.1
Signal	Above rated operation - 18 m/s						
Ω_{gen}	0.0	-0.1	-2.8	0.0	-0.1	-0.1	-0.1
$\dot{\Omega}_{gen}$	0.9	-0.1	1.4	0.0	-0.1	-0.2	0.0
P_{el}	0.0	-0.1	1.5	0.0	-0.1	-0.1	-0.2
θ_P	-0.2	0.1	-0.1	-0.1	0.2	0.4	0.2
$\ddot{y}_{tt}$	0.0	0.1	-6.4	-0.1	0.1	0.1	0.3
$\ddot{z}_{tt}$	0.0	-0.1	-146.1	0.1	-0.2	-0.3	0.4

Table E.13: Regression analysis: Variation of equivalent loads in percent per increase in **air density** of 0.01 kg/m^3. Densities of 1.165, 1.195, 1.225, 1.258 and 1.293 kg/m^3 have been considered, with 1.225 kg/m^3 as baseline.

Load	Equiv. range, m=6			Equiv. magnitude, p=6		
	6 m/s	12 m/s	18 m/s	6 m/s	12 m/s	18 m/s
M_{op}	0.9	0.5	0.6	0.9	0.2	0.0
M_{ip}	0.0	0.0	0.2	0.1	0.0	0.0
F_r	1.1	0.7	0.1	0.7	0.1	0.0
M_r	0.3	-0.3	0.4	0.6	0.1	0.0
M_{tt}	0.6	0.6	0.7	-0.1	0.8	0.2
M_{tb}	1.2	0.7	0.3	1.1	0.2	0.1

Table E.14: Regression analysis: Variation of statistical parameters of standard signals in percent per increase in **air density** of 0.01 kg/m^3. Densities of 1.165, 1.195, 1.225, 1.258 and 1.293 kg/m^3 have been considered, with 1.225 kg/m^3 as baseline.

Signal	Below rated operation - 6 m/s						
	$\bar{X}$	$Var(X)$	γ_3	γ_4	λ_1	λ_2	ΔS_{max}
Ω_{gen}	0.1	2.9	0.5	-0.3	1.0	1.4	1.1
$\dot{\Omega}_{gen}$	0.0	1.1	-3.6	-0.5	1.8	2.0	0.1
P_{el}	0.9	1.3	1.1	0.7	0.2	0.1	0.8
θ_P	0.0	0.0	0.0	0.0	0.0	0.0	0.0
$\ddot{y}_{tt}$	0.0	0.7	18.3	0.2	1.3	1.5	0.6
$\ddot{z}_{tt}$	0.0	1.3	-3.8	0.0	1.4	1.4	0.8
Signal	Rated operation - 12 m/s						
Ω_{gen}	0.0	-2.3	-1.3	-0.5	-0.9	-0.8	-0.9
$\dot{\Omega}_{gen}$	0.0	-0.8	2.5	0.0	-0.5	-0.2	-0.3
P_{el}	0.2	-2.7	2.1	3.1	-2.0	-2.3	-0.7
θ_P	1.4	1.1	-9.4	-1.0	0.4	-0.1	0.5
$\ddot{y}_{tt}$	0.0	0.4	-12.1	-0.2	0.5	0.6	0.0
$\ddot{z}_{tt}$	0.0	0.6	32.5	0.0	0.9	1.0	0.2
Signal	Above rated operation - 18 m/s						
Ω_{gen}	0.0	-0.5	0.8	0.1	-0.1	0.7	-0.1
$\dot{\Omega}_{gen}$	0.0	0.8	5.5	0.2	0.9	1.0	0.3
P_{el}	0.0	0.1	0.5	0.0	0.7	0.8	0.0
θ_P	0.3	-1.1	-0.7	-0.2	-1.2	-0.7	-0.6
$\ddot{y}_{tt}$	0.0	1.5	-13.1	-0.1	1.2	1.2	0.9
$\ddot{z}_{tt}$	0.0	0.9	134.4	-0.1	1.0	1.1	0.4

Table E.15: Regression analysis: Variation of equivalent loads in percent per one percent increase of the **overall turbulence intensity**. Turbulence intensities of 5, 10 15, 20 and 25 % have been considered, with 15 % as baseline.

Load	Equiv. range, m=6			Equiv. magnitude, p=6		
	6 m/s	12 m/s	18 m/s	6 m/s	12 m/s	18 m/s
M_{op}	6.0	4.9	5.8	1.3	-0.1	2.4
M_{ip}	0.3	0.8	1.7	0.1	0.1	0.7
F_r	7.1	4.6	6.8	0.9	-0.4	0.9
M_r	6.3	4.2	6.8	1.6	-0.2	0.2
M_{tt}	5.9	5.8	6.3	0.3	2.7	3.3
M_{tb}	7.3	4.9	7.3	1.8	-0.4	1.3

Table E.16: Regression analysis: Variation of statistical parameters of standard signals in percent per one percent increase of the **overall turbulence intensity**. Turbulence intensities of 5, 10, 15, 20 and 25 % have been considered, with 15 % as baseline.

Signal	Below rated operation - 6 m/s						
	$\bar{X}$	$Var(X)$	γ_3	γ_4	λ_1	λ_2	ΔS_{max}
Ω_{gen}	0.3	16.2	4.8	0.9	12.6	14.8	7.3
$\dot{\Omega}_{gen}$	0.0	14.0	-1.8	1.5	15.9	16.2	8.2
P_{el}	0.9	13.9	20.8	1.3	11.7	11.0	7.0
θ_P	0.0	0.0	0.0	0.0	0.0	0.0	0.0
$\ddot{y}_{tt}$	0.0	13.7	-40.8	0.8	15.5	16.4	7.3
$\ddot{z}_{tt}$	0.0	12.5	-21.5	0.0	12.8	13.1	6.7
Signal	Rated operation - 12 m/s						
Ω_{gen}	-0.1	22.6	0.8	-0.2	15.0	9.3	8.2
$\dot{\Omega}_{gen}$	0.0	9.4	7.8	-3.7	9.7	10.6	3.4
P_{el}	-0.6	11.6	-5.9	-13.9	10.4	10.5	5.4
θ_P	1.3	7.6	9.3	-0.5	8.7	8.1	3.6
$\ddot{y}_{tt}$	0.0	11.4	9.0	-0.8	11.1	11.2	5.3
$\ddot{z}_{tt}$	0.0	11.5	162.3	-0.4	12.5	13.0	5.5
Signal	Above rated operation - 18 m/s						
Ω_{gen}	0.0	11.6	-4.2	-0.5	12.7	14.2	6.0
$\dot{\Omega}_{gen}$	0.0	14.3	5.7	-0.1	14.2	13.8	6.8
P_{el}	0.0	145.4	-377.2	74.2	24.9	14.5	33.2
θ_P	-0.1	13.7	4.8	0.8	14.9	15.1	5.8
$\ddot{y}_{tt}$	0.0	14.2	7.9	0.2	13.9	13.9	6.9
$\ddot{z}_{tt}$	0.0	13.2	-314.5	0.2	13.2	13.3	7.1

Table E.17: Regression analysis: Variation of equivalent loads in percent per 0.1 increase of the **lateral turbulence ratio**. Lateral turbulence ratios of 0.6, 0.7, 0.8, 0.9 and 1.0 have been considered, with 0.8 as baseline.

Load	Equiv. range, m=6			Equiv. magnitude, p=6		
	6 m/s	12 m/s	18 m/s	6 m/s	12 m/s	18 m/s
M_{op}	0.3	0.5	0.5	0.2	0.0	0.0
M_{ip}	0.0	0.1	0.1	0.0	0.0	0.0
F_r	0.2	0.3	0.3	0.1	0.0	0.0
M_r	0.0	-0.3	0.4	0.2	0.0	0.0
M_{tt}	0.3	0.3	0.7	0.0	0.0	0.0
M_{tb}	0.1	0.3	0.3	0.2	0.0	0.0

Table E.18: Regression analysis: Variation of statistical parameters of standard signals in percent per 0.1 increase of the **lateral turbulence ratio**. Lateral turbulence ratios of 0.6, 0.7, 0.8, 0.9 and 1.0 have been considered, with 0.8 as baseline.

Signal	Below rated operation - 6 m/s						
	$\bar{X}$	$Var(X)$	γ_3	γ_4	λ_1	λ_2	ΔS_{max}
Ω_{gen}	0.0	0.7	0.4	-0.1	-0.2	0.4	0.2
$\dot{\Omega}_{gen}$	0.0	0.2	3.3	0.3	0.8	0.9	0.5
P_{el}	0.4	0.1	0.5	0.2	-0.4	0.4	0.1
θ_P	0.0	0.0	0.0	0.0	0.0	0.0	0.0
$\ddot{y}_{tt}$	0.0	1.4	5.5	0.1	0.5	0.4	0.4
$\ddot{z}_{tt}$	0.0	0.5	-1.0	0.3	0.8	0.9	-0.1
Signal	Rated operation - 12 m/s						
Ω_{gen}	0.0	-1.4	-0.3	0.2	-0.5	-0.1	-0.1
$\dot{\Omega}_{gen}$	-8.9	0.0	-2.0	0.4	0.1	0.2	1.0
P_{el}	0.1	-1.2	0.7	1.0	-0.8	-0.4	-0.3
θ_P	0.2	0.0	-1.4	-0.1	0.0	-0.7	0.1
$\ddot{y}_{tt}$	4.9	3.1	28.0	-0.2	1.0	0.9	1.6
$\ddot{z}_{tt}$	11.9	0.0	71.1	0.1	0.0	0.0	-0.6
Signal	Above rated operation - 18 m/s						
Ω_{gen}	0.0	0.0	-0.2	0.1	0.3	0.9	-0.1
$\dot{\Omega}_{gen}$	1.7	0.9	7.6	0.0	0.9	0.8	-0.4
P_{el}	0.0	0.3	-2.5	0.0	0.8	0.9	0.3
θ_P	0.0	-0.2	-0.2	-0.1	-0.1	0.0	0.0
$\ddot{y}_{tt}$	-173.8	5.2	-0.5	-0.2	1.4	0.7	2.7
$\ddot{z}_{tt}$	3.4	0.6	26.9	0.1	0.7	0.7	0.7

Table E.19: Regression analysis: Variation of equivalent loads in percent per 0.1 increase of the **vertical turbulence ratio**. Vertical turbulence ratios of 0.3, 0.4, 0.5, 0.6 and 0.7 have been considered, with 0.5 as baseline.

Load	Equiv. range, m=6			Equiv. magnitude, p=6		
	6 m/s	12 m/s	18 m/s	6 m/s	12 m/s	18 m/s
M_{op}	0.2	0.1	0.2	0.1	0.0	0.0
M_{ip}	0.0	0.1	0.2	0.0	0.0	0.1
F_r	0.1	0.0	0.3	0.1	0.0	0.0
M_r	0.1	-0.2	0.5	0.1	0.0	0.0
M_{tt}	0.2	0.3	0.1	0.0	0.0	0.1
M_{tb}	0.0	0.2	0.4	0.1	0.0	0.0

Table E.20: Regression analysis: Variation of statistical parameters of standard signals in percent per 0.1 increase of the **vertical turbulence ratio**. Vertical turbulence ratios of 0.3, 0.4, 0.5, 0.6 and 0.7 have been considered, with 0.5 as baseline.

Signal	Below rated operation - 6 m/s						
	$\bar{X}$	$Var(X)$	γ_3	γ_4	λ_1	λ_2	ΔS_{max}
Ω_{gen}	0.0	0.3	0.2	0.0	-0.2	0.3	0.1
$\dot{\Omega}_{gen}$	0.0	0.4	-8.9	0.2	1.0	1.2	1.0
P_{el}	0.2	0.0	0.3	0.2	-0.3	0.2	0.0
θ_P	0.0	0.0	0.0	0.0	0.0	0.0	0.0
$\ddot{y}_{tt}$	0.0	-0.6	43.3	0.2	0.7	1.0	-1.1
$\ddot{z}_{tt}$	0.0	0.6	-8.1	0.3	1.0	1.2	0.2
Signal	Rated operation - 12 m/s						
Ω_{gen}	0.0	-0.8	-0.1	0.3	-0.1	0.3	0.1
$\dot{\Omega}_{gen}$	0.0	0.4	2.3	-0.5	0.5	0.7	-0.8
P_{el}	0.0	-0.7	0.4	0.6	-0.3	0.1	-0.1
θ_P	0.1	-0.1	-0.8	0.0	0.2	-0.1	0.0
$\ddot{y}_{tt}$	0.0	0.6	13.4	-0.3	0.8	0.9	0.9
$\ddot{z}_{tt}$	0.0	0.5	49.2	-0.2	0.8	0.9	0.0
Signal	Above rated operation - 18 m/s						
Ω_{gen}	0.0	0.0	1.7	0.2	0.4	1.0	0.1
$\dot{\Omega}_{gen}$	0.0	1.1	5.6	-0.1	1.2	1.3	0.2
P_{el}	0.0	0.4	-3.4	0.0	0.9	1.1	0.3
θ_P	0.0	0.0	0.2	0.3	0.2	0.3	0.2
$\ddot{y}_{tt}$	0.0	0.9	15.0	0.1	1.0	1.1	-0.3
$\ddot{z}_{tt}$	0.0	0.6	-21.0	-0.1	0.7	0.7	-0.2

Table E.21: Regression analysis: Variation of equivalent loads in percent per 100 m increase of the **integral length scale** of longitudinal turbulence. Length scales of 170, 255, 340, 510 and 680 m have been considered, with 340 m as baseline.

Load	Equiv. range, m=6			Equiv. magnitude, p=6		
	6 m/s	12 m/s	18 m/s	6 m/s	12 m/s	18 m/s
M_{op}	-0.6	-2.4	-2.1	0.4	-0.3	0.0
M_{ip}	-0.2	-0.6	-0.8	0.0	-0.2	-0.3
F_r	0.4	-2.9	-3.1	0.4	-0.2	0.1
M_r	-0.6	-1.9	-5.7	0.5	-0.2	-0.2
M_{tt}	-2.4	-3.4	-3.2	-0.1	-0.7	-1.1
M_{tb}	0.0	-3.7	-5.4	0.7	-0.3	-0.3

Table E.22: Regression analysis: Variation of statistical parameters of standard signals in percent per 100 m increase of the **integral length scale** of longitudinal turbulence. Length scales of 170, 255, 340, 510 and 680 m have been considered, with 340 m as baseline.

Signal	Below rated operation - 6 m/s						
	$\bar{X}$	$Var(X)$	γ_3	γ_4	λ_1	λ_2	ΔS_{max}
Ω_{gen}	0.0	0.5	0.3	0.0	-0.2	-0.5	0.1
$\dot{\Omega}_{gen}$	0.0	-0.9	0.9	0.0	-1.1	-1.1	-0.5
P_{el}	0.0	0.5	0.8	0.1	-0.2	0.2	0.1
θ_P	0.0	0.0	0.0	0.0	0.0	0.0	0.0
$\ddot{y}_{tt}$	0.0	-1.0	1.8	0.1	-1.1	-1.1	-0.4
$\ddot{z}_{tt}$	0.0	-0.7	-0.4	0.0	-0.8	-0.8	-0.4
Signal	Rated operation - 12 m/s						
Ω_{gen}	0.0	0.6	1.0	0.6	-0.6	-1.0	0.2
$\dot{\Omega}_{gen}$	0.0	-1.0	-0.7	0.2	-1.1	-1.1	-0.4
P_{el}	0.0	0.7	-0.3	-0.4	-0.1	-0.5	0.2
θ_P	0.0	0.2	0.2	0.0	-0.6	-0.2	0.1
$\ddot{y}_{tt}$	0.0	-1.2	1.6	0.0	-1.1	-1.1	-0.6
$\ddot{z}_{tt}$	0.0	-1.0	-2.3	0.0	-1.0	-1.1	-0.5
Signal	Above rated operation - 18 m/s						
Ω_{gen}	0.0	-0.6	1.2	0.1	-0.9	-1.1	-0.3
$\dot{\Omega}_{gen}$	0.0	-1.1	0.0	0.0	-1.2	-1.2	-0.6
P_{el}	0.0	-1.0	-3.5	0.3	-1.1	-1.1	-0.4
θ_P	0.0	0.7	0.3	0.0	-0.3	-0.5	0.2
$\ddot{y}_{tt}$	0.0	-1.2	-0.9	0.0	-1.2	-1.2	-0.6
$\ddot{z}_{tt}$	0.0	-1.1	2.2	0.0	-1.1	-1.2	-0.6

Table E.23: Regression analysis: Variation of equivalent loads in percent per reduction in the **spatial coherence decay factor** of 1. Spatial coherence decay factors of 8.8, 10.4, 12.0, 13.6 and 15.2 have been considered, with 12.0 as baseline.

Load	Equiv. range, m=6			Equiv. magnitude, p=6		
	6 m/s	12 m/s	18 m/s	6 m/s	12 m/s	18 m/s
M_{op}	-0.5	-0.3	0.0	-0.3	0.1	-0.3
M_{ip}	0.0	0.2	0.3	0.0	0.1	0.1
F_r	-2.0	-1.5	-1.9	-0.2	0.0	-0.4
M_r	-1.4	-0.6	0.9	-0.3	0.1	0.0
M_{tt}	0.9	0.7	0.6	0.1	0.4	0.5
M_{tb}	-2.4	-2.8	-4.5	-0.4	-0.1	-0.9

Table E.24: Regression analysis: Variation of statistical parameters of standard signals in percent per reduction in the **spatial coherence decay factor** of 1. Spatial coherence decay factors of 8.8, 10.4, 12.0, 13.6 and 15.2 have been considered, with 12.0 as baseline.

Signal	Below rated operation - 6 m/s						
	$\bar{X}$	$Var(X)$	γ_3	γ_4	λ_1	λ_2	ΔS_{max}
Ω_{gen}	-0.1	-3.6	1.3	0.7	-5.9	-2.8	-2.3
$\dot{\Omega}_{gen}$	0.0	0.0	-8.9	3.2	2.8	2.9	2.0
P_{el}	-0.1	-3.7	1.4	-0.3	-5.8	-4.3	-2.5
θ_P	0.0	0.0	0.0	0.0	0.0	0.0	0.0
$\ddot{y}_{tt}$	0.0	0.6	28.7	0.5	2.3	2.5	0.1
$\ddot{z}_{tt}$	0.0	3.0	-6.1	0.2	4.2	4.7	1.4
Signal	Rated operation - 12 m/s						
Ω_{gen}	0.0	-6.4	-0.3	-0.2	-6.0	-0.5	-2.8
$\dot{\Omega}_{gen}$	0.0	-0.3	-11.1	-0.5	1.1	2.1	-0.3
P_{el}	0.1	-2.8	0.6	0.7	-3.7	-1.5	-1.6
θ_P	-0.1	-1.6	-2.8	-0.3	-5.1	-3.2	-0.8
$\ddot{y}_{tt}$	0.0	2.5	-4.3	0.2	4.3	5.1	2.0
$\ddot{z}_{tt}$	0.0	-0.9	-52.9	-1.2	2.0	3.0	-1.4
Signal	Above rated operation - 18 m/s						
Ω_{gen}	0.0	-5.1	8.7	0.3	-5.3	1.8	-2.4
$\dot{\Omega}_{gen}$	0.0	2.0	-14.4	0.1	3.7	4.1	0.9
P_{el}	0.0	-7.6	-12.5	-0.6	-0.6	3.0	-4.0
θ_P	0.1	-2.8	-0.7	-0.1	-5.6	-5.6	-1.6
$\ddot{y}_{tt}$	0.0	0.0	15.4	0.5	3.5	4.2	0.2
$\ddot{z}_{tt}$	0.0	-1.5	-63.0	0.0	1.9	3.0	-1.4

Table E.25: Regression analysis: Variation of equivalent loads in percent per increase in **rotor mass imbalance**, corresponding to an increase of mass of one blade by 1 %. Blade mass increases of 0, 0.375, 0.7, 1.125 and 1.5 % have been considered, with 0 % as baseline.

Load	Equiv. range, m=6			Equiv. magnitude, p=6		
	6 m/s	12 m/s	18 m/s	6 m/s	12 m/s	18 m/s
M_{op}	-0.1	0.3	0.2	0.0	0.0	-0.1
M_{ip}	0.7	1.0	1.1	0.7	0.5	0.5
F_r	0.0	1.0	0.2	0.0	0.0	0.1
M_r	0.3	0.2	0.3	0.0	0.0	0.0
M_{tt}	0.3	0.2	0.2	0.2	0.3	0.2
M_{tb}	0.1	7.0	1.9	0.0	0.5	0.3

Table E.26: Regression analysis: Variation of statistical parameters of standard signals in percent per increase in **rotor mass imbalance**, corresponding to an increase of mass of one blade by 1 %. Blade mass increases of 0, 0.375, 0.7, 1.125 and 1.5 % have been considered, with 0 % as baseline.

Signal	Below rated operation - 6 m/s						
	$\bar{X}$	$Var(X)$	γ_3	γ_4	λ_1	λ_2	ΔS_{max}
Ω_{gen}	0.0	0.0	-0.1	-0.1	0.2	0.3	0.0
$\dot{\Omega}_{gen}$	0.0	0.8	-1.8	-0.3	0.1	0.0	1.3
P_{el}	0.0	0.0	-0.2	0.0	0.0	-0.2	-0.1
θ_P	0.0	0.0	0.0	0.0	0.0	0.0	0.0
$\ddot{y}_{tt}$	0.0	1.0	28.3	1.2	0.3	0.2	2.1
$\ddot{z}_{tt}$	0.0	0.0	0.2	0.0	0.0	-0.1	0.3
Signal	Rated operation - 12 m/s						
Ω_{gen}	0.0	0.1	-2.0	-1.7	1.4	2.2	-1.2
$\dot{\Omega}_{gen}$	0.0	2.6	-12.6	1.1	1.8	1.3	2.1
P_{el}	0.0	0.0	-0.1	-0.2	0.3	1.7	0.0
θ_P	0.0	-0.1	0.4	0.2	1.0	5.8	0.2
$\ddot{y}_{tt}$	0.0	206.7	-76.5	-4.7	25.4	2.5	57.4
$\ddot{z}_{tt}$	0.0	23.4	129.0	-1.5	6.2	1.6	10.1
Signal	Above rated operation - 18 m/s						
Ω_{gen}	0.0	0.0	-0.9	0.1	0.6	0.7	0.8
$\dot{\Omega}_{gen}$	0.0	0.6	-2.3	0.1	0.2	0.0	0.5
P_{el}	0.0	1.5	-17.1	0.1	1.7	0.6	1.4
θ_P	0.0	0.0	0.0	0.0	0.2	0.7	0.2
$\ddot{y}_{tt}$	0.0	122.0	-61.2	-5.0	17.5	1.3	32.2
$\ddot{z}_{tt}$	0.0	2.8	-204.8	-0.1	0.6	0.0	2.2

Table E.27: Regression analysis: Variation of equivalent loads in percent with increasing **aerodynamic rotor imbalance**, corresponding to a pitch angle offset of 0.1 degree at one blade. Offsets of 0.0, 0.25, 0.50, 0.75 and 1.0 degree have been considered, with 0 degree as baseline.

Load	Equiv. range, m=6			Equiv. magnitude, p=6		
	6 m/s	12 m/s	18 m/s	6 m/s	12 m/s	18 m/s
M_{op}	-0.3	-0.1	0.3	-0.8	-0.7	-0.8
M_{ip}	0.0	-0.1	0.0	-0.1	-0.3	-0.5
F_r	-0.1	0.0	0.3	-0.2	-0.1	0.0
M_r	0.2	0.2	0.1	0.0	0.0	0.0
M_{tt}	1.8	1.5	0.9	0.1	0.4	0.3
M_{tb}	0.1	1.2	1.4	-0.2	0.0	0.2

Table E.28: Variation of statistical parameters of standard signals in percent with increasing **aerodynamic rotor imbalance**, corresponding to a pitch angle offset of 0.1 degree at one blade. Offsets of 0.0, 0.25, 0.50, 0.75 and 1.0 degree have been considered, with 0 degree as baseline.

Signal	Below rated operation - 6 m/s						
	$\bar{X}$	$Var(X)$	γ_3	γ_4	λ_1	λ_2	ΔS_{max}
Ω_{gen}	0.0	-0.2	-0.1	0.0	-0.1	0.0	-0.1
$\dot{\Omega}_{gen}$	0.0	-0.1	-2.6	0.2	-0.1	0.0	0.1
P_{el}	0.0	-0.1	-0.1	-0.1	-0.1	-0.2	-0.1
θ_P	0.0	0.0	0.0	0.0	0.0	0.0	0.0
$\ddot{y}_{tt}$	0.0	0.3	2.8	-0.2	0.0	0.0	-0.3
$\ddot{z}_{tt}$	0.0	0.1	-3.6	0.0	0.0	-0.1	0.3
Signal	Rated operation - 12 m/s						
Ω_{gen}	0.0	-0.1	0.2	0.1	-0.2	-0.2	-0.2
$\dot{\Omega}_{gen}$	0.0	0.1	-3.8	0.1	0.0	0.0	0.0
P_{el}	0.0	0.2	-0.2	-0.3	0.2	0.2	0.0
θ_P	0.0	-0.7	1.7	0.3	-0.4	0.3	-0.3
$\ddot{y}_{tt}$	0.0	4.9	7.4	-0.1	0.5	-0.1	2.2
$\ddot{z}_{tt}$	0.0	4.6	-5.2	-0.8	1.0	0.0	1.5
Signal	Above rated operation - 18 m/s						
Ω_{gen}	0.0	-0.3	0.4	0.0	-0.1	0.1	-0.1
$\dot{\Omega}_{gen}$	0.0	0.1	-1.6	0.0	0.1	0.1	0.1
P_{el}	0.0	0.0	-1.1	-0.1	0.2	0.1	0.0
θ_P	0.0	0.0	-0.1	0.0	0.0	0.2	0.0
$\ddot{y}_{tt}$	0.0	10.3	0.7	-0.6	1.5	0.2	3.2
$\ddot{z}_{tt}$	0.0	2.7	35.1	-0.1	0.6	0.1	1.2

F Estimation of spectral moments

Spectral moments are quantities related to the frequency content of a signal. Similar to the central moments in the time domain, the spectral moments are basic parameters to characterise the distribution of a signal's oscillations in the frequency domain.

For Gaussian processes, some spectral moments can be related directly to time domain characteristics, such as the variance of the process and its derivatives. This approach is for example used in offshore engineering [118, 119], where the moments are often estimated from variance, the mean period of zero up-crossings and the mean period of crests. However, in other disciplines they are more commonly calculated from an estimation of the power spectral density (PSD) representation of a signal. Hence, the density distribution has to be derived prior to the calculation of the moments. Many different techniques are available for this task. A comprehensive summary by Kay and Marple can for example be found in [87].

In this work, spectral moments are applied quite often. When computed from standard signals, they serve for example as inputs to neural networks in the estimation procedure, but moments from load signals are also applied at investigations related to the calculation of fatigue loads in the frequency domain. Therefore, several approaches have been compared in order to find the most suitable method for their calculation. Besides three PSD based approaches (the *periodogram method*, the *correlation method* and the *maximum entropy method*) a *series expansion* derived by Holm [120] has also been tested. This expansion allows for the direct estimation of spectral moments from the autocorrelation function without the preceding calculation of the PSD.

F.1 Periodogram and correlation methods

These two techniques are both based on Fourier transformation. Unfortunately, the Fourier transformation itself is not a consistent estimator of the PSD. As a consequence, estimations of the PSD from a Fourier transformation always tend to have a high variance which does not reduce even if the length of the input time series is increased.

To improve the quality of the estimates, averaging is applied (compare Figure F.1).

In the case of the periodogram, a time series is segmented into several (often overlapping) parts. Each segment is transferred into the frequency domain by a windowed Fourier transformation. The PSD finally computes as the average of several squared frequency spectra.

The correlation method exploits the fact that the autocorrelation function and the power spectrum are Fourier transform pairs. First, several estimates of the autocorrelation function from overlapping segments of a time series are calculated. The autocorrelation functions are then averaged in a second step and transferred into the frequency domain to yield a consistent estimation of the PSD.

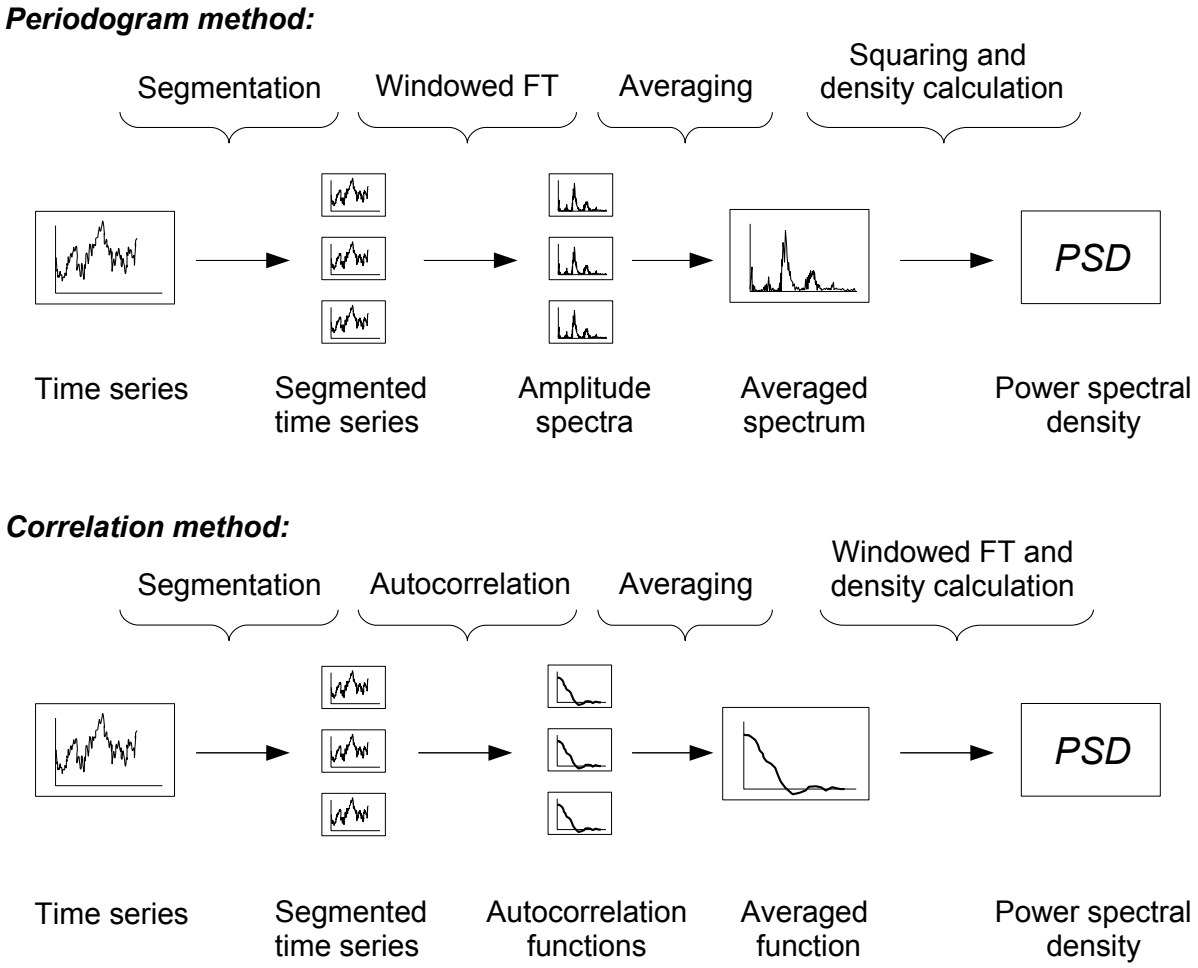

Figure F.1: Schematic of periodogram and correlation methods for power spectral density estimations

Both approaches are relatively easy to implement and therefore widely used. Nevertheless, they also have some disadvantages. First, they utilise segmented time series to derive consistent estimates. For a reasonable choice of the length of these segments, a priori knowledge of the frequency content of the signal has to be available. This is because the segment length influences the frequency resolution. Therefore, it

should be chosen long enough to get sufficient resolution, but at the same time still yield a reasonable number of segments for the averaging.

Second, both suffer from the common problems of the Fourier transformation when broad-banded data of finite length is processed. In such cases, the so-called windowing technique has to be applied, where a window function is added to the process either by multiplication in the time domain or by convolution in the frequency domain. Although windowing helps to improve results from a Fourier transformation of finite data, the method itself introduces some unwanted effects, such as leakage. These effects are discussed in many text books on frequency domain methods and no attempt is made to summarize them here. However, it should be pointed out, that one of the main differences of the periodogram and correlation method lies in the impact of the window function on the results: In the case of the correlation method, the windowing is applied relatively late in the process and the introduced effects on the PSD correspond exactly to what is known from a windowed Fourier transformation. For the periodogram, the resulting frequency spectrum has to be squared in order to yield the PSD and hence also the windowing effects on the PSD are squared (in the frequency domain).

F.2 Maximum entropy method

The maximum entropy spectral estimate (MESE) is related to the correlation approach in the respect that it is also based on the autocorrelation function, but at the same time it differs in an important aspect: For finite length input data, the autocorrelation function is of course also of finite length. Hence, the derived autocorrelation function can be considered as being a truncated estimate of the real function. Effects of the truncation on the PSD are smoothed out by the application of a window function in the correlation method. The MESE approach, however, tries to extrapolate the autocorrelation function instead of smoothing. In doing so, the estimate of the PSD gets more consistent than in the case of the correlation method while the necessity for windowing is removed at the same time (compare Figure F.2).

A brief outline of the extrapolation procedure can be found in Holm [120] or Holm and Hovem [121]. As a first step, the autocorrelation function is estimated from time series data up to a certain time lag. An autoregressive model is then fitted to match the estimated autocorrelation function. This can be done by solving a linear set of equations. The extrapolation is performed by extending the set of equations for time lags outside the available autocorrelation data. Because the solution of the extended set of equations does not require further information than the available autocorrelation

Maximum entropy spectral estimate:

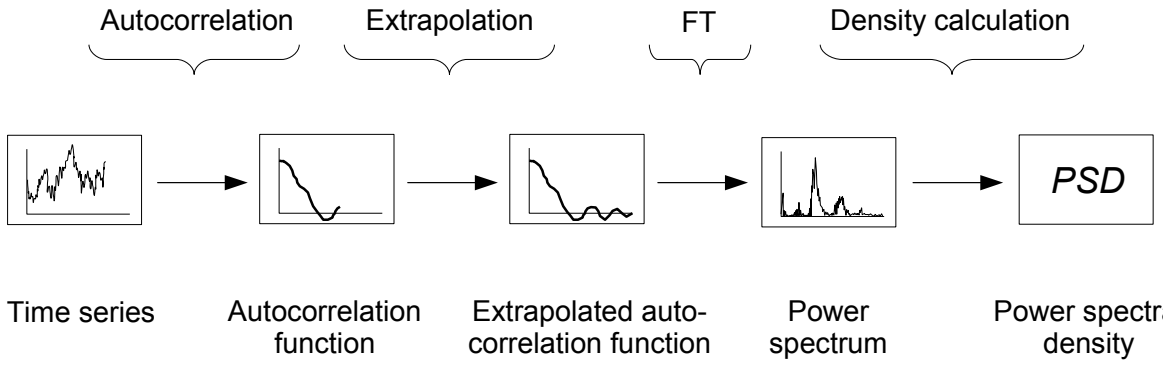

Figure F.2: Schematic of the maximum entropy spectral estimate method for power spectral density estimations

lags, the extrapolation is maximally random and hence fulfils the maximum entropy requirements.

The resolution of the resulting PSD is determined by the length of the autocorrelation function. Extrapolation can therefore also improve the frequency resolution quite a lot, compared to the correlation method outlined above. However, the MESE is computationally much more expensive and the computational costs increase further with an increasing number of extrapolated lags.

F.3 Direct estimation of spectral moments from series expansion

Holm [120] describes a series expansion of autocorrelation terms which can be used for the direct estimation of spectral moments. The derivation of the series is based on relating the autocorrelation function to the PSD by a series of cosine terms. These terms are then inserted into a discrete form of equation 5.3 and thereby link the autocorrelation function directly to the spectral moments. The expression is also extended to include a maximum-entropy extrapolated part of the autocorrelation function. In the end, it computes to

$$\lambda_n = \left[\frac{c_0^n}{2} R_{cor,xx}(0) + \sum_{k=1}^{M} c_k^n R_{cor,xx}(k) \right] + \sum_{k=M+1}^{\infty} c_k^n R_{cor,xx}(k) \tag{F.1}$$

where M is the number of available autocorrelation lags of the autocorrelation function $R_{cor,xx}$ and c_k^n are the series coefficients. The term outside the squared brackets is the extension of the formula for maximum-entropy extrapolated time lags.

Holm also derived a general expression for the coefficients and gave explicit formulas for the calculation of the first five. These are required to compute spectral moments up to fourth order:

$$c_k^0 = 0 \tag{F.2}$$

$$c_k^1 = \begin{cases} \frac{-2}{\Delta t}\frac{1}{(\pi k)^2} & \text{for } k = 1, 3, 5, \cdots \\ 0 & \text{for } k = 2, 4, 6, \cdots \end{cases} \tag{F.3}$$

$$c_k^2 = (-1)^k \frac{1}{(\Delta t)^2}\frac{1}{(\pi k)^2} \tag{F.4}$$

$$c_k^3 = \begin{cases} \frac{3}{4}\frac{1}{(\Delta t)^3}\left[-\frac{1}{(\pi k)^2} + \frac{2}{(\pi k)^4}\right] & \text{for } k = 1, 3, 5, \cdots \\ 0 & \text{for } k = 2, 4, 6, \cdots \end{cases} \tag{F.5}$$

$$c_k^4 = (-1)^k \frac{1}{(\Delta t)^4}\left[\frac{1}{2}\frac{1}{(\pi k)^2} - \frac{3}{(\pi k)^4}\right] \tag{F.6}$$

$$\tag{F.7}$$

Calculation of the spectral moments as series expansion from the autocorrelation function requires very little computational costs. This holds true at least as long as no maximum-entropy extrapolation is required. In general the computed moments seem to already converge often for a relatively small number of available lags. Because the length of time series used within this work is typically quite large, many lags can in theory be derived from the time series data. This means that in most cases convergence of the spectral moments can already be achieved without extrapolation.

F.4 Tests and conclusions

All of the above described methods have been tested extensively on measured and simulated wind turbine data. Because only time series of 10 minute length and with a high resolution ($>$ 10 Hz) have been processed, all methods give similar results. For time series with this length and resolution, the MESE obviously does not have a significant advantage in terms of accuracy anymore as it would probably be the case for shorter series.

As an example, the second and fourth order spectral moments of the rotor torque, calculated from simulations of the NREL 1.5 MW wind turbine model, are shown in Figure F.3. In this case, three different mean wind speeds have been investigated (6, 12 and 18 m/s), together with 6 different stochastic representations of the turbulent wind

field from different seeds. The turbulence intensity was set to 15 % for all simulations.

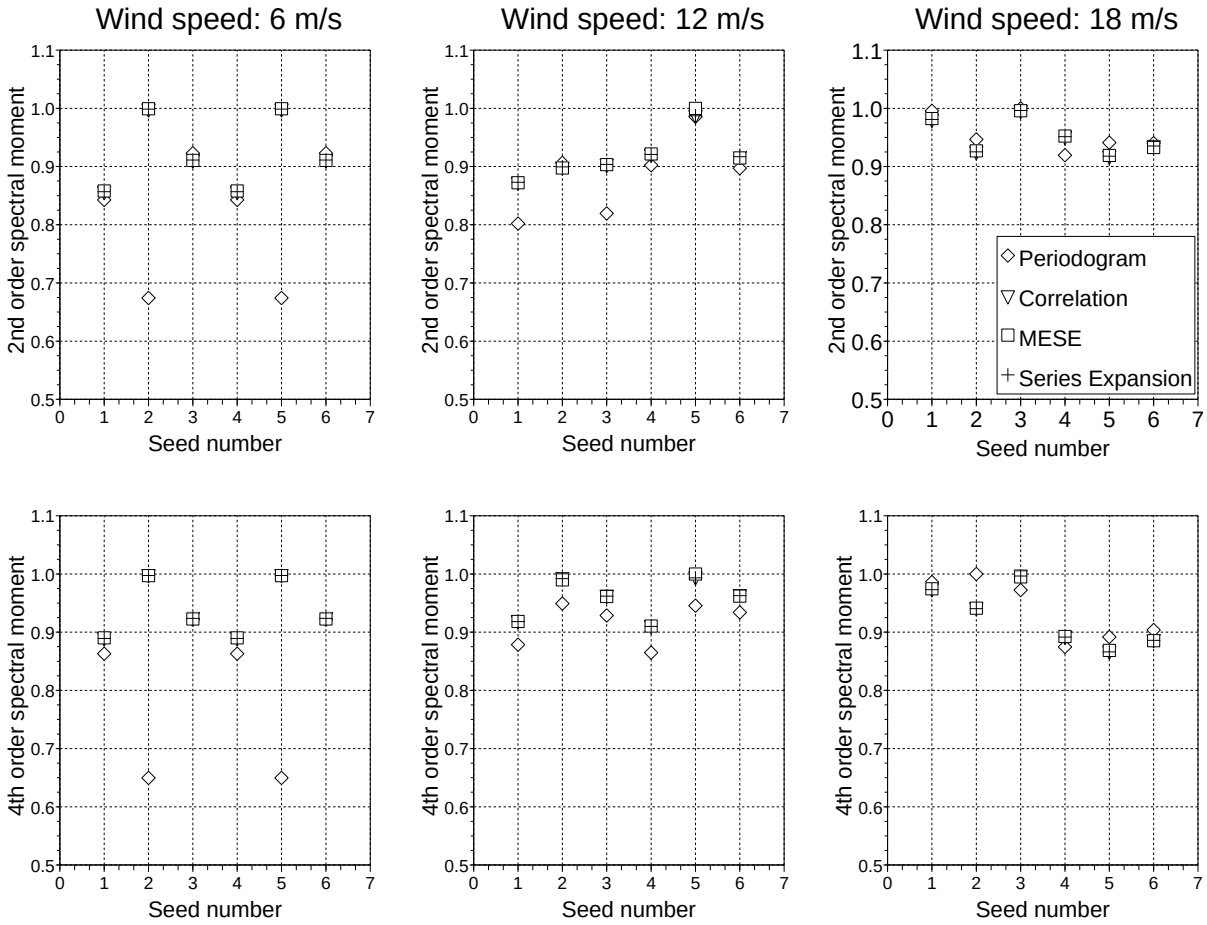

Figure F.3: Second and fourth order spectral moments from various methods for simulated rotor torque of the NREL 1.5 MW turbine

It can be seen, that there is some variation in the spectral moments with the applied stochastic wind field. Nevertheless, results from correlation method, MESE and series expansion are quite similar. This is not surprising, as all of them are based on the autocorrelation function. The results from the periodogram differ from the others and seem to give somewhat lower moments for the cases at wind speeds of 6 and 12 m/s.

It is difficult to judge which method yields the most accurate results from Figure F.3, as the real spectral moments are unknown in this case. Even additional tests, based on the analysis of filtered white noise (where the theoretical PSD is known from the filter response function) did not allow to draw clear conclusions on the superiority of one method over the others in terms of accuracy. Because all results are in a comparable range and show similar scatter, the choice of method within this work was based on practical considerations: Periodogram and correlation both need a priori knowledge of the frequency content of the processed time series in order to chose an appropriate segmentation length. Furthermore, their outcome is influenced by the applied window

function. These two facts imply, that the quality of the results from these methods also depends on the input and probably some (undesirable) parameter adaptations with respect to the input might occasionally be required. This is not the case for the MESE, if a relatively large number of extrapolation lags is used all the time. However, the method is computational expensive and takes some time to execute. Taking these aspects into consideration, the series expansion approach by Holm seems to be most suited. Therefore, this method has been chosen as the standard procedure for spectral moment estimation in this work.

G Investigations into the integral length scale of turbulence

The investigations on the influence of environmental and operational conditions on wind turbine loads and standard signals in Chapter 3 revealed, that the integral length scale of turbulent wind fields can have a significant impact on the fatigue loads of a wind turbine. While a reduced length scale means more gusts in a given period of time, very large length scales can cause trends in the measured data sets. The response of the turbine to these situations in terms of fatigue loads and its statistical parameters of standard signals differs. Hence, the introduction of length scale related parameters into the procedure for the load estimation based on standard wind turbine signals seems advisable.

Following a general overview, basic relations of length scales, power spectral density and fatigue loads are discussed briefly. Then, estimates of the average length scales from the met mast and nacelle anemometer data of the Multibrid M5000 and the Nordex N80 measurement campaigns are presented and evaluated. On the basis of the gained experience, length scale related parameters of standard signals are derived.

G.1 Overview on integral length scales

The integral length scale is one of the main parameters for the characterisation of the turbulent flow and serves as a measure of the average eddy scale size. Commonly, only the large 'energy-containing' eddies are of interest in wind energy applications and hence the term 'length scale' only refers to those in this investigation. As an illustration of the gusts of interest, the typical turbulent structure of a simulated wind field with a negative gust from about 150 to 250 m and a positive gust from about 200 to 350 m has been plotted in Figure G.1.

Many investigations of length scales at different sites can be found in literature. Counihan [56] has summarised the results from several measurement campaigns which have been conducted and published between 1915 to 1972 along with the find-

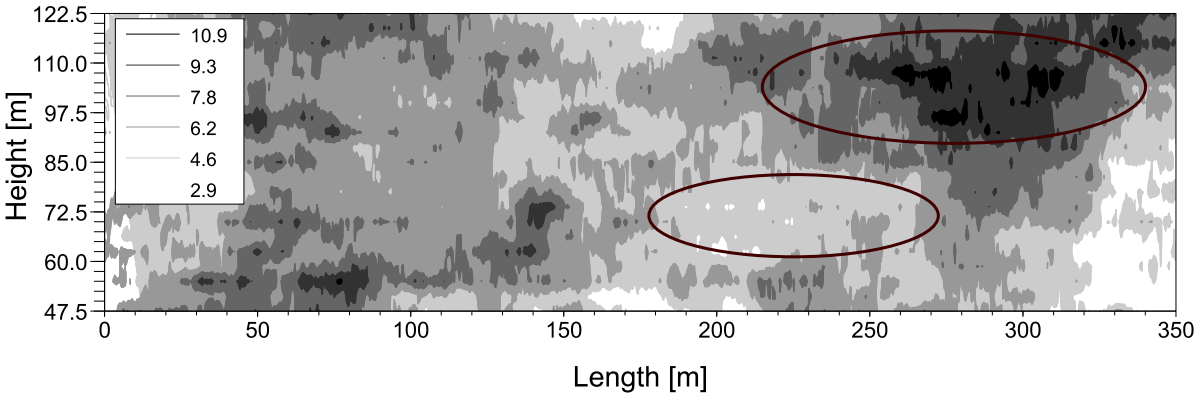

Figure G.1: Longitudinal cut through a simulated turbulent wind field. An average wind speed of 7 m/s has been used for the generation, along with a turbulence intensity of 20 %, a wind shear exponent of 0.2 and an integral length scale of 170 m

ings and conclusions of various researchers. In general it has been found, that the length scale decreases with increasing surface roughness and increases with height up to approximately 200-300 m. At greater heights it becomes independent of the surface roughness and decreases for further increases of height. From his analysis of measured data, Counihan also derived an expression to estimate the integral length scale for heights between 10-240 m.

Figure G.2 shows some of the length scales, that have been collected by Counihan. The available data has been divided into two groups of data sets for this plot. One contains length scales from sites with relatively small roughness lengths which have been denoted either as ‘Smooth’, ‘Coast’, ‘Grass’ or ‘Rural (flat)’. The other one includes all data that has been characterised as ‘Rough’ and ‘Woods’, where the roughness lengths is usually large. Although the data is subjected to much scatter, an increase of length scale with height and decreasing roughness length is indeed clearly visible.

In addition to height and roughness length, Frandsen et al. [57] reported a dependency on wind speed. They state that $L_u \approx 25 \cdot U$ for larger heights of 80 to 160 m at an investigated coastal site. The wind speed dependency is less pronounced for three sites investigated by Veldkamp [28](two coastal and one offshore site). A significant increase at wind speeds larger than 15 m/s was observed only for the offshore site Horns Rev. For most of the other wind speeds and sites, fairly constant values of about 200 m have been calculated.

It is evident, that wind turbines at various sites operate in different average gust lengths, depending on hub height and site conditions. But even at a single location the gust length varies significantly with time. For the Risø test site for large wind turbines Frandsen et al. [57] reported large standard deviations of length scales. They also showed, that even for the maximum measurement height of 160 m, the mean value of

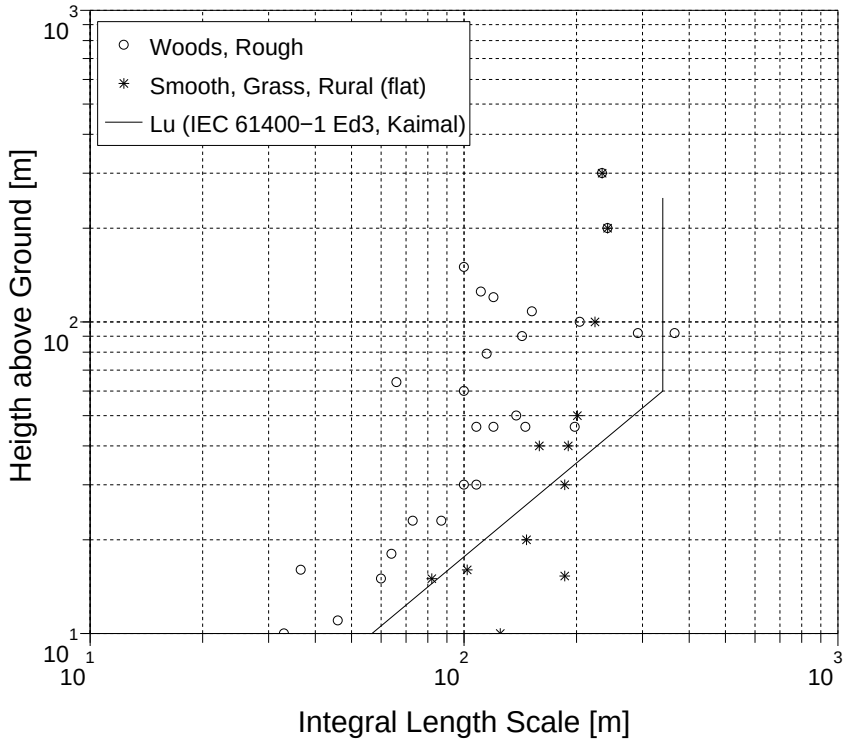

Figure G.2: Integral length scales from various sites summarised by Counihan [56]

the length scale for wind speeds between 10 to 12 m/s has still not fully converged. This corresponds to the findings by Counihan.

Petersen et. al. [122] showed length scales that have been measured at the offshore wind farm Vindeby, ranging from a few meters to several kilometres with an average value of 300 to 500 m. Contrary to the onshore sites investigated by Counihan, they found that the length scales already converge at very low heights of 30 to 40 m.

Figure G.2 also displays the length scale as defined in the standard IEC 61400-1 [16]. Neither a variation with roughness length nor with wind speed has to be taken into account according to the standard. At first glimpse, the values appear to be quite large when compared to the measured average site values. However, if the length scale varies with wind speed, much larger values than the ones proposed by the standard might appear for wind speeds above the annual average site wind speed. Realising, that for the fatigue loading of wind turbines the wind speeds above rated ($>$12-14 m/s) are most important [123], the IEC values are put into perspective. As an example, Frandsen et. al. [57] also outline, that the IEC values fit quite well to measurements at the Risø test site for wind speeds between 10 to 12 m/s and that the IEC in fact underestimates the gust length for higher wind speeds.

Length scales in the wake of a wind turbine are significantly smaller than those in free stream conditions, particularly closely behind the rotor. In [57] a reduction of approximately 70 to 75 % at 1D behind a turbine has been observed. These findings correspond to studies referred to by Vermeer et. al. [58] or Frandsen et. al. [47], where a reduction of the free stream length scale in the wake of a turbine to about half of the free stream conditions at a distance of 4D has been reported.

G.2 Length scales, power spectral density and fatigue loads

Because the integral length scale is a measure for the average gust length inside a wind field, it is also an important parameter for the modelling of turbulent flow. Length scales are often employed in particular for the definition of the power spectral density of wind speed time series.

Many different proposals for the power spectral density of wind speed have been published in the past. However, often definitions of Kaimal or von Karman are followed in wind energy applications, as these are the ones which are still or have been promoted by the IEC standard 61400-1 [16]. In its normalised form the Kaimal spectrum is defined as:

$$\frac{fS_u(f)}{\sigma_u^2} = \frac{4fL_u/U}{(1+6fL_u/U)^{5/3}} \tag{G.1}$$

where $S_u(f)$ is the power spectral density of wind speed, f is the frequency, σ_u is the standard deviation of wind speed and L_u is the integral length scale of turbulence.

Decreasing the length scale or increasing the wind speed corresponds to shifting the peak of the spectrum to higher frequencies (see Figure G.3). This means that more energy is present at relevant eigenfrequencies of the wind turbine, i.e. in frequency ranges above approximately 0.25 Hz which leads to stronger excitations of the turbine structure. Furthermore, for example as pointed out in [122], the characteristic frequency of gusts is linked to the mean wind speed and length scale by

$$f_{gust} \propto U/L_u \tag{G.2}$$

Hence, the characteristic frequency also increases when the length scale is reduced or the mean wind speed is increased. A higher characteristic frequency is equivalent

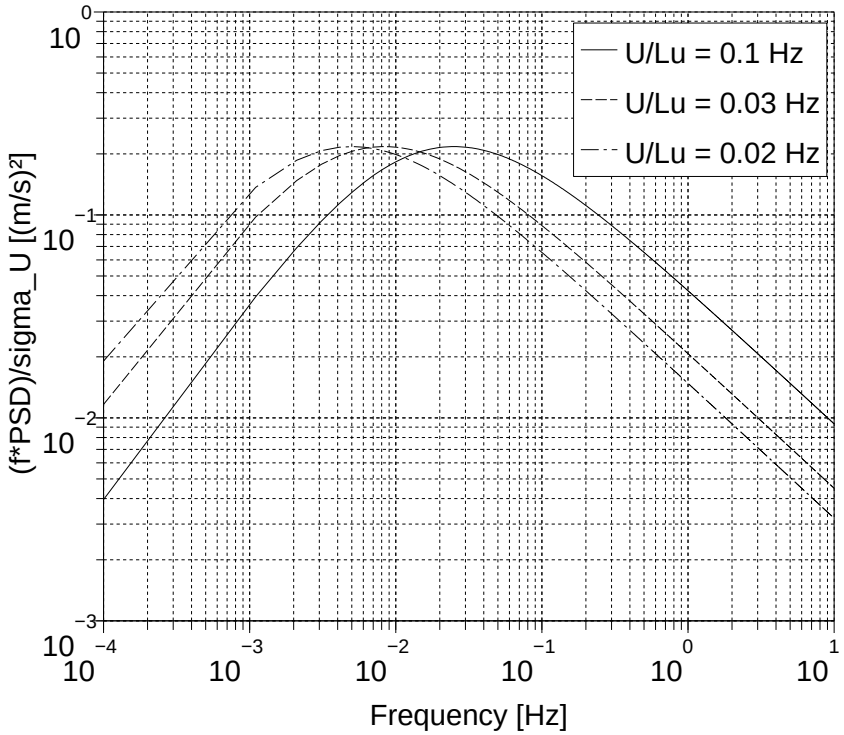

Figure G.3: Kaimal power spectral densities for different ratios of mean wind speed to integral length scale

to more gusts in a given time and the fatigue loads are likely to increase. Opposite effects apply if energy is shifted to lower frequencies.

In contrast to variations in length scales, an increased standard deviation of wind speed will add energy to all frequencies of the Kaimal spectrum. Hence, low and high frequency oscillations will be equally influenced and their ratio remains constant. In this case, the characteristic frequency does not change, but the amplitude of gusts increases.

The influence of length scales on fatigue loads and statistical parameters of standard signals can be very different. This raises additional challenges for a load estimation system. An example is a very large length scale which can provoke wind speed oscillations with periods larger than the length of the measured time series. These effects appear as trends in wind speed. Trends tend to have a great influence on some statistical parameters of loads and standard signals, for example on the variance. On the contrary, their impact on equivalent load ranges can be far less pronounced. As a consequence, the variance of a load signal alone is not a very accurate indicator of the corresponding equivalent load ranges. In addition, the *type* of variance also has to be considered.

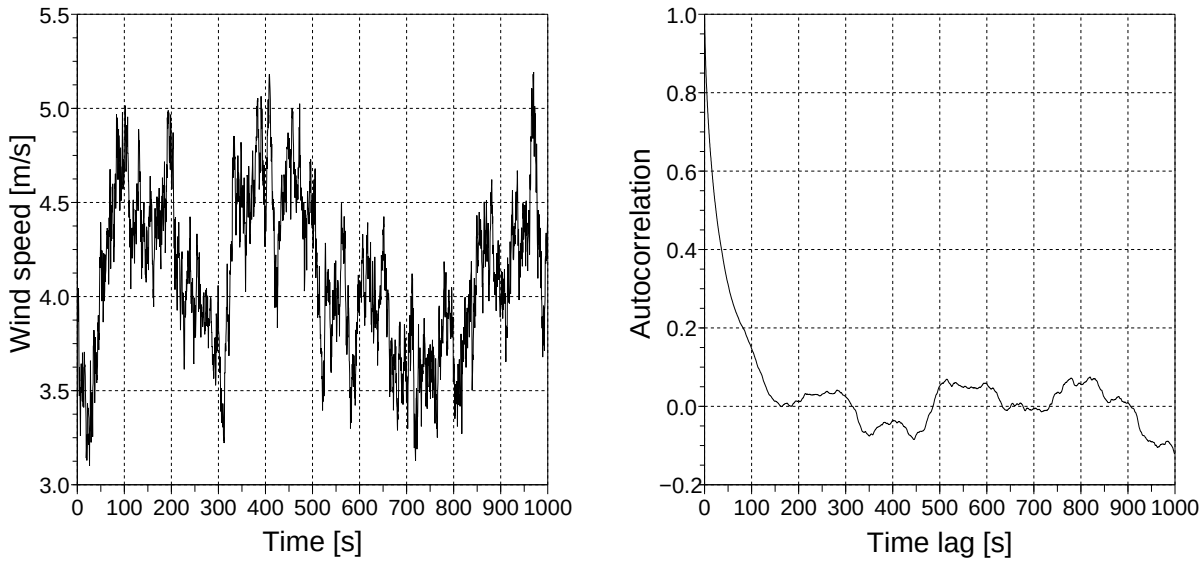

Figure G.4: Example of a simulated wind speed time series and its autocorrelation function

Knowing the integral length scale can potentially improve the accuracy of load estimations, because it allows to conclude on the distribution of energy in the wind. In the following, these scales are first derived from measured data at two sites. In a second step, efforts to relate them to statistical parameters of standard signals are undertaken.

G.3 Length scale computations

G.3.1 Autocorrelation approach

One common method to determine the integral length scale of turbulence is by means of autocorrelation (see for example [56], [19], [124] and [125]), where the integral of the autocorrelation function is multiplied by the mean wind speed to give the integral length scale. An example for the autocorrelation function is displayed in Figure G.4, where it is plotted together with the underlying wind speed time series.

The integral length scale derived by autocorrelation can be linked to the Kaimal spectrum. In 1938 Taylor [126] proved, that the power spectral density and the correlation coefficients are linked by

$$R_{cov,uu}(x) = \int_0^\infty S_u(f) \cdot cos\left(\frac{2\pi f x}{U}\right) df \tag{G.3}$$

$$S_u(f) = \frac{4}{U} \int_0^\infty R_{cov,uu}(x) \cdot cos\left(\frac{2\pi f x}{U}\right) dx \tag{G.4}$$

where $R_{cov,uu}(x)$ is the autocovariance function of a wind speed time series, $S_u(f)$

is its power spectral density, f the frequency, x the spacial distance to the origin of the time series and U the mean wind speed. Substituting $x = \tau \cdot U$ and $R_{cov,uu}(\tau) = R_{cor,uu}(\tau) \cdot \sigma_u^2$ into Taylor's expression G.4 yields

$$\frac{S_u(0)}{4\sigma_u^2} = \int_0^\infty R_{cor,uu}(\tau) d\tau \tag{G.5}$$

Multiplying with U gives

$$\frac{US_u(0)}{4\sigma_u^2} = U \int_0^\infty R_{cor,uu}(\tau) d\tau \tag{G.6}$$

where the left hand side corresponds to the length scale in the Kaimal power spectral density calculated for $f = 0$. Thus the integral length scale can in theory be computed from the integral of the autocorrelation function $R_{cor,uu}$ and the mean wind speed U.

In practice, however, this turns out to be not as straightforward as it may seem at first glance. Stationarity of a time series is an important requirement for the calculation of its autocorrelation function. Low frequency noise and trends can keep the autocorrelation function from approaching zero in a consistent manner [125]. Therefore, the integral of the autocorrelation function will not give correct length scales if the time series is too short and does not also appropriately capture low frequency wind speed fluctuations. O'Neill et. al. [124] calculated the integral length scale from autocorrelation based on DNS simulations of homogeneous isotropic turbulence. They found, that the derived length scale heavily underestimates the real value, if the simulation domain is too small.

The author's own investigations on the basis of a hundred simulated wind speed time series confirmed these findings. The time series length had to be significantly (about a hundred times) larger than the average gust length to give good estimations. This means, that a wind speed time series of about 1000 s is required to estimate a length scale of 100 m at a mean wind speed of 10 m/s with some accuracy. Because it is common that time series are restricted to 600 s in wind energy, the applicability of the autocorrelation approach for the estimation of length scales is limited. It should also be mentioned, that quite some scatter was present in the calculated length scales, with standard deviations of about 50 % for short time series but still about 20 % for very long time series.

Even for sufficiently long wind speed time series, the autocorrelation function will eventually start to oscillate about zero at some large time lag (Figure G.4). Several integration schemes have been developed in the past to overcome these issues, where for example the integration is carried out only up to the first zero crossing or up to the

first minimum. Sometimes, the integration is performed even on the basis of a fitted exponential function (see e.g. [125] and [124]). Although these schemes can increase the accuracy of the results, the lack of stability against low frequency noise will in practice always add some uncertainty to the derived length scale.

G.3.2 Length scale estimation from power spectral density

In theory, the integral length scale corresponds to the intersection point of the power spectral density with the ordinate:

$$\frac{US_u(0)}{4\sigma_u^2} = L_u \tag{G.7}$$

However, this value is difficult to compute in practice. Therefore, another often used method for the estimation of length scale is to fit a theoretical description of the power spectral density to the previously derived power spectral density of a wind speed time series. The length scale can then be extracted from the fit (see e.g. [57] or [127]).

Unlike the autocorrelation method, fitting of the data can be performed on the basis of relatively short time series (compared to the autocorrelation approach) with suitable methods. Only such parts of the spectrum are fitted which can be derived with sufficient accuracy from a 10 minute time series, e.g. the peak of the spectrum or some part to the right of it (Figure G.5). Excluding the extremely low frequency parts of the spectrum makes the estimation of the length scale from power spectral densities less sensitive to non-stationarity of wind speed time series than the autocorrelation method, something which has also been reported by Frandsen et. al. [57].

The decision upon which part of the spectrum is used has to be based on length and resolution of the time series as well as on the method which is used for the spectral estimation (compare for example Annex F). Furthermore, measurement devices can also influence the results. Dahlberg et. al. [43] showed, that the step response of an investigated cup anemometer is similar to a first order response with a time delay of approximately 0.15 s. Hence, the anemometer itself acts as a low-pass filter and higher frequencies will not be captured correctly in the wind speed time series. The time domain response of a first order model with a time constant of 0.15 s is shown in Figure G.6. In addition, the normalised PSD of its frequency domain response is plotted. As can be seen from this figure, frequencies of 0.5 Hz will appear only with approximately 80 % of their original value, when the time series has been measured with a cup anemometer. Of course, the reduction of the PSD at higher frequencies influences the results of a fit, if these frequency ranges are included. A correction

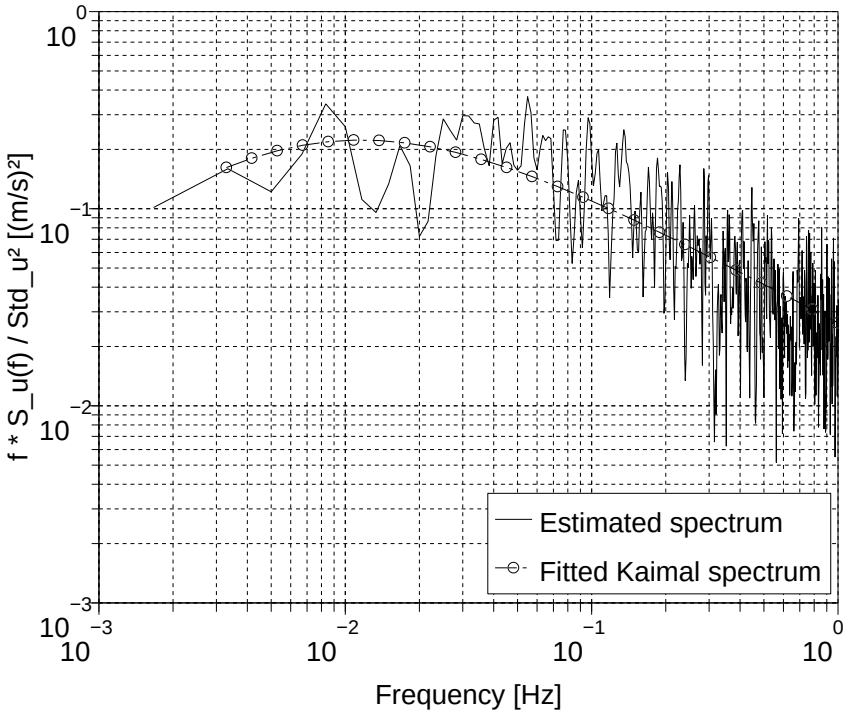

Figure G.5: Kaimal spectrum is fitted to a spectrum which is estimated from a measured wind speed time series by means of the correlation method.

of the measured spectra with a suitable transfer function is possible, if the response of the measurement device is known. As an alternative, measurement devices without significant response functions at frequency ranges of interest, such as ultra sonic anemometers, can be used.

G.4 Analysis of measured data

G.4.1 Length scales from wind speed measurements

Based on the power spectral density approach, data from the SWE met mast at Bremerhaven (Annex C) and the ECN test site at Wieringermeer (Annex D) have been analysed to derive length scales from wind speed time series. The PSDs have been estimated by means of the correlation method in conjunction with a Hanning window.

Met mast data at two different heights (102 m and 74 m) have been processed at Bremerhaven, while only data at 80 m hub height was available at Wieringermeer. In addition, data from the anemometers mounted on top of the nacelles have also been analysed.

The results are listed in Table G.1. Of course, they are not representative for the met mast locations, as only about 150 hours of data from a single wind direction sector

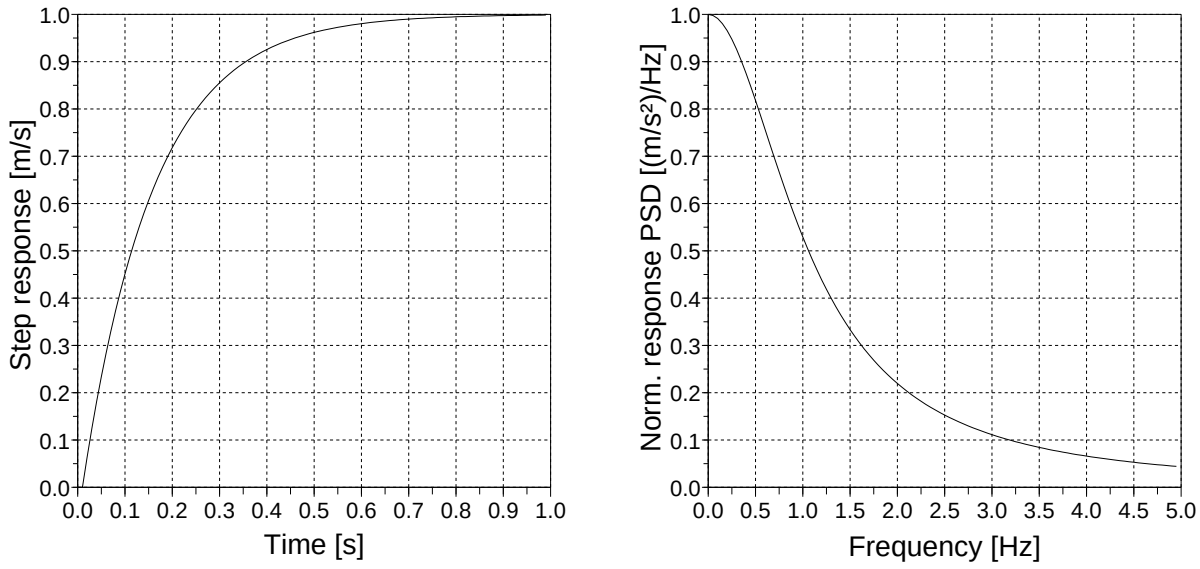

Figure G.6: Time and frequency response of an anemometer approximated as first order model

have been considered for each site.

In general, the length scales derived from the nacelle anemometer do not correspond to those derived from met mast data. In addition, they can not be related to each other easily, as for example a large free stream length scale does not necessarily lead to a large length scale from nacelle anemometry. The distortion of the flow by the rotor and the nacelle is probably too strong and even superimposes the effects of the large-range low-frequency oscillations. Therefore, the estimation of the integral length scale directly from the nacelle anemometer signal with sufficient accuracy seems to be difficult and other indicators have to be found.

Table G.1: Comparison of length scales from met masts and nacelle anemometry of the M5000 turbine at Bremerhaven and a N80 turbine at Wieringermeer

Site	Bremerhaven			Wieringermeer	
Location	Mast	Mast	M5000	Mast	N80 (T8)
Measurement height [m]	102	74	∼102	80	∼80
Wind speed					
Mean [m/s]	10	8.8	9.0	8.3	8.3
Mean turbulence intensity [%]	7	10	10	9.5	20
Integral length scales					
Mean [m]	310	170	100	340	830
Median [m]	150	120	30	210	640
0.1-quantile [m]	60	35	15	75	210
0.9-quantile [m]	700	300	230	640	1700

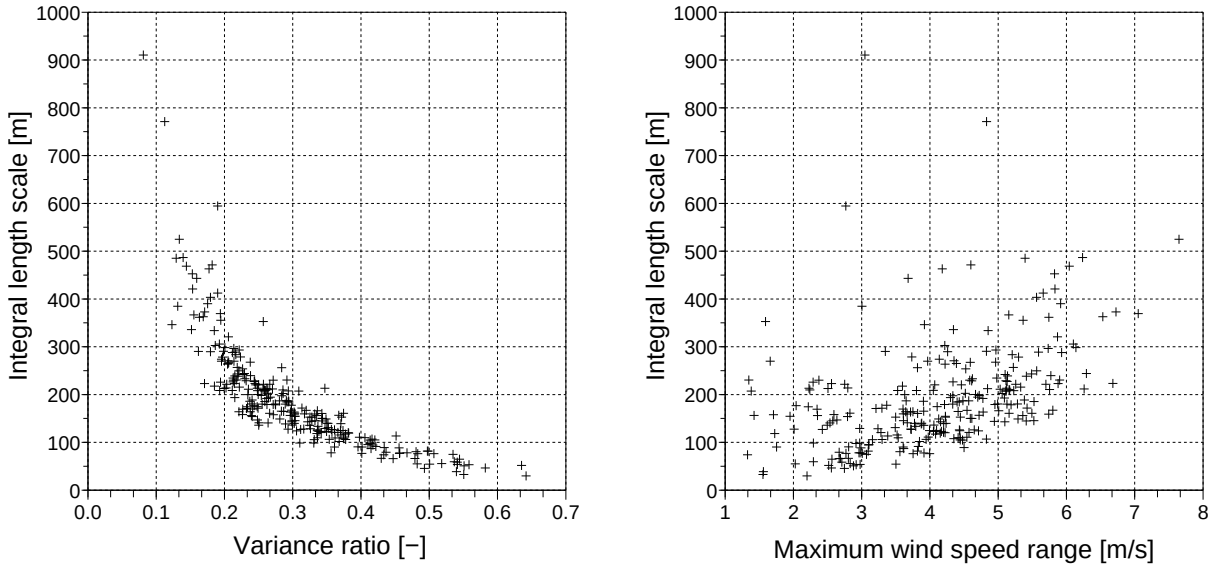

Figure G.7: Estimated length scales plotted over the variance ratios of filtered to unfiltered wind speed time series and over the measured maximum wind speed ranges. Only time series with mean wind speeds from 5 to 9 m/s have been considered.

G.4.2 Parameters related to the distribution of a signal's energy

A simple but effective way to characterise a signal's energy distribution is to compute the variance of the original time series and to relate it to those of filtered series. This has been tested taking measured wind speed time series at Bremerhaven as an example. On the left hand side of Figure G.7, the estimated length scales are displayed over the ratios of variances of high-pass filtered to unfiltered wind speed time series $\mathrm{Var}(U)_{\mathrm{hf}}/\mathrm{Var}(U)$. Only wind speed time series with a 10 minute mean between 5 and 9 m/s have been considered with turbulence intensities from 3 to 16 %. A cut-off filter frequency of 0.05 Hz has been applied.

The scatter plot suggests, that a relation between length scales and variance ratios exists. Although the data features a wide range of turbulence intensities, the shape of the plot is quite pronounced. This indicates the validity of the theoretical considerations regarding the length scale dependency of energy distribution. Further investigations, where the correlation of variance ratios and turbulence intensity has been analysed, emphasis this assumption. Their relation turned out to be much weaker.

In addition, the effect of length scale on other statistical parameters of wind speed time series has been investigated. At least a small correlation has been found for most of them. As an example, length scales are also plotted over the measured maximum wind speed ranges of 10 minute data sets at the right hand side of Figure G.7. Although the shape of the scatter plot is less pronounced, an increase of ranges with length scales is visible. Of course the ranges are not only influenced by length scales, but

Table G.2: Comparison of variances and variance ratios of wind speed and power signals with equivalent rotor torque ranges for several combinations of turbulence intensity and integral length scale of turbulence.

Wind conditions	$Var(U)$	$Var(P_{el})$	$\frac{Var(U_{hf})}{Var(U)}$	$\frac{Var(P_{el,hf})}{Var(P_{el})}$	$\Delta S_{eq,M_r}$
I_T=15 % and L_u=170 m	1.00	0.85	1.43	1.44	1.02
I_T=15 % and L_u=680 m	1.00	1.10	0.73	0.77	0.99
I_T=15 % and L_u=340 m [1]	1.00	1.00	1.00	1.00	1.00
I_T=10 % and L_u=340 m	0.44	0.44	1.00	1.06	0.68
I_T=20 % and L_u=340 m	1.78	1.87	1.00	0.94	1.33

also significantly by turbulence intensity. This explains the large scatter in the plot.

If the distribution of energy with frequency has got an impact on the derived loads, including related parameters into the load estimation procedure makes sense. As pointed out above, the variance ratios of filtered signals can serve as an indicator for the energy distribution with frequency. When calculated from standard signals such parameters allow to draw conclusions on the distribution of energy in load signals. Hence, they can improve prediction results.

Some basic tests regarding the relations between variance ratios of filtered standard signals and equivalent loads have been performed on the basis of simulations. Results are listed in Table G.2, where the variance ratios as well as the pure variances for the wind speed and the electrical power signal are given together with the equivalent load ranges of the rotor torque. An elliptical band-pass filter with a cut-off frequency of 0.05 Hz has been utilised to derive the high frequency data (with subscript $_{hf}$). The values in each row are averages from six simulations using different stochastic wind fields. All simulations have been performed with a mean wind speed of 6 m/s. It can be seen, that

- the general variance of the power signal is influenced stronger by turbulence intensity than by length scale.
- the variance ratio of the power signal is influenced stronger by length scale than by turbulence intensity.
- the equivalent load ranges of the rotor torque are influenced mainly by turbulence intensity.

[1] Baseline: Data in columns are relative values with respect to this row.

It is obvious from Table G.2, that variance ratios can be employed to distinguish, if for example a change in variance of the electrical power is caused by a variation of turbulence intensity or length scale. Therefore, it can generally be beneficial to provide statistical parameters of filtered and unfiltered signals as inputs for the neural network estimation to improve the identification of wind conditions and their effects on wind turbine loads.

As shown in Figure G.7 in the example of wind speed ranges, length scales influence other statistical parameters as well and hence this information is redundantly available in the input parameters. Hence, training of a network has not necessarily to result in the selection of variance ratios as input parameters, even though these are related more directly to the energy distribution. Instead the relevant information can also be extracted from other statistical parameters. Therefore, investigating acceptance or rejection of variance ratios by networks will not give a clear impression of their ability to reflect length scale related information.

G.5 Summary and conclusions

Wind turbine loads do not only depend on the variance of the wind speed, but also on the type of variance (the distributions of energy with frequency). As an example, large integral length scales increase the probability of low frequency wind speed oscillations, which cause different fatigue loads than fast changing fluctuations with the same total variance. This imposes additional challenges on the estimation of wind turbine loads.

Therefore, possibilities of including information on the distribution of energy over frequency into the estimation procedure have been investigated. Unfortunately, it turned out that the wind turbine anemometer signals are not well suited for this task. An alternative approach, based on the comparison of energy content at various frequency ranges of standard signals, seems more promising. Here, standard signals are filtered and a ratio of filtered to unfiltered time series is derived. These parameters can be related to the distribution of energy of load signals.

Although it seems that variance ratios are particularly suited for this task, this information is redundantly available from other statistical parameters of standard signals (albeit less clear). Hence, demonstrating the suitability of variance ratios by analysing neural network based transfer functions is difficult.

H Hermite moment models for non-Gaussian transformations

H.1 Winterstein's Hermite moment models

For the transformation of processes from the Gaussian domain into the non-Gaussian domain, Winterstein developed second order models based on Hermite polynomials. These models calculate the non-Gaussian distributions based on the normalised target moments of the process: the skewness γ_3 and the kurtosis γ_4. Utilisation of Hermite polynomials makes the transformation orthogonal, which means that the contributions from skewness and kurtosis are independent of each other. The models can be inverted to allow for the reverse transformation of processes.

In addition to the direction of transformation (from or into the Gaussian domain), the transformation functions also depend on the kurtosis of the process. Different models are applied for so-called 'softening' ($\gamma_4 > 3$) and 'hardening' ($\gamma_4 < 3$) responses.

Prior to some of the transformations, the time series have to be normalised by their mean value and standard deviation which yields the normalised non-Gaussian time series $Z_0(t)$ and the normalised Gaussian time series $X_0(t)$:

$$Z_0(t) = \frac{Z(t) - \bar{Z}(t)}{\sigma_Z} \tag{H.1}$$

$$X_0(t) = \frac{X(t) - \bar{X}(t)}{\sigma_X} \tag{H.2}$$

After the transformation, the time series can be rescaled in a similar manner to the desired mean and standard deviation.

It should be mentioned, that Winterstein published several approximations for the polynomial coefficients. The following equations are based on the approximations given in [99]. The time dependence of Z and X is disregarded in the following in favour of a better visual appearance.

In case of a *softening process* the coefficients can be approximated from:

$$\tilde{h}_3 = \frac{\sqrt{1 + 1.5(\gamma_4 - 3)} - 1}{18} \tag{H.3}$$

$$\tilde{h}_4 = \frac{\gamma_3}{4 + 2\sqrt{1 + 1.5(\gamma_4 - 3)}} \tag{H.4}$$

The transfer functions are defined by

- from Gaussian to non-Gaussian

$$Z_0 = \kappa \left[X_0 + \tilde{h}_3(X_0^2 - 1) + \tilde{h}_4(X_0^3 - 3X_0) \right] \tag{H.5}$$

- from non-Gaussian to Gaussian

$$X_0 = \left[\sqrt{\xi^2(Z_0) + c} + \xi(Z_0) \right]^{1/3} - \left[\sqrt{\xi^2(Z_0) + c} - \xi(Z_0) \right]^{1/3} - a \tag{H.6}$$

with the additional parameters

$$\kappa = (1 + 2\tilde{h}_3^2 + 6\tilde{h}_4^2)^{-0.5} \quad , \quad \xi(Z_0) = 1.5b \left(a + \frac{Z_0}{\kappa} \right) - a^3$$

$$a = \frac{\tilde{h}_3}{3\tilde{h}_4} \quad , \quad b = \frac{1}{3\tilde{h}_4} \quad , \quad c = (b - 1 - a^2)^3$$

For *hardening processes*, the coefficients are given by

$$h_3 = \frac{\gamma_3}{6} \tag{H.7}$$

$$h_4 = \frac{\gamma_4 - 3}{24} \tag{H.8}$$

$$\tag{H.9}$$

with the transfer functions

- from Gaussian to non-Gaussian

$$\begin{aligned} Z_0 = {} & \frac{9h_4^2(A(X_0) - B(X_0))^{2/3} - 3h_3h_4(A(X_0) - B(X_0))^{1/3}}{9h_4^2(A(X_0) - B(X_0))^{1/3}} \\ & + \frac{9h_4^2 + 3h_4 + h_3^2}{9h_4^2(A(X_0) - B(X_0))^{1/3}} \end{aligned} \tag{H.10}$$

- from non-Gaussian to Gaussian

$$X_0 = Z_0 - h_3(Z_0^2 - 1) - h_4(Z_0^3 - 3Z_0) \tag{H.11}$$

and the additional parameters

$$A(X_0) = \frac{27(h_4 X_0)^2 + (18h_3h_4 + 4h_3^3)X_0 - 108h_4^4 - 108h_4^3 + (-36h_3^2 - 36)h_4^2}{6\sqrt{3}h_4^2} + \frac{(-24h_3^2 - 4)h_4 - 4h_3^4 - h_3^2}{6\sqrt{3}h_4^2}$$

$$B(X_0) = \frac{27h_4^2 X_0 + 9h_3h_4 + 2h_3^3}{54h_4^3}$$

The Winterstein Hermite moment models are meant for mild non-Gaussianities only. For some values of γ_3 and γ_4 the model can become non-monotonic and the transformation fails. As an extension, Gurley proposed an iterative optimisation which will also find Hermite models suited to correct stronger non-Gaussianities.

H.2 Gurley's modified Hermite moment models

In [100] Gurley points out that a more robust method fo identifying the optimal coefficients of the Hermite model is to apply a numerical optimisation procedure (compare Figure H.1). This procedure minimises the error E between the target skewness γ_3^T and kurtosis γ_4^T and the measured skewness γ_3^M and kurtosis γ_3^M:

$$E = (\gamma_3^T - \gamma_3^M)^2 + (\gamma_4^T - \gamma_4^M)^2 \tag{H.12}$$

The optimised Hermite model should therefore give a more accurate match of target moments than the pure Winterstein model. However, the optimised skewness and kurtosis do not have a physical meaning anymore.

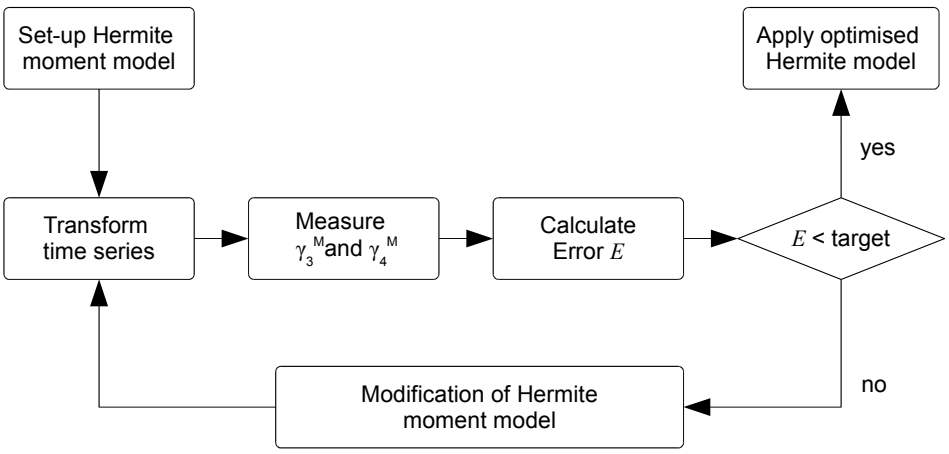

Figure H.1: Gurley's optimisation procedure for Winterstein's Hermite moment model

Curriculum vitae

Nicolai Cosack was born in Celle, Germany, on August 26th 1975. After finishing grammar school at the Gymnasium Uetze in 1994, he did one year of military service. In 1995 he started to study civil engineering at the Universität Hannover. Following an academic year abroad at the University of Bristol, he graduated with a masters degree from Hannover with a thesis in the field of offshore foundations for wind turbines.

From 2002 to 2004 he worked for GE Wind Energy on load and system simulations, first in Salzbergen and later in Berlin. He was involved in the validation of wind turbine simulation models with measured data and in the design of several new wind turbines, all based on the same general platform. While in Berlin he also spend time training colleagues from Germany, USA and India.

In 2004 he took a part time position at the Universität Stuttgart to pursue his PhD at the Endowed Chair of Wind Energy which was founded just a few months before. Besides his research work he also participated in teaching students in the courses Wind Turbine Design I and II and supervised several mid-study and master theses. Another focus was put on the design of tools for wind turbine simulation to support other research activities. He contributed to proposals and the organisation of research projects which currently finance several positions at the Universität Stuttgart and other universities.

In parallel to his PhD he has continued to work in the wind energy industry. In 2004 he also joined the engineering firm RSBconsult in Münster, where he participated in several projects ranging from technical consulting to the design of complete wind turbines. When RSBconsult was acquired by the Indian Kalyani Group in 2007, the company was renamed Kenersys and started to manufacture its own wind turbines. He is currently responsible for wind turbine system simulations there.